2001

Analytical and laboratory modelling of granular filters for embankment dams

Mark R. Locke
University of Wollongong

ANALYTICAL AND LABORATORY MODELLING OF GRANULAR FILTERS FOR EMBANKMENT DAMS

A thesis submitted in fulfillment of the requirements
for the award of the degree

DOCTOR OF PHILOSOPHY

from

UNIVERSITY OF WOLLONGONG

By

Mark R. Locke
B.E. (Hons)

FACULTY OF ENGINEERING
2001

DECLARATION

I, Mark Locke, declare that this thesis, submitted in fulfillment of the requirements for the award of Doctor of Philosophy, in the Faculty of Engineering, University of Wollongong, is wholly my own work unless otherwise referenced or acknowledged. The document has not been submitted for qualifications at any other academic institution.

Mark Locke

September 20, 2001

SUMMARY

Granular filters are used in embankment dams to protect the dam core material from internal erosion, while draining seepage water to prevent saturation of the downstream embankment. In this thesis, a mathematical model is developed to describe the time-dependent processes of filtration of non-cohesive base soils, modelling the rate of erosion and transport of particles into the filter. As particles are captured within the filter, they in-turn are able to retain progressively finer base soil particles until a self-filtration zone forms that is able to prevent any further erosion. The model predictions are verified with a series of laboratory tests in newly constructed, large scale filtration equipment, the largest of its kind in Australia.

Erosion and filtration of a crack through a cohesive dam core is described by analytical modelling. The processes of erosion of the crack walls, transport of particles through the crack, and capture of the particles within the filter are combined to produce a time-dependent model describing the sealing of a cracked core as a filter cake forms. The model is able to predict crack erosion for various filters and hydraulic conditions, and has been applied to several case studies to identify practical uses of the model.

Extensive laboratory work examining erosion and filtration of cohesive base soils provides an improved understanding of the filtration process. Particles eroded from the walls of a pinhole were shown to be coarser than the original base soil particles, and these coarser particles influence filtration. Based on the experimental data, a new design procedure for broadly graded base soils, called the Reduced PSD method, is developed.

ACKNOWLEDGEMENTS

I would like to thank Prof. Indraratna, my supervisor for this PhD project. For three years, since obtaining the research grant through until correcting this thesis, Prof. Indraratna has had a major role in the research. Constant encouragement to produce more work has kept me on track and seen this project finished on time.

This APA(I) research project has been sponsored by SMEC (Victoria) and the Australian Research Council. I would like to thank SMEC, and Managing Director Phil Cummins, for supporting new research both financially and through their intellectual input to the project. In particular I would like to thank Dr Gamini Adikari, who has acted as a co-supervisor of the project and given a lot of time and energy to ensure the project progressed well.

The assistance and friendship from students and staff in the Faculty of Engineering has been invaluable. Particular mention must go to Ailsa Taylor, who assisted with much of the laboratory work described in this thesis. Alan Grant, Ian Bridge and Ian Laird gave me a lot of assistance in the laboratories, particularly Alan who constructed the large scale filter equipment. He also kept me fit with a few tough games of basketball each week. The administration staff, particularly Pam Burnham and Elaine Rhodes, were always helpful and able to extract assistance from university administration when I could not.

Dr Fernando Delgado Ramos has recently completed a PhD in filter design, at the University of Granada in Spain. He and I have often liaised regarding our complimentary research, and some of the laboratory methods and data in this thesis are based on his work. His collaboration has been a great assistance.

Grateful acknowledgment is made to the various water authorities who have allowed me to use samples of material from their dams, provided staff to collect water samples, given permission to use dam data, performance records and drawings, and to publish this data. These include Melbourne Water, Wimmera-Mallee Water, North East Regional Water Authority, Goulburn-Murray Water, and Hastings Council at Port Macquarie.

My family and friends, both new and old, have provided a lot of support throughout the project. While some people think that my PhD has been about surfing, skiing and conferences in exotic locations, there has been a lot of work and some tough moments. It is amazing how a discussion with friends can clear your mind and help solve problems.

Thankyou all.

What did the fish say when it bumped into a wall? Dam.
(Janet Locke, 2000)

TABLE OF CONTENTS

TABLE OF FIGURES

TABLE OF TABLES

1. INTRODUCTION

1.1 Introduction to Granular Filters

In geotechnical engineering, granular filters are used to protect soils from erosion due to seepage. As water flows through a soil, fine particles can be washed out, leading to internal erosion (or piping) and eventual failure. A correctly designed filter will retain the loose soil particles thus preventing piping, while allowing seepage water to flow and avoiding the build up of high internal pore pressures. A granular filter is typically a well graded sand or sandy gravel. Granular filters are used in embankment dams, road pavements, behind retaining walls, for coastal protection and in landfills. The fundamental physics of filtration is essentially the same; however, designs differ slightly between the applications. This study deals predominantly with the behaviour of granular filters within embankment dams.

Filters are necessary in several locations within an embankment dam (Figure 1.1). The most critical filter is immediately downstream of the dam core. This filter must minimise internal erosion by retaining particles eroded from the core, while controlling the seepage flow and forming a drainage layer to avoid saturation of the downstream embankment. The critical filter is continued between the downstream fill and foundation to prevent particle movement either from the fill into the foundation or vice versa, and transport seepage safely to the downstream toe. Core erosion can lead to rapid failure of the dam by piping; hence, it is essential that this filter performs its function correctly.

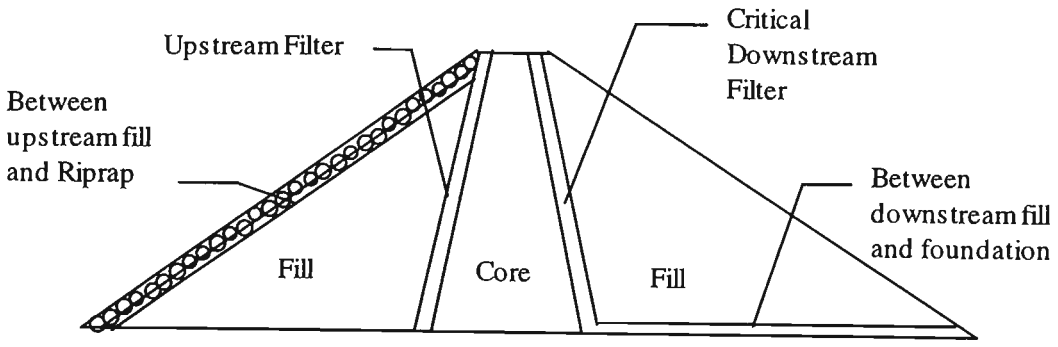

Figure 1.1 - Location of filters within a typical embankment dam

Within an embankment dam, filters are also often used beneath the upstream riprap to protect fine fill from erosion due to wave action. A filter upstream of the core is required to prevent erosion during drawdown of the reservoir. These other filters are illustrated in Figure 1.1. The focus of this study is the critical filter downstream of the core, since the success of this filter is essential to avoid internal erosion of the dam core. The concepts of filter behaviour developed in this thesis apply equally to filters in other locations.

The failure of dams by internal erosion and piping through inadequate filters is a real risk. Foster et al. (1998) examined historical records of dam failures and determined that the average probability of failure of large embankment dams is 1.2% over the life of the dam (136 dam failures out of 11192 large embankment dams constructed up to 1986). Of these failures, 46% were due to a piping mechanism, where the granular filter was either inadequate or not present. Uncontrolled erosion of the fine materials occurred, either by seepage into the foundation or through the dam structure, leading to the failure of the dam. The dam failures are not isolated to older dams, 13 of the recorded piping failures occurred in dams constructed during or after 1980. Hence, there is a need to improve dam design techniques and knowledge of the behaviour of granular filters.

There is an increasing push to replace granular filters with geotextiles, which can perform the same function. The advantages of geotextiles are numerous; often they are cheaper to install than granular filters, and they are constructed to careful requirements, so that the uncertainties due to variations in the properties of natural materials are removed. Some embankment dams have been built with geotextile filters, and nearly thirty years later these dams are still performing well (Faure et al. 1996). However, there is still a concern that the long-term performance of geotextiles may be unsatisfactory, given that a major dam usually has a design life approaching 100 years. A particular concern is that a geotextile may tear due to differential settlement or earthquake induced motion within the structure. Because of these concerns, granular filters are more commonly used than geotextiles in important structures such as embankment dams. This study will focus solely on the performance of natural, granular materials as filters.

Filtration is a complex process, the various erosion processes, hydraulic forces required for particle transport, and particle interactions resulting in the retention of particles are difficult to identify and describe. This thesis presents an examination of all of these aspects of filtration through analytical modelling and laboratory simulation. Theoretical models will be developed, describing erosion and filtration of non-cohesive base soils, and erosion and transport through a crack in cohesive materials and the effect of a filter to seal the crack. These processes are combined with a new model of particle capture in filters, producing two new, complete theoretical models of filtration. Laboratory results will be described, verifying the model predictions and outlining problems with current design criteria and resulting in recommended new filter design criteria.

1.2 The Function of a Granular Filter

Filters are used where water seeping out of an exposed face of a soil may cause erosion of the soil, due to removal of particles under hydraulic forces. To function correctly, filters must meet the following criteria:

1. The filter must be fine enough that the pore spaces between the filter particles are sufficiently small to capture some of the larger particles of the protected material (called the base soil), shown in Figure 1.2. These captured particles will block the filter voids and retain the remainder of the base soil.
2. The filter must be coarse enough that is has sufficient permeability to allow seepage flow to pass through the filter, preventing the build up of high pore pressures and draining all the seepage water from the dam, avoiding saturation of the downstream fill.
3. The filter must be non-cohesive, requiring a limit on the quantity of cohesive fines in the filter. Cavities or cracks may form within the cohesive core material, the protective filter must have negligible cohesion so that it can collapse and self-heal over the crack.

Piping failure within a soil mass can result from the continuation of three particle migration process causing erosion of the material: namely backwards erosion, suffusion or erosion through a crack. Backwards erosion is a process where seepage forces remove particles from the exit face of the soil body. Continued erosion leads to a backwards (upstream) movement of the erosion face, as a tunnel is formed and progresses towards the reservoir. This process occurs mainly in non-cohesive materials. Suffusion of internally unstable materials involves the loss of fines from within the structure of a soil. If a sufficient quantity of fines are eroded, then a volume reduction of the material may occur. Concentrated erosion requires a crack through the material or an interface with a

solid surface, such as a conduit or spillway structure. Higher velocity flows through the crack can result in erosion and transport of particles, and subsequent enlargement of the crack. If the material is cohesive it may be able to maintain a roof over the crack, allowing extensive erosion.

To demonstrate how a filter functions, Figure 1.2 shows a stable base - filter interface. Seepage forces have washed out some base soil particles into the filter, initiating the backwards erosion process. Initially, some fine base particles may be transported completely through the filter, but in a stable filter the larger base particles will be trapped by the pore constrictions (connections between pores) of the filter material. These trapped particles will then form smaller pores, subsequently retaining smaller base particles, and as this process continues the entire interface becomes stable. After formation of a stable interface, no further particle loss occurs. This process is called "self-filtration". The water flow rate will vary during this process, but generally reaches a steady state as the process stabilises.

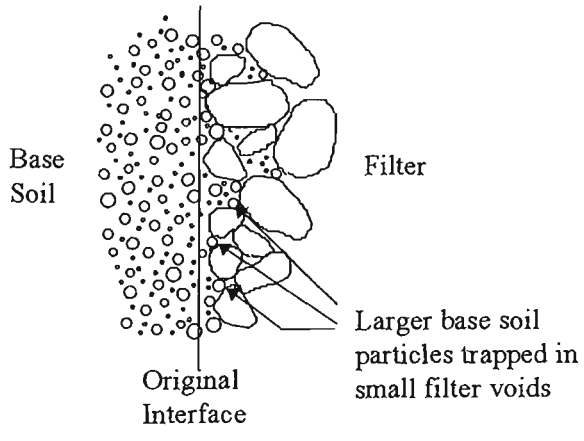

Figure 1.2 Stable Base-Filter Interface During Seepage

Filtration is controlled by the pore constrictions in the filter material. A pore constriction is the small, two-dimensional opening between two filter pores. These pore constrictions are smaller than the filter pores and are responsible for preventing the movement of loose soil particles. If a particle is larger than all of the constrictions exiting a pore, then it will be retained within that pore. The possible outcomes of the filtration process are dependent on the relative size of the base soil particles and can be grouped into the four cases shown in Figure 1.3, each of which is described below.

A. The pore constrictions are finer than all the base particles, and no particles penetrate the filter. This case is excessively conservative, and often leads to insufficient permeability to allow drainage of seepage water as the base and filter material have almost the same grain sizes.

B. This case describes a stable base - filter combination. Some base material penetrates the filter, but these particles eventually encounter a smaller pore constriction and are captured. These retained particles form smaller voids that are able to capture further base particles, hence a stable interface results. The formation of a stable interface is often accompanied by a decreasing flow rate that becomes constant with time.

C. The figure shows a stable or semi-stable base - filter combination. Here, fine base particles are initially able to wash through the filter without being impeded, while coarser particles are retained. The retained particles block the pores and form a self-filtering interface. The acceptable degree of fine particle washout defines the failure or success of this case. If an excessive amount of fines are eroded, the base permeability increases and subsidence can occur, both of which may be unacceptable.

D. This is an unstable base - filter combination, where the filter is too coarse to retain any base particles, hence, the formation of a stable interface is not possible

A successful filter will be somewhere between case B and case C depending on the base material to be protected. Case B is safe, but may be somewhat conservative. Case C may be acceptable, but it is necessary to have detailed knowledge of the filtration process and properties of the materials before designing a filter near the success/failure boundary. In many applications, it may be acceptable to allow some loss of fine material before a stable interface can be established.

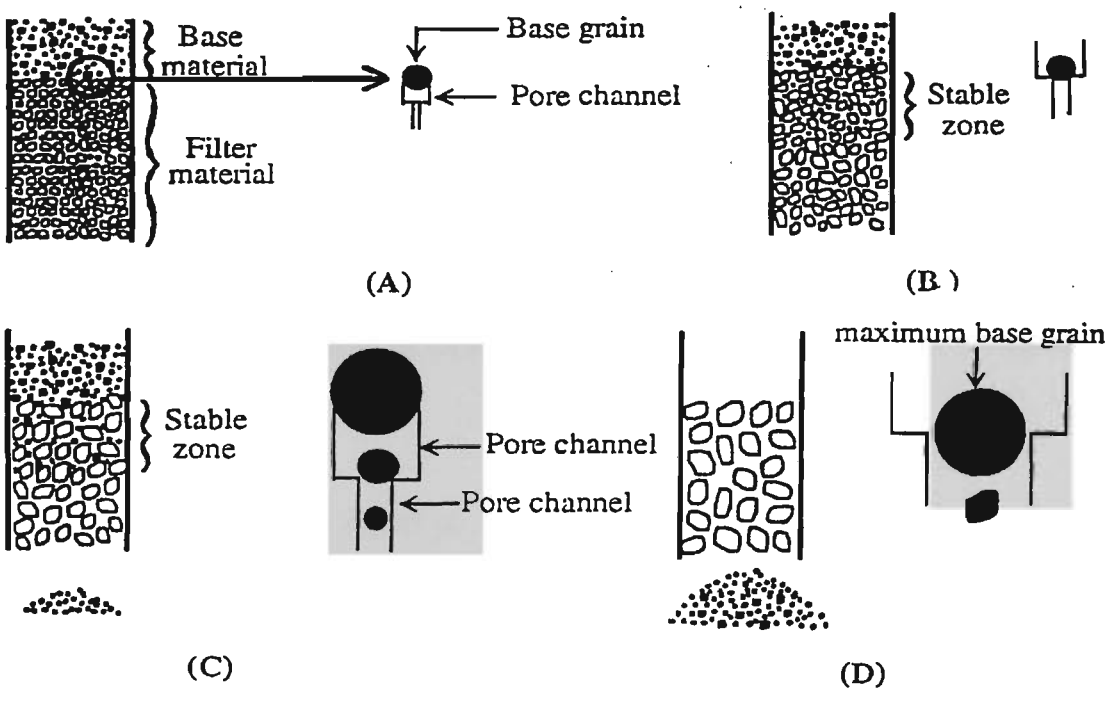

Figure 1.3 Possible Outcomes of Filtration

1.3 Research Aims

The research described in this thesis aims to improve knowledge of the processes occurring within a granular filter, through the following activities:

- A critical review of literature in this field and a discussion of the findings of this literature, including discussion of which areas of filter behaviour are still uncertain.
- Analytical modelling of the movement of non-cohesive base soil particles through a granular filter. Using fundamental physical concepts, the time-dependent erosion and capture of base soil particles within the filter can be described. This will provide a description of what occurs, and the changes in material properties, during the filtration process. The modelling predictions will be verified through laboratory testing.
- Laboratory study of the erosion of cohesive soils including the rate of erosion and size of eroded particles. Comparison with published data and laboratory tests on the same materials will provide a basis for describing what occurs during filtration of cohesive materials. This will include an examination of current design criteria on the basis of the new laboratory results.
- Analytical modelling of filtration of cracks through cohesive materials, based on the observations of the laboratory experiments. Current analytical models are inadequate when describing filtration of cohesive soil. Factors such as erosion resistance, physico-chemical forces on cohesive particles, and concentrated leaks through cracks will be considered to produce a complete model of filtration of a crack through a dam core.

Through these four approaches, the thesis will describe many important aspects of granular filter behaviour. The main aim being to produce analytical models of filtration that can be applied in practical situations for the design and analysis of filters.

1.4 Scope of Research and Thesis Structure

The research described in this thesis significantly extends knowledge of granular filter behaviour through a number of approaches:

1. The development of a new analytical model describing the time-dependent transport of non-cohesive base soils into granular filters. The analytical modelling incorporates geometric, hydraulic and physical factors of the protected soil and granular filter in order to produce a detailed model. This model is able to describe the time-dependent changes in flow rate and mass transfer rate, base soil and filter grading, permeability and porosity.
2. Large scale testing of base soil and filter combinations in a new, purpose built, large-scale apparatus. The behaviour of coarse, non-cohesive materials during filtration can be examined in detail with minimum boundary effects due to a large filtration chamber.
3. Development of an analytical model to describe the time-dependent filtration of cracks through cohesive base soils. The complete model will describe cracking of dam cores, the subsequent erosion and transport of fine particles due to flow through the crack, and the filtration of these particles at the filter interface.
4. New laboratory tests developed to examine erosion of cohesive materials due to flow through a hole, and the correlation of this data with standard filtration tests. A new method to predict a safe filter for broadly graded cohesive materials is described.
5. A series of standard No Erosion Filter tests, performed to relate the erosion tests with analytical modelling and examine the current filter design criteria.

The research described in this thesis begins with a critical review of previous literature, presented in Chapter 2. This literature review describes previous work in filtration including both empirical research and analytical methods.

Chapter 3 is dedicated to "Modelling Filtration of Non-cohesive Soils". The theory behind a new model of filtration is described. This chapter is subdivided to describe the development of the model, comparisons with published research and comparison with a new series of large and small-scale laboratory experiments.

Chapter 4 on "Laboratory Study of Erosion and Filtration" describes the laboratory experiments examining erosion and filtration of cohesive soils. These tests were intended to investigate erosion rates and the size of particles eroded from clayey base soils, and to compare these results with filtration tests. Various materials are identified for which suitable filters do not meet current design criteria. The reasons for these variations from the expected behaviour are explained, and a new method to predict safe filters for broadly graded base soils is developed. The observations of these experiments show that the model developed for non-cohesive base soils (Chapter 3) is not sufficient to describe filtration of cohesive base soils.

Chapter 5 describes "Modelling Filtration of Cohesive Materials". In this chapter, a new model is developed to describe the time-dependent changes occurring during filtration of cohesive materials. The model developed in Chapter 3 is extended to consider cracking of the dam core, erosion and transport of particles due to flow through the crack and filtration of these particles if they reach the filter interface. The laboratory observations described in Chapter 4 form an important part of this modelling.

Chapter 6 presents a "Comparison with Empirical Criteria". This chapter compares the predictions of both the model for filtration of non-cohesive base soils developed in Chapter 3, and the crack erosion model developed in Chapter 5, with current filter design guidelines. Recommendations are given on the use of these empirical criteria and the limitations of the modelling and empirical criteria are identified. A new design procedure is described based on this comparison and a newly developed method to examine broadly graded base soils.

In Chapter 7, various practical applications of the modelling work are described using four case studies. Various aspects of the filters in a new dam, currently under construction in Australia, are examined through modelling and laboratory experiments. A dam rehabilitation project is examined to determine the effectiveness of the rehabilitation solution. Existing filters in old embankment dams are studied with the non-cohesive analytical model. In the fourth case study, the published failure of Balderhead Dam in England is examined to describe the reasons for the failure of this dam.

Chapter 8 presents the "Conclusions and Recommendations". This chapter sets out the main research findings and presents a detailed recommended procedure for filter design and some future directions for research in this field.

2. LITERATURE REVIEW

2.1 Introduction

Filters are a very important element of embankment dams, providing protection to the dam core. The core provides an impermeable barrier, limiting seepage flows through the dam. A filter downstream of the core is essential to protect the fine material from being eroded by internal seepage. Sufficient evidence exists to show that concentrated leaks commonly develop in the core of well designed and constructed dams (Sherard and Dunnigan 1985). These leaks are usually attributed to cracking due to differential settlement, earthquake movement, shrinkage or hydraulic fracturing. A suitable filter, downstream of the dam core, is able to retain eroded particles from the core and seal any concentrated leaks.

The design of granular filters is usually based on the particle size distribution of the soil to be protected (the base soil). Terzaghi (1922) was the first to develop granular filter design requirements. He envisaged two requirements that must be fulfilled:

- The filter should be fine enough to prevent erosion of the base soils and arrest piping (ie. the retention requirement). In order to ensure this, Terzaghi (1922) recommended a retention ratio:

  $D_{15F}/d_{85B} \leq 4\text{-}5$

- The filter should be many times more pervious than the base soil to allow the free seepage of water without altering the grain structure of the filter, and without causing excessive head loss (ie. the permeability requirement). To ensure this he recommended a permeability ratio:

  $D_{15F}/d_{15B} \geq 4$

In this thesis, D_{15F} refers to the filter particle diameter for which 15% of particles are finer, and d_{85B} represents the 85% largest base soil particle diameter. The Terzaghi (1922) requirements describe the important and conflicting grain size relations of a suitable filter. The filter must be fine enough to retain the base soil while being coarse enough to drain the seepage flow.

While the design criteria of Terzaghi (1922) are still used for simplified filter design, extensive subsequent research into the behaviour of filters has greatly improved knowledge in this field. The large majority of research has been laboratory based. A series of experiments on sets of base soil - filter combinations has usually led the researcher to recommend an empirical relationship for a stable combination (Sherard and Dunnigan 1985). Laboratory research has led to design criteria that provide simple empirical relations for stable base soil - filter combinations. These criteria are used in most dam filter designs. However, these empirical criteria can only be reliably applied to the range of soils tested, and may have certain laboratory bias due to different testing methods, definitions of failure etc. They neither provide an understanding of the mechanisms involved with base soil - filter interaction, nor the time-dependent properties of the filtration process. Hence, most empirical criteria do not give the designer a confident picture of what may occur within the dam, the long-term effects on filtration and the level of safety involved with design decisions.

With increasing use of computers, many researchers are now concentrating on more advanced numerical analysis of filtration, including the modelling of base soil - filter combinations, with particular focus on particle movement through filters. These approaches recognise the fact that soil masses are made up of a random distribution of

varied particle sizes. These analytical methods provide detailed models of what may be occurring during filtration. They give an idea of the filter thickness required, and can estimate a probability of failure. The assumptions used in developing the model are very important. Often the assumption of spherical particles or a certain particle size distribution curve shape cannot be applied to a real soil. The models may be difficult to apply to real design situations because of their reliance on a number of empirical parameters or impractical mathematical models.

This literature review is a summary and discussion of the findings of past researchers in filter design using the approaches outlined above. Firstly, the review examines some of the factors influencing filtration, and then describes separately both the empirical research and analytical modelling of filter behaviour. The final sub-section introduces the main focus of the current research.

2.2 Factors Influencing Filtration

The three requirements of a filter (retention of particles, sufficient permeability to allow seepage, and no cohesion) place conflicting requirements on the filter particle size. Designing a suitable filter to meet these functions requires knowledge of the factors influencing base soil - filter interaction under seepage flows. The interaction of real granular materials leads to a very complex process of particle migration in a porous medium, with many factors involved in the process. These factors can be broadly termed geometric, physical, hydraulic, chemical and biological as briefly explained below:

- Geometric factors define the shape of grains and the particle size distribution of both filter and base soil, and also the structure of the filter medium (pore constriction size and distribution). In all empirical approaches, the particle size distribution of the base soil and filter is considered by far the most important and hence, often the only factor considered in the laboratory.
- Physical factors may include inter-particle friction and cohesion, particle surface roughness, density or specific gravity etc. The seepage fluid physical characteristics include viscosity, density and temperature effects. Consideration of equilibrium of forces on a loose particle within a filter requires modelling of some of the above physical properties (Indraratna and Vafai, 1997).
- Hydraulic factors include the applied total head, hydraulic gradients of seepage water and the corresponding particle velocities and mass flow rates. Considering hydraulic forces may allow a relaxation in filter design criteria (de Groot et al. 1993).
- Chemical factors that affect particle sizes (dispersion or flocculation) and flow characteristics are associated with both water and soil chemistry. It is well known that

the reservoir water chemistry on limestone terrain has the beneficial effect of increased floc sizes, leading to more economical filter design (Indraratna et al., 1996). Reddi and Bonala (1997) have shown that pore fluid chemistry can influence the capture of clay particles by filters.

- Biological effects generally involve the change in porosity of the filter media due to bacterial and fungal growth.

Because of this large number of parameters and complex interaction between them, it has been necessary to simplify the problem and concentrate only on certain aspects in modelling filter behaviour. Most researchers have considered the soil and filter grain size distribution as the most important parameters (Sherard and Dunnigan 1985). Some have also included a simple model of the hydraulic effects and/or physical properties (Indraratna and Vafai 1997). Hydraulic effects are often ignored because it is conservative to assume that the hydraulic force is sufficiently high to mobilise particles that are not stopped by geometric constraints. However, consideration of hydraulic effects gives a better indication of the true process of filtration (de Groot et al. 1993).

2.3 Empirical Filter Research

Extensive empirical research has been carried out in the past 60 years. This Section describes the basic experimental approach adopted by most researchers, including some recent developments in laboratory methods. The findings of previous researchers are summarised to describe the many factors affecting the filtration process. The factors discussed here include: the effect of hydraulic gradient and flow direction; appropriate grain size ratios to determine design criteria; additional requirements for broadly graded materials; problems with internally unstable soils; alternative criteria relating base soil grain size to permeability; and additional problems with cohesive base soils.

2.3.1 Experimental Approaches

Experiments have typically been conducted using a vertical cylinder, called a permeameter, similar to that shown in Figure 2.1. The cylinder is typically 150 to 300mm long and 100 to 250mm diameter. Sherard et al. (1984) describe a typical method for these standard tests. In summary, the experiment involves vertical flow of water through the base soil and filter. Effluent water is collected to measure flow rates and the amount of base soil in the effluent slurry. Often a range of hydraulic gradients are applied, varying from 0.5 to as high as 50. This has been done to examine the effect of different water pressures and to ensure more severe hydraulic conditions in the test than may exist within a real dam. The apparatus is often vibrated or tapped with a rubber mallet, as this has been shown to break up soil bridges that may form over the filter pores (Section 2.3.3). Most researchers have employed similar experimental methods; however, various researchers have defined criteria for success and failure in the tests slightly differently. Generally accepted failure criteria include:

- visual inspection - the base soil gradually sealing the filter or passing through the filter;

- permeability changes throughout the test;
- measurement of the change of mass of both the soil and filter, which gives a quantitative measurement of the movement of soil particles;
- determination of the grain size distribution difference before and after the test.

A common alternative test method is the slurry test (Sherard et al. 1984b, Indraratna et al. 1996). In this test the filter is compacted in the standard filtration apparatus, then a slurry of the base soil is applied to the filter under high pressure to examine whether individual base soil particles can move through the filter. The filter is successful if the slurry forms a thin skin on the face of the filter, and unsuccessful if the slurry passes through the filter.

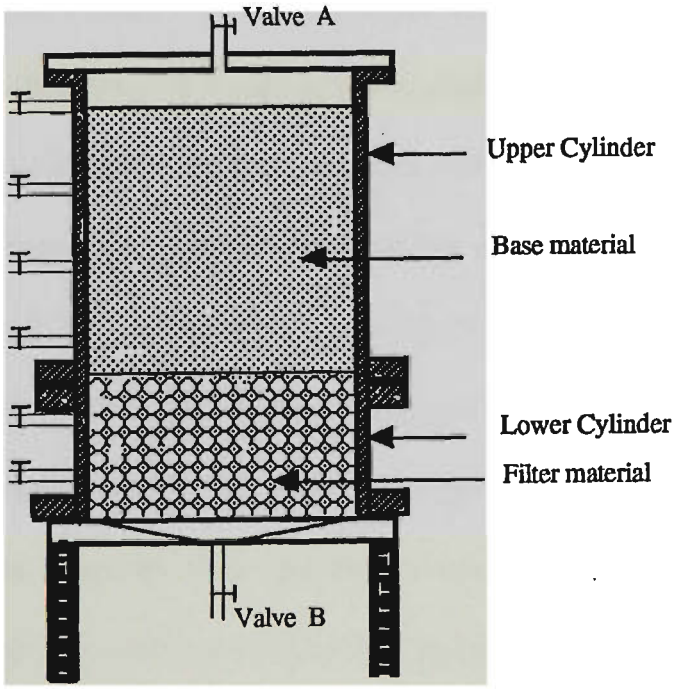

Figure 2.1 Typical Laboratory Apparatus

Several other tests have been developed to identify particular facets of filter behaviour or parameters effecting filtration. Examples include the cack erosion test proposed by Maranha das Neves (1989) and physical examination of the filter pores by filling a filter

material with glue and cutting it into slices (Wittmann, 1979). The findings of these specialist tests will be described in more detail later. The design criteria recommended by some researchers based on empirical research are shown in Table 2.1. While this list is by no means complete, it provides a good summary of the most commonly adopted criteria for dam filter design.

2.3.2 The No Erosion Filter Test (NEF Test)

Sherard and Dunnigan (1985) realised that the standard filter test described above (Section 2.3.1) was not suitable for examining the filtration of fine cohesive soils, particularly when the material is cracked. Noting this problem, Sherard and Dunnigan (1985) proposed the "no-erosion" filter (NEF) test to determine stable base - filter combinations. This test utilised the standard permeameter apparatus (Figure 2.2). The filter material is compacted in the cylinder, and a thin layer of base material compacted on top of it (typically 25mm thick). A hole (1mm in diameter for fine soils and 5-10mm for coarse soils) is formed in the base soil. Then a high water pressure ($4kg/cm^2$) is applied to the system to investigate erosion of the base soil through the filter. The base soil - filter combination is declared successful if no visible erosion of the pinhole through the base soil occurred during a 20 minute test, and a thin layer of fine base particles covered the filter interface, significantly blocking the flow. The boundary filter particle diameter, D_{15Fbdy}, is defined as the largest filter D_{15} size, at which no visible erosion of the pinhole occurs. Filters coarser than this boundary allow some erosion before the filter seals. Sherard and Dunnigan (1989) state that the NEF test is the best test available for evaluating critical filters located downstream of impervious cores in embankment dams. They also mention that the conditions in the test duplicate the most severe conditions that can develop inside a dam from a concentrated

erosive leak through the core discharging into a filter. A detailed procedure for the NEF test, developed during this work is described in Appendix 1.

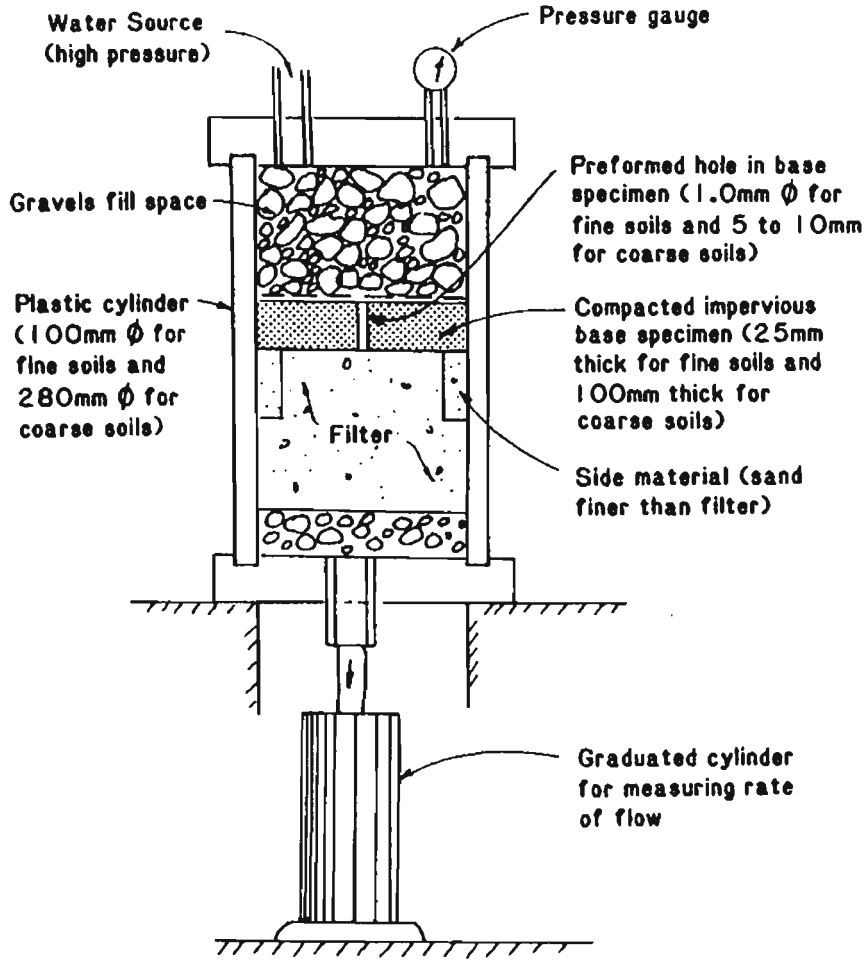

Figure 2.2 NEF Test Apparatus (Sherard and Dunnigan, 1985)

Table 2.1 - Summary of Empirical Filter Design Criteria

Author	Base Material	Filter Criteria	Comments
Terzaghi (1922)	Uniform sand	$D_{15F}/d_{85B} \leq 4\text{-}5$ and $D_{15F}/d_{15B} \geq 4$	Probably based on experience
Karpoff (1955) adopted by US Bureau of Reclamation (1963)	C_u=3-4	$5 < D_{50F}/d_{50B} \leq 10$ (fine sand)	Also required: 100% passing 75mm sieve, <5% passing 75μm sieve, finer section of base and filter should have parallel grading.
	C_u>4	$9 < D_{50F}/d_{50B} < 30$ and $6 < D_{15F}/d_{15B} < 18$ for crushed rock filters or $12 < D_{50F}/d_{50B} < 58$ and $12 < D_{15F}/d_{15B} < 40$ for natural, graded filters	
U.S. Army Corps of Engineers (1971)	uniform base with Cu<6	$D_{15F}/d_{85B} \leq 5$ and $5 < D_{15F}/d_{15B} < 20$ and $D_{50F}/d_{50B} \leq 25$	For medium to high plasticity clays use D_{15F}=0.4mm also require $C_{uf} \leq 20$
Vaughan and Soares (1982)		$k_{filter} < 6.7 \times 10^{-6} \times \delta^{1.52}$ where δ is a representative base particle size (usually d_{85B} or the mean floc size)	δ in μm, k in m/s Filter permeability used rather than particle size
Sherard and Dunnigan (1985)	Fine Silts/Clays (>85% passing 75μm)	$D_{15F}/d_{85B} \leq 9$	% Passing 75μm is based on the base soil fraction finer than 4.76mm. Filters for fine soils (>40% passing 75 μm) also should have <60% coarser than 4.76mm and maximum particle size 50mm
	Silty/Clayey Sands (40-85% passing 75μm)	$D_{15F} \leq 0.7$mm	
	Coarse material (<15% passing 75μm)	$D_{15F}/d_{85B} \leq 4$	
	Intermediate (15-40% < 75μm)	interpolate between previous categories based on % passing 75μm	
Honjo and Veneziano (1989)	Broad grading up to $d_{95B}/d_{75B} \leq 7$	$D_{15F}/d_{85B} \leq 5.5\text{-}0.5\ d_{95B}/d_{75B}$	Based on statistical analysis of compiled previous research.
Indraratna et al. (1996)	Lateritic soil, S.E. Asia	for d_{85} 50 to 60 μm: D_{15F}/d_{85B} <5 to 5.5 for d_{85} 60 to 80 μm: D_{15F}/d_{85B} <4 to 5	Slurry tests on cohesive lateritic soil.

2.3.3 Effect of Hydraulic Gradient and Flow Direction

This Section describes the findings of several experimental programs intended to examine various flow regimes through the base soil – filter combinations. The US Army Corps of

Engineers (USACE, 1971) performed extensive filtration experiments, varying the hydraulic gradient and rate of increase of the hydraulic gradient, to find the following:

- Failure of the base - filter combination usually occurred at a hydraulic gradient below unity. However, at higher gradients, the susceptibility to piping increases when the filter is subjected to vibrations (applied by tapping the apparatus with a rubber mallet);
- The rate of increase of the hydraulic gradient may affect the performance of the filter. A rapid increase in hydraulic gradient has the same effect as vibration. This is attributed to the rapid head increase preventing bridging of base soil grains over filter pores. The bridging phenomenon is shown in Figure 2.3. A number of particles smaller than the pore size, under an applied load such as that applied by seepage forces, can maintain a stable arch over the pore and prevent particle movement. These bridges are destroyed by vibration or rapid changes in hydraulic gradient;
- The downward flow condition is believed to be more critical than upward flow if vibration is applied.

Kenney et al. (1985) noted an increase in the maximum safe ratio D_{15F}/d_{85B} for progressively finer base soil - filter combinations. This occurred because the hydraulic transport conditions in finer filters were inadequate to move the largest possible particles through the pore constrictions. In finer filters, a larger pore velocity is required to obtain the same transport conditions as result in coarser filters. Kenney et al. (1985) defined a hydrodynamic number, R', and found that values of $R' \geq 10$ allow transport through the filter of the largest possible particles:

$$R' = qD_{5F}/n_f\nu \qquad (2.1)$$

Where, q is a unit flux (discharge rate divided by total cross sectional area), n_f is the filter porosity and ν is the kinematic viscosity of the seepage water.

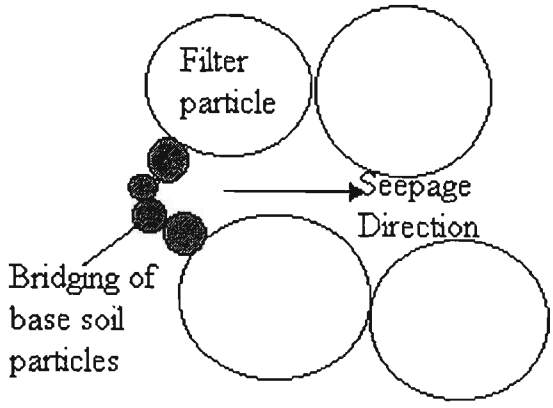

Figure 2.3 Bridging Phenomenon at base soil-filter interface (after USACE, 1971)

2.3.4 Grain Size Ratios

It seems well accepted that base soil - filter stability can be ensured, provided an empirically determined grain size ratio (or combination of ratios) is met, for example $D_{15F}/d_{85B}<5$ or $D_{50F}/d_{50B}<30$. Because so many different grain size ratios have been adopted, a discussion of their application is necessary. The aim of this Section is to determine which grain sizes are representative of the soil and filter for determining filtration stability (eg. d_{50B} or d_{85B}, and D_{15F} or D_{50F}).

Firstly, consider a representative base soil grain size, d_{iB}; where, i represents a percentage of base soil particles finer than d, eg. the 50% or 85% largest particle. Experiments using a wire screen as a filter can study *self-filtration* of the base material. *Self-filtration* is the phenomenon where the coarser base particles are first retained at the filter interface, and these coarse base particles are then able to retain some finer base particles. Continuation of this process results in a stable, self-filtering interface, able to retain even the finest particles. If a wire screen is able to retain a soil containing both particles coarser and finer than the screen opening size, then self-filtration must be occurring. Otherwise the fines

would continually move through the screen. Many researchers using metal sieves as filters have shown that very little particle loss occurs when the filter opening size is less than d_{80B} and that the particle loss is great when the filter opening size is greater than d_{90B} (Vaughan and Soares 1982, Kwang 1990). This implies that the use of d_{85B} to represent the stability of self-filtering base soils is acceptable.

Fischer and Holtz (1996), based on statistical analysis of previous research, suggest the ratio D_{15F}/d_{75B} accurately predicts granular soil retention behaviour, regardless of the coefficient of uniformity of the base and filter soils. However, there is no physical justification for adopting d_{75B} to represent the base soil.

Next consider a representative filter particle size, D_{iF}. Kenney et al. (1985) studied the retention capability of granular filters by examining the controlling constriction size, D_c*, which is the diameter of the largest particle that can pass through the filter material. D_c* can be related to the size of particles in the fine fraction:

$$D_c^*/D_{5F} \leq 0.25$$

$$\text{or } D_c^*/D_{15F} \leq 0.20 \qquad (2.2)$$

Kenney et al. (1985) found that these relations were independent of the filter thickness beyond a thickness of about $200D_{5F}$. Equation (2.2) reinforces the use of D_{15F} as a representative value of the filter size. Witt (1993), through probabilistic analysis of filter void sizes, also found that a single controlling pore size exists and is related to the finer fraction of filter particles.

The mid-size ratio, D_{50F}/d_{50B}, or similar ratios have been proposed by some researchers including the U.S. Army Corps of Engineers (USACE, 1971) and Karpoff (1955). The

combination of this ratio with another (eg. D_{15F}/d_{15B}) was intended to better represent the full gradation curve of well-graded materials. Sherard and Dunnigan (1985), Honjo and Veneziano (1989) and Fischer and Holtz (1996) suggest that this ratio does not correlate to filter performance and should not be used in design. A direct limitation on the coefficient of uniformity, C_u, may be more sensible for broadly graded materials.

The fine size ratio D_{15F}/d_{15B} has been used both to represent filter permeability and retention criteria, eg. U.S. Army Corps of Engineers (1971) suggest:

$$5 < D_{15F}/d_{15B} < 20 \qquad (2.3)$$

Sherard et al. (1984a) suggest that d_{15B} has no significant influence on the retention properties of the needed filter. In many design situations it is necessary to ensure that the permeability of the filter is sufficiently greater than the base soil permeability to drain the soil and prevent a build up of high pore pressures. However, it seems reasonable to adopt a direct permeability relation (eg. filter permeability > 20 times base permeability) rather than an indirect grain size relation to meet the permeability requirement. Hence, the use of d_{15B} is not recommended to represent filter performance.

Honjo and Veneziano (1989) have performed a statistical analysis of extensive data from previous research efforts. The results show that D_{15F}/d_{85B} is the most important parameter in predicting filter performance. Based on this extensive evidence, it seems reasonable to adopt D_{15F} as a representative filter particle size, and Terzaghi's retention ratio D_{15F}/d_{85B} is suitable to represent the stability of a base - filter combination. Recent researchers have concluded that the safe D_{15F}/d_{85B} ratio decreases when applied to broadly graded base soils (Honjo and Veneziano, 1989). This leads to a discussion of broadly graded materials.

2.3.5 Filtration of Broadly Graded Materials

Broadly graded materials, having a wide range of particle sizes, occur often in nature. Broadly graded materials can be considered as having C_u greater than 20, where $C_u=d_{60}/d_{10}$. This section will consider both well graded and broadly graded soils, with a coefficient of uniformity, C_u, greater than 6. Honjo and Veneziano (1989) examined published laboratory data of 287 experiments from 11 references, so that a statistical analysis of filter performance could be made. The statistical analysis determined that, in addition to the retention ratio D_{15F}/d_{85B}, the ratio d_{95B}/d_{75B}, called the *self-healing index*, is a less important but still significant parameter. The self-healing index is related to the capability of the base soil to form a satisfactory self-healing layer. Honjo and Veneziano (1989) proposed a new design rule for cohesionless, well graded and broadly graded soils (Equation 2.4). As can be seen, as the base soil becomes more broadly graded, the safe retention ratio, D_{15F}/d_{85B}, reduces.

$$\frac{D_{15F}}{d_{85B}} \leq 5.5 - 0.5\frac{d_{95B}}{d_{75B}} \quad \text{for } d_{95B}/d_{75B} < 7 \qquad (2.4)$$

There have been a number of incidents involving embankment dams with broadly graded cohesionless tills as the core material. Lafleur (1984) examined these materials to study the self-filtration phenomenon. The base materials ranged in particle size from 2μm to 19mm, with C_u of 8 to 360, containing 15 to 50% fines. An examination of the base soil particle size distribution (PSD) showed that although base particles coarser than 1mm make up as much as 30% by weight of the total particles, they are so few in number that they are floating in a matrix of finer material. Hence, these coarse particles do not influence filtration.

In one test, an unstable filter resulted with the filter retention ratio $D_{15F}/d_{85B}=2.2$. Lafleur (1984) re-calculated this ratio considering only the fraction of base soil finer than 5mm and found the retention ratio nearer to 9, in agreement with experimental data for uniform base soils. Based on this, Lafleur (1984) speculated that self-filtration acts on base particles finer than a representative diameter that fortuitously was the same as that given by the fraction passing 5mm. This representative diameter was likely to be related to the shape of the grain size curve. Coarser particles are not numerous enough to affect self-filtration.

Lafleur et al. (1989) examined filtration of broadly graded cohesionless materials. The work began with the basic assumption that for successful filtration, the allowable opening size of the filter, O_f, must be smaller than some indicative base particle size d_{iB}:

$$O_f < d_{iB} \qquad (2.5)$$

For uniform materials it is accepted that d_{iB} is the d_{85B} diameter. However, Lafleur et al. (1989) showed that a finer indicative particle size is required for broadly graded base soils in order to reduce the extent of erosion before the filter seals and self-filtration occurs. Based on the previous findings of Kenney et al. (1985), the pore opening size can be estimated from $O_f \leq D_{15F}/5$. Using this relation, Lafleur et al. (1989) examined stable base-filter combinations in the laboratory, to examine d_{iB} for various types of material such as broadly graded, gap graded and internally unstable soils. Tests of base and filter combinations show the indicative base particle size, d_{iB}, depends on the type of material used. For materials with linear PSD (on the log scale) and $C_u>20$, d_{iB} is in the range d_{50} - d_{80}. For gap graded materials, d_{iB} corresponds to the d_{85} size of the lower side of the gap, since the coarse particles play no part in filtration. Once the indicative base particle size is found, normal design criteria can be applied, by replacing d_{85B} with d_{iB}. This will be investigated further in Chapter 4, when the *Reduced PSD* is introduced.

Experiments by Lafleur et al. (1989) using wire screens as filters showed that for internally stable base soils, there is some particle rearrangement at the filter as self-filtration occurs. This zone of particle rearrangement was called the self-filtration zone. This zone is small for well graded soils (having $6<C_u<20$), but is quite extensive for broadly graded soils, with $C_u>20$. This is because there are fewer large particles in the broadly graded material to initiate self-filtration, and also a larger range of particles must be captured. Hence, more fines are lost before the interface stabilises, and broadly graded base soils will lose a large volume of fines before successful filtration is established. This is why a finer indicative base soil size must be adopted to reduce erosion during filtration of broadly graded soils.

Broadly graded filter materials also deserve discussion. These materials are attractive to designers because they are able to retain fine base soils (a property controlled by the fine filter fraction, D_{15F} or smaller), while still having coarse particles that can be easily retained by the downstream fill of an embankment dam. This often means that a single filter can be used, rather than multi-stage filters. Often broadly graded material is significantly cheaper to manufacture than a uniform material, or may be available in local natural deposits. However, broadly graded filters do have their drawbacks (ICOLD 1994). Segregation during placement is a major concern because the fine fraction of the filter material is relied upon for base soil retention. If the fine fraction is not present due to segregation, then piping can occur. In addition, a single layer of a broadly graded filter material will usually have a lower permeability than the overall permeability of a multi-stage filter. Hence, the filter may not provide the necessary drainage properties. Clogging of broadly graded filters is also more likely, leading to high pore pressures in the dam core. To reduce the risk of segregation or clogging within critical filters in embankment dams, the US Soil

Conservation Service recommends $C_u<6$ for the coarse and fine sides of the filter band (this is the band between the maximum and minimum gradings in the design specification). In addition, the ratio of maximum and minimum allowable particle diameters (the width of the filter band) should be limited to 5, for the fraction finer than D_{60F} (ICOLD, 1994).

2.3.6 Internally Unstable Soils

Internal instability means that the coarse particles of a broadly graded material form a skeleton that takes all of the external stress within the soil. Some fine particles are not part of this soil structure, and are not restrained by the external stresses. These particles, under the influence of seepage or vibration forces, can move through the skeleton of coarser particles, causing internal erosion. This process is often called suffusion. Filter design criteria relying on the coarse fraction of the base soil (e.g. D_{15F}/d_{85B}) are not suitable for internally unstable soils since extensive mass loss may occur even when the coarse fraction of the base soil is retained. Internally unstable soils generally have a concave upwards grading curve or are gap graded. Lafleur et al. (1989) showed that internally unstable soils which are successfully retained by a filter (ie. the filter is fine enough to retain the loose fine base particles) may "self clog". This is a process where fine particles are washed out through the base material and accumulate at the filter interface, producing a layer of low permeability and increased pore pressures at the interface.

Kenney and Lau (1985) investigated the internal stability of soils. They suggest that for a material to be internally unstable, three conditions are necessary:

- The compacted granular material must possess a primary fabric of coarse particles which support the imposed loads;

- Within the pores of the primary fabric, there must be loose particles which can be moved by forces such as water flow;
- The size of constrictions in the pore network formed by coarse particles, must be larger than some of the loose particles.

These conditions require that there is a deficiency in number of particles of a certain mid-size range, such that not all pore constrictions of a smaller size can be blocked. This requires a gently inclined particle size distribution (wide range of particles) or gap grading in the lower part of the grading curve. Kenney and Lau (1985) describe a method based on the particle size distribution (PSD) to determine the internal stability of a soil. However, they suggest that the best method to determine internal stability is to perform a hydraulic test in a permeameter. For internally unstable soils, the filter could be designed to retain the fraction of fine base particles that are stable, using normal design criteria. However, the problem of "self clogging" must still be considered.

Kwang (1990) performed experimental research on gap-graded materials, having a distinct gap in the particle size distribution. Kwang (1990) showed that instability of gap-graded materials occurs when the diameter ratio of the gap range (the ratio of the minimum diameter of the upper end of the gap to the maximum diameter of the lower end of the gap) is greater than four. This simple relation can be used to determine the internal stability of gap-graded materials.

2.3.7 Particle Size - Permeability Relations

Vaughan and Soares (1982) suggested an alternative method for designing filters for non-cohesive soils based on a base soil size - filter permeability relationship, as shown in Figure 2.4. Since the permeability of a filter intrinsically reflects the porosity and

differences in grading and grain shape, this relation should take into account all of these factors. Vaughan and Soares (1982) suggest a design rule:

$$k = 6.7 \times 10^{-6} \times \delta^{1.52} \quad \text{k in m/s and } \delta \text{ in } \mu\text{m} \qquad (2.6)$$

In the above equation, δ represents the soil particle size to be retained. For an internally stable, non-cohesive base material, δ should be taken as d_{85B}. For cohesive base soils, Vaughan and Soares (1982) suggest that the filter should be designed to retain the mean size of the clay flocs, as will be discussed shortly.

Indraratna et al. (1996) developed an alternative particle size – permeability relationship for filtration of cohesive, lateritic soils, based on the observation of slurry tests. This relationship is based on the d_{85B} size of the base soil:

$$k_f = 6.3 \times 10^{-4} \times (d_{85B})^{1.25} \quad d_{85} \text{ in mm, k in cm/s} \qquad (2.7)$$

Indraratna et al. (1996) showed that a relationship exists between the permeability and the size of fine soil particles for non-cohesive soils given by;

$$k = 0.96(D_{5F} D_{10F})^{0.92} \quad D_{5,10} \text{ in mm, k in cm/s} \qquad (2.8)$$

where, D_{5F} and D_{10F} are in mm, and k in cm/s. Since permeability can be related to the fine particle sizes of the filter material and it has been shown that the fine filter particles are responsible for filtration, the relationship suggested by Vaughan and Soares (1982), between filter permeability and the base soil size, sounds a plausible design criteria. Indraratna et al. (1990) compared their experimental results examining the effect of filter permeability on the filtration of lateritic clay with those of Vaughan and Soares (1982) finding similar results (Figure 2.4). These observations suggest that a base soil particle size – filter permeability relationship is adequate for the design of granular filters. However, there are practical problems with determining the in-place filter permeability during dam construction as the permeability may change appreciably with small fluctuations in the

fines content and extent of compaction. The standard filter grain size ratios are generally easier to control during dam construction.

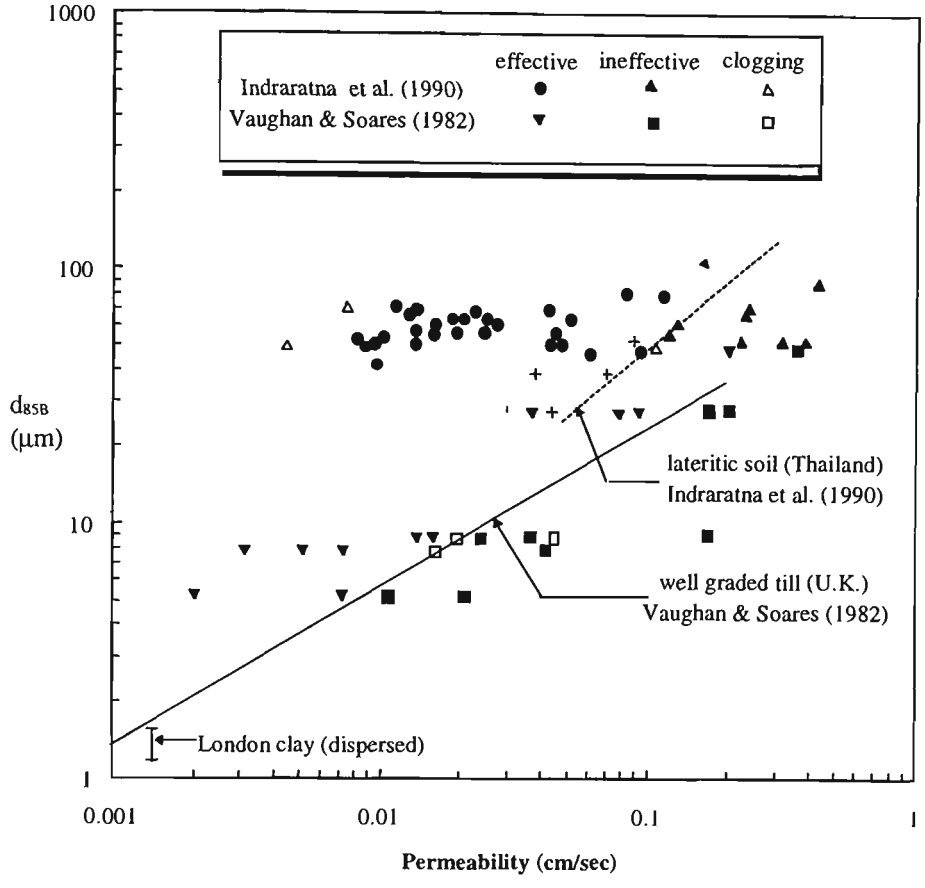

Figure 2.4 Base Particle Size vs Filter Permeability Relationship (Indraratna et al. 1996)

2.4 Filtration of Cohesive Base Materials

Most dam cores are made of cohesive materials such as sandy or silty clays. This is because the core must be sufficiently impermeable to prevent the loss of water from the reservoir. However, the majority of design criteria described so far have been developed using non-cohesive base materials. Many designers have applied design principles developed for non-cohesive base materials to cohesive bases, assuming that they will be conservative since the cohesion of the base soil will reduce erosion rates. However, Vaughan (2000) suggested that observations of dam failures showed that the rules for non-cohesive soils were invalid for two reasons. First, the cohesive forces in the clay did not prevent filter failure, rather they had allowed cracks to stay open and stable while their walls were eroded by the small flow of water. Second, segregation had invalidated reliance on self-filtering to prevent loss of material. Self-filtering is explicitly assumed in the design criteria for non-cohesive soils.

Some early attempts were made to examine the effect of erosion resistance in filtration of cohesive soils, which is the ability of a cohesive material to resist erosion due to shear forces induced by water flowing over the surface of the material. Wolski (1970) examined erosion of silty clay at a filter interface by measuring changes in porosity and pore pressures, and through x-ray examination of samples during seepage. The findings of these tests were that two stages of erosion occur. The first stage, at relatively low hydraulic gradient, involves removal of base particles at the filter interface, until arching of several small particles over the filter pores stops erosion. The thickness of the erosion zone was observed to be half the pore diameter in the filter material. Then, at higher hydraulic gradients, the arches break down and further erosion occurs through progressive particle loss and the formation of piping failure. This suggests that for intact cohesive materials,

filters will most likely be conservative if designed using the design criteria developed for cohesionless soils. However, there are two particular problems associated with cohesive base materials: cracking and dispersive clays, as described below.

2.4.1 Concentrated Leaks through Cracks

Sherard and Dunningan (1985) state that "... hydraulic fracturing is much more common than was previously considered likely. Concentrated leaks occur in most embankment dams of all types and sizes without being observed. This is somewhat surprising; however, the evidence available for this conclusion is now so strong that it must be accepted." Hydraulic fracturing is made possible by differential settlements and internal stress transfer. This occurs even in dams without unusual settlement. This is supported by observation of wet seams and concentrated leaks observed in many dams and also finite element computations which show that only relatively small settlements are needed to create zones of low total stress in the dam capable of allowing hydraulic fracture. After a crack develops, erosion of the crack by high velocity flow may occur as shown in Figure 2.5. Eroded particles may be transported to the filter interface. If the filter is fine enough, these particles are captured at the filter interface and form a skin over the filter. This low permeability skin or *filter cake* reduces the flow rate through the crack and prevents further erosion. If the filter is too coarse, eroded particles will pass through the filter and the crack may enlarge as erosion continues.

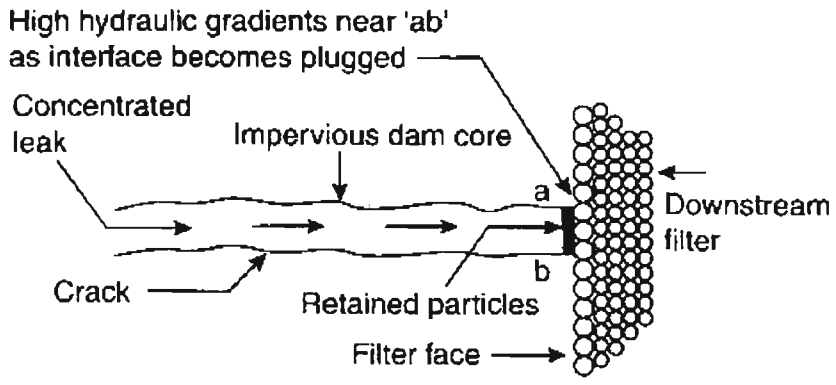

Figure 2.5 Concentrated Leak Through a Crack in a Cohesive Core (after Sherard et al. 1984b).

2.4.1.1 Development of a Crack

Many factors may contribute to cracking in embankment dams; some possible causes of cracking include differential settlement of embankment materials, foundation movement, shrinkage, earthquake-induced movement, slope instability and hydraulic fracturing. Hydraulic fracturing has been identified as a major cause of cracks in embankment dams. In a zoned embankment dam, any differential settlement of the more compressible clay relative to the stiffer filter and embankment shell zones will result in a transfer of stress onto the stiffer zones and a reduction in the stresses within the core. If the reservoir pressure is greater than the minor principal stress at some point in the core, then hydraulic fracture can occur. Kulhawy and Gurtowski (1976) have used finite element procedures to demonstrate that load transfer can reduce the minimum principal stresses to significantly lower than the total hydrostatic water pressure. Other causes of stress transfer can include abrupt changes in foundation profile, rigid structures such as conduits, or variations in materials, density and moisture content etc. Lo and Kaniaru (1990) presented detailed modelling and laboratory testing of hydraulic fracturing. They indicated that the hydraulic fracturing pressure can be estimated based on the minimum principal stress, ie. hydraulic fracture can occur when:

$$\gamma_w h_w \geq T + \sigma'_{min} + p_0 \qquad (2.9)$$

Where, $\gamma_w h_w$ is the hydrostatic water pressure, T is the tensile strength of the core material, σ'_{min} is the minimum effective stress in the core and p_0 is the pore pressure in the core. If the hydrostatic water pressure is sufficiently high then a crack can be opened within the clay core, resulting in water infiltrating the crack and 'jacking' it open. This may result in the crack continuing through the dam core, if the insitu stress conditions allow. The hydraulic fracture process requires some initial discontinuity or hairline crack to exist in the upstream face of the dam core, so that water can infiltrate the core and enlarge the crack. It is most likely that such discontinuities will exist in all cohesive cores due to construction drying cracks, narrow zones of permeable material, or areas of soil compacted against rock joints, rigid structures etc. Sherard (1986) concludes that this hydraulic fracturing process can occur in all types of embankment dams, from low homogeneous dams to high central core dams.

Indraratna et al. (1996) examined the cracking potential of lateritic soils, by examining the tensile behaviour of the soil in Brazilian tests at varying moisture content. The tensile strain was measured normal to the vertical diameter, and the tensile strain at failure recorded. The tensile strain ratio was defined as percentage difference in the tensile strain at cracking at any moisture content, compared with the tensile strain at cracking at standard Proctor optimum moisture content (OMC). The tensile strain ratio is plotted against moisture content in Figure 2.6. As the moisture content is reduced to below OMC, the risk of tensile cracking becomes pronounced as shown by the rapidly decreasing tensile strain ratio. Conversely, the ability to resist tensile cracking increases at greater than optimum moisture contents. As shown in Figure 2.6, increased compaction (from standard Proctor to modified compaction) increases the risk of tensile

cracking at the same moisture content. Penman and Charles (1981) showed that drier, more rigid cores will settle less but have a greater difference between major, intermediate and minor principal stresses in early life, leading to cracking at lower hydrostatic pressures.

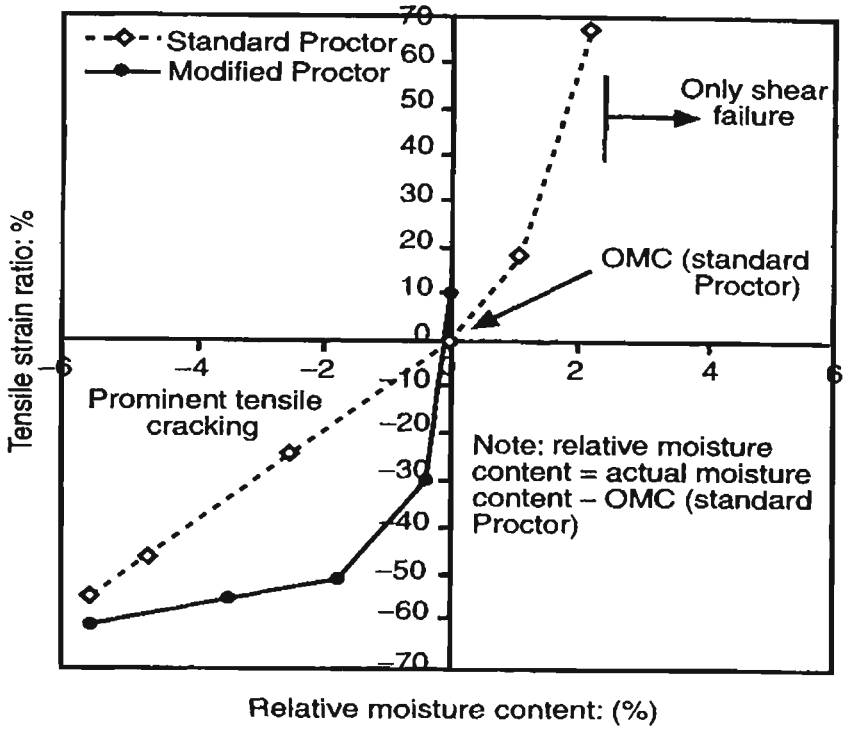

Figure 2.6 Tensile Behaviour of Compacted Soil at Varying Moisture Content

The prediction of internal stresses within an embankment dam is difficult. These stresses depend on the levels of stress relief and load transfer, dissipation of pore pressures etc. The location of potential cracks is also difficult to predict. This again depends on the internal stresses, reservoir level, localised variations in materials and their density, and construction processes. The thickness of a crack depends on a complex function of many variables such as the local stress and pore pressure conditions, hydrostatic pressure, material properties, swelling and slaking of the material. The most important variable influencing the crack thickness is the pressure of the water entering the crack. Cavity

expansion theory could be used to predict the size of a crack if the internal stresses and external hydrostatic water pressure were known (Carter et al. 1986). However, the great number of uncertainties makes any mathematical formulation unreliable. For low dams, the crack thickness is probably only fractions of a millimetre, whereas for high dams, cracks of several centimetres may develop. Sherard (1986) suggests that an excess hydrostatic water pressure of 10-20m of water could result in development of a crack up to 5-10cm thick.

Foster (1999) examined reports of cracking in many embankment dams, and concluded that in most cases the crack occurred at depths from the crest of less than or equal to about 30m. The depth of cracking appears to be related to the source of the low stress condition:

- Cracks associated with small scale irregularities in the rock foundation profile generally occur close to the bedrock surface and usually in the lower half of the dam height.
- Cracks associated with narrow cores and arching of the core between the shell zones are generally located at depths from the crest of 1/3 to 2/3 of the height of the dam.
- Cracks and piping associated with broad changes in the abutment profile are generally located within the upper 1/3 of the height of the dam. This is where tensile stresses might be expected to occur due to large-scale changes in abutment slope.
- Earthquake induced cracking is usually assumed to induce cracks in the upper 1/3 of the dam, however, foundation movement may lead to cracking in the lower sections of the dam.

2.4.2 Filtration of Concentrated Leaks through Cracks

Vaughan and Soares (1982) found that cracks up to a certain size and shape in a cohesive material remained stable even when they were flooded. They suggested that, at low flow velocities, slow erosion of these cracks may be accompanied by segregation of the eroded debris within the crack, this segregation may result in only fine particles reaching the filter. In the absence of coarse base soil particles, a self-filtering layer cannot form and the finer particles are continually lost and the crack enlarges, leading to possible piping failure. Based on this, Vaughan and Soares (1982) defined a "perfect filter" to protect a cracked, cohesive base material. The perfect filter will retain the smallest particles that can arise during erosion, even if they arrive at the filter interface after complete segregation, unaccompanied by larger particles that would allow self-filtering to occur. These smallest particles are the clay flocs that form when the base material is dispersed in the reservoir water. The perfect filter concept is a conservative approach, intended to provide a filter that cannot allow particles to erode.

Vaughan and Soares (1982) performed a detailed study on floc sizes. It was shown that the average floc size is dependent on both the material properties and water chemistry. As shown in Figure 2.7, flocs increase in size with increasing water ion content, but reach a maximum size beyond which a further increase in ion content has no effect. Either traditional empirical design rules or the particle size - filter permeability relationship (Section 2.3.7) can be used to determine the filter size required to retain these clay flocs.

A number of authors have discussed the "perfect filter" concept, and most believe that the concept is unduly conservative and that some degree of self-filtering can be relied upon (Ripley 1982). A criticism is that some filters designed in this way will be so fine that they

will possess some cohesion, which is unacceptable as cracks can propagate through the filter. Sherard (1982) in his discussion of the perfect filter concept states:

- Laboratory tests give confidence that clean sand (or gravelly sand) with D_{15F} size of 0.5mm will conservatively seal concentrated leaks in fine-grained cores.
- Because of the silt sized particles (30-70 microns) that comprise a substantial portion of all fine-grained clayey soils and which must be available to seal concentrated leaks, it is not necessary to provide a "perfect filter" to catch flocs of 10-20 microns diameter.

It is generally agreed in subsequent literature that the "perfect filter" is conservative. There is much evidence suggesting that clay cores are adequately protected by well constructed filters containing fine sand and that self-filtering can occur (Sherard et al. 1984b).

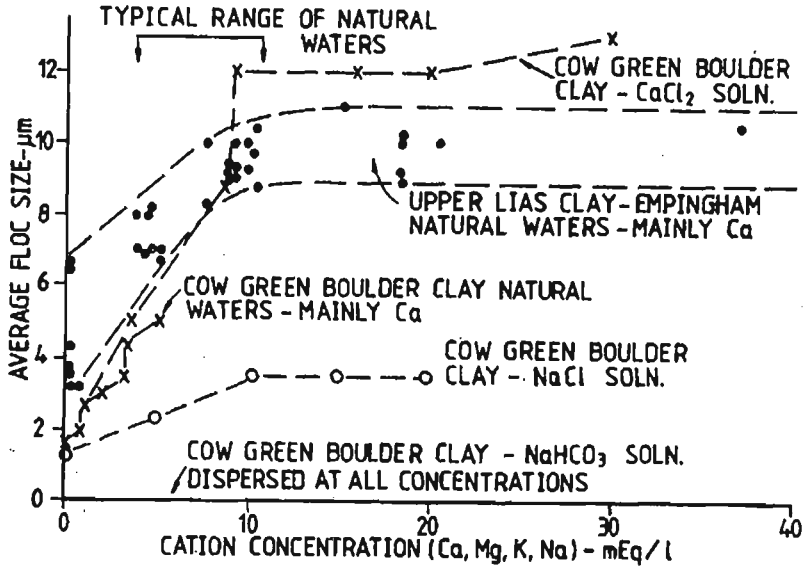

Figure 2.7 Variation of Floc Size with Water Chemistry (after Vaughan and Soares, 1982)

The 'critical filter concept' devised by Sherard and Dunnigan (1985), adopting the no-erosion filter (NEF) test, was proposed as an alternative approach to the design of filters to seal cracks in cohesive materials This is a conservative test of filters to seal concentrated

leaks through cohesive soils; the test was described in detail in Section 2.3.2. The empirical design criteria of Sherard and Dunnigan (1985), presented in Table 2.1, are based on the NEF test. These design criteria, in most cases, allow a coarser filter than that required by the perfect filter concept. Vaughan (2000) criticises the use of the NEF test, suggesting that the test fails to reproduce the features of crack behaviour in two ways. First, it is conducted in a rigid cylinder. If pieces of clay are washed onto the filter, the filter face can seal. Being rigidly constrained, the filter and the walls of the crack can resist the hydraulic pressure applied, and the filter is defined as a success. In a dam core, a crack can be sustained and re-opened by hydraulic pressure, if this pressure is larger than the total stress. The mechanism in the test is strain controlled, whereas the mechanism in the field is stress controlled. The second point raised by Vaughan (2000), is that the segregation or eroded debris and migration of only fine particles is specifically avoided in the NEF test. Sherard and Dunnigan (1985) performed NEF tests at very high hydraulic gradients in vertical apparatus. These tests show the suitability of the filter to retain particles eroded by high velocities, but do not examine this possible segregation at low velocities. Thus, the NEF test cannot predict field behaviour if segregation of debris is possible.

To examine these low flow velocities, Maranha das Neves (1989) developed a 'crack erosion test', where water flows at varying velocity over the flat surface of a soil sample and then through a filter, to examine the behaviour of the simulated crack and filter. Important observations include:

- There was no visible segregation during transport of the eroded material, ie. all the eroded material is transported and there is no preferential movement of fines.
- When erosion occurs, low flow velocities (2cm/s) are sufficient to transport sand sized particles to the filter surface, thus enabling self-filtration to occur at the filter interface.

- Before self-filtering is established, even the most conservative filters were unable to retain the fine particles.

Based on these observations, Maranha das Neves (1989) stated that segregation at low flow velocity is not a problem in filter design. This suggests that the NEF test is suitable for determining successful filters for cohesive materials, and the Sherard and Dunnigan (1985) criteria can be adopted for the design of filters for most cohesive base soils.

The design criteria of Sherard and Dunnigan (1985) have been shown to have limitations, particularly when applied to broadly graded and gap graded cohesive materials. Khor and Woo (1989) performed a number of NEF tests on sandy clays. They believe that particles coarser than fine sand cannot be relied upon to help seal the filter, and that it is necessary to provide a protective filter that will retain the fines but not necessarily the clay floc-size particles. They recommend the use of a new parameter, d_{85B}^*, which is the 85% largest size of the base soil fraction passing 75μm. Filters must satisfy the relation:

$$D_{15F}/d_{85B}^* \leq 12 \qquad (2.10)$$

Indraratna et al. (1996) examined the filter requirements for a cohesive, lateritic soil, a typical residual soil of Thailand and other parts of South East Asia. This material lacks much of the silt-size particle fraction usually present in other natural soils. The experiments involved forcing a slurry of base material into the filter under high pressure, to examine the retention of clay flocs. Based on these tests, Indraratna et al. (1996) showed that the following particle size ratios are appropriate for this material:

$$\text{For } d_{85} = 50 \text{ to } 60\ \mu\text{m}: \quad D_{15F}/d_{85B} < 5 \text{ to } 5.5$$
$$\text{For } d_{85} = 60 \text{ to } 80\ \mu\text{m}: \quad D_{15F}/d_{85B} < 4 \text{ to } 5 \qquad (2.11)$$

The retention ratios of Equations (2.11) for filtration of a lateritic soil are considerably lower than those proposed by Sherard and Dunnigan (1985), for fine soils ($D_{15F}/d_{85B} \leq 9$). This is most likely because the lateritic soil is gap graded and potentially internally unstable, lacking the silt size fraction. These lower safe ratios suggest that the current filter criteria for cohesive fine soils may not be universally applicable and testing of proposed combinations is usually necessary. The current practice of using concrete sand as a filter material to protect fine-grained soils reflects the general indistinctness in determining correct filter materials to protect cohesive soils, for example the Sherard and Dunnigan (1985) requirement, $D_{15F} < 0.7$mm, for sandy silts and clays. This issue requires further investigation and forms an important part of this thesis.

2.4.3 Erosion of Cohesive Materials

Different cohesive materials have greatly varying resistance to erosion, from dispersive soils to materials that are not eroded by high velocity water flow. Erosion resistance may significantly affect filtration. In order to understand the erosion process in cohesive soils it is advantageous to look at the physico-chemical forces acting within cohesive materials. These forces lead to significant variations in the physical behaviour and erosion resistance of soils. This discussion will look first at the least erosion resistant materials - dispersive clays. These clays tend to disperse into solution in the presence of water, leading to rapid erosion. The discussion then investigates the erosion resistance of cohesive materials.

2.4.3.1 Chemistry of Clay Dispersion

Soil dispersion is related to the clay mineralogy and pore water chemistry. Rallings (1966) examined dispersive soils through literature studies and experimentation, his findings are summarised here. We will consider three common clay types: montmorillonite, kaolinite and illite. Each has a different internal structure, which leads to different physical properties. For the purposes of this explanation, clay particles can be considered as plate-like particles with an overall negative charge. These negatively charged particles attract cations (positively charged ions) to attain electrical neutrality. The cations form a cloud (double layer) around the clay plates. The cations normally attracted comprise calcium, magnesium and sodium. These cations are called exchangeable cations, because they can be replaced by ions in the pore water. The term cation exchange capacity (CEC) is used to describe the ability of clay to adsorb and exchange cations. Table 2.2 shows the usual range of CEC for the three major clay types. Montmorillonite has a significantly larger cation cloud that kaolinite due to its higher CEC.

Table 2.2 Cation Exchange Capacity of Clay Minerals

Clay Mineral	CEC (milliequivalents / 100g)
Kaolinite	3-15
Illite	10-40
Montmorillonite	80-150

Clay dispersion is related to the charge on the adsorbed cations. Sodium ions, Na^{+}, are monovalent, whereas Calcium and Magnesium ions, Ca^{2+} and Mg^{2+}, are divalent. This means that twice as many sodium ions are required to balance the charge of the clay particle. Because there is very little difference in the size of the ions, the cation cloud (double layer) between clay particles must be thicker for monovalent Na^{+} ions, to

accommodate the extra cations. When two clay particles approach one another, there are two opposing sets of forces acting;

- Repulsive electrostatic forces due to the interaction of the two positively charged diffuse double layers (cation clouds), and
- Attractive Van der Waals forces that act between the clay surfaces.

The variation of potential energy between clay colloids with interparticle spacing is shown in Figure 2.8. As the cation cloud will be thicker for Na^+ ions (ie. greater intermolecular spacing), the net potential energy may reach the unstable repulsion zone and dispersion may occur.

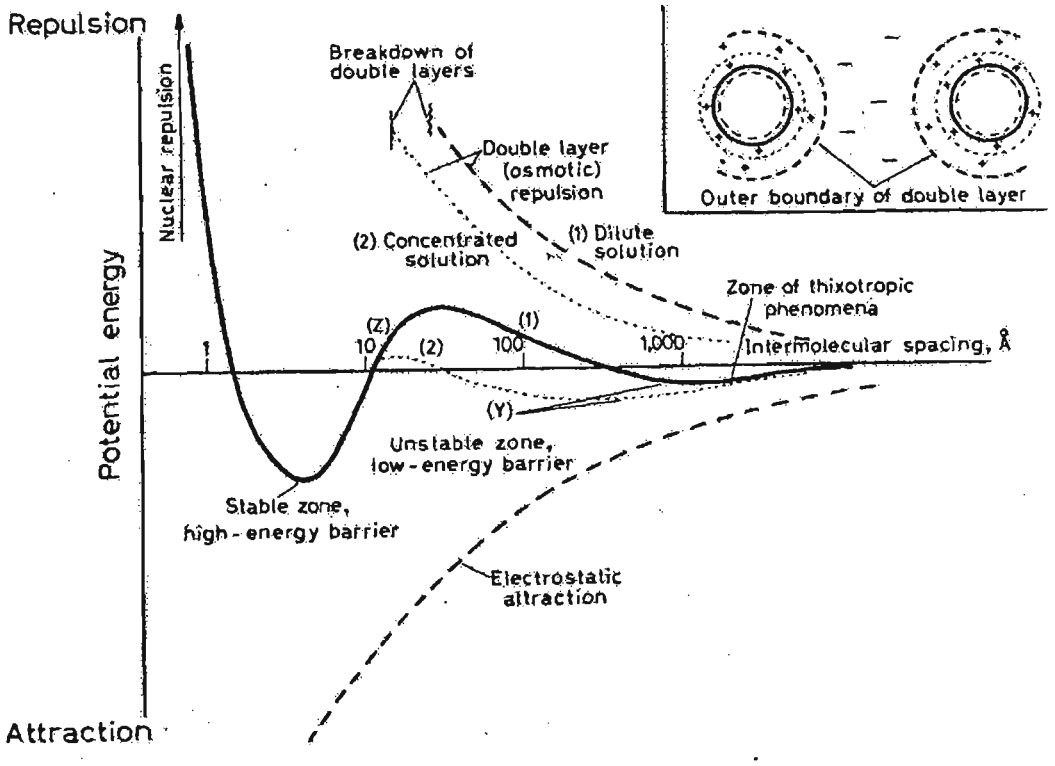

Figure 2.8 Potential energy curves for molecular and colloidal particle interaction (Lee 1968)

The ion content of the pore water also influences dispersion. In the presence of concentrated ionic solutions, the ion clouds on the clay crystals contract, the repulsive

forces at a given distance are reduced, and with them the barrier to flocculation. Conversely, relatively pure waters will tend to encourage dispersion.

A number of soil and pore water properties have been proposed to predict dispersion. Heinzen and Arulanandan (1977) suggest that while there are many complex factors leading to dispersion, the sodium adsorption ratio (SAR) of the pore water and the ion concentration of the eroding water are significant indicators.

$$SAR = \frac{Na^{+}}{\sqrt{Ca^{2+} + Mg^{2+}}} \qquad (2.12)$$

Sherard et al. (1976a) proposed the pinhole test to identify dispersive materials, where water is passed through a 1mm pinhole. If the sample erodes under a very low water head then it is dispersive. Sherard et al. (1976b) used the pinhole test and the SCS dispersion test to examine dispersion, and proposed a figure grouping soils into highly likely to disperse, unlikely to disperse and intermediate Figure 2.9). The graph relates the percent sodium to the total dissolved salts in the pore water extracted from a sample of the clay.

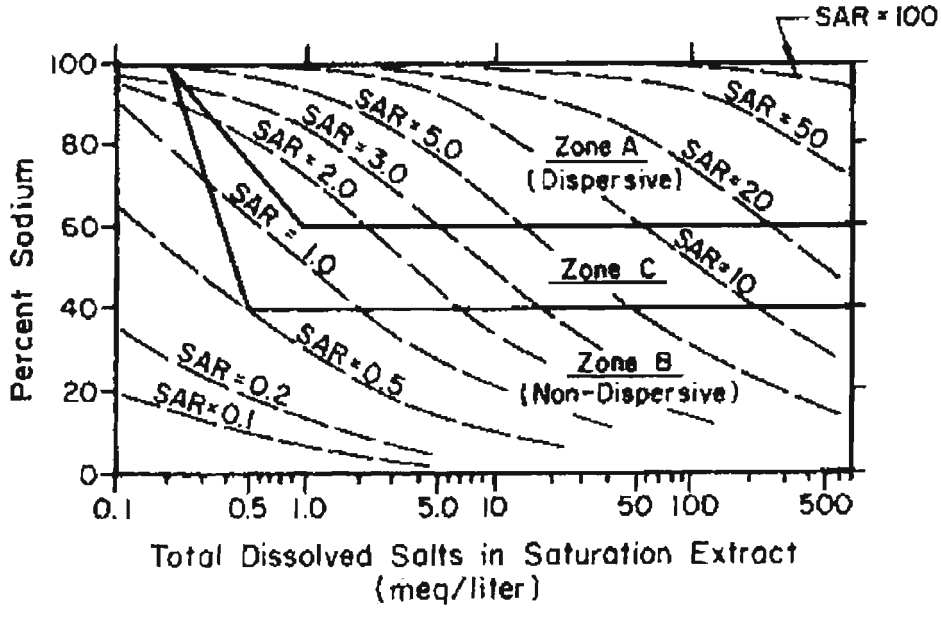

Figure 2.9 Likelihood of soil dispersion (Sherard et al. 1976b)

2.4.3.2 Dams with Dispersive Materials

Rallings (1966), in research on homogeneous earth dam failures in Queensland, Australia, showed that 25 of the 26 failures involved dams with dispersive materials. A large homogeneous dam should not be constructed of dispersive material. Sherard and Dekker (1977), after extensive research on dispersive materials, determined that:

- Filters with some fine sand sizes will generally control piping through dispersive clay.
- It is reasonable practice to build major embankment dams with cores of dispersive clay with appropriate design details.
- Existing dams of dispersive clay that have given no trouble are not usually considered unsatisfactory structures.
- Piping of dispersive clay in dam foundations is believed generally unlikely below the depth where the clay is continuously saturated in nature.

Sherard and Dunnigan (1985) stated that in the "No Erosion" filter test there is no difference between suitable filters for dispersive and erosion resistant materials. This may be due to the very high hydraulic gradient applied in these tests. Sherard and Dunnigan (1985) tested only two dispersive clays in coming to this conclusion. Foster and Fell (1999) performed further NEF tests on some dispersive clays and found the safe filter was slightly finer than that predicted by the Sherard and Dunnigan (1985) guidelines. The previous discussion of segregation due to low flow velocity through cracks is even more important for dispersive soils. If the fines of a dispersive clay core can be carried through the filter in suspension, then extensive mass loss can occur with no movement of larger particles to initiate self-filtration. This issue in filter design has not been satisfactorily resolved, and will be studied further in this research.

2.4.3.3 Erosion Resistance of Cohesive Material

Cohesive materials often present significant resistance to erosion. The effects of clay mineralogy, ion content and eroding fluid ion content, discussed previously in the context of dispersive clays, apply to the general erosion resistance of a cohesive material. Hence, erosion resistance can be related to the total dissolved salts and SAR of the material. Arulanandan et al. (1975) performed extensive tests on the erosion rates of clays in a rotating cylinder apparatus. They showed that a relation that has often been used in soil science could describe the erosion rate (E):

$$E = \alpha(\tau - \tau_c) \text{ g/m}^2\text{s} \qquad (2.13)$$

Where, α is an erosion rate parameter (g/Ns), τ is the applied shear stres (N/m^2) and τ_c is a critical shear stress below which no erosion will occur. This is shown in Figure 2.10.

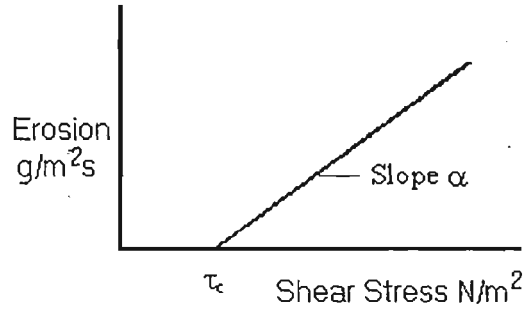

Figure 2.10 Erosion Rate vs Shear Stress (Arulanandan et al. 1975)

Arulanandan et al. (1980) presented the results of further rotating cylinder tests and flume tests, where samples of the soil are placed flush with the base of a flume and eroding water flows over the samples. The following characteristics were found to be important to the erodability of cohesive soils:

- Amount and type of clay fraction,
- Chemical composition of the pore fluid (dissolved cations) and of the eroding fluid
- Grains size distribution of the non-cohesive portion,
- Soil pH, temperature and water content,

Arulanandan et al. (1980) observed that erosion of cohesive soil is essentially a surface phenomenon. This explains why bulk engineering properties of soils, such as vane shear strength, unconfined compressive strength and dry unit weight have not proved useful as erosion predictors. Figure 2.11 shows a predictive chart developed by Arulanandan et al. (1980) to predict the critical shear stress, τ_c, from the soil SAR, dielectric dispersion and total salt concentration. Figure 2.12 shows the variation of the erosion rate parameter (α) with τ_c for remoulded soil samples.

Arulanandan and Perry (1983) considered the erosion resistance of cohesive core materials in embankment dams, particularly dams that have experienced piping failures. Based on measured properties of the failed material, the predicted erosion resistance or critical shear stress, τ_c, of these soils was very low (below 4 dynes/cm^2). Arulanandan and Perry (1983) suggest the following erosion categories for dam cores:

- Erodable soils with $\tau_c < 4$ dynes/cm^2. Core materials in this category warrant extensive, detailed filtration tests of the proposed filter material.
- Moderately erodable fines with 4 dynes/cm^2 $< \tau_c < 9$ dynes/cm^2. Core materials in this category also warrant filtration testing of the proposed filter material.
- Erosion resistant soils with $\tau_c > 9$ dynes/cm^2. For core materials in this category filter gradation can be determined based on simple filter design criteria.

Khilar et al. (1985) examined the erosion rate parameter, α, and discovered a large variation in the parameter, depending on the test method. The parameterα determined by a flume test was up to two orders of magnitude higher than that determined for the same material using a flow through slot test, and potentially five orders of magnitude higher

than for erosion due to flow through the pores of the material. This difference from one flow test to another was attributed to differences in the concentration of particles in the eroding fluid. Hence, in the case of erosion of a cracked dam core, the erosion rate will vary depending on the concentration of particles suspended in the eroding water.

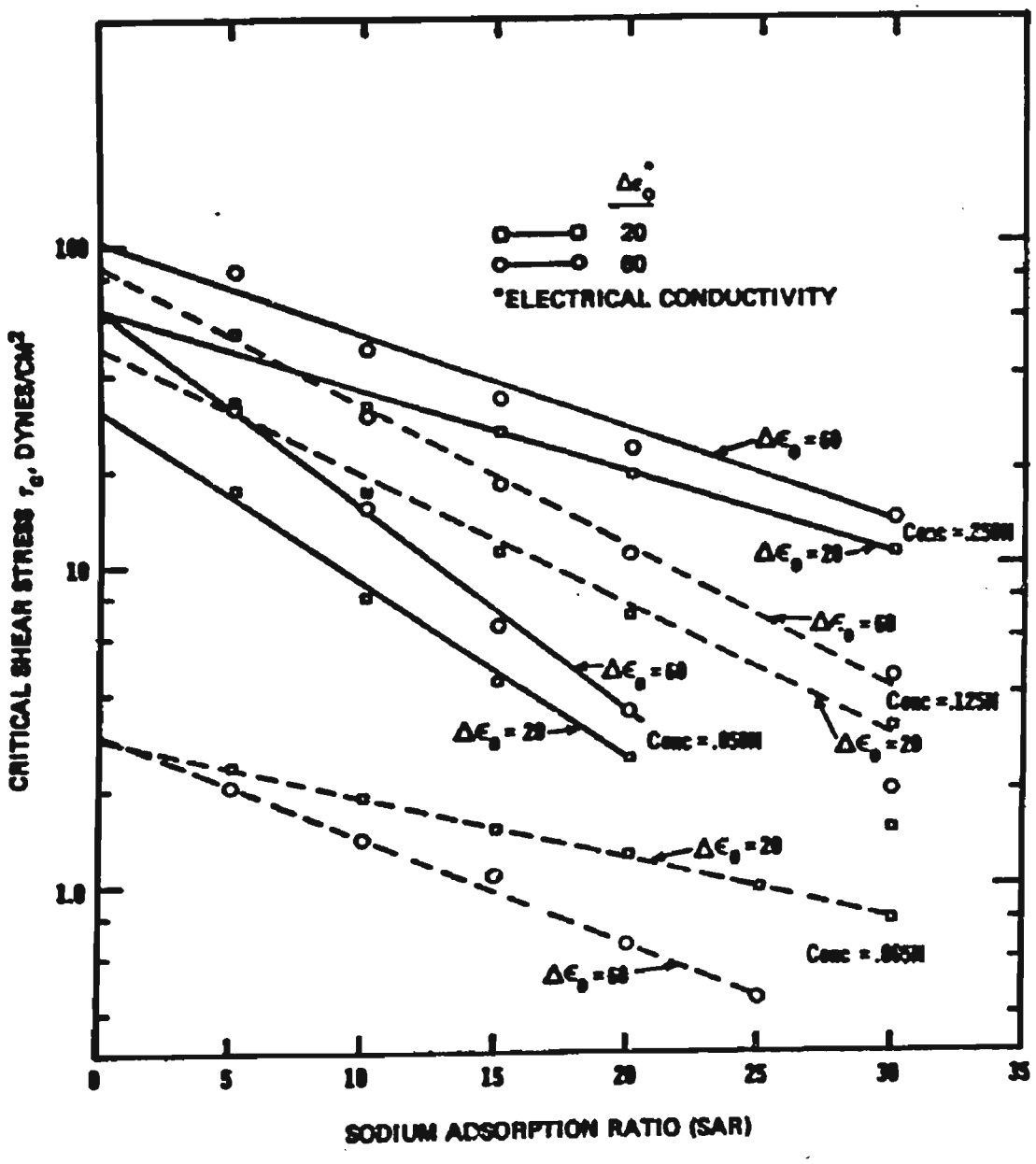

Figure 2.11 Predictive chart for critical shear stress from laboratory tests in rotating cylinder apparatus (Arulanandan et al. 1980)

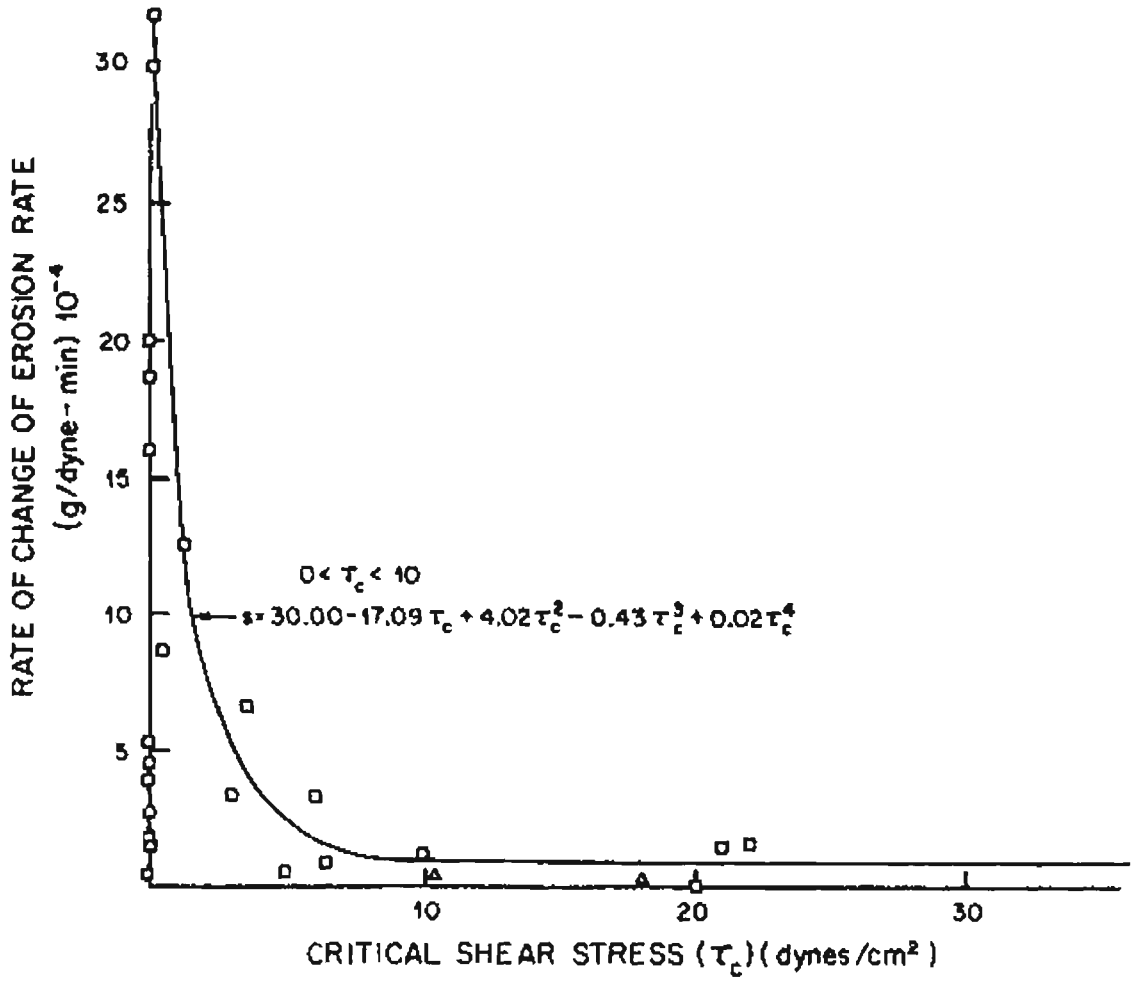

Figure 2.12 Rate of change of erosion rate α vs critical shear stress for remoulded soils in rotating cylinder apparatus using distilled water (Arulanandan et al. 1980)

Hjeldnes and Lavania (1980) studied cracking and erosion of dam materials directly through a laboratory test developed specifically for this purpose. The apparatus consisted of an inner and outer cylinder, ie. a hollow annulus, mounted vertically. The soil sample was compacted into the ring between these cylinder walls. The apparatus was made in two sections that could be pulled apart at the mid-height. A measured vertical tensile force was applied by raising the upper half of the cylinder, causing the material to crack horizontally at mid-height. A hydraulic gradient applied across the apparatus resulted in water passing through the crack into the centre of the hollow annulus. This water was collected and the flow rate and volume of solids in the effluent was recorded. In this way, the erosion and cracking properties of the materials were measured directly. The

observations of these experiments for two very different dam core materials are summarised below.

A well graded silty sand with gravel (non-cohesive), exhibited a self-healing effect. Erosion began after cracking, but diminished and ultimately vanished with time. This shows that the coarser particles are stable and self-filter the fines after some time. Further increases in crack width produced further flushes of turbid effluent water, followed by self-healing. Continual rapid erosion occurred when the crack width approached the maximum particle size. At this crack width, all the particles could be eroded and the coarser particles could not self-filter because they were not retained. Hence, a granular filter will be necessary to protect against large cracks through a dam core constructed with this material.

The second material tested was a silty-clayey fine sand (cohesive). This material had no self-healing effect. Initial crack deformation produced no erosion. As the crack width was increased, leading to an increase in flow rate, the eroding shear stress exceeded the critical shear stress and erosion began, and continued with no self-healing or reduction in the erosion rate. This demonstrated the erosion resistance of cohesive materials, but also demonstrated that once the critical shear stress is exceeded, the fine particles are not able to self-filter and a protective filter is necessary.

2.4.4 Summary of Filters for Cohesive Materials

The problem of cracking of cohesive cores, and particularly cracks through dispersive clays or materials with low erosion resistance, means that design criteria developed for cohesionless materials may not be applicable. The "perfect filter" concept, developed by Vaughan and Soares (1982) is a conservative concept that ensures that the filter will retain any particles that may reach it, under any seepage conditions. The No Erosion Filter (NEF) test, developed by Sherard and Dunnigan (1985), is suitable to test cohesive base soil - filter combinations, including dispersive base soils, assuming no segregation is possible in practice. Erosion resistance may mean no erosion occurs, but if the seepage forces exceed the critical shear stress, then a protective filter is required. There is still some uncertainty concerning the application of empirical design rules to all cohesive materials. Little is known about the size of particles that are eroded from a crack in a cohesive material and the effect on these particles when they reach the filter interface.

2.5 Analytical Models of Filtration

Many researchers are now focussing on analytical models of base soils and filters to describe the microscopic and macroscopic response of base soil – filter combinations to water flow under various conditions. With increased use of computers in engineering research, it has been possible to perform detailed simulations of the particle movement at the base soil - filter interface. Recent years have seen a number of new models described in the literature, some of which will be described here. This section will begin by describing the requirements of an analytical model. Secondly, the more common methods used to model filter voids will be described. Thirdly, an examination of some methods used to predict the movement of particles into a filter. Finally, a comparison of the proposed models will lead to recommendations of the best available models and possible improvements.

2.5.1 Requirements of Numerical Analysis

The first requirement of a numerical model of filtration is to represent the properties of the base and filter soils. The base soil particle size distribution (PSD) is usually sufficient to represent the base soil as an assembly of spherical particles of different size. A shape factor is sometimes used to describe non-spherical particles. Cohesive base soils complicate the modelling process greatly, factors such as erosion resistance, particle size and shape and physico-chemical forces should be considered.

Within the filter, it is the voids rather than the particles that control seepage and filtration. In particular, base particles are usually trapped by the smallest part of a connection between two voids, often called a void constriction or pore throat. The size of these constrictions is dependent on the size and packing geometry of the filter particles. The

normal approach is to adopt a filter void model and determine the filter void constriction size distribution (CSD) in some way, usually based on the filter PSD. Section 2.5.2 describes some of the void models adopted by various researchers.

The numerical analysis must also consider the movement of base particles under seepage forces, and the mechanisms of capture of these particles within the filter. Particle capture is usually modelled by a probabilistic comparison of base particle and filter constriction sizes. A particle smaller than the filter constriction between pores can pass through to the next pore where the probabilistic comparison is repeated (Silveira 1965, Schuler 1996). In this way, the expected infiltration distance of base soil particles can be simulated by a probabilistic analysis of the base PSD and filter CSD. Several particle infiltration models are presented in Section 2.5.4. Other factors that a good model may consider include the amount of base particles mobilised by applied seepage forces and changes in the filter CSD as particles are captured, these particle transport models are described in Section 2.6.

2.5.2 Filter Void Models

Silveira (1965) proposed a simple filter void model where base soil particles encounter constrictions at uniform spacing in the direction of flow. The constriction size is randomly determined from the constriction size distribution. If a particle is smaller than the randomly generated constriction, then it can move to the next constriction, where the comparison is repeated. This process is represented graphically in Figure 2.13. Probability functions are used to estimate the number of confrontations with randomly generated voids until a base particle will be retained by a void.

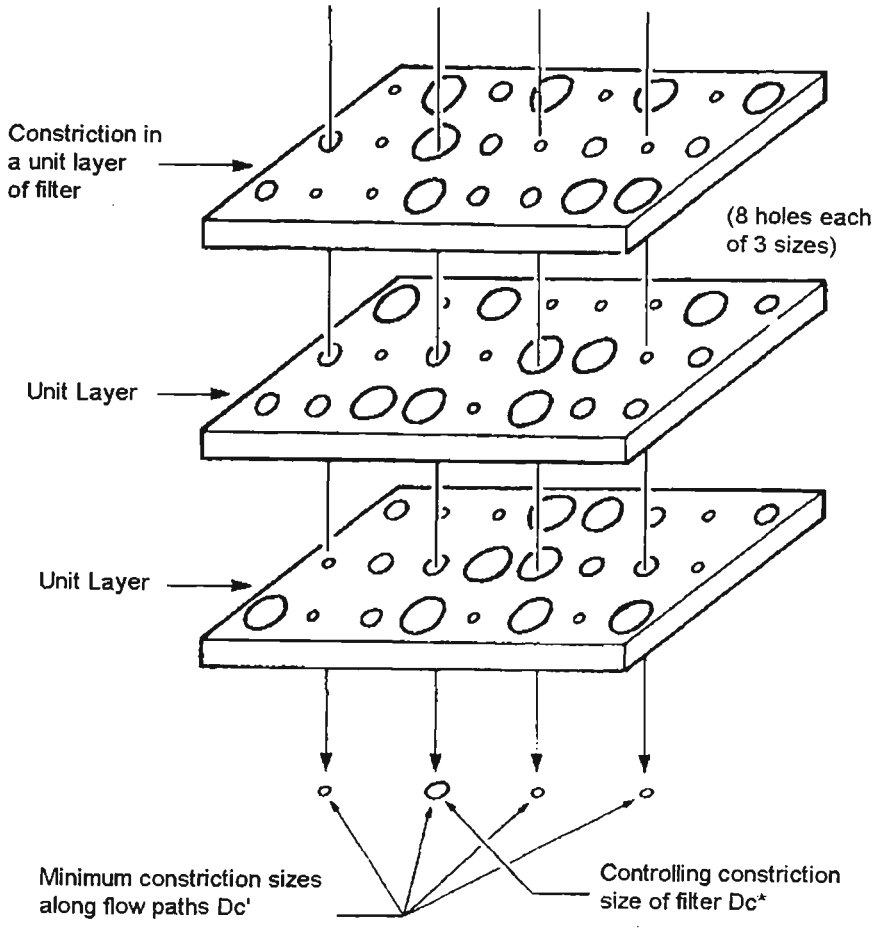

Figure 2.13- Layered Filter Model - Kenney et al. (1985)

An alternative void model represents the filter voids as a series of channels of varying diameter (Figure 2.14). The smallest of the pore constrictions within the pore channel governs the size of a base particle that can pass through the pore channel. Indraratna and Vafai (1997) adopted a model of this type. The model has been shown by Kovacs (1981) to be a good representation of the large and small pores in a natural soil. In this model, the minimum pore channel diameter, d_0, is given by:

$$d_0 = 1.63 \frac{n_e}{1-n_e} \frac{D_h}{\alpha} \qquad (2.14)$$

Where, D_h is a mass weighted equivalent diameter and α is a shape coefficient. Methods to determine these values can be found in Indraratna and Vafai (1997).

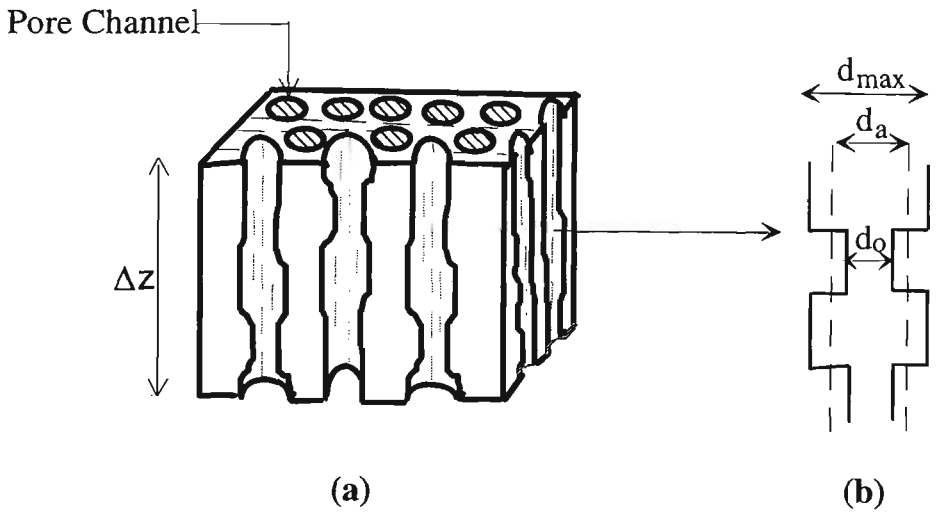

Figure 2.14 Void Channel Model - Indraratna and Vafai (1997)

A recent development has been the use of a three-dimensional pore network model. Witt (1993) developed a pore model of spheres (pores) interconnected by pipes (pore constrictions) (Figure 2.15). Particles can move from one pore to another through any of the constrictions, provided the particle is smaller than the constriction diameter. Witt (1993) assumed that from each pore, there are a number of possible exits (or pore constrictions), and the largest constriction size determines whether a particle can move from the pore.

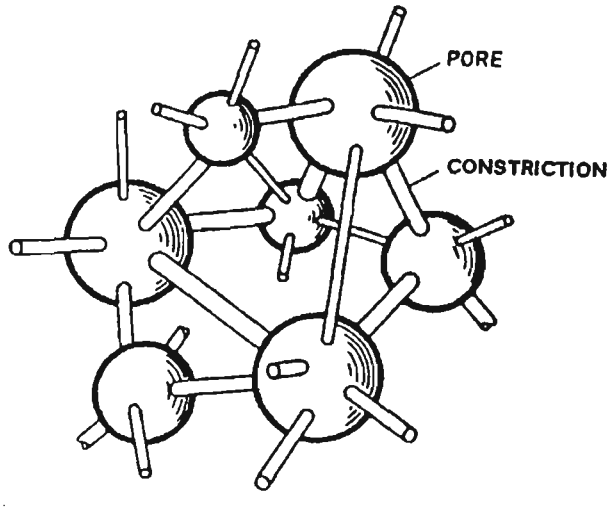

Figure 2.15 Pore Network Model - Witt (1993)

Schuler (1996) used a regular cubic network model of pores interconnected by six constrictions, similar to that of Witt (1993), as shown in Figure 2.16. Schuler (1996) determined that there were on average 5.7 constrictions per pore, and hence adopted the cubic network with six constrictions connecting every pore. This model was shown to accurately predict particle movement.

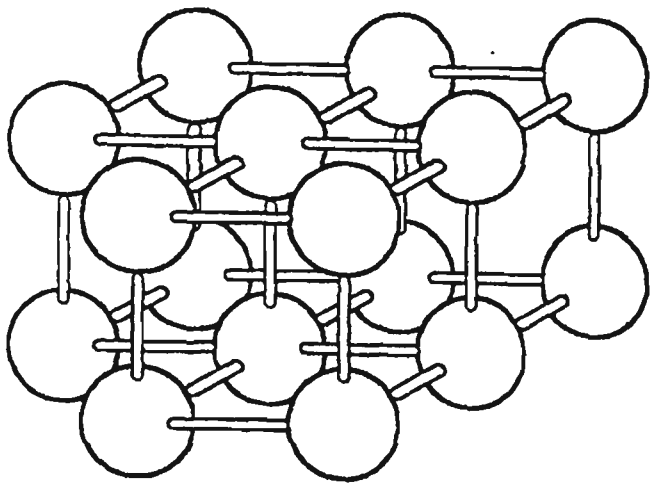

Figure 2.16 Cubic Pore Network Model - Schuler (1996)

2.5.3 Methods to Determine the Constriction Size Distribution

All of the filter void models described above require a constriction size distribution in order to determine the size of particles that can pass through the filter. Various modelling and laboratory methods have been used to estimate the size of constrictions. Silveira (1965) proposed a constriction size model that assumes the size of a constriction to be the largest circle that can fit between three tangent filter particles (Figure 2.17a). The model assumed that the grains are spherical, the filter is at its maximum density, and the relative positions occupied by the grains are random. Based on the probabilities of occurrence of each filter particle diameter, determined from the filter PSD, a combination of these probabilities can lead to the probability of different constriction sizes, and hence, a CSD curve. Since filters are not always compacted to maximum density, Silveira et al. (1975) proposed an

alternative void model for the least dense state of a soil, where four particles combine to form a void. This model is shown in Figure 2.17b.

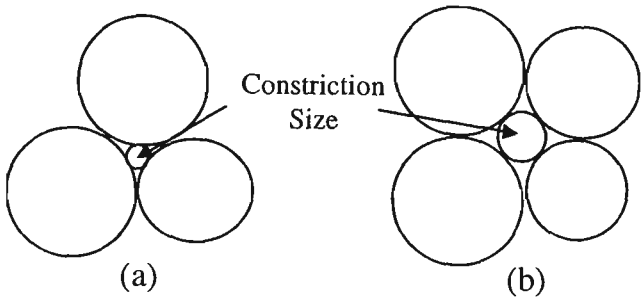

Figure 2.17 Particle packing arrangement for a) most dense and b) least dense states

The Silveira (1965) void size model has been shown to be a good approximation for uniform filters. However, in more broadly graded filters, the use of the particle size distribution by mass (as determined by sieving), to represent the frequency of filter particles, introduces errors. This is because large particles, with a high individual mass but low number, will be over-represented in the model and produce a high number of large pores. In reality it is unlikely that these few large particles will meet to form a large pore. De Mello (1977) showed that Silveira's model predicts an increase in the ratio of large void sizes to median filter particle sizes, d_{v85}/D_{50}, as the coefficient of uniformity of the soil increases (Figure 2.18). It is expected that as C_u increases, the number of small particles filling voids between the larger particles would increase, leading to smaller void sizes. Hence, the PSD by mass should not be used to model the voids of well graded filters.

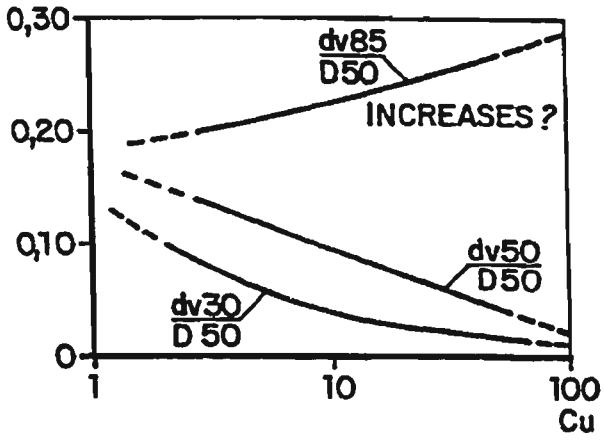

Figure 2.18 Comparison of Filter Void Model (DeMello 1977)

Kenney et al. (1985) and Federico and Musso (1993) deal with this problem by converting the PSD by mass to a PSD by number of particles. This approach gives a better approximation of the real CSD, but still has been shown to give errors for broadly graded filters. Humes (1996) and Schuler (1996) have adopted a PSD by surface area. This is considered more representative of the possible particles which may form a void, since, although there will be only a small number of larger particles, they have a great number of contacts with other particles, due to their large surface area.

Schuler (1996) produced a model of the size of pore constrictions using an adaptation of the geometric method of Silveira (1965). The model is shown in Figure 2.19. Four particles are present and form two constrictions in a variable geometric assembly. Importantly, the model considers the effect of filter density. The angle, α, in Figure 2.19, decreases with increasing density, producing smaller constriction sizes. The least dense particle packing is considered when $\alpha=90^{\circ}$, while the most dense packing is the case where α is a minimum and filter particles B and D are touching, producing two small constrictions.

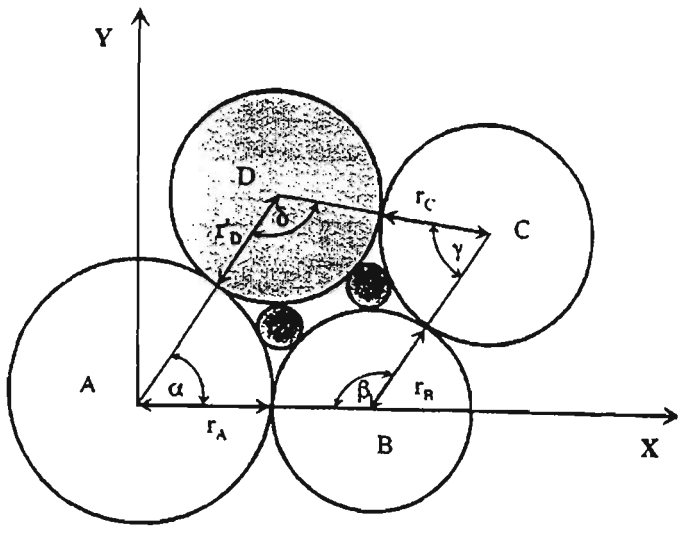

Figure 2.19 New Method to Determine CSD - Schuler (1996)

Some researchers have taken a direct approach and measured the constriction sizes within a filter, rather than estimating the sizes. Wittman (1979) filled a filter medium with resin and then, after hardening, cut the sample into sections to examine the void size distribution. Using this measured CSD as a probability density function, he developed a model of a flow path in the form of a pore channel with irregular width in the direction of flow. Some criticism was directed at the work of Wittman (1979), because a slice of the filter material will show a random plane through both pores and pore constrictions, rather than the smallest part of the voids (the pore constrictions), which form the restrictions to particle movement.

Witt (1993) measured the pore constriction size distribution of a real material; silicon rubber was poured into the voids of a gravel and cut open to reveal 3D representations of the pores and constrictions. In this case, the true, three-dimensional shapes of the filter pores were obtained, overcoming the problem of measuring constriction sizes in slices of the material. This lead Witt (1993) to a statistical distribution of the largest constriction size associated with each pore. The distribution of exit sizes was found to be log-normal.

2.5.4 *Infiltration of Base Soil into Filters - Probabilistic Methods*

The next step of analytical modelling is to describe the movement of base soil through the filter void model. The two broad categories of infiltration models are probabilistic methods (described here) and particle transport models (described in Section 2.6). Probabilistic methods simulate the probable depth of base particle penetration into the filter voids by comparing the probability of a base particle encountering a void through which it can pass. Some of the proposed methods are described in the following sections.

2.5.4.1 *Direct Probabilistic Methods*

Silveira (1965) assumed that particles move only in the direction of flow and encounter random void constrictions at uniform intervals. The probability p that a base particle, of diameter d', can pass through a single, random filter void constriction is the cumulative fraction of constrictions larger than d', which can be found directly from the CSD (ie. p is the fraction coarser than d' from the CSD). Then the number of confrontations, n, until the particle encounters a smaller void constriction through which it cannot move, based on a confidence level of $\overline{P}$ can be estimated:

$$n = \frac{Log\left(1-\overline{P}\right)}{Logp} \tag{2.15}$$

And the distance, L, the particle can infiltrate into the filter is:

$$L = n.s \tag{2.16}$$

Where, s is the distance between each confrontation with a pore constriction. In other words, s is the distance between unit layers in the filter pore model, often called a unit step (Figure 2.13). Silveira (1965) assumed that s is given by the mean diameter of filter grains (from the PSD by mass). Humes (1996) improved on the Silveira (1965) model by considering the PSD by surface area to represent the filter particles.

Kenney et al. (1985) used the Silveira (1965) constriction size model and the unit layers void model as shown in Figure 2.13. Rather than a probabilistic analysis of the infiltration depth of particles, the analysis then considered the probability of occurrence of minimum constriction sizes along flow paths perpendicular to the unit layers. Kenney et al. (1985) found that the minimum constriction size encountered along any flow path soon approached a constant value as the filter thickness was increased. This was called the controlling constriction size, D_c^* and was found to be related to the finer fractions of filter particle sizes:

$$D_C^* / D_5 \leq 0.25 \text{ or}$$

$$D_C^* / D_{15} \leq 0.2 \qquad (2.17)$$

2.5.4.2 Stochastic Methods

Using stochastic methods, based on a pore model and the size distribution of the pore constrictions, the probability that a grain meets a constriction through which it cannot pass in a number of confrontations can be determined. Witt (1993) used a three-dimensional pore network model (Figure 2.15) to show that as the number of confrontations with constrictions increases (ie. the filter thickness increases) the minimum constriction size of any path tends to a constant value d_p for all paths, and that for a depth of penetration, L:

$$d_p = 0.27\ d_g \quad \text{for } L \approx 60\ D_{5F}$$

$$d_p = 0.23\ d_g \quad \text{for } L \approx 300\ D_{5F} \qquad (2.18)$$

In the above equations, d_g is the mean grain diameter of the filter (by number), usually between approximately D_{5F} to D_{10F}. Particles finer than diameter d_p can pass through the filter. An important observation, similar to that of Kenney et al. (1985), was that if L is

increased beyond $300D_{5F}$ the decrease in the minimum constriction size is negligible. If there are grains in the base soil which are larger than d_p, then these particles will be retained and self filtration is initiated (provided the base soil is internally stable).

2.5.4.3 Monte Carlo Simulation

Schuler (1996) used percolation theory to model the movement of individual base particles through the pore network model of Figure 2.16. Percolation theory suggests that a network can be percolated infinitely if the probability of penetration (passing from one pore to the next through a void constriction) is greater than a critical probability, specific to the number of dimensions and the structure of the network in question. This means, in theory, that a base particle can pass through an infinitely thick filter, if the probability that it will be smaller than a random pore constriction is greater than the critical probability, p_{cr}. A Monte Carlo simulation was used to examine the infiltration depth of a large number of base particles of different sizes into the filter model. The simulation showed that the critical probability is approximately p_{cr}=37% (ie. base soil particles finer than the 63% largest pore constriction from the CSD can move infinitely through the filter). This is shown in Figure 2.20, where the infiltration depth, E, refers to the number of unit steps (or levels) in the direction of flow. Monte Carlo simulation showed that the relation of Equation (2.18) can be used to estimate the mean penetration depth, E (number of confrontations with constrictions or layers in the 3D model), of a particle into the filter.

$$E = 123(36.3 - p)^{-0.88} \quad \text{for } p<36.3\% \qquad (2.19)$$

While there is no comparison of this model with laboratory experiments or field results, it appears to be theoretically sound. The model combines many concepts from previous research and produces probably the most accurate model of this form.

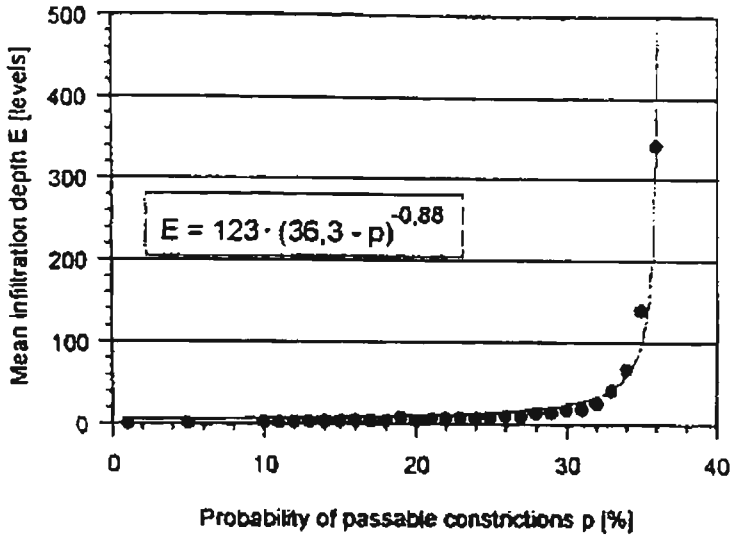

Figure 2.20 Infiltration Depth vs % Voids Larger than Particle Size (Schuler, 1996)

2.5.4.4 Other Probabilistic Models

Alternative probabilistic approaches commonly provide an alternative method for determining the constriction size distribution curve, or a new probabilistic approach for particle transport through an assumed void network. However, many proposed models are not practical for application to design situations, often requiring a number of empirical parameters or extensive computer modelling. A major criticism of these models has been that the void models do not adequately describe broadly graded materials. In addition, they generally only deal with non-cohesive, spherical particles.

Imdakm and Sahimi (1987) have used a Monte Carlo simulation to model filtration in chemical engineering. Particles move through a weighted random walk where two possible exits from each pore are considered. The probability of a particle taking either exit is based on the ratio of flow volumes through both exits. Particles are retained if they encounter a void constriction smaller than the particle diameter (randomly generated from the constriction size distribution). The model has the advantage of considering the effects of

particle capture within the voids. Clogged voids are assumed to reduce the permeability and possible number of flow paths within the filter. This concept of continually decreasing permeability and narrowing flow paths could be combined with the Schuler (1996) void model to produce a time-dependent model of filtration.

Aberg (1993) considered the void ratio and mean pore size of a granular soil, as a function of the particle size distribution, and proposed a model of the void structure in cohesionless soils. The model considers any random line drawn through a collection of particles and compares the length of sections through particles (a grain chord) and the length of sections through voids (a void chord). By considering the average length of these chords, a model is produced to estimate the average void sizes. The Aberg (1993) model has the advantage of considering both soils where all particles form the skeleton of the material, and soils where finer particles are loose within the structure of the coarser particles. The model has been applied to determine the permeability, void ratio, bubbling pressure and filtration opening size of cohesionless soils. Aberg (1993) found a good correlation between the predictions of his model and tests conducted by Kenney et al. (1985).

2.6 Particle Transport Models

Particle transport modelling has been considered extensively in both contaminant transport and chemical filtration. However, the use of these models to describe the movement of large particles, such as through granular filters, has been limited. The usual approach is to consider basic physical concepts such as conservation of mass and momentum, to model the flow of a fluid containing solid particles through the voids of a filter. Honjo and Veneziano (1989) developed a soil particle transport model based on conservation of mass in the solid and liquid (slurry of soil and water) phases. The model is capable of describing absorption and release of soil particles with time in different elements of the base and filter. Various soil particle sizes can also be considered. The model was used to demonstrate self-healing of the base soil as coarser particles collect at a screen. In addition, internal stability and instability were investigated using the model.

Indraratna and Vafai (1997) adopted the particle transport approach, incorporating a simple pore channel model (Figure 2.14) that provides the geometric constraint to movement. The model also considers the hydraulic forces required to mobilise the base soil particles. A critical hydraulic gradient, i_{cr}, is determined based on a balance of the frictional resisting forces with the hydraulic and gravitational disturbing forces. Figure 2.21 shows the situation considered, where the contact friction resists erosion, unless the applied hydraulic gradient is large enough to overcome the frictional resistance. The frictional forces (F_{xz} and F_{yz}) are assumed to be caused by the horizontal confining stresses σ_x and σ_y acting on the projected sides of the particle. In an irregular pore channel it is difficult to estimate the exact friction mobilised at a given location. For the analytical model, it was postulated that the upper limit of the frictional force is proportional to the fully mobilised lateral stress in the filter. This lateral stress can be estimated from the overburden depth h_s and hydraulic

head h_w (ie. an effective vertical stress of $h_s\gamma_s - h_w\gamma_w$). Hence the upper limit of the frictional forces will be:

$$F_{xz} = F_{yz} < 0.5\pi d^2 K\left(\gamma_s h_s - \gamma_w h_w\right)\tan\phi' \qquad (2.20)$$

A critical hydraulic gradient, i_{cr}, is determined based on a balance of the frictional resisting forces with the hydraulic and gravitational disturbing forces, given by:

$$i_c < \frac{4K}{\delta z \gamma_w}\left(\gamma_s h_s - \gamma_w h_w\right)\tan\phi' - \frac{2d}{3\delta z \gamma_w}\left(\gamma_s - \gamma_w\right) \qquad (2.21)$$

where, $K < \tan^2\left[\frac{\pi}{4} - \frac{\phi'}{4}\right]$ and ϕ' is the effective friction angle between base and filter particles.

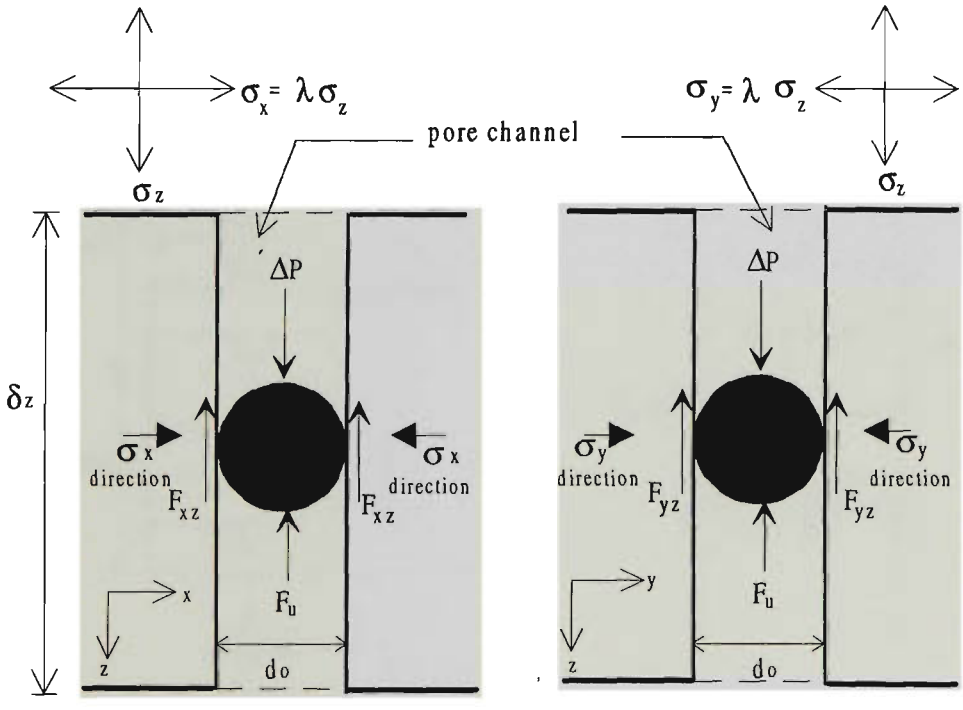

Figure 2.21 Equilibrium of Particle "Plugging" a Vertical Pore Channel in a)XZ Plane; b) YZ Plane (Indraratna and Vafai, 1997)

If seepage forces exceed the critical hydraulic gradient, and the particle is smaller than the geometric constraint, d_0, it will move. Moving particles are controlled by the governing differential equations of mass and momentum conservation. The base-filter interface is

divided into elements as shown in Figure 2.22. Considering the mass flow rates in and out of a typical element shown in Figure 2.22b, and the rate of mass accumulation within the element during a time period, *dt*, the principle of mass conservation requires:

$$\frac{d(\rho_m u)}{dz} = \frac{d\rho_m}{dt} \tag{2.22}$$

The principle of momentum conservation is applied to the volume of slurry, V_m, to give:

$$\sum F = \rho_m V_m \left(\frac{du}{dt} + u\frac{du}{dz} \right) \tag{2.23}$$

The external forces, ΣF, include surface forces due to hydrodynamic pressure and body forces resulting from gravity and viscous drag. Defining R as the viscous drag per unit mass of the slurry, the external forces can be determined from:

$$\sum F = -\frac{\partial P}{\partial Z} V_m - \rho_m g V_m + \rho_m R V_m \tag{2.24}$$

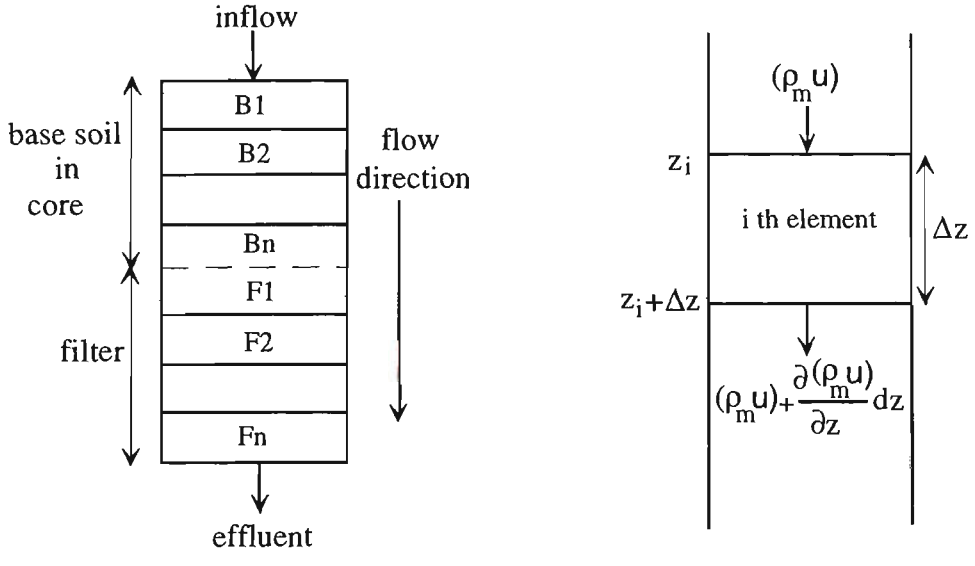

Figure 2.22 Illustration of (a) base and filter elements and (b) generalised slurry flow through a filter element (Indraratna and Vafai, 1997)

By considering a number of elements at the base - filter interface, the movement of particles is modelled by a finite difference analysis. The process predicts the change in slurry density (ρ_m) and the slurry velocity (u) within the time-step, Δt. The slurry velocity is then incorporated in Darcy's law (u=ki) to compute the corresponding hydraulic gradient

at each time-step. The flow rate is easily determined from the continuity equation, according to the slurry velocity and element porosity.

The PSD of each element at any given time is computed based on the mass and PSD of the element at the previous time step and the subsequent rate of erosion and retention. The PSD of each element is recalculated for each time step and the finite difference procedure repeated. This analysis shows the gradual change in particle size distribution, permeability and porosity of the base soil and filter elements, and hence, describes what is occurring at the base - filter interface with time for the entire particle size range. This is the only method to date that uses the entire PSD and considers time variant changes in PSD. The choice of a single value for the minimum pore channel diameter, d_0, can be justified by the work of Kenney et al. (1985) and Witt (1993) who found that after a short distance the smallest constriction on any pore channel will tend to a single value, the controlling constriction size, D_c^*. However, the pore channel diameter, d_0, is often higher than the controlling constriction size, hence the accuracy of the model is compromised.

2.7 Comparison of Filter Models

Many different techniques were presented above for modelling particle movement through filters. This section provides a brief comparison of some of these models. The general process of most numerical methods is to predict the depth of infiltration of base particles of varying diameter, based on geometric conditions. The expected infiltration of various particle diameters can define the base soil erosion and retention within the filter. The models of Schuler (1996) and Humes (1996) predict particle infiltration directly. The controlling constriction sizes of Witt (1993) and Kenney et al. (1985) can be compared also since they predict a single base particle size, below which infiltration will be infinite. The time-dependent predictions of the Indraratna and Vafai (1997) model cannot be compared directly with other models, however, the pore channel model and the minimum diameter, d_0, can be compared.

Two filter materials will be used for the comparison, a uniform sand filter with D_{15}=1.3mm and C_u=2, and a well graded sand filter with D_{15}=1.3mm and C_u=6. Figure 2.23 and Figure 2.24 show the model predictions for the uniform sand and well graded sand filters respectively. The figures show on the y-axis the predicted depth of infiltration of base soil particles of varying diameter (x-axis) into these two materials. Also shown are the controlling constriction sizes predicted by Witt (1993) and Kenney et al. (1985), and the minimum pore channel diameter of the Indraratna and Vafai (1997) pore model. Kenney et al. (1985) present two formulae for controlling constriction size based on D_{15} and D_5 of the filter, only the highest value is shown, as this is the conservative value. The predicted controlling constriction sizes are similar for uniform filters (Figure 2.23), but become widely scattered for more broadly graded materials, due to the increased difficulty of quantifying the particle size and shape effects (Figure 2.24). For both filter materials, the

model of Schuler (1996) predicts a percolation diameter close to the controlling constriction diameter of Kenney et al. (1985) and Witt (1993). The model of Humes (1996) predicts that much finer particles are required to infiltrate the same distance; this is because the model only allows particles to move in the direction of flow and considers the filter to be in the densest state.

The pore channel model of Indraratna and Vafai (1997) predicted a minimum pore channel diameter larger than other models for the well graded filter. Vafai (1996) has pointed out that the validity of 'd_0' tends to decrease as the C_u value is increased above 6. The Indraratna and Vafai (1997) model assumes nearly spherical particles (shape factor α=6), which decreases the accuracy when considering broadly graded filters. For broadly graded materials, the shape factor, α, should be calibrated such that the minimum pore channel diameter is equivalent to the controlling constriction size predicted by Witt (1993) or Kenney et al. (1985). For example, when α=8 (cubic particles) the minimum constriction size, 'd_0', in the Indraratna and Vafai (1997) model is about 20% less, approaching the controlling constriction size of Kenney et al. (1985) in Figure 2.24. The equations for controlling constriction size determined by Witt (1993) and Kenney et al. (1985) have been verified by extensive laboratory experimentation and are therefore more likely to be accurate. This suggests that the pore model adopted by Schuler (1996) is generally more representative of real soils than the Humes (1996) adaptation of the Sileira (1965) model.

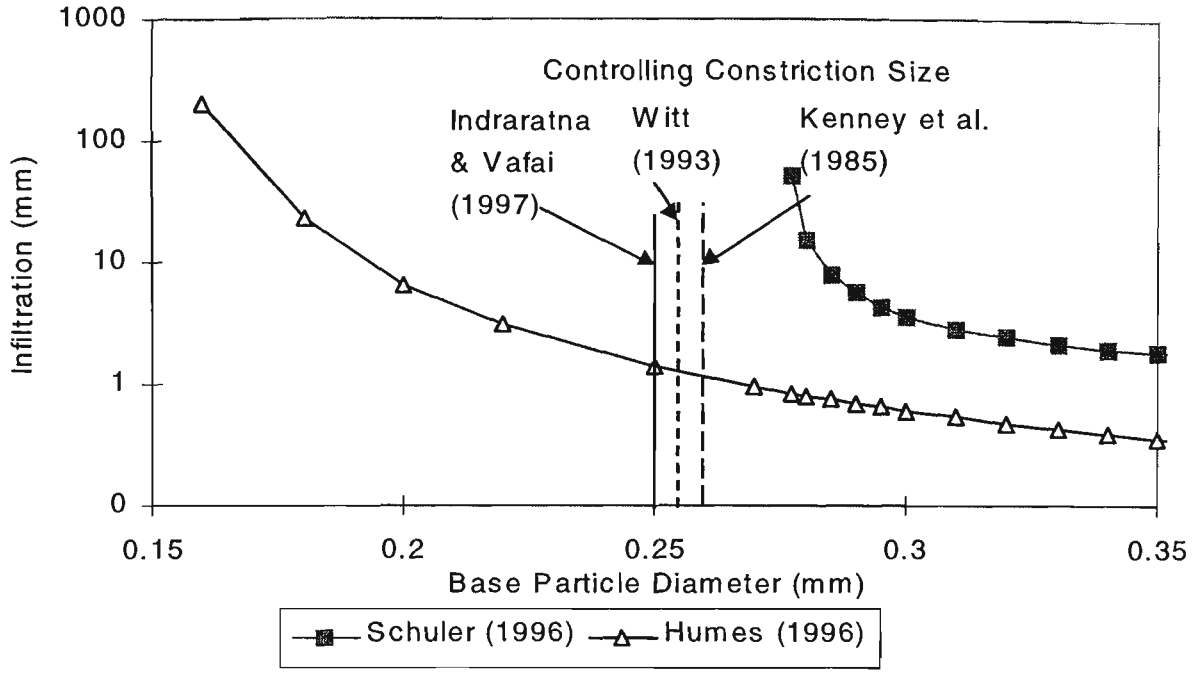

Figure 2.23 Predicted infiltration depth into a uniform filter with D_{15F}=1.3mm and C_u=2

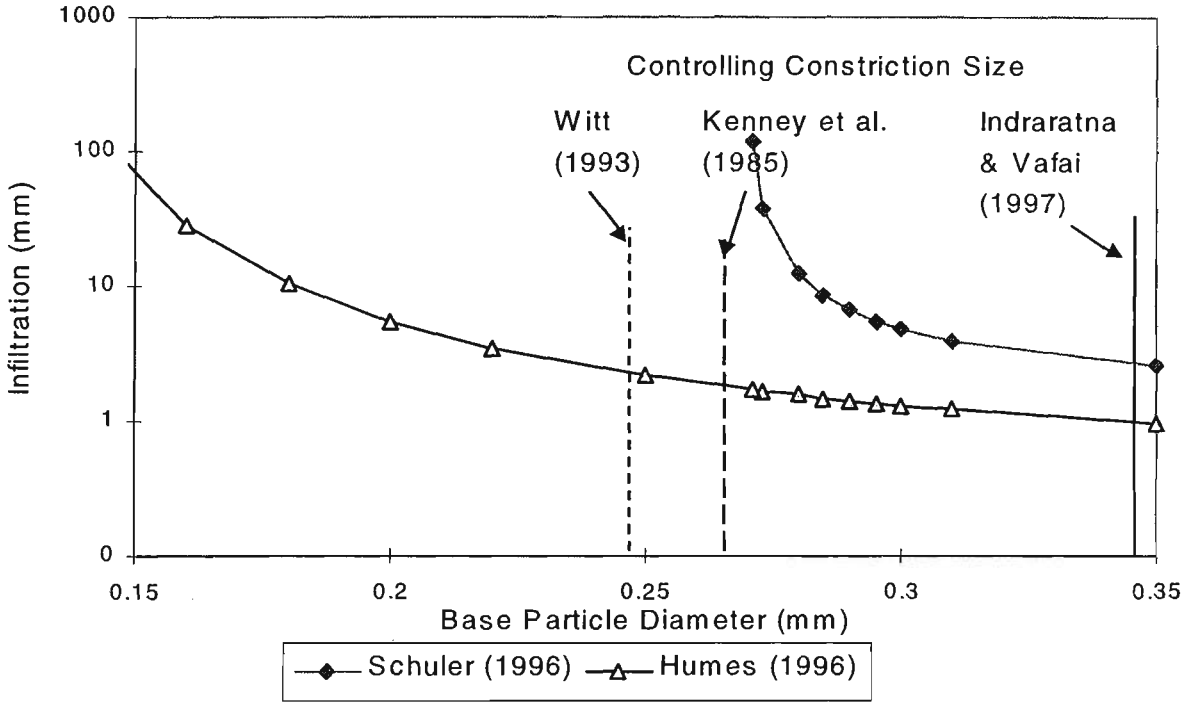

Figure 2.24 Predicted infiltration depth into a well graded filter with D_{15F}=1.3mm and C_u=6

2.7.1 Modelling Physico-Chemical Effects

The behaviour of cohesive base soils can be affected by physico-chemical forces that may retain fine particles within the filter, when they would normally pass through the filter pore constriction. In addition, the erodability of cohesive materials is related to the concentration of ions in the eroding water and pore fluid. While physico-chemical capture is minimal for relatively pure reservoir water, these effects may become dominant when considering filtration of brackish water, contaminants, dams in karstic terrain or mine tailings dams.

To consider these physico-chemical effects, Rege and Fogler (1988) produced a network model of pores and pore constrictions, similar to that of Witt (1993) to model filtration. They suggested that the capture of particles smaller than the void constriction size is dependent on fluid velocity, ionic strength, pH, and the particle density and concentration. Reddi and Bonala (1997) used these concepts of particle capture due to physico-chemical effects to produce a model of long-term accumulation of fines in filters. A single particle deposition coefficient, λ, was defined such that the amount of physico-chemical capture was related linearly to the slurry concentration C, ie. deposition = λC. The deposition coefficient was related to the pore and particle sizes, fluid velocity, ionic strength and pH. This additional deposition of cohesive fines within the filter, could be included in time-dependent models of granular filters which currently only consider geometric constraints to particle movement. Physico-chemical capture is important because progressive accumulation of fine particles in filters over a long period may lead to unacceptable permeability reductions and a build up of excessive pore pressures, leading to instability of geotechnical structures.

Reddi et al. (2000) extended the particle accumulation model to describe the decrease in permeability with time due to physico-chemical clogging of pores. A pore channel model was used to describe the filter voids. The pore sizes decrease as fine particles accumulate on the pore walls. The Hagen-Poiseuille equation relating permeability to pore size was used to predict the decrease in permeability as the pores became clogged. The model was verified through laboratory experimentation. Permeability reductions of more than one order of magnitude occurred even for filtration of particles that were smaller than the majority of soil pores, and hence, were not retained by the physical capture mechanism described earlier (Section 2.5.4).

2.8 Focus of the Current Research

The empirical criteria proposed by Sherard and Dunnigan (1985) are based on extensive experimental data and have been verified by other researchers (Foster and Fell 1999, Delgado 2000). These criteria have been used successfully to design filters for many dams throughout the world. However, the criteria have been shown not to apply universally to all base soils (Indraratna et al. 1996). In addition, these empirical guidelines do not describe the processes occurring within the filter and are unable to identify potential problems with unusual materials. Sherard and Dunnigan (1985) note that some samples used in developing the criteria had a safe filtration ratio (D_{15F}/d_{85B}) lower than the safe design criteria. Hence, further research is necessary to describe the time-dependent changes occurring within the base soil and filter material, and determine why some samples do not behave as expected. A laboratory study of erosion and filtration processes for cohesive base soils will be described to improve the understanding of how cohesive materials behave during filtration. This will include a series of large scale erosion tests and correlation of the observations of these tests with the results of no erosion filter tests on the same materials. This laboratory study is presented in Chapter 4.

Due to the assumptions and simplifications made, the analytical approaches described in this literature review all have limitations. The majority of models only describe the initial infiltration of particles into the granular filter, and do not consider the time-dependent changes in filter properties and behaviour. Time-dependent description of filtration is essential to demonstrate the formation of a self-filtering interface, and predict the amount of mass lost before this interface forms. The rate of erosion and particle transport give a designer a significantly better idea of warning times if piping failure is going to occur. The Indraratna and Vafai (1997) model provides a basic description of these time-dependent

changes. The current research will expand on the concepts proposed by Indraratna and Vafai (1997) and Vafai (1996) by adopting a more accurate void model, and considering in more detail the realistic geo-hydraulic processes of filtration. This modelling will describe in detail the filtration of a non-cohesive base soil, and is presented in Chapter 3. Comparison will be made between these predictions and published laboratory data, empirical criteria and new laboratory studies.

To date, no analytical approach has adequately described the filtration of cohesive base soils. The model developed for non-cohesive base soils will be expanded in Chapter 5 to describe filtration of cohesive base soils also. Observations of laboratory experiments on the erosion and filtration of cohesive soils, described in Chapter 4, will be used to describe the behaviour of these materials. Concepts such as resistance to erosion, aggregation of cohesive particles, physico-chemical capture of particles and concentrated flow through cracks in cohesive soils will be considered in developing the model described in Chapter 5 of this thesis.

The extensive previous research described in this literature review has produced a large number of empirical design criteria and case studies. The predictions of the models of filtration developed in this thesis will be compared with the empirical criteria in Chapter 6, and with new and existing case studies in Chapter 7.

3. MODELLING FILTRATION OF NON-COHESIVE BASE SOILS

3.1 Introduction

The design of granular filters is generally based on empirical guidelines, as outlined in Chapter 2. These empirical guidelines were developed through extensive laboratory tests, whereby the stability of various base soil - filter material combinations was evaluated under different hydraulic gradients (Sherard et al. 1984, Delgado 2000). However, the mechanisms of filtration, interface behaviour and the time-dependent changes that occur within the filter medium cannot be described by empirical criteria. In contrast, mathematical models can be formulated to explain the fundamental mechanics of particle interaction and migration, within a framework of well-defined geo-hydraulic constraints. Considering the mass flow and momentum conservation principles, combined with appropriate seepage criteria, governing equations can be developed to simulate time-dependent changes in particle size distributions, mass flow rates, filter retention capacity and base soil erosion rates as related to the change in porosity and permeability of the filter medium. This Chapter will describe a new analytical model developed to describe the time-dependent behaviour of the interface between non-cohesive base soils and granular filters.

Existing numerical models of filtration have certain limitations. Many adopt simplified pore models that are only applicable to a limited range of filter materials. Very few models consider the time rate of formation of a stable filter interface. Instead, the models only determine the amount of particle infiltration into a clean filter, while ignoring the change in filter void sizes and permeability, due to capture of base soil particles. Considering time-dependent changes is essential to describe the formation of a self-

filtering interface. The description of time-dependent changes in flow rate, filter permeability, base soil erosion etc. can be very useful to the dam designer. Additionally, most existing filter void models are inaccurate for broadly graded soils. In this Chapter, a revised particle transport model is developed to describe filtration of non-cohesive soils, which significantly extends the previously proposed analytical model by Indraratna and Vafai (1997) for particle transport. The entire model, described in Section 3.2, includes: a) a filter pore model based on a three dimensional pore network model, b) determination of particle infiltration based on a probabilistic analysis of the filter pore model and c) principles of conservation of mass and momentum describing the movement of soil particles through the filter voids. The model is calibrated against previously published laboratory results in Section 3.3. Comparisons with new laboratory results are described in Section 3.4. The time dependent model predictions are presented in Section 3.5.

3.2 Theoretical Development of the Analytical Model

The analytical model is intended to describe the rate of erosion of non-cohesive base soils due to seepage flow, and the transport distance and possible retention of these particles in the filter. As particles are captured they alter the filter properties; in particular, they reduce the size of filter voids and allow retention of progressively finer particles. The model will describe this time-dependent change in mass flow and particle retention, and linked to this are the time-dependent changes in flow rate, permeability and porosity. The first requirement of the analysis is a model of the filter geometry, in particular a model of the filter pore voids.

3.2.1 Filter Pore Model

At the base soil – filter interface, eroding base soil particles move through the void space of the filter. The particles move under the influence of the seepage water, until they encounter a pore where all the exits or pore constrictions from the pore are smaller than the particle diameter. The particle is then retained within that pore. In order to model this process, the first important requirement is a suitable model of the filter pore voids. Many different filter pore models have been adopted to model filtration. Some of these pore models were introduced in Chapter 2, and are not elaborated here.

A granular soil is a three dimensional collection of particles which form pores of different size and shape, having constrictions between the pores, which may be of different size, shape and orientation. It is not feasible to model the random arrangement of pores and constrictions, without making simplifications. The regular pore network models appear to provide a reasonable approximation of the filter voids. These models assume the pores have a regular three-dimensional structure, such as a cubic or

tetrahedral arrangement, and each pore is connected to the surrounding pores by pore constrictions. After examination of the pores of a gravel, Schuler (1996) suggested that there are, on average, 5.7 constrictions from every pore. Based on this, Schuler (1996) developed a regular cubic network model of pores and constrictions, shown in Figure 3.1a, where the spheres represent pores, while the small cylinders represent constrictions. Each pore has six exits or constrictions, connecting the pore to surrounding pores (Figure 3.1b). A particle that has entered a pore through a constriction, may exit the pore through any of the other five constrictions, provided the particle is smaller than the constriction diameter. While the analysis of particle movement will be 2D, this 3D model at the microscopic scale provides a better simulation of particle movement.

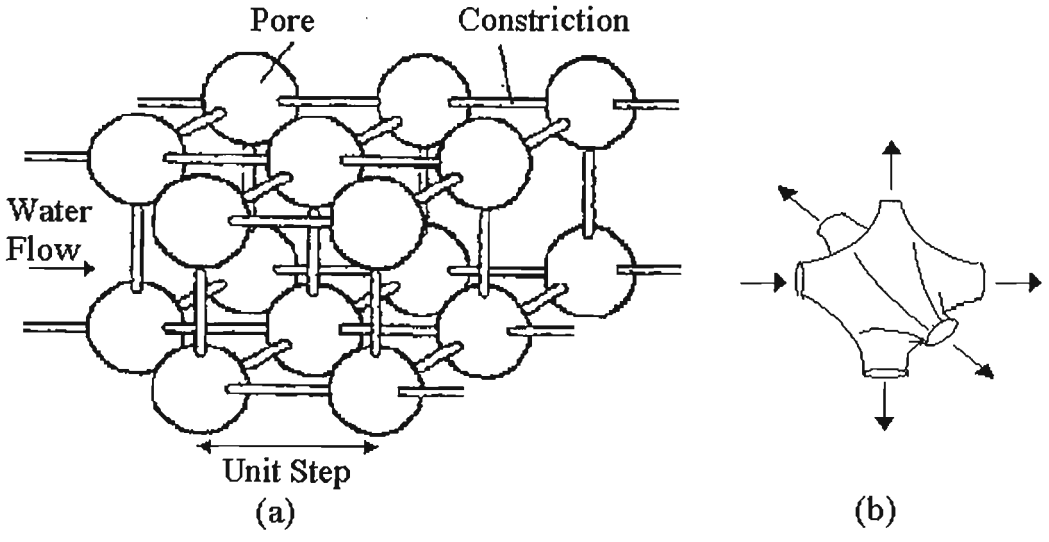

Figure 3.1a) Cubic network pore model (after Schuler 1996); b) Single pore with six constrictions.

3.2.2 Constriction Size Distribution

The pore network model assumes that the size of each pore and constriction is randomly determined from a pre-determined size distribution. The pore constrictions, represented as bonds (cylinders) between the pores in Figure 3.1a, form the smallest link between pores, capturing moving particles. Hence, the important geometric factor for modelling

non-uniform granular filters is the pore *constriction size distribution*, hereafter called the CSD. An assumption made here is that the filter CSD is dependent on the particle size distribution (PSD) and relative density of the filter. A geometric model is be developed to determine the size of constrictions based on the size of particles forming the constriction.

In Chapter 2 (Section 2.5.3), it was shown that the normal PSD by mass, as determined by sieving, is not suitable for modelling the size of particles encountered in a granular soil. This is because large particles, which have a large mass, will be over-represented in the distribution. Humes (1996) showed that the PSD by surface area is more suitable for calculating the CSD than the usual PSD based on mass. This is because the filter voids are formed by the surfaces of particles. The distribution of filter particles by surface area is determined by assuming that the density of all particles is constant, and that all grains have the same shape. The number of particles of a particular diameter is determined from the PSD by mass, and the surface area of these particles is their frequency times a function of the square of the diameter (Humes, 1996). Equation (3.1) is used to convert the PSD by mass to the PSD by surface area.

$$P_{SA} = \frac{\frac{P_{mass,i}}{D_i}}{\sum \frac{P_{mass,j}}{D_j}} \qquad (3.1)$$

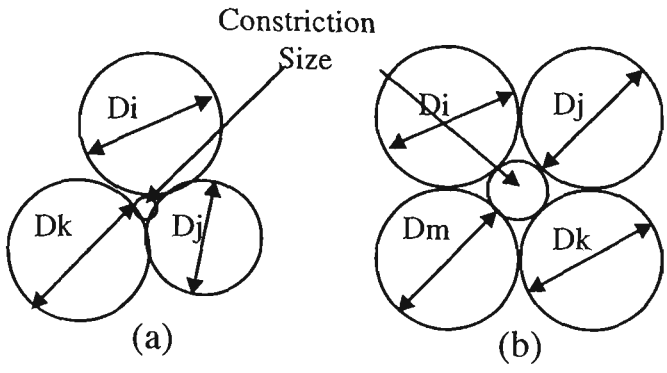

Figure 3.2 Pore Constriction Size for a) Most Dense and b) Least Dense states.

Constriction sizes can be estimated by considering one of the two geometric conditions shown in Figure 3.2. These two geometric conditions represent, in two dimensions, (a) the most dense and (b) the least dense packing condition of a soil. The diameter of a circle which can fit between the three or four filter particles, represents the size of the constriction formed by these particles. Considering the *most dense* particle packing, where the constriction is formed by three tangent spheres of diameters D_i, D_j and D_k, (Figure 3.2a), the theory of standard mean error can be used to estimate the constriction diameter D_v, as given by Equation (3.2).

$$\left(\frac{2}{D_i}\right)^2+\left(\frac{2}{D_j}\right)^2+\left(\frac{2}{D_k}\right)^2+\left(\frac{2}{D_v}\right)^2 = 0.5\left[\left(\frac{2}{D_i}\right)+\left(\frac{2}{D_j}\right)+\left(\frac{2}{D_k}\right)+\left(\frac{2}{D_v}\right)\right]^2 \tag{3.2}$$

In order to produce a constriction size distribution, the frequency of each possible constriction size must be determined. The constriction of diameter D_v is formed by 3 particles with diameters D_i, D_j, and D_k (Equation 3.2). Hence, the probability of occurrence, P_v, of the constriction size D_v, is a function of the probability of occurrence of the three particle sizes, taken from the filter PSD. P_v is calculated using Equation (3.3),

where r_i, r_j and r_k represent the number of times the particle diameters D_i, D_j, and D_k appear in the combination of three particles being considered. Hence, r_i, r_j and $r_k = 0, 1, 2$ or 3 and $r_i + r_j + r_k = 3$. The most dense constriction size distribution, CSD_{MD}, is then the cumulative distribution of constriction sizes D_v, and the corresponding probability is P_v.

$$P_v = \frac{3!}{r_i! r_j! r_k!} (P_i)^{ri} . (P_j)^{rj} . (P_k)^{rk} \qquad (3.3)$$

Now consider the least dense particle packing geometry (Figure 3.3a), where the constriction is represented by the shaded area formed by four particles. Silveira et al. (1975) noted that the geometry of the least dense packing problem is very difficult to solve directly. A simplifying assumption is made, that the constriction size is equivalent to a circle with the same area as the enclosed area formed by four tangent particles, ie. the shaded area of Figure 3.3b. This shaded area has the same area, S_v, as the equivalent circle of diameter D_v, in Figure 3.3c.

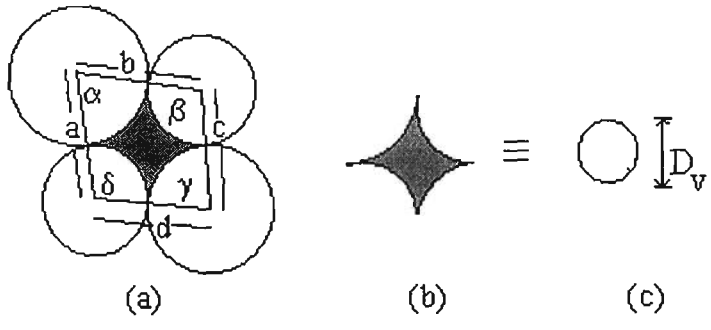

Figure 3.3 a) Pore constriction formed by 4 particles b) Constriction area formed by tangent particles, S_v c) Circle of equivalent area

The constriction area S_v (Figure 3.3b) is the area of two triangles with sides a,b and c,d (dimensions are defined in Figure 3.3a) and a common diagonal minus the area of the enclosed sector of each particle, which gives:

$$S_v = \frac{adSin\alpha}{2} + \frac{bcSin\gamma}{2} - \frac{1}{8}\left(D_i^2\alpha + D_j^2\beta + D_k^2\gamma + D_m^2\delta\right) \qquad (3.4)$$

The angles β, γ and δ can be related to α by geometry. The angle α should be varied so that S_v is a maximum, giving the maximum constriction size. Then the equivalent pore diameter D_v is:

$$D_v = \sqrt{\frac{4S_v}{\pi}} \qquad (3.5)$$

The probability of occurrence of the combination of four filter particles producing a constriction with diameter D_v is given by:

$$P_v = \frac{4!}{r_i! r_j! r_k! r_m!} p_i p_j p_k p_m \qquad (3.6)$$

In the lease dense packing state, pore constrictions usually do not form on a plane through the centres of the four particles making up the constriction. If a plane is cut perpendicular to the direction of water flow and through the centre (smallest cross section) of the void constriction it will most likely intersect the four particles at various apparent diameters, which will be smaller than the actual diameter. Schuler (1996) suggests that the mean of all possible chord lengths through the circular particle be used to represent the apparent diameter of particles, ie. a diameter of 0.82 times the actual diameter may be used. This seems a reasonable assumption since the mean chord length represents the mean of all apparent diameters on all planes through the spherical particle.

The two geometric cases shown in Figure 3.2 represent the extremes of relative density. Real filters are unlikely to exist either in the most dense or least dense states, but rather at some intermediate density. A more representative pore model should also consider the filter relative density. Schuler (1996) examined the CSD of a soil at varying relative

density and proposed that all the CSD curves have the same shape. However, Giroud (1996) suggests that in certain locations within a medium dense to dense granular material, a number of particles will group together to form a maximum density arrangement. These two observations imply that, within a granular filter, the smallest pore constrictions will be the same size regardless of the filter density, and the distribution of coarser pore constrictions will vary, having the same shape as the minimum and maximum CSD curve. The assumption is made that the coarser pore constrictions increase in size proportionally (ie. linearly) with a decrease in relative density, between the most dense and least dense packing models. In addition, the smallest constrictions are equal in size to the smallest constrictions of the *most dense* packing arrangement. This allows a simple formulation for the actual CSD based on: (a) the most dense CSD, (b) the least dense CSD and (c) the filter relative density, R_d, defined in Equation (3.7). The actual CSD is calculated using Equation (3.8). The *most dense* and *least dense* constriction size distributions are divided into n discrete portions. The integer i represents these discrete portions of the CSD such that i/n is the fraction of constrictions finer than constriction diameter $D_{v,i}$, representing the median diameter of the i^{th} portion of the CSD.

$$R_d = \frac{e_{max} - e}{e_{max} - e_{min}} \tag{3.7}$$

$$D_{V,i} = D_{VMD,i} + \frac{i}{n}(1 - R_d)(D_{VLD,i} - D_{VMD,i}), i = 0,1,2,...n \tag{3.8}$$

where, $D_{VMD,i}$ and $D_{VLD,i}$ are the $(100\, i/n)\%$ coarsest constrictions from the most dense and least dense constriction size distributions respectively. To explain the application of Equation (3.8), for i=0 the finest constriction diameter $D_{v,0}$ is the finest diameter of constrictions from the most dense CSD. If n=20, then i=1 corresponds to the constriction

diameter with 5% (or 1/20) of constrictions finer. The actual constriction diameter for 5% passing, ie. $D_{v,1}$, is found using Equation (3.8).

The pore model then consists of a 3D cubic network of pores with six constrictions connecting each pore to its neighbours, as shown in Figure 3.1. The size of each constriction is randomly generated from the CSD, which is calculated based on the filter PSD and relative density. Figure 3.4 shows the predicted CSD for the least dense, most dense and two intermediate cases (R_d= 0.8 and 0.5). As can be seen, the intermediate constriction size distributions have similar shape and share the same finest point.

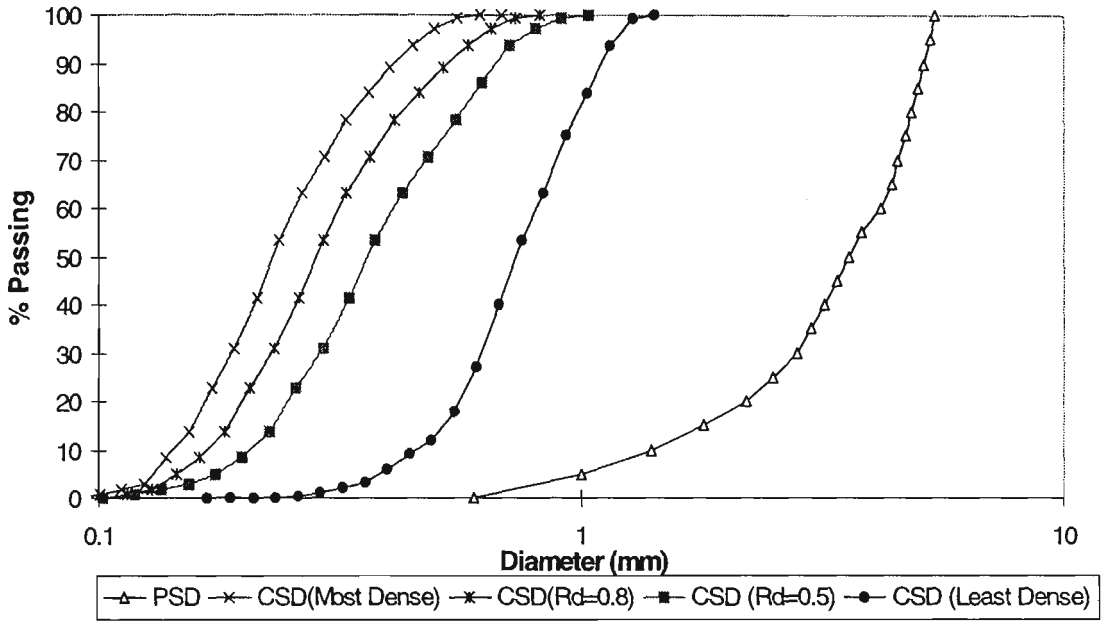

Figure 3.4 Comparison of Constriction Size Distributions at various relative densities.

3.2.3 Constriction Sizes of Broadly Graded Materials

Broadly graded base and filter materials present a further problem in modelling, particularly the determination of the constriction size distribution (CSD). In some cases, the fine particles may not contribute to the stable structure of the soil, but may be loose within the pores formed by the stable skeleton of larger particles. In the opposite case, the coarse particles may be 'floating' in a matrix of fines. The voids between these coarse

particles are filled with finer particles, and no large voids remain. These two structures are shown in Figure 3.5, the difference in particle sizes is exaggerated to demonstrate the concept. In either case, the filter PSD should be truncated to discount particles that do not contribute to the CSD.

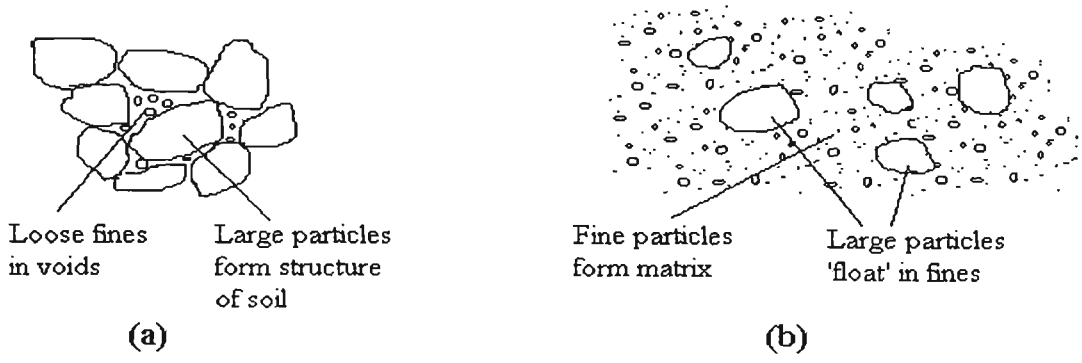

Figure 3.5 a) Fine particles loose between soil skeleton, b) Large particles floating in a matrix of fines.

Skempton and Brogan (1994) define an 'ideal' grading curve, represented by Equation (3.9), which defines a sequence of grading that allows all voids to be infilled and provides the most dense possible particle arrangement when compacted, ie. fine particles exactly fit between the voids formed by coarser particles. The ideal curve is plotted in Figure 3.6. If there are excess fines than predicted by this ideal curve (ie. the PSD has a longer fine tail than the ideal curve) then some fine particles will be loose within the soil skeleton and the material will be internally unstable. Alternatively, if the coarse particles are larger than predicted by the ideal curve (ie. the PSD stretches to the right of the ideal curve), these coarse particles will be floating within a matrix of fines, because there is insufficient quantity of the size fraction required to fill the voids between these particles. An unstable and a stable grading are shown in Figure 3.6. The ideal curve is given by Equation (3.9), where, S_n is the fraction passing diameter D_n and D_{max} is the largest particle diameter.

$$S_n = \sqrt{\frac{D_n}{D_{max}}} \tag{3.9}$$

Equation (3.9) can be re-written to relate different particle sizes within the grading curve and eliminate D_{max}. The equation becomes:

$$D_n = D_m \left(\frac{S_n}{S_m} \right)^2 \tag{3.10}$$

where, S_m is the fraction passing diameter D_m. By noting that fine particles are loose if D_n is finer than predicted by Equation (3.10). By substituting m=2n into Equation (3.10), particles finer than D_n are loose within the soil skeleton if:

$$D_n < \frac{D_{2n}}{4} \tag{3.11}$$

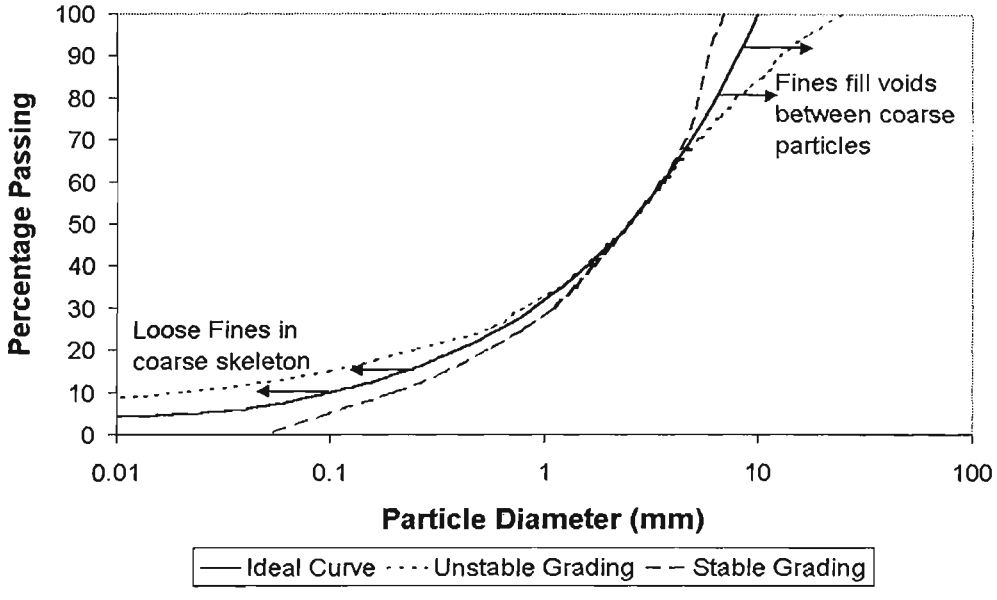

Figure 3.6 Ideal curve and stable and unstable filter gradings

Equation (3.11) can also be used to describe the upper portion of the PSD curve, ie. particles coarser than D_{2n} will float in a matrix of fines if D_{2n} is coarser than $4D_n$. Therefore, combinations of particles coarser than D_{2n} do not contribute to the constriction size distribution. These coarse particles are still present and combine with smaller particles to form constrictions, but do not meet particles of the same size. Only the finer and coarser particles should be considered for truncating the PSD by this method, and in

the current modelling, the finest 20% and coarsest 20% have been examined. If $D_{20}<D_{40}/4$, then it is assumed that all particles finer than D_{20} are loose within the soil and the PSD is truncated to consider only particles coarser than D_{20}. If this is not the case then progressively finer diameters are considered (ie. consider $D_{15}<D_{30}/4$ etc.), in order to find the coarsest particle size for which Equation (3.11) is true.

Similarly for the coarsest 20% of the PSD, if $D_{80}>4D_{40}$, then the particles coarser than D_{80} do not form constrictions. If $D_{80}<4D_{40}$ then D_{2n} is incrementally increased to find the finest D_{2n} for which Equation (3.11) is true. The truncated PSD, determined in this fashion, is then used to calculated CSD_{MD} using Equations (3.2) and (3.3), and also using Equations (3.5) and (3.6) to calculated CSD_{LD}. Equation (3.8) then defines the actual CSD based on the relative density of the filter.

A complete geometric model of the filter has now been developed. A three-dimensional network of pores connected by constrictions in a cubic arrangement describes the filter voids. The size of pore constrictions is randomly determined from the constriction size distribution. Next the analysis will consider how far the base soil can infiltrate into the granular filter model.

3.2.4 Particle Infiltration Depth

A method will be described to estimate the distance a base soil particle of diameter *d*, can infiltrate into the three-dimensional pore network model (Figure 3.1). The particle infiltration depth is predicted by a probabilistic analysis of the particle sizes, represented by the base soil PSD and the filter constriction sizes from the filter CSD. If a particle is smaller than a constriction, then it can move through to the next pore. The probability

that a base particle of diameter d, can pass a single, random constriction can be denoted by p, which is the cumulative probability of pore constrictions larger than d (the fraction of constrictions coarser than d, from the CSD). Therefore, the probability of the particle moving one step through the network model in the direction of flow from the fist pore (a *forward step*), is p. The assumption is made that, if the particle cannot make a forward step from the first pore, then the particle may move in any of the four directions perpendicular to the flow, if there is a pore constriction larger than the particle. It is assumed that the particle cannot move against the flow direction or return to the pore from which it originated. Hence, if the particle does not move forward, within the sample space (1-p), then there are four possible perpendicular exits (a *sideways step*). The probability of perpendicular (sideways) movement, $P(1S)$, is then:

$$P(1S) = \left[1 - (1-p)^4\right](1-p) \tag{3.12}$$

Within the next pore (after any sideways step), the particle again has a probability p of moving forwards in the direction of flow. Hence the conditional probability of a forward step, within the first pore or any of the neighbouring four pores, P(F|1S), is:

$$P(F|1S) = p + \left[1 - (1-p)^4\right](1-p)p \tag{3.13}$$

Equation (3.13) can be extended to consider the probability of one or more additional sideways steps before a forward step, recognising that there are now only three possible sideways exits from the pore. Continuing this process leads to Equation (3.14), describing the overall probability of one forward step after any number of sideways steps, P(F), in the direction of flow through the network model:

$$P(F) = p + \sum_{i=0}^{\infty}\left[1 - (1-p)^4\right](1-p)p\left\{\left[1 - (1-p)^3\right](1-p)\right\}^i \tag{3.14}$$

where, $i+1$ is the number of sideways steps before a forward step. Noting that the series term of Equation (3.14) tends to zero as i increases, it is possible to neglect higher order terms beyond the first 3-4 terms. In reality, it is possible that a particle encountering a constriction in the direction of flow, through which it cannot pass, would be retained in that void by fluid drag forces, rather than making a perpendicular movement. However, the intention here is to model the worst possible geometric case. Hence, unhindered perpendicular movement (sideways steps) has been considered. Silveira (1965) proposed a method to determine the number of confrontations, n, with randomly generated pore constrictions, required to stop a particle moving forwards through the filter, with a level of confidence $\overline{P}$. This equation can be adapted to consider the number of layers a particle can move through the pore network model, based on the probability of passing one layer, P(F):

$$n = \frac{\ln\left(1-\overline{P}\right)}{\ln P(F)} \tag{3.15}$$

This equation defines the depth of infiltration of a base particle of diameter d into the filter, expressed as a number of layers of the three-dimensional network model. This is based on the constriction size distribution and level of certainty $\overline{P}$. A certainty level of 50% could be adopted to determine the mean expected infiltration depth. Of greater concern is the probabilistic maximum infiltration depth of particles, thereby a higher level of certainty is required. Soria et al. (1993) adopted a value of 98% in their analysis, while Silveira (1993) suggests a value close to 100% as appropriate. Figure 3.7 shows the probability of forward movement, P(F), against the probability of passing one constriction, p (shown as the solid line). Also shown on the right hand y-axis, is the predicted number of layers a particle can infiltrate the filter for three values of $\overline{P}$ (from Equation 3.15). The trend of the predicted infiltration depth is similar for each value of

$\overline{P}$, tending to increase rapidly at some critical probability. This rapid increase in infiltration depth occurs at increasing probability p, as the certainty, $\overline{P}$, is increased. As previously described, the CSD curve is significantly steeper (ie. more uniform) than the PSD curve (see Figure 3.4). This means that there is only a small variation in the constriction size corresponding to the various critical values of p. Therefore, the constriction diameter corresponding to the critical probability for various values of $\overline{P}$ will not vary greatly. This suggests that the model is not sensitive to the chosen value of certainty, $\overline{P}$. A value of $\overline{P}$=95% has been adopted for the current modelling, as this gives a reasonable correlation with other models. The predictions of Figure 3.7 could be used to estimate the infiltration depth of particles into clean filters, based on the probability of a particle passing a single constriction (p) and the predicted infiltration depth 'n'.

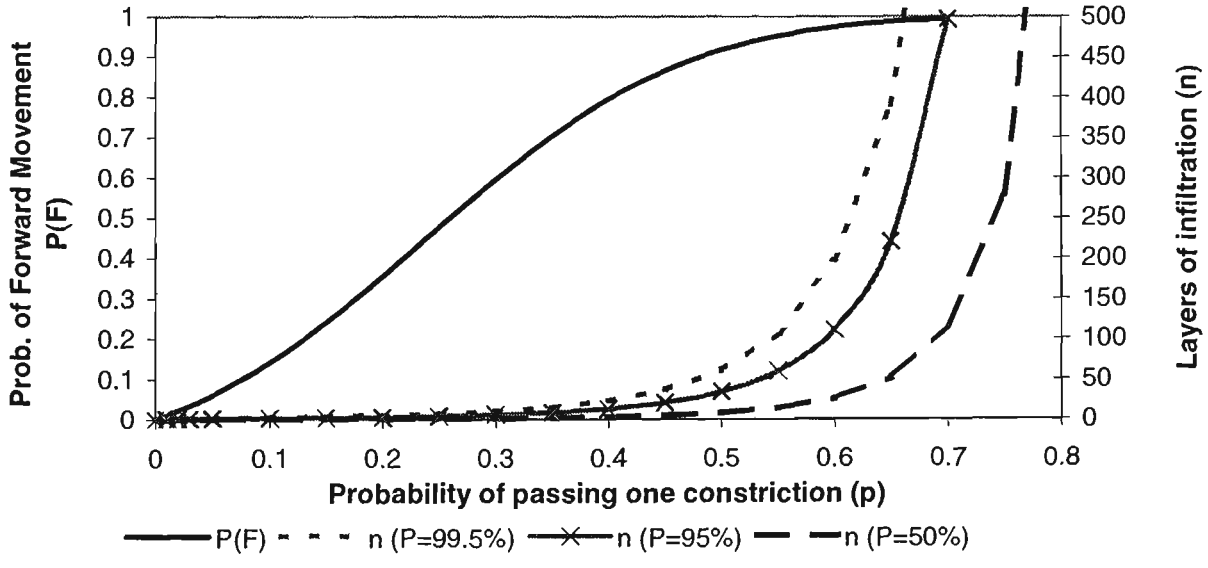

Figure 3.7 Infiltration Model – Probability of forward movement and predicted depth of infiltration.

Now it remains to find the spacing of the network (distance between pores) to determine the actual depth of infiltration into the filter. The filter voids were assumed to be represented by a cubic network of pores with an equal distance between each pore (Figure 3.1). This distance is described as a *unit step* in many previous models. Since constrictions form near the centre of a filter particle and the next constriction will form near the centre of the next filter particle, it seems reasonable to adopt the mean filter particle size, $D_{f,mean}$ as a unit step. This mean particle diameter should be based on the actual number of particles not the PSD by mass. Multiplying the unit step by the number of layers 'n' the particle can infiltrate, the expected length of infiltration (L) of a base soil particle into the filter is:

$$L = \frac{\ln\left(1-\overline{P}\right)}{\ln P(F)}.D_{f,mean} \qquad (3.16)$$

This completes the geometric model of filter voids and the expected infiltration depth of individual base soil particles of varying diameter into the filter. Hence, the behaviour of each individual base soil particle can be predicted, based on the filter PSD and relative density and the base soil particle size. In order to describe the overall behaviour and time-dependent changes within the filter, the rate of particle transport must be determined.

3.2.5 Rate of Particle Transport

Base soil particles are dislodged and transported into the filter due to drag forces exerted by the seepage water. Indraratna and Vafai (1997) developed a comprehensive particle transport model to simulate particle movement within granular media for non-cohesive soils. In this model, all base soil particles finer than the filter voids are assumed to be loose and available to be transported. These loose soil particles are assumed to be

suspended in a homogeneous slurry, the rate of movement of this slurry is controlled by the governing differential equations of conservation of mass (Equation 3.17) and momentum (Equation 3.18), relating the slurry flow velocity and density changes with time and distance. The current model extends these concepts by incorporating the infiltration depth of particles into the cubic network structure, as developed in Section 3.2.4.

$$\frac{d(\rho_m u)}{dz} = \frac{d\rho_m}{dt} \tag{3.17}$$

$$\sum F = \rho_m V_m \left(\frac{du}{dt} + u \frac{du}{dz} \right) \tag{3.18}$$

In Equations (3.17) and (3.18), ρ_m, V_m and u are the slurry density, volume and velocity respectively, while ΣF represents the external forces acting on the slurry, including the external hydraulic gradient and fluid drag. If the flow is laminar, then the rate of change of velocity will be negligible ($du/dt \approx 0$), and the flow velocity can be determined from Darcy's law. The external forces in Equation (3.18) include surface forces due to hydrodynamic pressure and the body forces resulting from gravity and viscous drag. Defining R as the viscous drag per unit mass of the slurry, and P as the hydraulic pressure, the external forces can be determined from:

$$\sum F = -\frac{\partial P}{\partial Z} V_m - \rho_m g V_m + \rho_m R V_m \tag{3.19}$$

The Indraratna and Vafai (1997) model assumes that the pore water and loose particles move at the same speed, and ignores the additional friction and energy loss due to particles in the flow. However, the drag forces necessary to mobilise the base soil particles will reduce the available energy in the flow, and also reduce the flow velocity. Observation of the flow of particles through a filter has revealed that particles generally move in intermittent bursts. A stream of particles will pass one obstruction (small

constriction) and move through a number of similar confrontations, until stopping again due to bridging of the particles over another constriction. These particles may later become mobile again and repeat the process. Joy et al. (1993) described this process with a stochastic model of the probabilities of movement, however, the model parameters are difficult to estimate and would greatly confuse the current particle transport modelling. In order to estimate this increased energy loss due to entrained particles, the current model adopts the simplifying assumption that the pore water and particles move as a mixed, homogeneous slurry. Because the slurry contains suspended particles, its viscosity (η) is higher than that of clear water (η_0). A relation developed by Happel and Brenner (1965) is adopted to determine the increase in viscosity due to interaction effects between the particles and pore walls, based on the slurry volumetric concentration (C), as given by:

$$\frac{\eta}{\eta_0} = 1 + 2.5C\left(1 + \frac{5dD_v}{8(2D_v - d)^2}\right) \qquad (3.20)$$

In the above expression, d may be taken as the mean diameter of loose particles, and D_v as the mean pore constriction diameter. This increase in viscosity causes an increased energy loss in the flow. This can be represented by decreasing the effective media permeability (k), ie:

$$k = k_w \frac{\eta_0}{\eta} \qquad (3.21)$$

where, k_w is the media permeability to flow of pure water. Visual observation of the filtration process revealed that large base soil particles travel at a slower rate than finer particles, as expected. Faure and Gendrin (1989) and John and Watson (1996) separately examined soil washout through geotextile apertures, and they showed that particles coarser than half the aperture diameter would form bridges over the geotextile opening. Bridging is a process where particles smaller than an opening form a 'log-jam' over the

opening and do not pass through (Section 2.1.3). While bridging is not relied on to retain particles in this current model of granular filters, it can be assumed that base soil particles with a diameter greater than half the pore constriction diameter will move at a slower rate than finer particles, due to partial retardation by bridging. In the current analysis, it is assumed that the base particles coarser than half the mean constriction size move at half the pore water velocity, while finer particles move at the same velocity as the pore water.

3.2.6 Complete Transport Model

The two independent models developed so far, ie. a geometric prediction of particle infiltration depth and the particle transport equations, can be combined by considering a number of elements at the base - filter interface (Figure 3.8a). A finite difference or finite element solution to the differential equations of conservation of mass and momentum can model the movement of loose particles. The rate of particle erosion and movement is determined from the slurry density ρ_m and velocity u, determined from Equations (3.17) and (3.18), as summarised in Figure 3.8b, where the slurry density ρ_m is limited by the fraction of base soil fines able to infiltrate the filter.

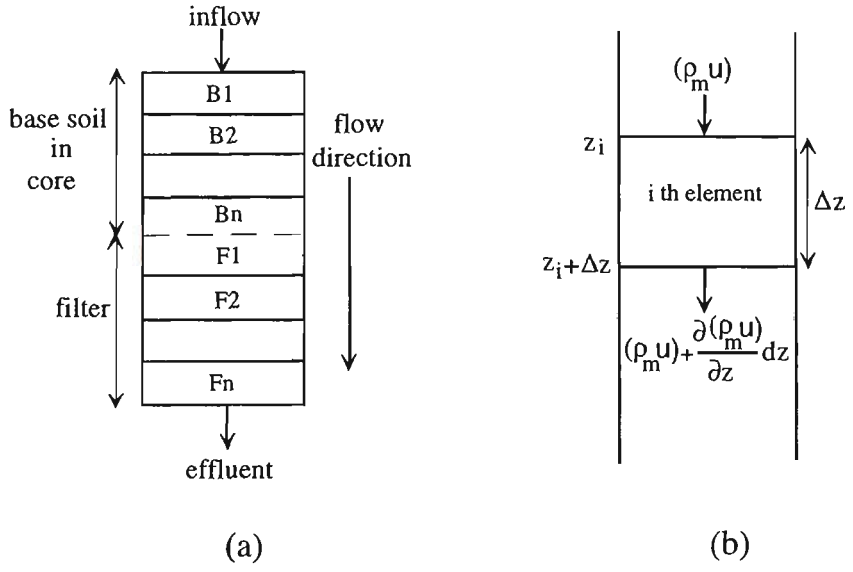

Figure 3.8 Illustration of (a) base and filter elements and (b) generalised flow of slurry through a filter element (Indraratna & Vafai, 1997)

The length of infiltration into the filter, incorporating Equation (3.16) to determine the infiltration distance, L, models the geometric constraint to movement. In order to use Equation (3.16) to determine whether particles can move from one element to the next, it is necessary to define three base particle size ranges for each filter element:

1. Fine particles that have an infiltration distance (L) greater than the distance from the filter interface to the end of the element; these particles can pass through the element. The coarsest diameter in this particle size range, corresponding to an infiltration distance (L) equal to the distance from the filter interface to the end of the element, is defined as the diameter passing the element, d_p.
2. Particles larger than d_p, which can pass more than one unit step into the filter element, ie. $n>1$ in Equation (3.15), are considered as moving into the next element and are then retained within the element. Once a particle is retained in an element, it cannot be moved further. The coarsest particle within this range (the particle diameter corresponding to n=1) is defined as the retained particle diameter d_r.
3. Particles coarser than d_r, which cannot pass one unit step into the filter element, remain in their current location.

The diameters d_p and d_r are determined for each base soil and filter element. It is assumed that particles larger than diameter d_r, that cannot pass one unit step, into the next filter element are retained within the previous element. This particle size, d_r, corresponds approximately to the 95% largest filter void. It seems reasonable that particles larger than this cannot move into the next element, while particles smaller, within the size range d_p to d_r, may move a small distance before being retained. Particles finer than diameter d_p move through to the next element and remain in suspension. The retained particles are

essential in the formation of a self-filtering zone. Once retained, these particles form part of the element PSD, resulting in smaller pore constrictions that are able to retain finer base particles. At the next time-step the diameters d_p and d_r will be smaller. Eventually through this time-dependent retention of finer particles, the diameter of pore constrictions becomes smaller than the finest base soil particles, and the filter interface will stabilise. This is the important advantage of modelling the time-dependent changes in the filtration process.

In order to solve the governing differential equations, (3.17) and (3.18), initial conditions are required for the flow velocity and slurry density. It is assumed that all particles finer than d_r can be mobilised, and there is no selective erosion of finer particles. Therefore, the maximum density of the slurry is limited by the volume fraction of particles finer than d_r within each element. However, very high flow concentrations have not been observed in laboratory testing. Calibration against laboratory observations suggests that the initial maximum slurry concentration should be limited to 20-25% solids by volume. Within each element, the initial slurry density is determined from the minimum of either the volume of solids within the element finer than d_r, or the maximum concentration of 20-25%. The filter elements will usually have zero initial particle concentration (ie. the slurry density is the density of water), unless the filter fines are internally unstable. The initial flow velocity is determined by Darcy's equation, based on the applied head and the combined permeability of the base soil and filter. During the analysis, a further boundary condition is that the seepage water entering the first base soil element has zero particle concentration.

The rate of movement of the loose material is controlled by the equations of conservation of mass and momentum. A finite difference procedure is used to apply these equations. Equations (3.17) and (3.18) can be discretised in a finite difference process as:

$$\frac{\rho_{mi}^{t+1} - \rho_{mi}^{t}}{\Delta t} = -\left(u_i^{t} \frac{\rho_{mi+1}^{t} - \rho_{mi}^{t}}{\Delta z} + \rho_{mi}^{t} \frac{u_{i+1}^{t} - u_i^{t}}{\Delta z} \right) \tag{3.22}$$

$$\sum F = \left(\rho_{mi} V_{mi}\right)^{t} \left[\frac{u_i^{t+1} - u_i^{t}}{\Delta t} + u_i^{t} \frac{u_{i+1}^{t} - u_i^{t}}{\Delta z} \right] \tag{3.23}$$

where, the subscripts refer to the element number, and the superscripts refer to the time step. From Equations (3.22) and (3.23), the change in slurry density (ρ_m) and the slurry velocity (u) can be determined within the time-step Δt. The flow rate is easily determined from the continuity equation, according to the slurry velocity and element porosity.

The volume of particles moving between elements is defined by the slurry density and velocity, while the size distribution of these loose particles is governed by the diameter d_r and the base soil PSD. The following describes how the PSD of each element at any given time is computed based on the mass and PSD of the element at the previous time step and the subsequent rate of erosion and retention.

3.2.7 Prediction of Change in PSD

The total volume of effluent from an element (V_{out}), the volume of soil eroded from the element (V_{Sout}), and the volume of water flowing out of the element (V_{Wout}) for each time-step, are related to the effluent flow rate, Q, where:

$$V_{out} = Q\Delta t = V_{Sout} + V_{Wout} \tag{3.24}$$

An overall mass balance of soil, water and slurry gives:

$$\rho_S V_{Sout} + \rho_w V_{Wout} = \rho_m V_{out} \tag{3.25}$$

Solution of Equations (3.24) and (3.25) yields the values of V_{Sout} and V_{Wout}. The total volume of solids in element *i* can be determined from Equation (3.26), incorporating the balance between the solids in the incoming slurry from element *i*-1 and the outgoing material from element *i* during the time period Δt:

$$\left(V_S\right)_i^t = \left(V_S\right)_i^{t-1} + \left(V_{Sout}\right)_{i-1}^t - \left(V_{Sout}\right)_i^t \qquad (3.26)$$

If in element *i* there are S_r% of particles finer than diameter d_r, then the volume of soil corresponding to each discretised diameter range, *j*, can be estimated by (Indraratna & Vafai, 1997):

$$(V_{Sout})_j^t = (V_{Sout})^t \frac{P_j^{t-1}}{S_r} \qquad (3.27)$$

$$P_j^t = \frac{(V_s)_j^{t-1} - (V_{Sout})_j^t}{V_s^t} \qquad (3.28)$$

In the above equations, P_j is the percentage of soil by total volume (V_s) corresponding to a specific diameter j. Particles of diameter, d_j, within the size range $d_p<d_j<d_r$ are retained in the next element, whereas finer particles, $d_j < d_p$, will remain in suspension and pass through to the next element. These suspended particles should not be considered as part of the PSD for calculating the CSD of the element in the next time-step. This analysis predicts the gradual change in particle size distribution of the base and filter elements; hence, it describes what is occurring at the base - filter interface with time for the entire particle size range.

3.2.8 Change in Element Permeability

As particles are eroded, transported and retained, the permeability of each element will change. The coefficient of permeability of non-cohesive granular soils is governed by the finer particles in the soil. Koenders and Williams (1992) present Equation (3.29) to

determine the permeability of a granular soil, based on the mean particle diameter ($D_{f,mean}$) and porosity n_e. This equation has been incorporated in the current particle transport model, to determine the base soil and filter permeability at each time-step.

$$k = \frac{1}{\eta}\left(D_{f,mean}\right)^2 n_e \chi \left(\frac{n_e}{1-n_e}\right)^2 \qquad (3.29)$$

where, $\chi = 0.0035 \pm 0.0005$. Permeability is a complex combination of different soil properties including particle size and shape, density, mineralogy, fabric, etc. For simulating the behaviour of real materials, It would be advisable to calibrate the model by varying the constant, χ, in Equation (3.29) so that the predicted initial permeability matches the measured initial permeability. Then the model should predict the changes in permeability more accurately.

3.2.9 Change in Element Porosity

The time dependent change in porosity (and relative density) of each element can be estimated based on the original porosity and the changes in void space within each element. This can be related to the volume of water in each element, which can be calculated from:

$$\left(V_W\right)_i^t = \left(V_W\right)_i^{t-1} - \left(V_{Wout}\right)_i^t + \left(V_{Wout}\right)_{i-1}^t \qquad (3.30)$$

where, V_{Wout} is calculated from Equations (3.24) and (3.25). Assuming full saturation of the elements and considering the total volume of each element to be V_T, the porosity of the element is given by:

$$n_i = \frac{\left(V_W\right)_i}{\left(V_T\right)_i} \qquad (3.31)$$

The entire process described above is repeated at each time-step. The model is able to describe the rate of erosion and the distance base soil particles can infiltrate into a filter,

the formation of a self-filtration zone as these particles are retained, and the reduction in infiltration distance and eventual stabilising of the filter due to this self-filtration zone. The time-dependent changes in flow rate and particle transport, and the permeability and porosity of each element are predicted by the model, leading to a complete description of the filtration process. These time-dependent predictions can give a designer a better understanding of the rate of erosion and formation of a stable self-filtering interface or warning times before piping failure.

3.3 Comparison of Model Predictions with Published Research

The model has been implemented in a computer program using Visual Basic in Microsoft Excel, this allowed easy viewing and plotting of the data as the files were presented as simple spreadsheets. The model predictions have been calibrated and verified through a comparison with previously published laboratory results. While no published laboratory tests have examined the complete time-dependent changes within base soils and filters, some published results are relevant to certain modelling predictions. This section will firstly compare the filter pore model and CSD model with the published constriction and void size distributions of Soria et al. (1993) and Wittmann (1979).

Few published results describe the infiltration of particles into a filter. Kenney and Lau (1985) presented the changes in PSD of both internally stable and unstable materials after extended water flow, and Lafleur et al. (1989) examined the movement of broadly graded base soils into broadly graded filters. The changes in PSD and mass movement predicted by the current model will be compared with both of these published studies. Further verification of the model will be given in Chapter 6, where the model predictions are compared with published empirical design criteria, and Chapter 7 where several case studies are considered.

3.3.1 Verification of the Constriction Size Distribution Model

The filter pore model is essentially composed of two sections: the constriction size distribution (CSD) and the predicted length of infiltration into the cubic network model. In order to verify the constriction size distribution model (Section 3.2.2), the predicted CSD from the model is compared with the published results of two experiments, determining constriction and void size distributions. The first set of experimental data is

from Soria et al. (1993). These experiments used an indirect approach, passing uniform sized particles through filters of varying length to find what size particle could pass different filtration lengths, then back calculating the CSD, using a method proposed by Silveira (1993). Larger constriction sizes are found from particle infiltration into very thin filters and smaller constrictions from progressively thicker filters. The PSD and measured CSD, along with the CSD calculated by the method proposed in this paper, are shown in Figure 3.9. The predicted CSD corresponds closely with that measured by Soria et al. (1993), the coarser measured constrictions are slightly larger than those predicted because of inaccuracies in measuring the maximum size of particles that can move through very thin filters.

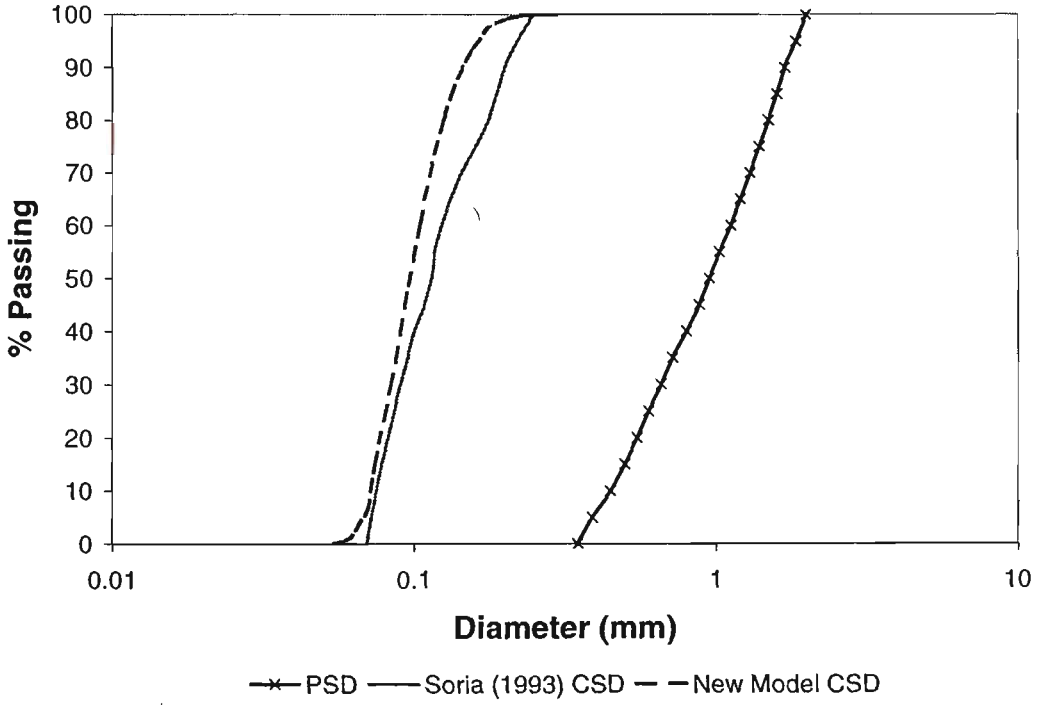

Figure 3.9 Comparison of calculated CSD with measured CSD of Soria et al.(1993)

The second set of published experimental data is from Wittmann (1979), who filled a gravel filter with resin, and cut slices through the solid material after the resin dried. Pore sizes on the face of each slice were measured using a planimeter. Because the slice is a plane through the random filter material, the slice does not intersect all of the pore constrictions. The pore sizes measured are neither the constrictions nor the pores, but fill a broad range between and including these extremes. Therefore, the CSD predicted by the current model is expected to be more uniform than the distribution measured by Wittmann (1979), with sizes equal to the smaller measured pores (Figure 3.10). The predicted CSD of Silveira's (1965) most-dense model is also shown for comparison; the shape of the two CSD curves is similar, but the new model predicts larger pores because the filter is not at its maximum density. In both sets of experimental data, the porosities or relative densities of the filters were not reported. A relative density of 80% was assumed by the writer.

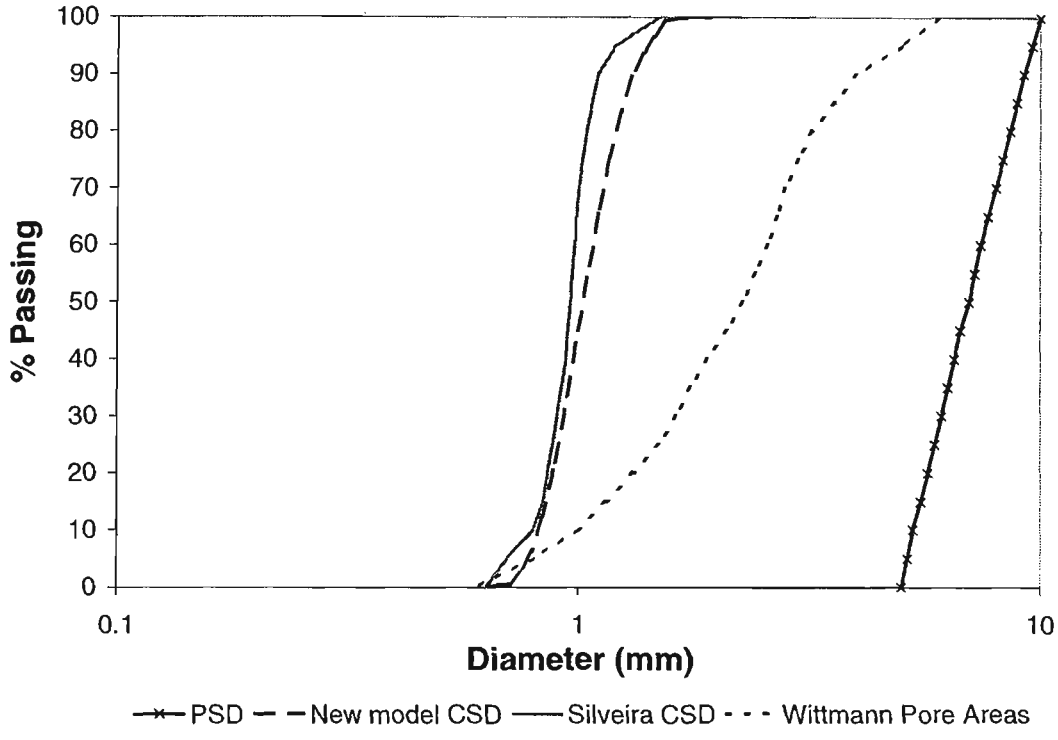

Figure 3.10 - Comparison of CSD model with measured pore sizes of Wittmann (1979)

3.3.2 Verification of the Infiltration Depth Model

To verify the infiltration length model, the predictions of Equation 3.16 can be compared with a number of other models for infiltration of particles of various sizes into a filter. The prediction of infiltration length requires both the CSD and probabilistic comparison of particle and constriction sizes within the pore network model. Therefore, verification of the infiltration length will confirm that the entire geometric model is predicting suitable results.

The general process of most analytical methods is to predict the depth of infiltration of base particles of different diameter. The models of Schuler (1996) and Humes (1996) lead to this directly. Witt (1993) and Kenney et al. (1985) define a controlling constriction size, which is a single diameter estimating the boundary between finer particles that will pass through the filter and coarser particles that are retained. Kenney et al. (1985) present two different formulae for the controlling constriction size based on D_{15} and D_5 of the filter, of which the coarser value is shown.

Chapter 2 presented a comparison of the infiltration distance of base particles into two different filter materials, as predicted by various models. The predictions of the new model will be compared with the predictions of the other models for these two materials. The first filter material is a uniform sand with D_{15}=1.3mm and a coefficient of uniformity C_u=2. The comparison is shown in Figure 3.11. All the models considered predict a rapid increase in infiltration length of particles near a diameter near the controlling constriction diameter defined by Witt (1993) and Kenney et al. (1985). The model of Humes (1996) predicts that a finer particle diameter is required for extensive infiltration. The Schuler (1996) model predicts a very rapid increase in infiltration distance, which is unlikely to

occur in reality. The model proposed in this chapter predicts a rapid increase in infiltration from 5mm for a 0.27mm diameter particle to 20mm for a 0.25mm particle, and 100mm for a 0.23mm particle. This corresponds closely to the predicted controlling constriction diameter of 0.26mm. Hence, the model predictions are likely to be correct for uniform filters.

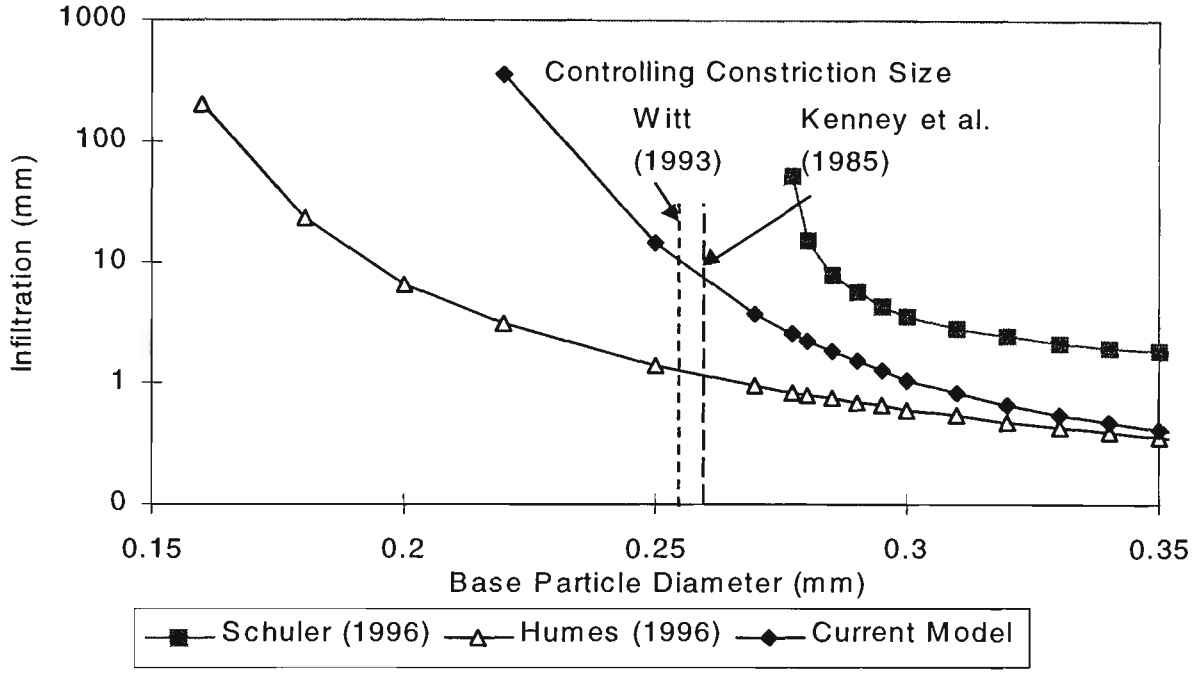

Figure 3.11 Comparison of Base Particle Infiltration Depth Models - Uniform Sand Filter, C_u=2, D_{15F}=1.3mm

Most infiltration models give similar predictions for uniform materials (C_u<3), but predictions become increasingly scattered for more broadly graded filters. Figure 3.12 describes the predicted depth of infiltration of particles of different diameters into a well graded gravelly sand, with a uniformity coefficient (C_u) of 6. The model of Schuler (1996) predicts a rapid increase in particle infiltration close to the controlling constriction size of Witt (1993) and Kenney et al. (1985). The model of Humes (1996) predicts that much finer particles are required for the same infiltration. As indicated in Figure 3.12, the current model predicts low infiltration depths similar to those of both Schuler (1996) and

Humes (1996) for base particles coarser than the controlling constriction size of Witt (1993), although the predicted infiltration depth for these coarse particles is greater than the depth predicted for infiltration into the uniform filter, which reflects the higher number of large pore constrictions in a well graded material. For particles finer than the controlling constriction size, the rapid increase in infiltration depth (log scale) implies the potential risk of wash out.

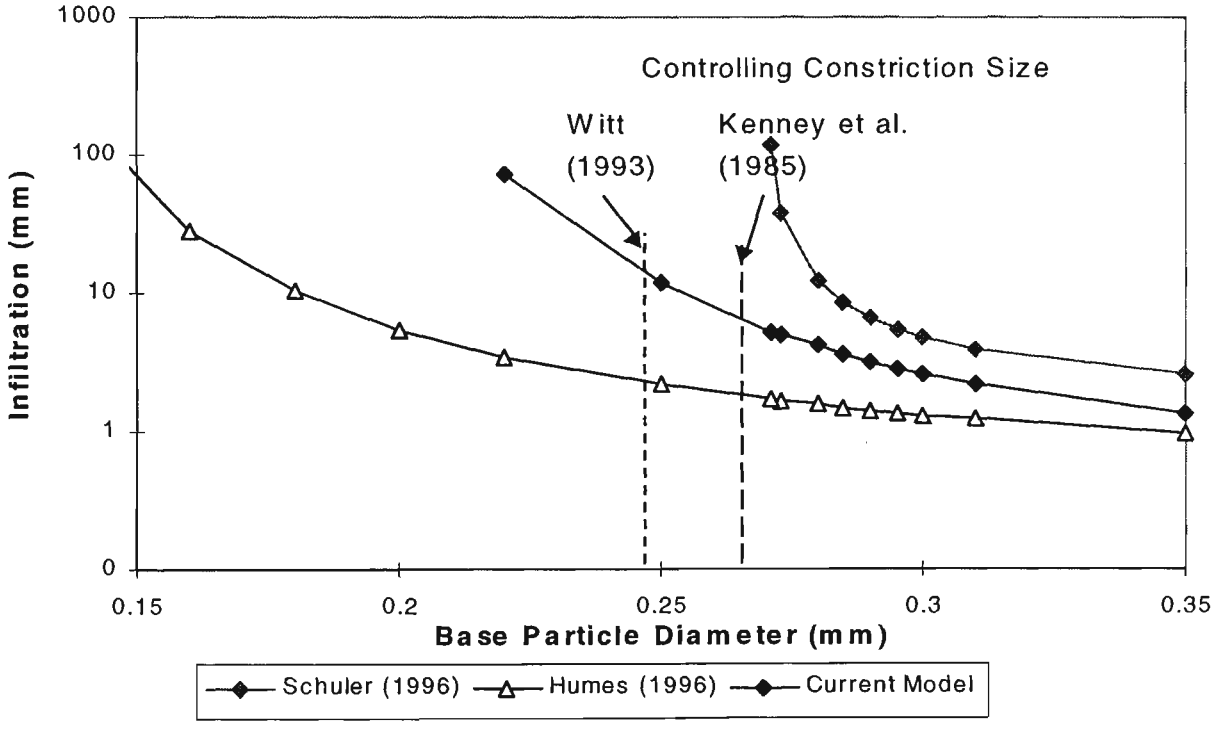

Figure 3.12 Comparison of Base Particle Infiltration Depth Models for Well Graded Sandy Gravel Filter, C_u=6, D_{15F}=1.3mm

3.3.3 Model Verification - Prediction of Internal Stability

In order to demonstrate the entire filtration model, the predicted changes in PSD of some broadly graded samples after prolonged seepage are compared with published laboratory data. Kenney and Lau (1985) describe a number of tests on broadly graded soils, measuring the extent of particle loss in different layers of the materials after prolonged water flow, to determine whether the material is internally stable or not. The

experimental data of Kenney and Lau (1985) includes the particle size distribution (PSD) of the soil elements before and after prolonged seepage. A sample of material compacted in a vertical cylinder was subjected to downward seepage flow. The material was retained with a wire sieve in the base of the apparatus. After testing, the sample was divided into layers (elements) and the PSD of each layer determined. Here, a comparison is shown between the model predictions and the measured particle size distributions for an unstable material (Figure 3.13), and a stable material (Figure 3.14). The predicted and measured PSD for several elements are shown. The sample was divided into five elements, with Element 1 as the top element and seepage vertically downwards.

For the unstable material (Figure 3.13), the predicted change in PSD is similar to that measured. In an unstable material, because the fines are eroded through the material, the PSD becomes increasingly coarser with time. Element 1 looses a significant amount of fines before stabilising. The model underestimates the loss of material from Element 1, this may be due to some dilation of the sample surface due to seepage during the experiment, allowing coarser particles to move. Subsequent elements loose a lesser amount of fines because fines from elements above enter and are retained within these elements. Hence, the overall change in PSD is smaller in subsequent elements than in Element 1.

For the stable material (Figure 3.14), the model again predicts a change in PSD similar to that measured. In a stable material, very little particle transport occurs and the initial and final PSD should be very similar. Element 1 looses some fines before stabilising. The remaining elements show insignificant changes in PSD, because the small amount of fines lost from each element is balanced by the mass retained from the previous element.

To summarise, the model predicts that material A is internally unstable (Figure 3.13), and material 3 is internally stable (Figure 3.14). These predictions are in accordance with the observations of Kenney and Lau (1985). The particle size distributions predicted by the model for each element within the experiment are close to those measured by Kenney and Lau (1985). The model slightly under-estimates the amount of base loss.

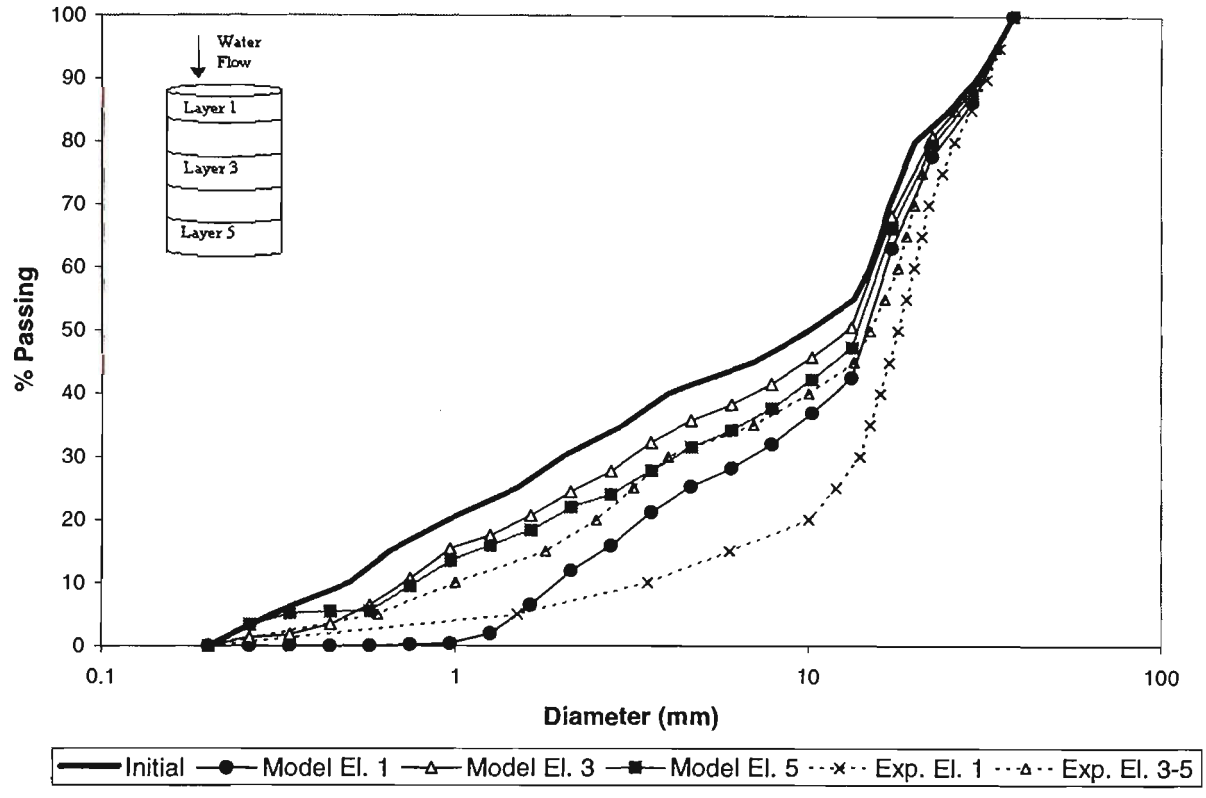

Figure 3.13 Comparison of Model and Experimental Results: change in PSD After Test - Unstable Material A (Kenney & Lau, 1985)

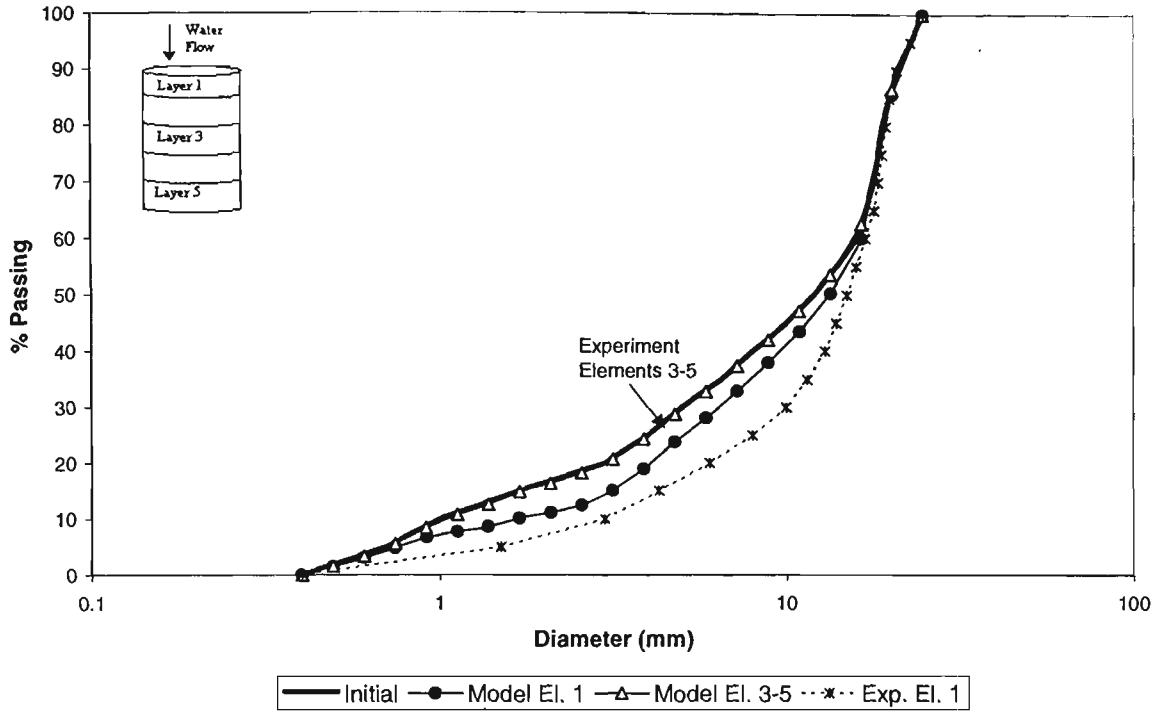

Figure 3.14 Comparison of Model and Experimental Results: change in PSD After Test - Stable Material 3 (Kenney & Lau, 1985)

3.3.4 Model Verification - Broadly Graded Materials

Most previous models of filtration have not been able to describe the behaviour of broadly graded soils. The current model will be compared with published laboratory tests to show its application to broadly graded materials. Lafleur et al. (1989) described a series of filtration experiments on broadly graded, non-cohesive base soils. Tests on a nearly-linearly graded base soil with C_u=40 (material B2) and a base soil with coarse particles floating in a matrix of fines with C_u=15 (material B6) are compared with the predictions of the current model. The PSD of these two base soils, and the four filter materials used, F2, F3, F4 and F5 are shown in Figure 3.15.

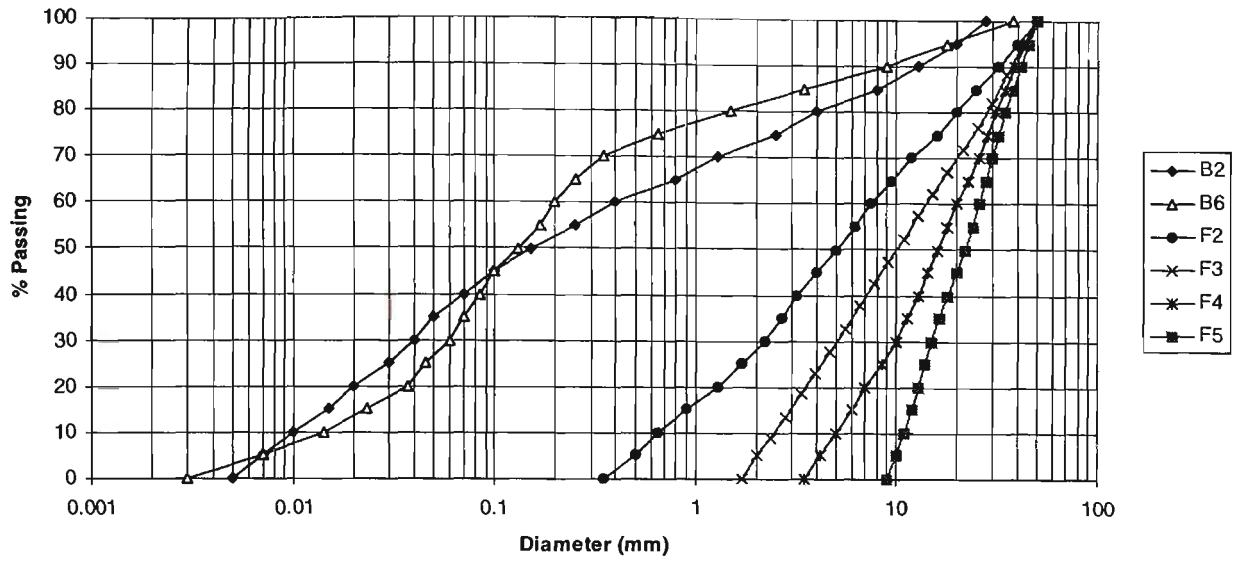

Figure 3.15 PSD of base and filter materials from Lafleur et al. (1989)

It is significantly more difficult to define success or failure of filtration of broadly graded base soils. The erosion of the base soil will eventually stop for most base soil - filter combinations, but the extent of base soil erosion may be unacceptable. It is the total mass of base soil lost before stable filtration is effected that is important in defining the success or failure of a filter. Figure 3.16 demonstrates the predicted mass of migrated particles against distance from the filter interface for base material B2 and the four different filters. The predicted mass passing through the filter (y-axis) is defined as the total mass of base material infiltrating a greater distance into the filter than the x-axis distance. Consequently, a rapid decrease in mass passing indicates a zone of particle retention. In all cases, the formation of a self-filtering zone near the filter interface can be clearly observed, where the majority of mass is retained. The mass required to form this self-filtration zone increases significantly as the filter D_{15F} size is increased. Figure 3.17 shows the extent of material loss for base soil B6, and again, the same self-filtering layer is visible.

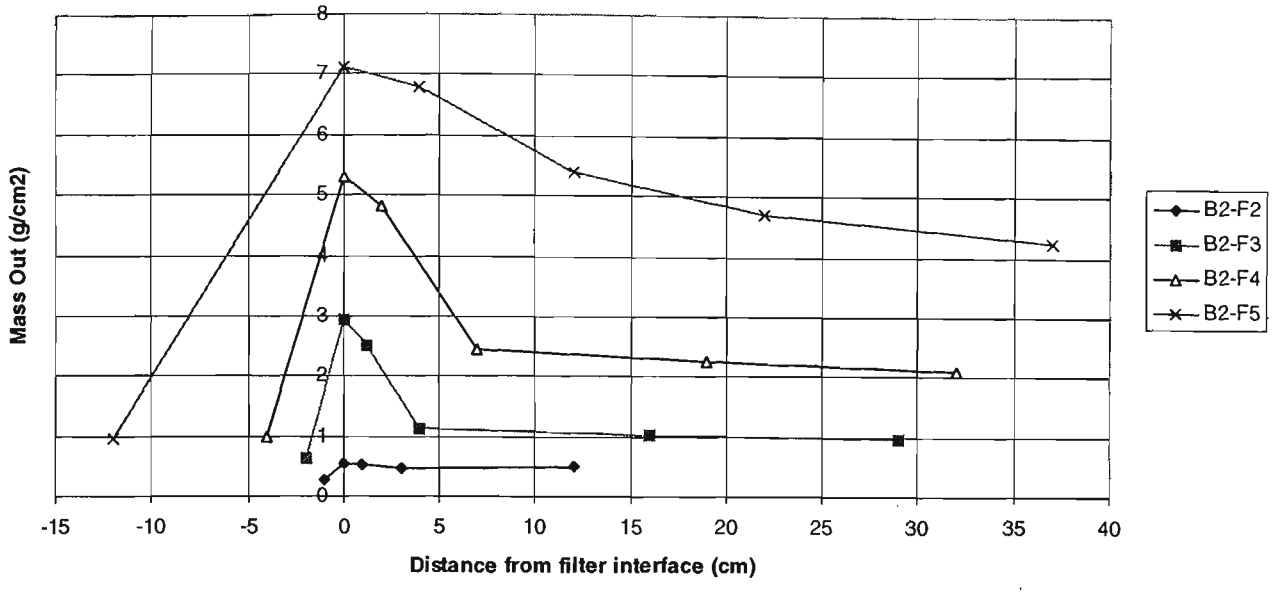

Figure 3.16 Predicted mass loss during filtration - material B2 protected by various filters

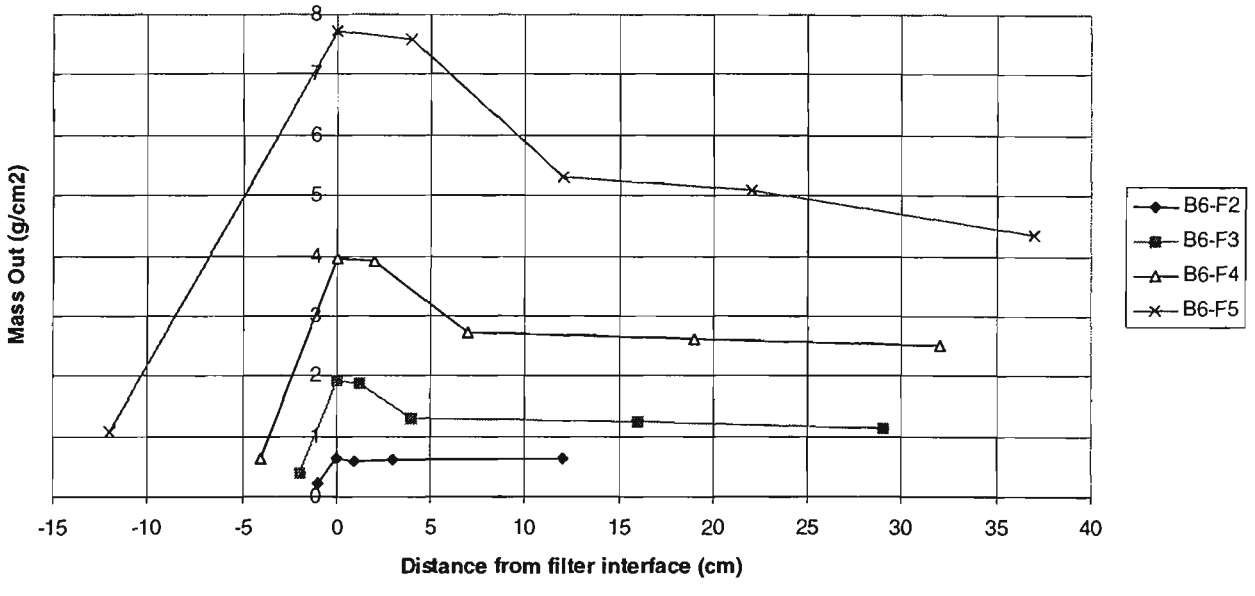

Figure 3.17 Predicted mass loss during filtration - material B6 protected by various filters

Lafleur et al. (1989) measured the mass of base soil particles washed out during filter tests on the two base soils. Their tests had a 15cm thick filter, so the predicted mass passing more than 15cm through the filter, from Figures 3.16 and 3.17, is compared with the measured values in Table 3.1. The predicted mass loss is approximately four times

the measured mass loss. This is partly due to the modelling assumption that any particle finer than the controlling constriction size, d_r, will move. The main reason for the difference may be that, as noted by Lafleur et al. (1989), the apparatus was not vibrated during the tests. As a result, bridging of base particles over the voids could occur, and the significant interlocking between silt and clay particles would prevent some fines eroding through the filter. Hence, it is expected that incomplete particle movement occurred in the lab tests. However, the trends predicted are similar, and the formation of a self-filtering zone is clearly visible in the model predictions.

Lafleur et al. (1989) adopted a mass loss of less than $0.25 g/cm^2$ in their experiments to define a successful base - filter combination. For the same combination, the model predicts a mass loss of about $1.0 g/cm^2$. Since the model uses a probability of passing constrictions of $\overline{P}$=95% and ignores the effects of soil arching and cohesion, it could be considered as representing the worst case for real conditions. Based on this, a predicted mass loss of less than $1 g/cm^2$ could be considered a successful filter.

Table 3.1 Predicted and measured mass of migrated particles in filter test.

	Base Material B2 - Mass loss g/cm^2		Base Material B6 - Mass Loss g/cm^2	
Filter	**Model**	**Lafleur et al. (1989)**	**Model**	**Lafleur et al. (1989)**
F2	0.5	0.12	0.7	0.13
F3	1.0	0.23	1.2	0.14
F4	2.3	0.54	2.7	0.69
F5	5.2	1.31	5.3	2.74

3.4 Comparison of Model Predictions with Laboratory Tests

The majority of filter tests performed to determine empirical criteria, have been carried out on fine base soils and sand filters. In an embankment dam, it is often necessary to construct multi-layer filters, where a gravel drainage layer is in contact with a sand filter. The normal filtration apparatus is only about 150mm diameter, and is not generally suitable for testing this sand - gravel filter interface. In order to test these materials successfully, a large-scale filter permeameter was purpose built for the project. This apparatus is a clear acrylic cylinder, 500mm diameter and 1m high, with steel endplates. A schematic diagram of the apparatus is shown in Figure 3.18. Filter material was placed and compacted in the cylinder to a maximum depth of 800mm. Finer gravel was placed around the top perimeter of the filter to a depth of about 50mm. This fine material is termed the *side material* (Sherard et al. 1984) and is intended to prevent the formation of large voids and preferential flow paths between the filter particles and the wall of the cylinder. Then a 100mm layer of base soil was placed and compacted above the filter. A layer of geofabric was placed and a small surcharge load of 2kPa applied to the base soil to prevent heave. Erosion was induced by a downward flow of up to 2.5 *l*/s. The flow was frequently interrupted (every minute) to avoid particle bridging and facilitate particle movement. After a test (usually of 1-2 hours duration), the filter was sampled at increasing depths to determine the change in PSD due to infiltration of base soil particles. The experiment was repeated for different base soil-filter combinations with varying filter retention ratios, D_{15F}/d_{85B}. The cylinder has been rated to retain water pressures up to 150kPa, and flow rates up to 2.5 litres/sec have been used. A photograph of the apparatus can be seen in Figure 3.19.

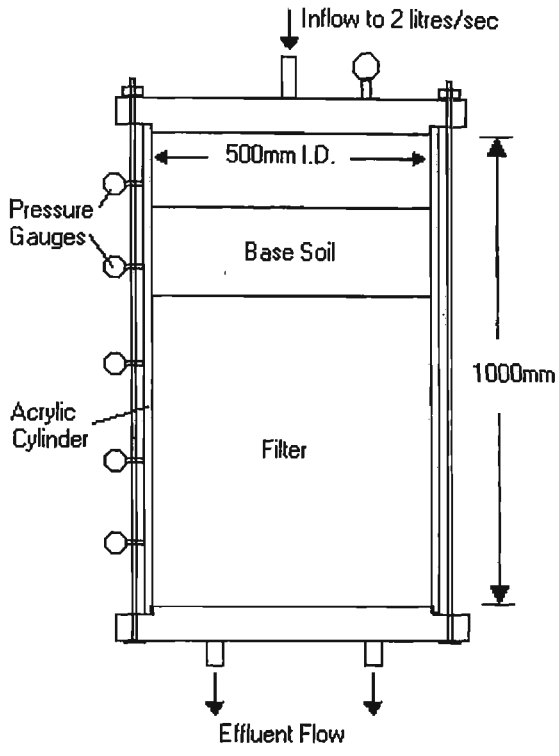

Figure 3.18 Schematic diagram of large-scale filtration apparatus.

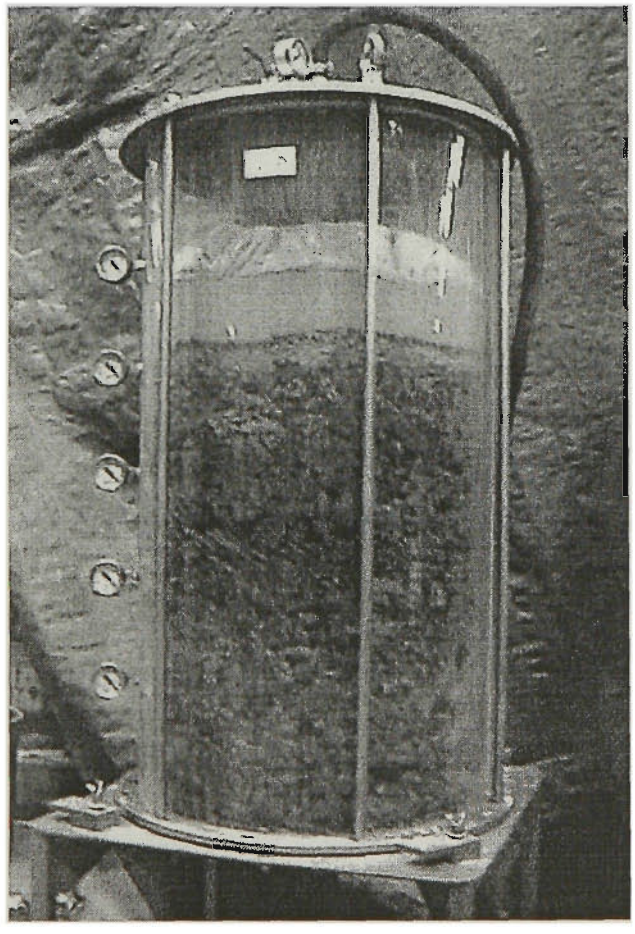

Figure 3.19 Large scale filter permeameter

3.4.1 Change in Base and Filter PSD

The large-scale apparatus is capable of showing more clearly the migration of base soils into a granular filter. Particle infiltration and the amount of soil lost can be clearly seen during the test and measured afterwards by taking samples of the filter material at different depths and determining the change in PSD from the original material. The analytical model predicts this change in PSD of the base and filter soils during filtration. For effective filters, the PSD of the base and filter soils eventually reaches a stable distribution, where no further erosion occurs. Hence, the stable PSD of various filter elements, as predicted by the analytical model, can be compared with the measured PSD of the filter material at increasing depths at the end of laboratory tests. Samples of filter material were carefully taken from the filtration apparatus at various depths from the filter interface to determine the laboratory (lab) PSD. The final predicted PSD of filter elements located at 5cm and 20cm from the base - filter interface are compared with the measured results for the same filter material with two different base soils giving retention ratios D_{15F}/d_{85B} of 4 and 7, as shown in Figures 3.21 and 3.22, respectively. The PSD of the base and filter materials before and after the experiment and simulation are shown. The higher retention ratio ($D_{15F}/d_{85B}=7$) allows significantly more infiltration of base soil into the filter, as shown by the larger 'tail' of fines in the filter PSD after testing. The model predicts similar trends to those observed in the laboratory.

As expected, for both filter retention ratios the content of fines in the filter increases dramatically near the filter interface (at 5cm depth), as a self-filtration zone is formed. The long tail of fine particles indicates the retention of base soil particles within the filter, as vividly described in an earlier study by Indraratna and Vafai (1997). At 20cm depth there are fewer retained fines, indicating that the majority of particle retention occurs

near the filter interface. In general, the model predicts a lesser amount of retained particles near the interface than measured, (ie. the laboratory curve at 5cm depth plots to the left of the model curve). This may be due to the bridging of soil particles over the filter voids. In addition, the assumption was made in the model that any particle with an infiltration distance, L (Equation 3.16), greater than one unit step will pass through to the next element. However, in reality, it is unlikely that all of these coarser particles will be located over a large pore constriction. Hence, fewer coarse particles are expected to migrate. The model also predicts fewer particles will be retained further from the interface (20cm depth). This is because of the rapid increase in infiltration distance (L) predicted for particles finer than the controlling constriction size. In reality, combinations of small constrictions will retain some fine particles, which according to the probabilistic particle infiltration model, could move further.

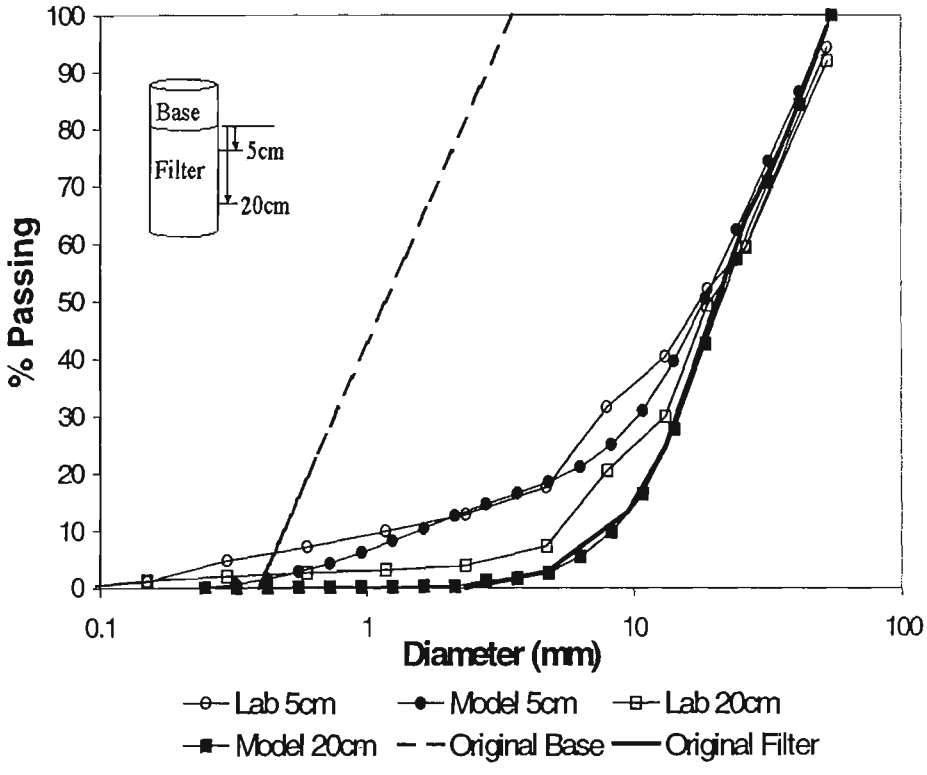

Figure 3.20 Comparison of predicted PSD and laboratory results for $D_{15F}/d_{85B}=4$

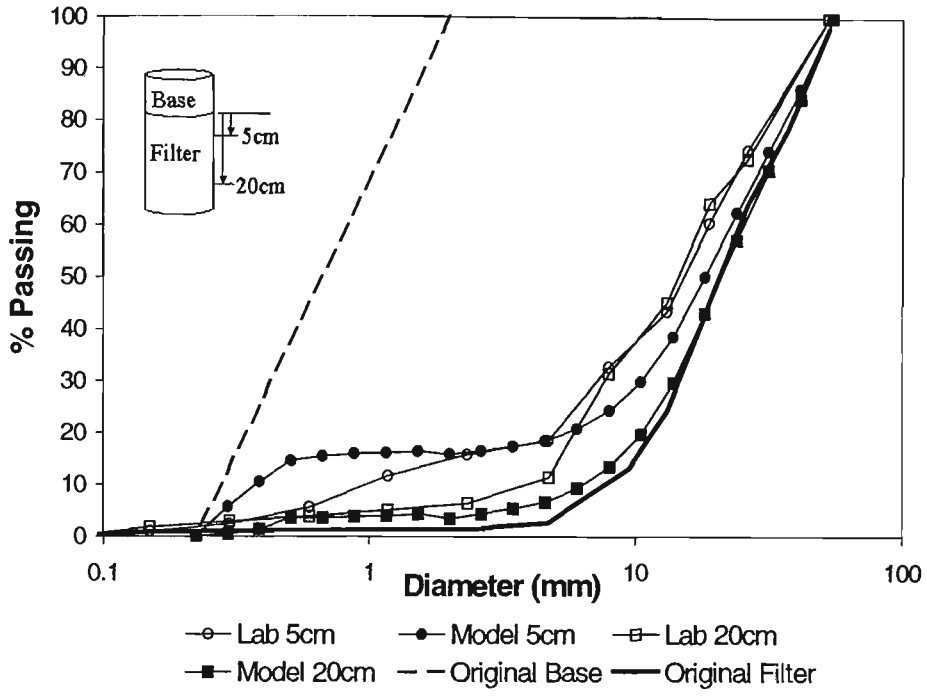

Figure 3.21 Comparison of predicted PSD and laboratory results for $D_{15F}/d_{85B}=7$

3.4.2 Extent of Mass Movement

Most important in determining the success or failure of filtration of well-graded and broadly-graded soils is the mass of base soil eroded before a self-filtration zone is formed. For the same experiment as outlined above, Figure 3.22 shows both the predicted and measured mass of base soil eroded and transported into and possibly through the filter, for three different retention ratios ($D_{15F}/d_{85B}=4$, 7 and 10). As described previously, a sharp decrease in mass passing (y-axis) indicates particle retention at that depth (x-axis), while a constant mass passing (near horizontal sections of Figure 3.22) suggests that the fine particles continue to move through the filter. The correlation between the model predictions and measured results is encouraging. The model overestimates the amount of mass passing entirely through the filter, for the reasons mentioned earlier. The model predicts that, for these internally stable base soils, mass loss from the base soil occurs almost entirely within five to ten centimetres of the filter interface. Within the

filter, the eroded base soil is quickly retained in the self-filtering zone, which forms in the first five to ten unit steps (or 15-30cm) of the filter void model. The unit step is defined as the mean filter particle diameter by number, $D_{f,mean}$, (usually corresponding to D_5-D_{10}). Beyond the self-filtering zone, mass loss is almost constant, indicating insignificant retention of the fine particles that pass through the filter. On the basis of these observations, the minimum filter thickness for effective filtration is 10 times the mean filter particle diameter $D_{f,mean}$. Beyond this depth, the filter thickness has little additional effect. This effect has been observed in many experiments and model simulations with a range of base and filter materials.

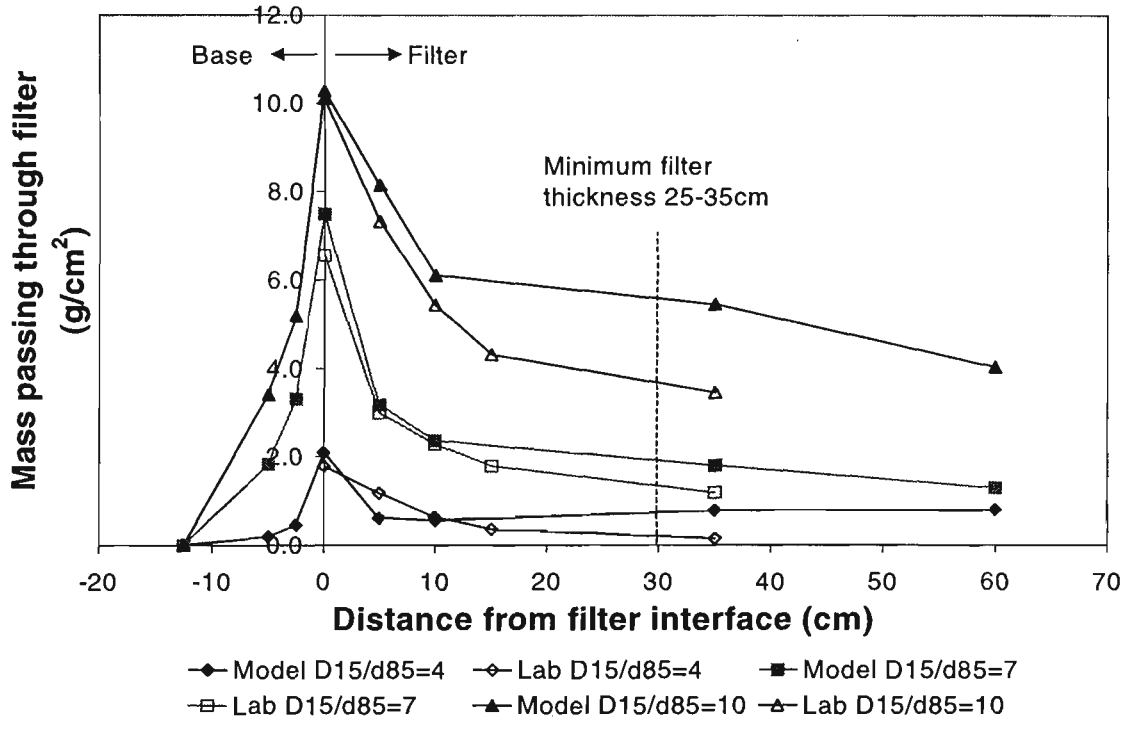

Figure 3.22 Comparison of predicted and measured mass loss during filtration of non-cohesive materials

3.5 Model Prediction of Time-Dependent Filter Behaviour

An important feature of the proposed model is the ability to predict time-dependent changes in flow-rate and the permeability and porosity of the base and filter soils. The time-dependent changes during simulation are described here, for the same filter material described in the laboratory tests above (D_{15F}=10.1mm, C_u=2.5), with four different base soils. The base soils are graded such that C_u=3, and d_{85B} is selected to obtain grain size ratios of D_{15F}/d_{85B}=4, 7, 10 and 12. The initial porosity of all the base soils was assumed constant at 35% for ease of comparison, and the initial filter porosity was estimated at 40%. The permeability values of the base and filter materials were calculated using Equation (3.29). The hydraulic gradient in each simulation was varied to ensure an initial flow rate of 0.2 l/s/m^2 for each base-filter combination.

The analytical model predicts the time-dependent erosion and retention within the base soil – filter system. Figure 3.23 shows the predicted mass of base soil passing out of the second filter element with time (10cm from the filter interface). This depth was chosen to exclude the majority of mass retained within the self-filtration zone. For a low retention ratio (D_{15F}/d_{85B}=4), the self-filtration zone stabilises quickly and little mass passes through the filter. For increasingly finer base soils (ie. higher retention ratios), the time taken for the self-filtration zone to prevent particle movement, and the quantity of particles passing into the filter, increases greatly. The finest base soil (D_{15F}/d_{85B}=12) is too fine to be retained by the filter, and hence, the filter is ineffective. This material exhibits continuous erosion, and the cumulative mass passing through the filter increases until complete erosion (ie. failure).

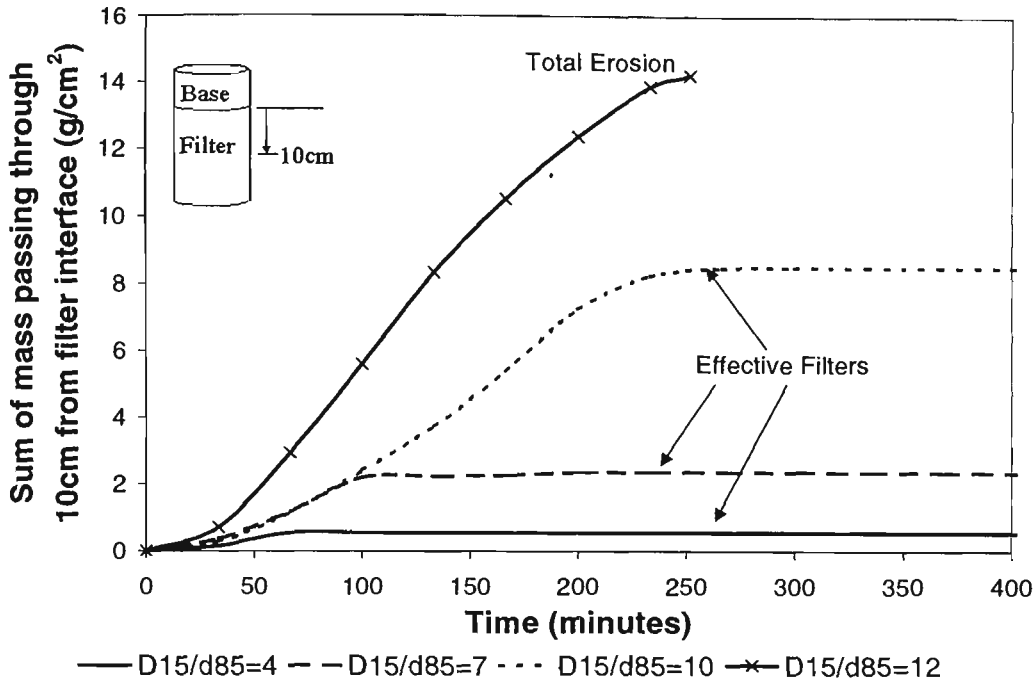

Figure 3.23 Mass passing 10cm from filter interface with time

Figure 3.24 shows the predicted change in flow rate through the four base soil and filter combinations. The coarsest base soil ($D_{15F}/d_{85B}=4$) initially exhibits an increase in flow rate as the fines of the base soil are transported through the filter. Following this initial increase in flow rate, the filter permeability decreases as base soil particles are retained, and the flow rate diminishes again. The flow rate stabilises at a value only slightly greater than the initial flow rate. A finer base soil ($D_{15F}/d_{85B}=7$) shows unstable flow for a longer period and a greater increase in flow. As the filter stabilises, the flow rate becomes constant at a significantly higher value than that of the $D_{15F}/d_{85B}=4$ case, which is due to a greater loss of base soil, resulting in a greater increase in the base soil permeability. The base soil with $D_{15F}/d_{85B}=10$ does eventually stabilise, but indicates a five-fold increase in flow rate corresponding to a large loss of mass. Although eventually effective, this is an example of a borderline filter. The finest base soil ($D_{15F}/d_{85B}=12$) is not retained by the filter. The flow rate increases continually throughout the simulation, as particle erosion accelerates and the porosity of the base soil increases, until complete washout.

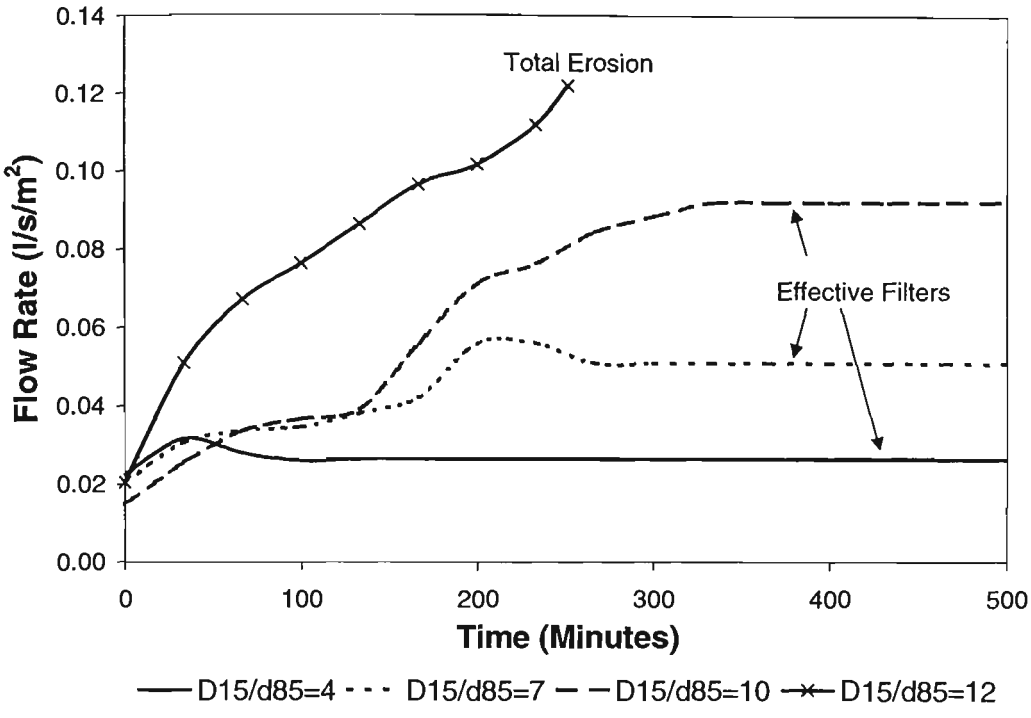

Figure 3.24 Predicted change in flow rate with time

Consider now the time-dependent changes in permeability of the base soil, shown in Figure 3.25. In all three simulations where a stable interface results (D_{15F}/d_{85B}=4, 7 and 10), the base soil permeability increases, attaining a constant value as the filter interface stabilises. The permeability of the coarsest base soil (D_{15F}/d_{85B}=4) increases from 0.075mm/s to 0.46mm/s during filtration. The permeability of the borderline base soil (D_{15F}/d_{85B}=10) increases from 0.02mm/s to 0.25mm/s, and this increase is almost 100% more than the permeability increase for the coarsest base soil. The permeability of the unsuccessful base soil (D_{15F}/d_{85B}=12) increases steadily until failure, indicating continued erosion and limited particle capture in the filter.

The time-dependent changes in base soil porosity are also shown in Figure 3.25. For the effective base soil – filter combinations, the base soil porosity increases steadily as mass is lost, approaching a constant value as the self-filtration zone is formed. The coarsest

base soil ($D_{15F}/d_{85B}=4$) shows the greatest resistance to erosion, and is characterised by the lowest increase in porosity with time. As expected, the rate of erosion (indicated by the change in porosity) increases as the size of the base soil decreases, in relation to the same filter material. In the case of unsuccessful filtration, the porosity increases steadily until a value of 0.6 is reached (ie. the definition of failure in the model).

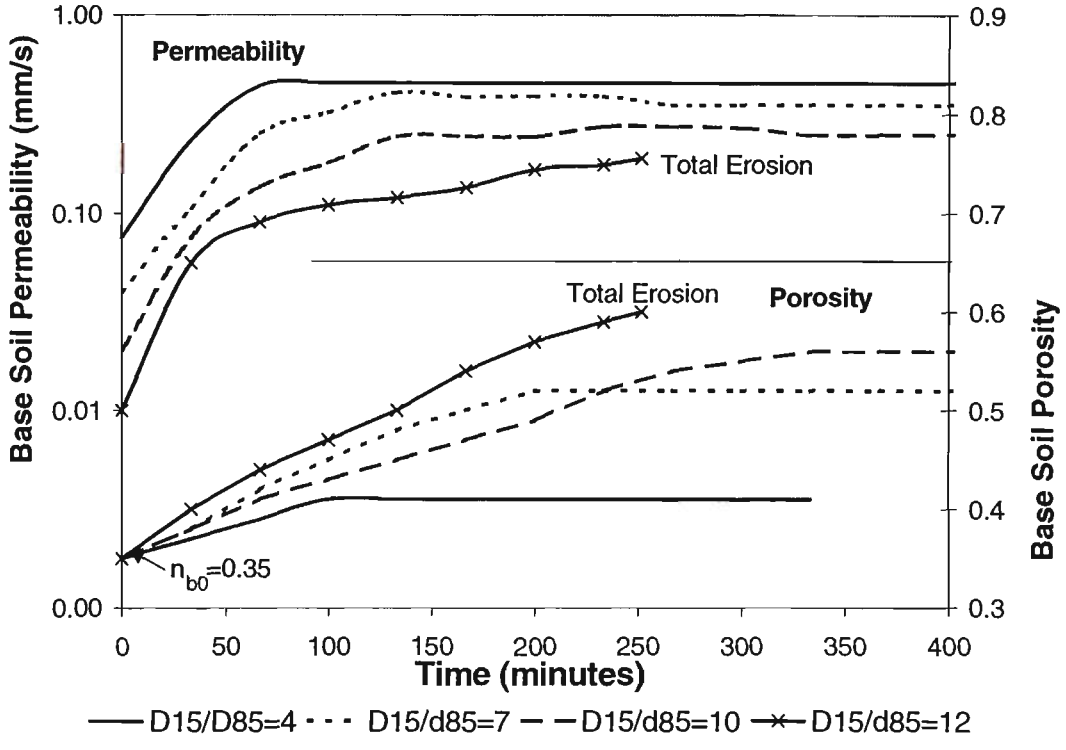

Figure 3.25 Change in permeability and porosity of base with time

Next consider the filter permeability (Figure 3.26), which initially decreases as some base soil particles are captured. However, the filter material is internally unstable, containing approximately 5% loose fines. The rate of wash out of these filter fines becomes larger than the mass rate of base soil retained by the filter, and hence, the filter permeability increases again. In successful filter combinations, after this initial fluctuation, and once the loose filter fines are almost washed out of the filter element, the permeability stabilises as erosion ceases. The borderline base soil ($D_{15F}/d_{85B}=10$) leads to a significantly lower final filter permeability than the two coarser base soils, because a

larger mass of finer particles is eventually captured in the filter. The permeability of the filter element for the unsuccessful combination (D_{15F}/d_{85B}=12) exhibits similar trends initially to the successful filters as base soil particles within the filter reduce the permeability. However, these base soil particles continue to move through the filter and failure is predicted before the interface can stabilise.

The time-dependent filter porosity (Figure 3.26) initially decreases as base soil particles migrate into the filter. For the three effective filtration cases, D_{15F}/d_{85B} = 4, 7 and 10, the filter porosity stabilises at a value lower than the initial, due to the retained particles. The reduction in the filter porosity indicates the amount of base soil retained within the filter. The filter porosity of the unsuccessful case, increases to a value greater than the initial porosity of 40%. This is because, as previously mentioned, the filter material is internally unstable. This leads to an increase in the filter porosity as the filter fines are washed out.

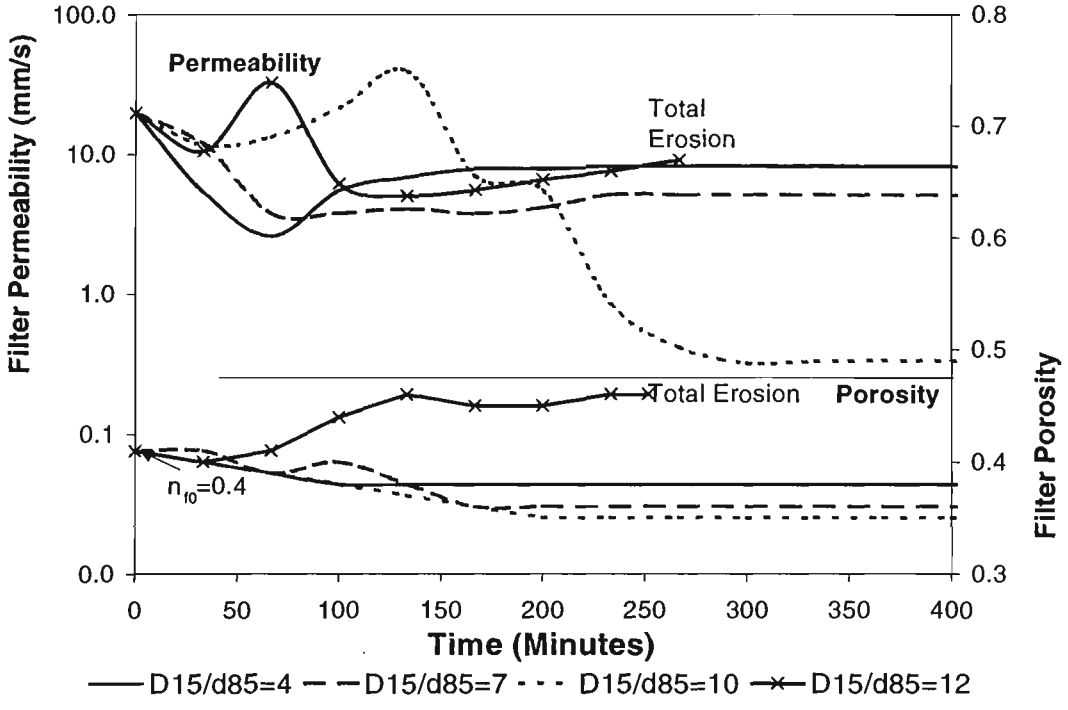

Figure 3.26 Change in permeability and porosity of filter with time

3.6 Summary of Modelling

A revised analytical model for the movement of non-cohesive base soil particles in granular filters, extending the particle transport concept of Indraratna and Vafai (1997) has been described. The model consists of three important sections:

1. A filter void model based on a three dimensional cubic network proposed by Schuler (1996). The size of pore constrictions linking the pores is determined from the filter particle size distribution (by surface area) and relative density.
2. A deterministic equation for particle infiltration into the filter model based on the probability of movement of a particle through the filter void constrictions. This equation defines the retention of particles within the filter.
3. Particle transport equations of conservation of mass and momentum, proposed earlier by Indraratna and Vafai (1997), which have been modified to consider the increased flow viscosity due to suspended particles in the pore water. The particle transport model defines the erosion and transport of base soil particles.

Within broadly graded soils, some fine particles may not contribute to the skeleton of fixed particles which form the structure of the soil, but are loose within the pores of this skeleton and do not affect particle capture during filtration. Therefore, these particles should not be considered when determining the size of constrictions in the filter voids. At the other extreme, some coarse particles may be 'floating' in a matrix of fines, where the voids formed between coarse particles are filled by finer filter particles. In this case, the coarser particles do not contact each other to form large constrictions, although they are still able to form constrictions with the smaller particles. A method has been described to determine which particle sizes should be excluded from the particle size distribution

(PSD), when determining the constriction size distribution (CSD) of a broadly graded material.

The model predicts the erosion of base soil particles and retention within a granular filter, and predicts for a suitable base soil - filter combination, the time-dependent formation of a self-filtering layer at the filter interface. As base soil particles are captured within the filter, void sizes will decrease and finer base soil particles will be retained. This leads to the formation of a stable, self-filtering layer approximately 5-10 "unit steps" in thickness, where each unit step corresponds to the mean filter particle diameter by number $D_{f,mean}$ (approximately D_5-D_{10}). Beyond this self-filtering layer, there is limited retention of particles, suggesting that increasing the filter thickness does not greatly increase the capture of particles, and the minimum thickness for an effective filter is 10 times $D_{f,mean}$. Time-dependent particle capture and changes in flow-rate, permeability and porosity are calculated by the model, leading to a full description of the filtration process.

The model predictions show that, irrespective of the initial retention rates of base soil in the filter, an effective filter is characterised by a stable (constant) permeability and porosity with time. This prediction describes what occurs within a granular filter when water first starts flowing through the base soil (eg. first filling of a dam reservoir). If a further perturbation occurs (such as cracking of the core, changes in seepage patterns, a change in the reservoir water chemistry etc.) then a subsequent load of base soil may reach the filter. The model could then be used to consider the effect of this new flow of base soil particles into the filter material that has already been modified by previous infiltration. If a filter is predicted to be effective in the first instance, the model may predict a further decrease in filter porosity and permeability until steady state conditions

are reached once again. In this way, the full life of the filter can be simulated. The base soils and filter described in this Chapter were coarse, non-cohesive sands and gravels. Similar trends in experimental results and model predictions have been obtained by the writer, for several finer non-cohesive materials.

Comparison with laboratory results and previously published experimental findings has shown that the current model predicts particle movement and capture similar to the measured data. The model is able to predict particle movement and changes in flow-rate, permeability and porosity for non-cohesive, uniform and broadly graded base and filter materials, and is a significant extension of the original Indraratna and Vafai (1997) analytical method. In addition, this revised model has been shown to predict internal stability, based on fine filter particle washout.

The theory developed in this Chapter was intended to describe the behaviour of non-cohesive base soils which erode as a backwards erosion front of the soil mass into the filter. Cohesive base materials behave differently, factors such as cracking, erosion resistance and physic-chemical forces will have an effect on filtration. The next Chapter describes a laboratory study designed to investigate some of these factors and describe the fundamentals of filtration of cohesive materials.

4. LABORATORY STUDY OF EROSION AND FILTRATION

4.1 Introduction

Protection of cohesive base soils using granular filters involves a complex process of particle erosion, transport and capture within the filter. This is a significant extension to the filtration of non-cohesive base soils described in Chapter 3. When designing filters for cohesive soils, it is generally accepted that the most critical situation to consider is a concentrated leak through a crack in the base soil. In this case, particles are eroded when the shear forces exerted by water flowing through the crack exceed the critical shear stress of the crack wall and initiate erosion. The majority of laboratory filtration tests have been conducted at high pressure, resulting in high shear stresses ensuring erosion occurs (the NEF test) or apply the base soil as a slurry of particles, ignoring the erosion of the base soil completely (slurry test). The majority of applications of filters will be at considerably lower pressures, where the erosion resistance of the base soil may have a significant effect. This Chapter describes a laboratory program which separately examines the processes of erosion and filtration of cohesive base soils, to attempt to explain some of the changes occurring during filtration for a range of hydraulic conditions.

The erosion of cohesive materials has been examined in several previous studies (Arulanandan et al., 1975, 1980). These studies and some predictive methods to estimate erosion parameters were presented in Chapter 2. Khilar et al. (1985) showed that the rate of erosion depends on the type of erosion test, showing that erosion parameters vary with different experiments due to changes in the particle concentration in the eroding fluid. Hence, an erosion test that models flow through a cracked cohesive material is necessary. In this study, a large-scale pinhole test (after Sherard et al. 1976a) has been used to

measure the erosion rate and the size of particles eroded due to flow through a 3mm pinhole. It is assumed that flow through a circular pinhole produces similar erosion to flow within a crack. The test methodology and results of tests on fifteen samples are described in Section 4.2. A series of NEF tests on the same 15 materials has been carried out to try to relate the measured erosion properties to filtration (ie. erosion rate and particle sizes), this is described in Section 4.3. Based on these NEF tests and a study of previous literature, a new method to estimate the safe filter boundary for cohesive base soils, and particularly broadly graded soils, is described in Section 4.4.

Several authors have suggested various different sizes of particles may be eroded from the crack walls and influence filtration. Vaughan and Soares (1982) assume that the clay erodes as flocs. Due to segregation, these fine flocs may arrive at the filter without any coarser particles. Sherard (1982) argued that silt sized particles (30-70 microns) within fine-grained clayey soils will also be available to seal concentrated leaks. Khor and Woo (1989) suggest that particles coarser than fine sand cannot be relied upon to assist in sealing the filter, and that it is necessary to provide a protective filter that will retain the fines (fraction<75μm), but not necessarily the clay floc size particles. These differing theories imply that the issue of particle sizes eroded and transported due to flow through a crack needs to be addressed. The large scale pinhole tests, described in Section 4.2.3 are also used to examine the size of particles eroded by flow through a pinhole in a compacted cohesive soil. A prediction of the size of eroded particles is necessary for modelling filtration of cohesive materials, considered in Chapter 5. A method to estimate the soil particle sizes influencing filtration is outlined in Section 4.5.

4.2 Laboratory Study of Erosion

The size of particles eroded, and the corresponding erosion rates due to concentrated flow through a crack, are important factors to assist in understanding of the filtration mechanism in cohesive soils. The literature review presented in Chapter 2, described the basic chemistry behind the erosion resistance of cohesive materials, and some previous experiments performed to measure erosion rates. In order to investigate erosion further, this Section describes the large scale pinhole test, and the results of extensive testing to determine erosion rates and the size of particles the particles eroded by concentrated flow through a pinhole.

4.2.1 Test Procedure – Modified Pinhole Erosion Test

The erosion test is essentially a modification of the pinhole test described by Sherard et al. (1976). The apparatus is shown schematically in Figure 4.1. The soil sample was compacted in five 40mm layers, in the 150mm diameter permeameter, subjected to 50 blows of the standard compaction hammer per layer. This gave approximately 90% standard Proctor compaction energy. The sample was covered and sat for at least 48 hours, before a 3mm diameter pinhole was pushed through the 200mm long sample. The permeameter was sealed and connected to a water supply, which provided a variable head from 0.3m to 2.2m. This produces flow velocities through the 3mm hole of approximately 0.7 to 3.5 m/s. An initial head of 0.3m was applied, and the flow rate through the pinhole was recorded. If the effluent water contained visible eroded particles, then 1-2 litres (accurately measured) of the effluent was poured into an aluminium foil lined sample tray. These samples were oven dried, and the sediment remaining in the tray was carefully scraped from the aluminium foil and weighed, to determine the erosion rate as a mass per volume of eroding fluid. The sediment was retained for later testing to

determine the particle sizes. The process was repeated, and the flow rates and erosion rates were similarly determined for several different pressure heads up to 2.2m.

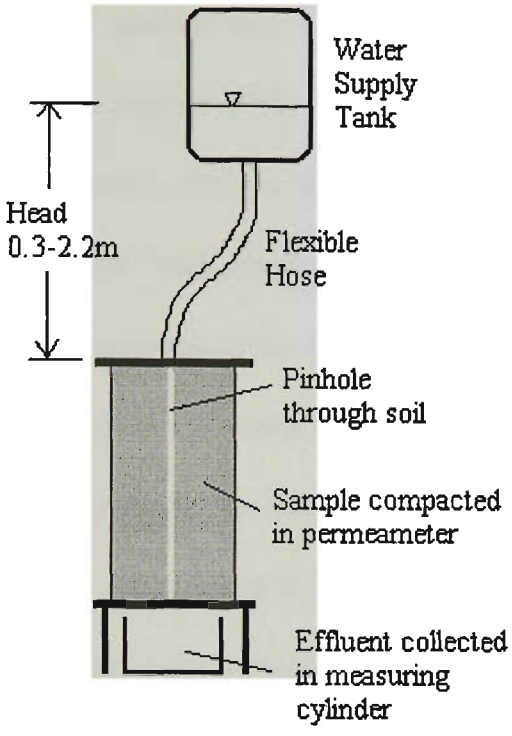

Figure 4.1 Schematic of apparatus for the large-scale pinhole test

A Melvern Particle Size Analyser (PSA) was used to determine the particle size distribution of the eroded sediment. The PSA uses a laser refraction method to determine the sizes of particles. This method is significantly more accurate than conventional hydrometer testing for determining the particle size distribution (PSD). However, the PSA does rely on the assumption of spherical particles (similar to the hydrometer test) and produces a PSD by volume, requiring the assumption that all particles have the same density.

Measurement of the PSD of the eroded material revealed that the sample eroded in the form of large aggregates (or clumps) of the cohesive material, rather than individual particles. The PSA is able to mechanically disperse the particle aggregates by applying

an ultrasonic vibration. It was observed that after some period of ultrasonic dispersion (usually 5-10 minutes), the aggregates obtained a stable minimum size distribution. These aggregates would not break down further without a chemical dispersant in the water, regardless of the mechanical dispersion energy applied. This mechanical dispersion was assumed to represent the potential break down of particles at the filter interface due to high hydraulic forces. It is difficult to imagine the particles breaking down further than this stable minimum distribution due to hydraulic forces alone. The eroded material before dispersion was termed the erosion product before dispersion, *EPbefore*. After ultrasonic dispersion was applied to disperse the eroded sample, the PSD was termed the erosion product after dispersion, *EPdisp*. The PSD of the original soil after drying and grinding, also obtained in the PSA, is termed the *original PSD*. The larger eroded particles are termed *aggregates* of primary particles. This terminology will be used throughout this Chapter. In most cases the erosion product *EPdisp* was larger than the original PSD due to this aggregation of particles.

4.2.2 Measured Erosion Rate of Cohesive Soils

The modified pinhole test, described above, was intended as an approximate method to determine the erosion rate due to concentrated flow, and to confirm that an erosion equation developed for other applications is suitable to describe erosion due to confined flow through a crack. The equation most commonly used to define the erosion rate, E, is:

$$E = \alpha(\tau - \tau_c) \text{ g/m}^2\text{s} \qquad (4.1)$$

where, α is an erosion rate parameter (g/Ns), τ is the applied shear stress (N/m^2), and τ_c is the critical shear stress below which no erosion will occur.

Fifteen samples were obtained from dam cores and other sources throughout eastern Australia. The samples range from pure kaolinite clays (BB3 and BB4) to dispersive

sandy clays (Hume) and coarser sandy clay (Thomson). Table 4.1 shows the erosion parameters τ_c and α measured in the laboratory for these fifteen samples. These values were determined by fitting a line of best fit to at least 3 (usually 4-6) data points from the erosion tests. The regression index (R^2) indicates the acceptability of this line of best fit. A high R^2 value (close to unity) indicates that most points lie close to the straight line defined by Equation 4.1, whereas low values indicate poor data correlation. Most of the erosion tests had $R^2>0.7$, which is acceptable for this approximate test method. However, some samples, notably the AS1 and Cowarra materials, had large variations in the mass eroded with little relation to the flow rate. These samples exhibited high initial erosion at a low flow rate, and then the erosion rate decreased and was relatively constant, regardless of the flow rate. It is likely that, initially, loose surface material was rapidly eroded, and following this any further erosion required plucking of particles from a solid structure at a much lower rate of erosion. In these cases, where the erosion parameters cannot be reasonably determined in a controlled laboratory test, a more conservative estimate of the erosion rate should be used. A conservative approach may be to assume that there is little or no critical shear stress, ie. $\tau_c \equiv 0$, and to adopt some representative value for α when modelling erosion (this representative α is shown in the fifth column of Table 4.1). The final two columns of Table 4.1 show the original material particle size, d_{85Orig}, and the percentage of fines in each sample. While there is a basic trend that the erosion rate becomes greater as the representative particle size increases or the percentage of fines decreases, there is no clear relationship between these parameters (or others) and the erosion rate. Arulanandan et al. (1980) predicted that the erosion of cohesive soil is dependent primarily on the inter-particle bonding force and only partly linked to the bulk soil properties such as particle size or fines content.

For the purposes of predicting erosion, if the regression index (R^2) of the line of best fit is higher than some acceptable value (say 0.7), then the erosion parameters determined

using this test could be applied in Equation 4.1. If the experimental data has a lower R^2 value, the modified erosion rate assuming the critical shear stress to be zero, $\alpha(\tau_c=0)$, could be adopted, or the test may be repeated. This laboratory method is not sufficiently accurate to identify the critical shear stress of highly erodable soils, with $\tau_c<0.5N/m^2$. These erodable materials are shown as having a critical shear stress $\tau_c<1N/m^2$. A more precise method of measuring the shear stress and erosion rate is required for these materials. For estimation purposes, if a material is not dispersive it generally will have a critical shear stress of at least $0.5N/m^2$.

Table 4.1 Results of Erosion Tests

Sample	τ_c (N/m^2)	α (g/Ns)	R^2	$\alpha(\tau_c=0)$	d_{85Orig} (μm)	%<75μm
BB1	9	0.05	0.9		120	88
BB3	10	0.17	0.9		16	95
BB4	23	0.12	0.8		11	100
CA1	12	0.1	0.8		36	95
CO1	8	0.08	0.7		45	90
RO1	2	0.06	0.9		35	92
SF1	<1	0.03	0.4	0.03	23	98
AS1	28	0.07	0.1	0.03	38	98
AS2	10	0.28	0.8		90	82
AP1	25	0.02	0.9		75	85
YanYean	10	0.05	0.7		35	98
Thomson	<1	0.23	0.8		170	55
Cowarra	0.5	0.09	0.2	0.08	25	96
Kerferd	0.5	0.04	0.8		28	95
Hume	<1	0.07	0.4	0.07	33	98

Some further observations from the erosion rate tests include:

- The clays tested generally had a moderate to low erosion rate and a high critical shear stress. The erosion rate of clayey sands increased as the clay content decreased,

indicating a lack of inter-particle bonding. Exceptions include the Cowarra and Hume dam core materials, which are slightly dispersive.

- Generally, samples at very low or very high moisture content (relative to optimum) had a higher erosion rate than the samples at or near the optimum moisture content.
- Samples were often highly erosive directly after compaction, but in tests performed after the samples were left for 2-3 days, the erosion rate reduced markedly. The erosion parameters in Table 4.1 were determined after the sample had been sitting for at least 48 hours.

In summary, the modified pinhole test provides a reasonable estimate of erosion parameters for modelling erosion due to a confined flow through a cracked base soil. The method cannot differentiate a critical shear stress less than about $0.5N/m^2$. The erosion Equation (4.1) can be used to predict the erosion rate related to the shear stress applied by the eroding fluid, for flow through a hole or crack. This equation will be used in developing an analytical model of filtration of cohesive base soils in Chapter 5.

4.2.3 Size of Eroded Particles

In order to describe the processes occurring during filtration of cohesive materials, it is necessary to investigate whether the erosion process will erode individual particles or larger aggregates and flocs, and if so, what size will these aggregates be. This first requires the PSD of the original materials. Following standard methods, a sample of each material was dried and ground, then the original PSD was determined by mechanical sieving for the fraction coarser than 600μm, and the PSA used for the finer fraction. The PSD was determined after ultrasonic dispersion had reduced the particles to a constant size distribution. The fines fraction and representative particle sizes d_{98}, d_{85}, and d_{50} of the original PSD are shown in the first 4 columns of Table 4.2. The 6^{th} column shows the

coarse fraction broadness coefficient d_{98}/d_{85}. Implications of this ratio will be discussed later.

Effluent water from the modified pinhole test was collected to measure the size and stability of the eroded particles. The next 7 columns in Table 4.2 show the measured particle sizes of the erosion product, before and after ultrasonic dispersion, *EPbefore* and *EPdisp*, determined using the PSA. The particle diameters shown for each material are the average of at least three samples of eroded material, obtained from erosion tests at different flow rates. Generally, the size distribution of each sample, collected at different flow rates, varied from the average by less than 10%. There was no correlation between the eroding shear stress (or flow rate) and the size of particles in the erosion product after dispersion. Some other important observations of the tests are described in the following paragraphs.

The eroded particles before dispersion, *EPbefore,* were significantly larger than the primary particles of the soil, indicating that erosion produced aggregates of the material rather than primary particles. Many materials eroded as large flakes up to 5mm long and this is reflected in the *EPbefore*. The ratio of eroded particle sizes to primary particle sizes decreased as the primary particle sizes increased, ie. coarser materials produced a lower degree of particle aggregation, as expected. The eroded particles had essentially the same PSD, regardless of the eroding shear stress, suggesting that if the critical shear stress is exceeded, the eroded particles will have the same size, regardless of the flow velocity.

The large flakes of eroded material quickly broke down under ultrasonic dispersion, suggesting they would not be stable under the high hydraulic forces expected at the filter interface. The eroded particles after dispersion, *EPdisp,* were often still larger than the

original particles after dispersion. This is because some clays form aggregates and flocs of many particles that cannot be broken down to basic particles by the mechanical dispersion forces. To represent this increase in particle size, the *aggregation ratio* (*A.R.*) is defined in Equation (4.3). Figure 4.2 shows the variation of A.R. with the d_{85Orig} size of the primary particles. The general trend is that finer materials produced a higher degree of aggregation. This is expected since these finer materials contain a higher proportion of clay particles that have strong cohesive bonds leading to the formation of clay flocs and aggregates of clays and coarser particles. There are exceptions to this correlation, notably the Thomson core material. This material is coarser than all others tested, but had an erosion product significantly coarser than the original sample, represented by an A.R.=2.6. While care was taken during the drying and grinding of materials, this variation in particle size may be due to crushing of the friable sand size particles while grinding the sample of original material before particle size analysis. For this reason the Thomson core material was excluded from Figure 4.2.

$$A.R. = \frac{d_{85EP(disp)}}{d_{85Orig(disp)}} \qquad (4.2)$$

Erosion tests on five samples (BB1, BB3, BB4, CO1 and CA1) were carried out for two or three different moisture contents to examine the effect of moisture content on the eroded particle size. The PSD after dispersion was almost identical, regardless of the moisture content. The moisture contents tested were all within 10% of OMC. The erosion product PSD may vary when the sample is compacted at the dry or wet extremes.

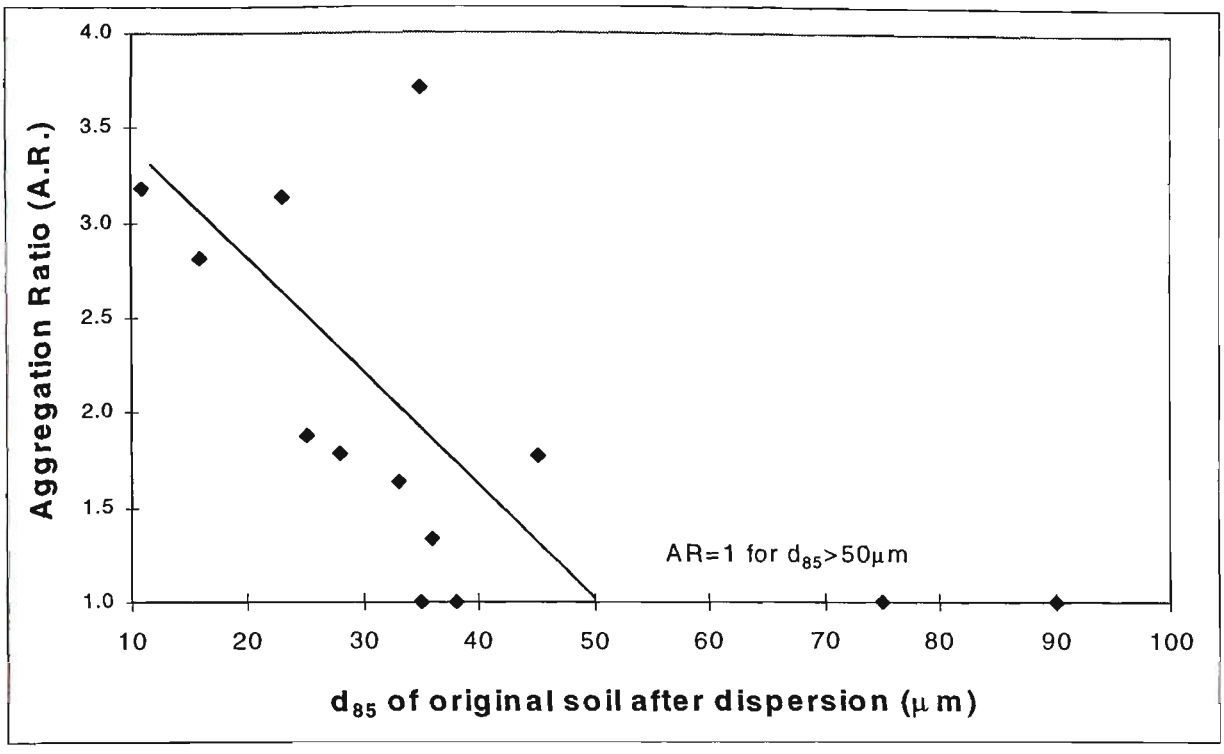

Figure 4.2 Extent of particle aggregation with particle size

In summary, the tests showed that erosion of a clayey soil due to flow through a pinhole produces pieces of eroded material that are generally larger than the primary soil particles. This eroded material can be easily broken down by mechanical dispersion. Once a steady minimum size is reached, additional dispersive energy does not break down the particle aggregates further. It is assumed that this stable minimum size represents the size of particles at the filter interface in a dam, since high hydraulic forces may break down the larger, unstable aggregates of particles. The PSD of this dispersed erosion product varies very little with erosion rate or moisture content. The dispersed eroded particles, *EPdisp,* were generally larger than the dispersed original particles of fine cohesive materials. The ratio of representative particle sizes of the *EPdisp* and Original PSD has been defined as the *aggregation ratio*, A.R. (Equation 4.2). The aggregation ratio was shown to increase with an increase in fines content, most likely due to a larger clay fraction. Variations in clay particle bond strength probably accounts for the variations in aggregation ratio.

Table 4.2 Results of erosion tests and NEF tests (particle diameters in μm)

Sample Name	PSD of Original Material After Dispersion					PSD of Erosion Product							A.R.	NEF	Ratio	Ratio
						EP(Before)			EP(Disp)							
	%<75μm	d_{98Orig}	d_{85Orig}	d_{50Orig}	d_{98}/d_{85}	$d_{98before}$	$d_{85before}$	$d_{50before}$	%<75μm	d_{98EP}	d_{85EP}	d_{50EP}	D_{85EP}/d_{85Orig}	Boundary D_{15bdy}	D_{15bdy}/d_{85EP}	$D15_{bdy}/d_{85Orig}$
BB1	82	650	120	12	5.4	700	350	140	95	700	120	32	1.0	780	6.5	6.5
BB3	99	40	16	5	2.5	350	200	70	90	70	45	22	2.8	125	2.8	7.8
BB4	100	35	11	4	3.2	220	100	25	90	65	35	11	3.2	100	2.9	9.1
CA1	91	500	36	5	13.9	750	650	420	96	500	48	10	1.3	325	6.8	9.0
CO1	90	400	45	8	8.9	500	400	150	89	400	80	35	1.8	800	10.0	17.8
RO1	92	250	35	2.2	7.1	700	600	250	70	180	130	40	3.7	750	5.8	21.4
SF1	98	75	23	8	3.3	650	500	200	95	95	72	30	3.1	540	7.5	23.5
AS1	100	65	38	20	1.7	500	300	75	98	65	38	20	1.0	270	7.1	7.1
AS2	82	250	90	12	2.8	400	300	160	82	200	90	12	1.0	1100	12.2	12.2
AP1	85	550	75	8	7.3	700	550	350	98	550	75	18	1.0	190	2.5	2.5
YanYean	98	75	35	7	2.1	300	200	90	95	75	35	7	1.0	630	18.0	18.0
Thompson	55	550	190	70	2.9	750	650	370	40	700	500	110	2.6	2000	4.0	10.5
Cowarra	94	100	25	7	4.0	600	400	45	92	88	47	15	1.9	530	11.3	21.2
Kerferd	96	120	28	9	4.3	700	500	180	97	80	50	19	1.8	350	7.0	12.5
Hume	94	400	33	6	12.1	650	450	100	96	90	54	16	1.6	370	6.9	11.2

4.3 Relating Erosion Tests to Filtration of Cohesive Soils

The No Erosion Filter (NEF) test, proposed by Sherard and Dunnigan (1985), is commonly accepted as a standard test for determining suitable filters to protect cohesive materials in embankment dams. A series of NEF tests were performed on the same 15 materials as used in the modified pinhole tests described previously. Appendix 1 outlines the detailed procedure followed for the NEF test, as proposed by Delgado and Locke (2000), based on the recommendations of Sherard and Dunnigan (1985). The aim of these experiments was to examine whether there was a correlation between the size of particles eroded from an open pinhole, *EPdisp*, and the boundary filter size, D_{15bdy}, determined in the NEF test. Table 4.2 shows the NEF boundary filter size for each material, along with ratios D_{15bdy}/d_{85EP} and D_{15bdy}/d_{85Orig}.

4.3.1 Correlation of the NEF Boundary with the Erosion Product

A correlation appears to exist between the no erosion filter boundary, D_{15bdy}, and a representative eroded particle size after ultrasonic dispersion, d_{85EP}, (Figure 4.3). Testing and modelling of non-cohesive soils by the writer, described in Chapter 3, determined that for a filter retention ratio of $D_{15F}/d_{85B}=4$, very little movement of the base soil particles occurs before the filter interface stabilises. Whereas for $D_{15F}/d_{85B}=6$, some mass loss occurs before a self-filtration zone is formed. Similarly, Kenney et al. (1985) defined the controlling constriction size of a filter, $D_c^*=D_{15F}/5$. Particles coarser than the controlling constriction size are rapidly retained within the filter, while particles finer than this size can pass through the filter. The writer postulates that the same mechanism may also apply to cohesive materials in the NEF test, ie. stable particles coarser than $D_{15F}/4$ are retained at the filer interface and form a filter cake, while finer particles can initially move through the filter.

This concept can now be investigated since the size of eroded particles has been defined. A filter retention ratio $D_{15F}/d_{85EP}<4$ would produce minimal erosion before particles are captured at the filter interface and seal the filter, ie. a filter with no erosion. Coarser filters would allow some mass loss before a sufficient quantity of particles were captured to seal the interface. The boundary line $D_{15F}/d_{85EP}=4$ has been plotted on Figure 4.3, which is almost representative of a lower bound for the data. Only three points plot below this line, of which two materials are pure kaolinite clays (BB3 and BB4), with a uniform coarse fraction ($d_{98}/d_{85}<2.5$). Sherard and Dunnigan (1989) also noted that fine soils with a uniform coarse fraction had boundary filter sizes lower than predicted by the design criteria. The other material (AP1) behaves unusually because it is very broadly graded, this will be discussed in detail in Section 4.4.

Figure 4.3 suggests that it is these stable eroded particles that are captured at the filter interface. Particles larger than $D_{15bdy}/4$ are retained to form a filter cake, which rapidly seals the pinhole and results in a successful NEF test. This geometric filtration has also been described by Yuen and Styles (1995) when examining filtration of kaolinite slurry. Reddi and Bonala (1997) showed that physico-chemical capture of clay flocs also effects long-term filtration, however this effect is unlikely to have any influence on the short duration, high pressure NEF test.

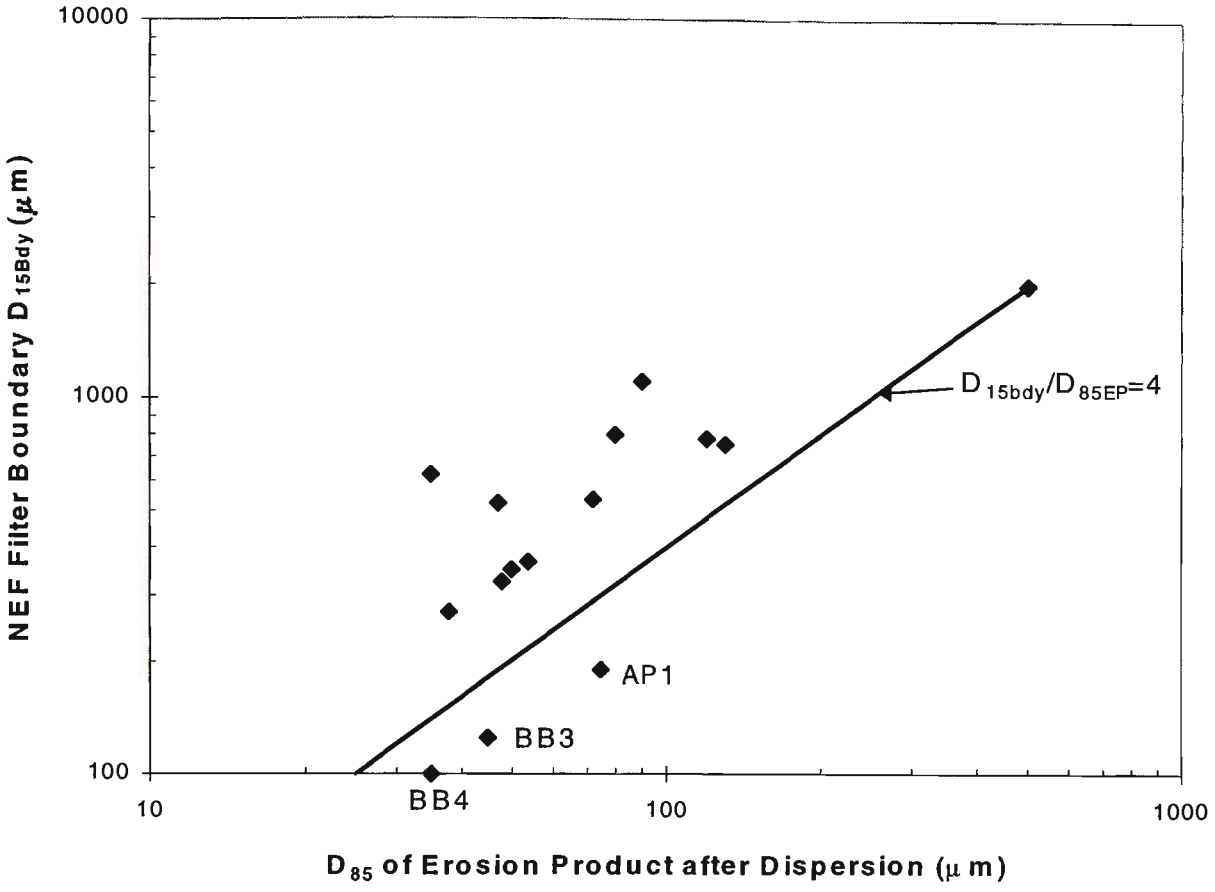

Figure 4.3 Relation between D_{85EP} of the dispersed erosion product and experimentally determined D_{15bdy}

It is quite clear from the data in Table 4.2 that the size of eroded particles before ultrasonic dispersion has no bearing on the results of the NEF test. These particles very quickly break down to the dispersed erosion product PSD. It is likely that incomplete breakdown of these aggregates during filtration (ie. the presence of larger particles than the dispersed erosion product, *EPdisp*) is the main reason for some samples having D_{15bdy}/d_{85EP} ratios significantly larger than 4. In other words, some materials have weak bonds forming these large aggregates, which break down at the filter face and leave finer particles, represented by *EPdisp*. Other materials may have significantly stronger bonds, which cannot be completely broken by the hydraulic forces.

4.3.2 Correlation of NEF Tests with the Original PSD of the Base Soil

Sherard and Dunnigan (1985) determined a linear correlation for the NEF boundary filter and the d_{85B} size of fine base soils, $D_{15bdy}/d_{85B}=9$. Figure 4.4 shows the relation determined in the laboratory between D_{15bdy} and d_{85Orig} (from the dried and ground base material) and the Sherard and Dunnigan (1985) empirical design criteria for fine silts and clays (group 1 soils), $D_{15bdy}/d_{85Orig}=9$; and for sandy silts and clays (group 2 soils), $D_{15bdy}=0.7$. Three samples plot below the line representing the empirical criteria. Two of these materials, BB3 and AS1, are uniform clays with $d_{98}/d_{85}<2.5$. As noted above, uniform fine materials often have boundary filters finer than those predicted by the empirical criteria. The Melvern PSA is able to show quite clearly whether a material is uniform or well graded and predictions of stable D_{15bdy}/d_{85Orig} ratios can be made based on the measured PSD. The third material is AP1, a broadly graded soil that will be discussed further in Section 4.4. Hence, the new laboratory data confirms the Sherard and Dunnigan (1985) design criteria for fine base soils with $d_{98B}/d_{85B}>2.5$.

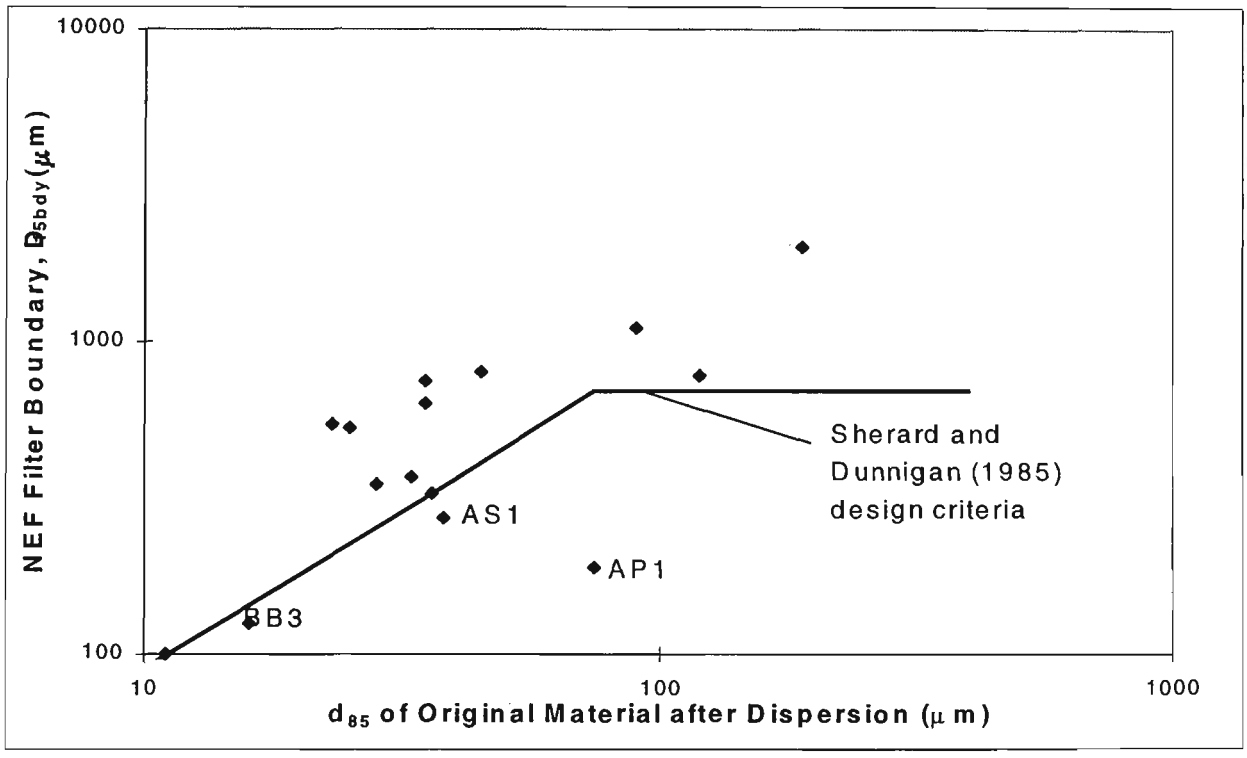

Figure 4.4 Relationship between d_{85} and experimentally determined filter boundary D_{15bdy}

Delgado (2000) found that a more representative relation for fine soils in groups 1 and 2 as defined by Sherard and Dunnigan (1989), is the relation between D_{15bdy} and the amount of fines (%<75μm). This relation is shown in Figure 4.5, excluding sample AP1. The relatively good correlation (R^2=0.87) confirms that the fine fraction is important in determining the no erosion filter boundary.

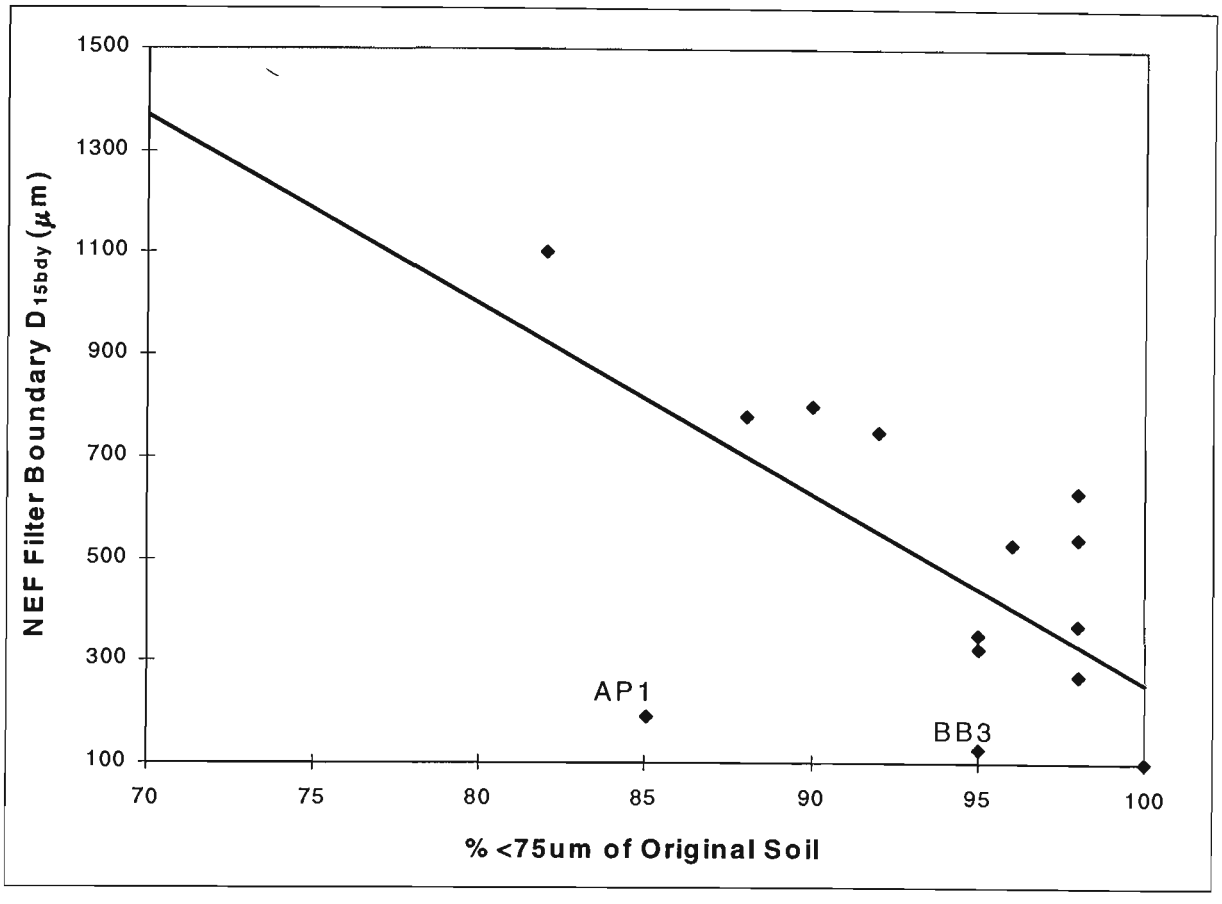

Figure 4.5 Relation between fines content and D_{15bdy}

4.4 Filtration of Broadly Graded Base Soils – The *Reduced PSD* Method

All of the 15 materials tested in this series of NEF tests are either group 1 or 2 materials, with >40% of particles finer than 75μm, as defined by Sherard and Dunnigan (1985). The relationship between critical filter sizes, D_{15bdy}, and base soil size d_{85orig}, determined from these tests is reproduced in Figure 4.6. This Figure also presents some published data of NEF tests from:

1. Khor and Woo (1989), who performed NEF tests on several broadly graded, sandy impervious soils,
2. data for group 2 soils tested by Sherard (1984), as reported by Foster (1999),
3. Delgado (2000), who performed an extensive series of NEF tests on materials from dams throughout Spain.

The Sherard and Dunnigan (1985) design criteria are also shown as a solid line in Figure 4.6.

The majority of the lab data in Figure 4.6 meet, or are very close to, the design criteria, the notable exception being material AP1, which has a safe critical filter size significantly finer than predicted. Some of the group 2 materials in the current laboratory data set, and the majority of the Khor and Woo (1989) and Sherard (1984) data, plot below the line $D_{15F}=9d_{85B}$ and the boundary filter seems to have little correlation with increasing d_{85B}. This is why Sherard and Dunnigan (1985) determined the somewhat arbitrary design guideline $D_{15F}=0.7$mm for these materials. The intention here is to investigate why this sharp divide occurs between the safe filter boundaries for group 1 and 2 materials, and why material AP1 has such a fine D_{15bdy}.

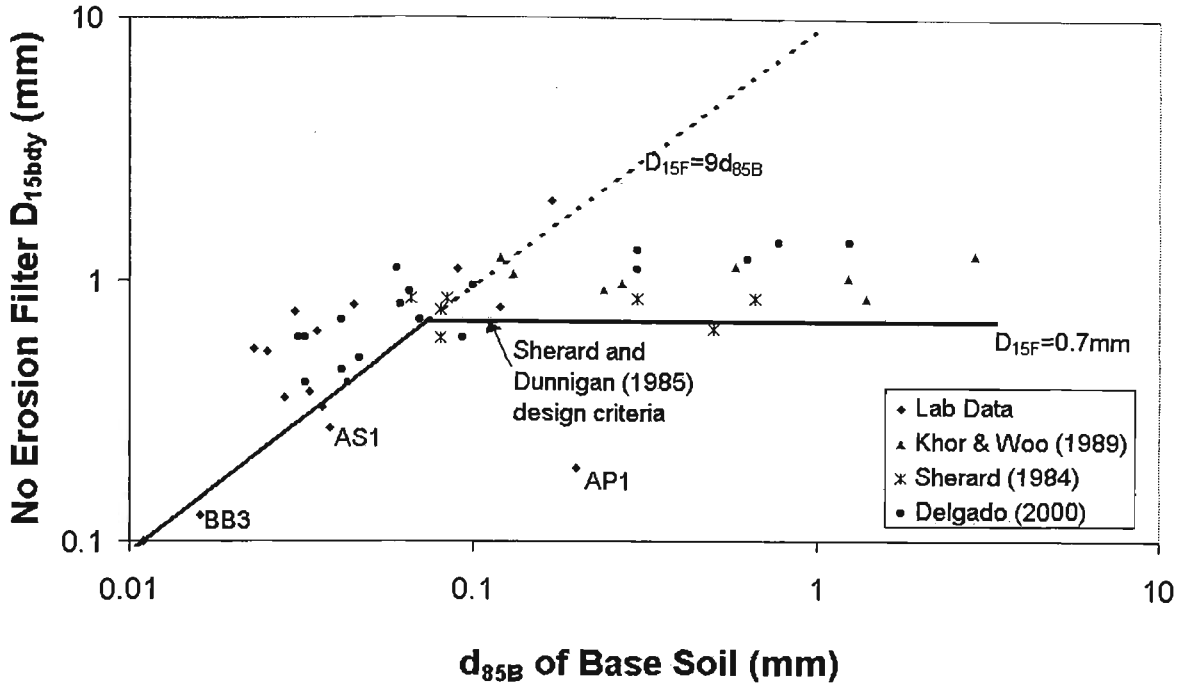

Figure 4.6 Results of NEF Tests compared with Sherard and Dunnigan (1985) design criteria.

The PSD of the AP1 material is shown in Figure 4.8. This material is broadly graded, with approximately 25% medium to coarse sand and 75% fines. The NEF boundary filter has a particle size typical of a filter able to retain fine clay, while the sand fraction of material AP1 has particle sizes approximately equal to the filter particle sizes. This suggests that, similar to filtration of non-cohesive soils, the coarse fraction of material AP1 is unable to retain the fine fraction, ie. the coarse fraction is an ineffective filter for the fine fraction, and self-filtering does not seem to occur. In this case, a successful filter must be able to retain the stable, fine fraction of the material. The stable fraction can be determined by examining whether the coarse fraction can act as a filter for the fine fraction. Splitting the PSD at any point n (where n is the percent passing diameter D_n), we can define D_{15} of the coarse fraction and d_{85} of the fine fraction:

$$d_{15coarse} = d_{n+0.15(100-n)} \quad (4.3)$$

$$d_{85fines} = d_{0.85n} \quad (4.4)$$

The coarse fraction is able to retain the fine fraction, ie. the material can self-filter if:

$$d_{15coarse} / d_{85fines} < 5 \quad (4.5)$$

This method is shown graphically in Figure 4.7. While the figure is a semi-log plot, the y-axis is not logarithmic and the multipliers of n in Equations 4.3 and 4.4 (ie. 0.85n) will not be affected by the log scale. The diameter corresponding to various values of n is fixed for the soil and does not vary with the scale, ie. $d_{0.85n}$ is the same regardless of whether the x-axis scale is logarithmic or not. The PSD should be divided at some point, n; an initial value of n=50% is reasonable unless the material is obviously gap graded. Equation (4.5) is checked to determine if this part of the PSD is stable, based on $d_{15coarse}=d_{57.5}$ and $d_{85fines}=d_{42.5}$. These diameters were found by substituting n=50% into Equations (4.3) and (4.4). As an example, reading from Figure 4.8 for the AP1 material when n=50%, $d_{15coarse}$=0.011mm and $d_{85fines}$= 0.007mm. This gives a ratio $d_{15coarse}/d_{85fines}$=1.6, suggesting that this fraction is stable.

If Equation (4.5) is satisfied then the fraction finer than $d_{15coarse}$ is stable, and increasing values of n should be considered, until Equation (4.5) is not satisfied. The largest diameter $d_{15coarse}$ complying with Equation (4.5), is the coarsest particle of the stable PSD. All larger particles may be captured at the filter interface, but will not be able to retain the finer particles of the base soil. Continuing the example for material AP1, the maximum diameter of the stable PSD, was found to be $d_{15coarse}$=0.055mm. This corresponds to n=68% and $d_{85fines}$=0.011mm. A new PSD, considering only the particles finer than this diameter, defines the stable self-filtering fraction of the soil. This is called the *reduced PSD* and is shown in Figure 4.8 for the AP1 material. This procedure has been called the *Reduced PSD* method. A successful filter must be able to retain the

reduced PSD. The AP1 material has an NEF critical filter with D_{15bdy}>0.19mm, and hence, $D_{15bdy}/d_{85reduced}\approx12$ which is closer to the expected filter ratio and a vast improvement on the previous ratio D_{15bdy}/d_{85}=2.5.

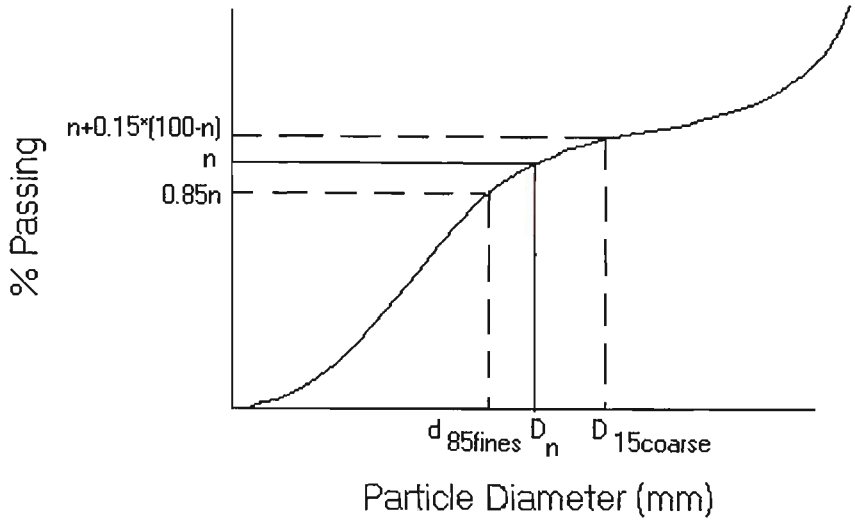

Figure 4.7 Method to assess self-filtration of a soil

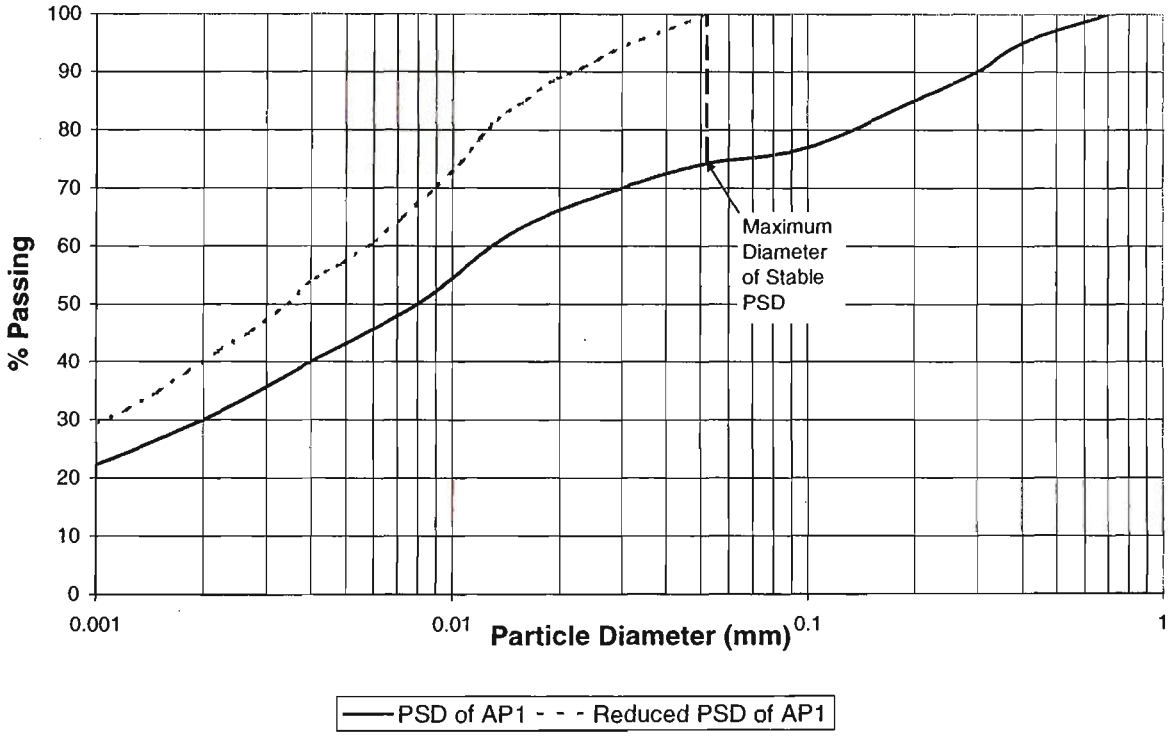

Figure 4.8 PSD and reduced PSD of material AP1

The *reduced PSD* procedure has been followed for each of the base soils tested, and for the Khor and Woo (1989), Delgado (2000) and Sherard (1984) data. The comparison of the measured D_{15bdy} and the $d_{85reduced}$ from the reduced PSD is shown in Figure 4.9. The majority of data points for the reduced PSD of both group 1 and 2 materials now plot above the line $D_{15F}/d_{85(Reduced)}=9$. This suggests that the design guidelines for group 1 soils can be extended to group 2 soils, provided they are able to self-filter, and the reason that many group 2 materials have a surprisingly low D_{15bdy} is that they cannot self-filter. Material AS1 plots below the design line, this material is a fine clay with very uniform PSD, ($d_{98B}/d_{85B}<2$). Sherard and Dunnigan (1985) also noted that uniform materials have a slightly lower D_{15bdy} value, so this result is not unexpected. Group 2 materials S5, BJV-C1 and BJV-C2 plot below the design line. These three materials are silts and sands with negligible cohesion, suggesting that particle aggregation would not occur with these materials, and they may behave more like a coarse material (group 3 or 4 soils) than a fine material, and a retention ratio $D_{15F}/d_{85B}<4$ is probably more appropriate.

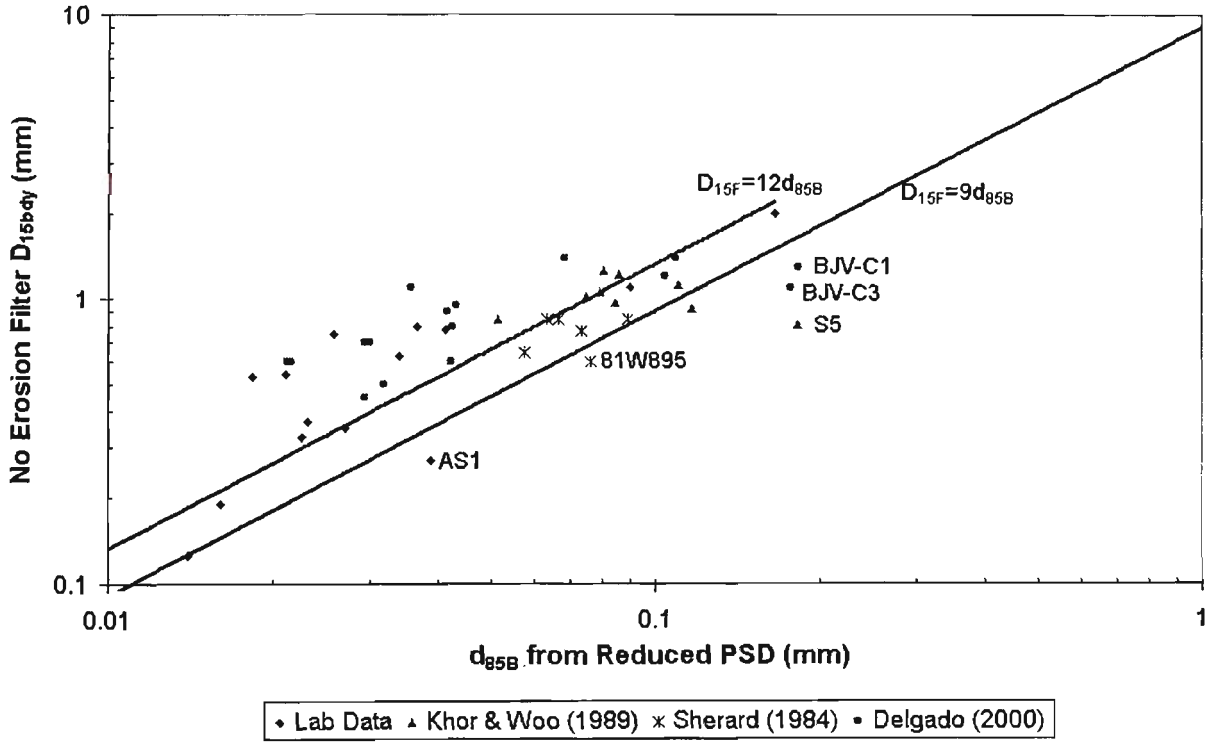

Figure 4.9 Relationship between D_{15bdy} and $d_{85(Reduced)}$ from the *reduced PSD* of the original base soil

Having shown the applicability of the *Reduced PSD* method, the results are divided into soil groups 1 and 2 to examine the effects on these two groups separately. The data is replotted for group 1 materials only in Figure 4.10. The Sherard and Dunnigan (1985) design criterion, $D_{15F}/d_{85(Reduced)}=9$ is also plotted in the Figure. This criterion when applied to the reduced PSD seems overly conservative for most of the data. The line $D_{15F}/d_{85(Reduced)} =12$ forms a lower bound for the majority of the measured NEF boundaries. The only exceptions are materials AS1 and BB3, which are fine clays with uniform gradings. Based on these observations, a new design criterion for group 1 soils is proposed:

$$D_{15F} \leq 12 d_{85reduced} \qquad (4.6)$$

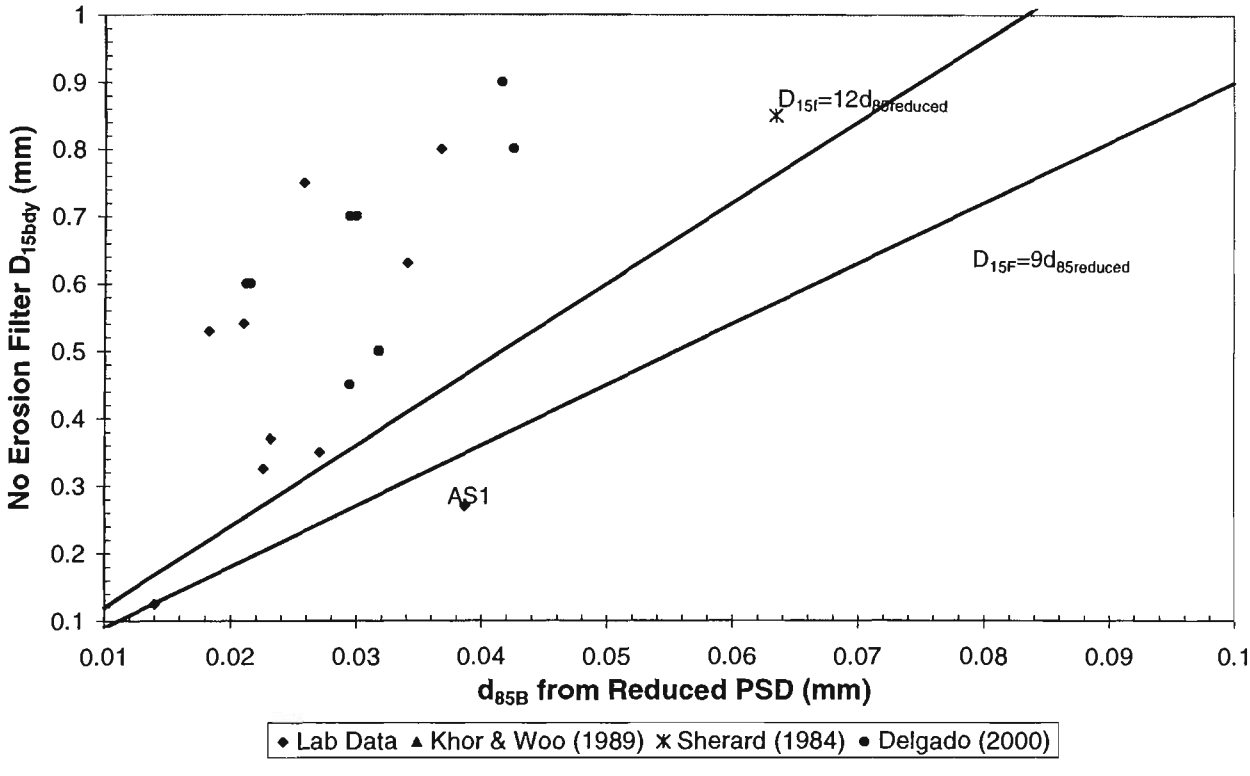

Figure 4.10 NEF boundary against d_{85} of the reduced PSD for soil group 1 materials only

The NEF boundary filter diameter and d_{85B} of the reduced PSD are replotted for group 2 materials in Figure 4.11. The line $D_{15F}/d_{85(Reduced)}=9$ is a lower bound for the majority of the measured NEF boundaries. Notable exceptions are silty materials S5, 81W895, BJV-C1 and BJV-C2. These four materials have a low plasticity index, PI<6, while the remaining group 2 materials were sandy clays and clayey sands with PI>10. The low PI can be related to a small clay fraction, and essentially non-cohesive fines. This suggests that the clay fraction affects particle aggregation, and produces larger particles that are stable during filtration. This aggregation of particles does not occur in low plasticity materials such as sandy silts. These non-cohesive materials should be designed by the criterion for group 3 base soils, $D_{15F}/d_{85B}<4$. Based on these observations, a new design criterion is developed for group 2 materials:

If PI>10:

$$D_{15F} \leq 9d_{85reduced} \quad (4.7)$$

If PI<10:

$$D_{15F} \leq 4d_{85reduced} \quad (4.8)$$

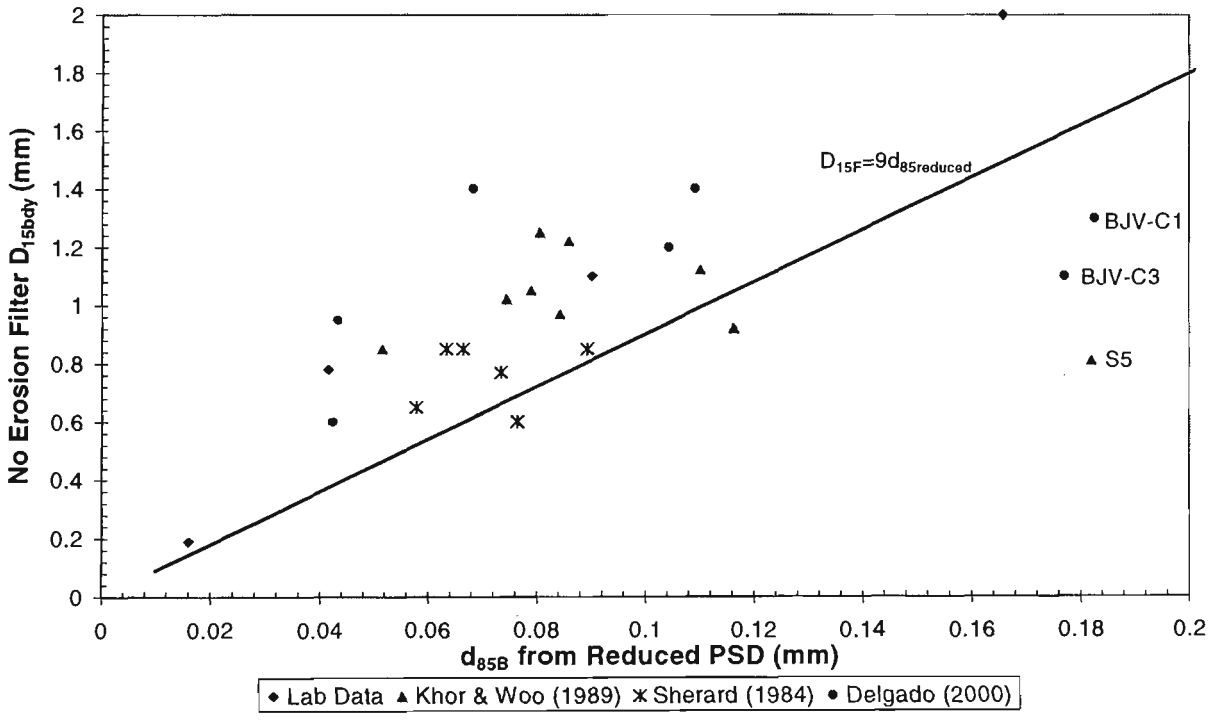

Figure 4.11 NEF boundary against d_{85} of the reduced PSD for soil group 2 materials only.

The Reduced PSD method has been followed to produce the *reduced PSD* of the erosion product (EP) from the laboratory tests. The relation between the reduced erosion product PSD and D_{15bdy} is shown in Figure 4.12. The line $D_{15bdy}/d_{85EP(Reduced)}=4$ represents a reasonable lower bound of the data. Based on the previous argument (Section 4.3.1), that filter voids can retain particles coarser than $D_{15F}/4$, this correlation with the internally stable erosion product suggests that the mechanically dispersed erosion product can be used to conservatively estimate the size of particles involved in filtration. This observation will be used in the next Section to estimate the size of particles effecting filtration of cohesive materials.

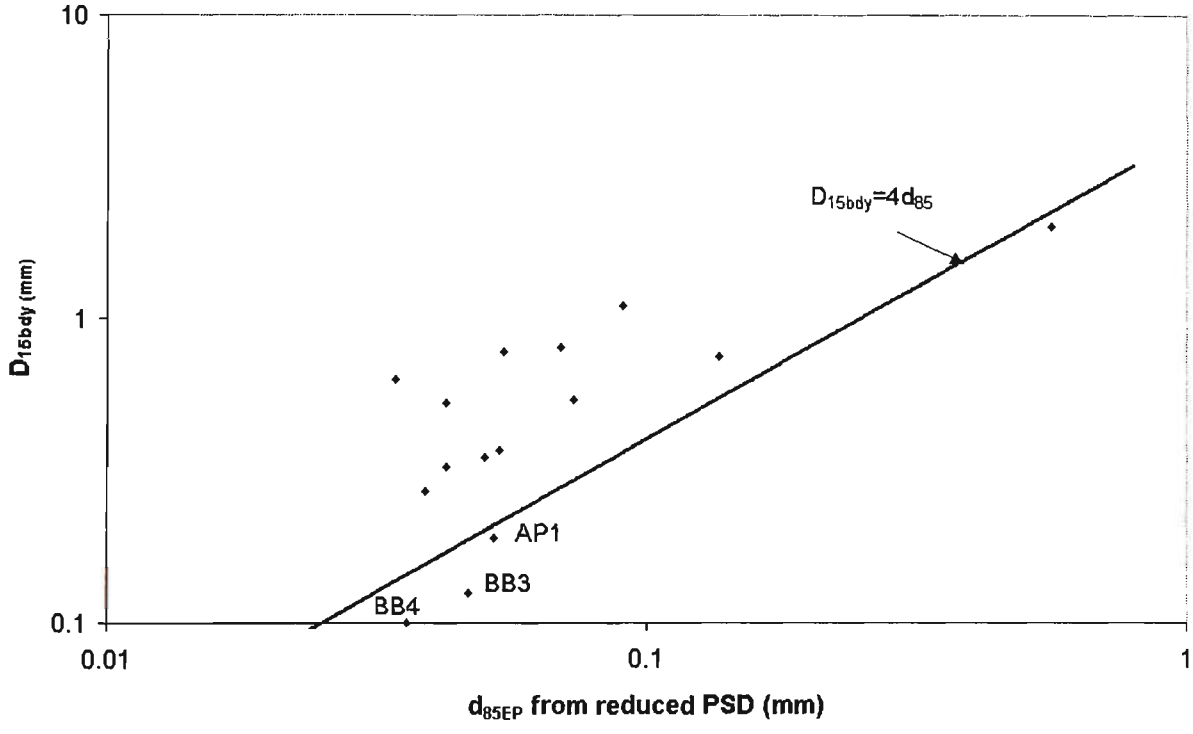

Figure 4.12 Relationship between D_{15bdy} and d_{85EP} of the reduced erosion product PSD.

4.5 Size of Particles for Modelling Filtration

In Chapter 5, a theoretical model of erosion and filtration of cohesive materials will be developed. For this model, it is necessary to define the size of particles that will be eroded, transported and retained within the filter. In Section 4.2.3, it was suggested that fine, cohesive particles erode as aggregates and flocs of many particles rather than individual particles, and that even after extensive mechanical energy is applied, stable aggregates will remain. For fine materials, the d_{85} size of these aggregates may be up to 3-4 times larger than the d_{85} size of the original material. The laboratory results are insufficient to recommend a relation for the size of eroded particles, based on the original particle sizes. However, these results do suggest that some aggregation does occur, and that larger particles are present to influence filtration.

Most dam designers adopt the empirical guidelines of Sherard and Dunnigan (1985) for filter design. These guidelines have been shown to be an adequate lower bound for the size of safe filters for most base soils (Figure 4.6). To ensure that the mathematical model developed predicts conservative results, the eroded particle sizes will be predicted based on the Sherard and Dunnigan (1985) guidelines. The comparison of NEF test results and the size of the erosion product, EP_{disp}, (Section 4.3.1) suggests that a ratio of $D_{15Fbdy}/d_{85EP}=4$ is a lower bound for most test results, ie. no erosion occurs if $D_{15F}/d_{85EP}<4$. Similarly, the analytical modelling and laboratory study of filtration of non-cohesive soils, developed in Chapter 3, suggests that very little erosion occurs for a retention ratio of $D_{15F}/d_{85B}=4$, whereas some erosion occurs for a retention ratio of 6. This suggests that the geometric model developed in Chapter 3 to describe infiltration of non-cohesive particles into a filter can also be used to model cohesive base soils, provided an estimate of the erosion product size is made. The size of the eroded particles

could be estimated by relating the Sherard and Dunnigan (1985) design criteria to the relation $D_{15F}/d_{85rep}=4$, where d_{85rep} is the *representative base soil particle size*. This terminology is adopted to describe the estimated rather than measured size of the EP.

A PSD multiplier, A, is applied to the base soil particle sizes to produce a *representative PSD* (ie. $d_{85rep} = A \times d_{85Orig}$), such that $D_{15F}/d_{85rep}=4$, and the Sherard and Dunnigan (1985) design criteria are met. The entire PSD should be multiplied by A. This multiplier is shown in Table 4.3 for the four different base soil groups. The %<75μm should be calculated based on the original base soil PSD, not the representative PSD after multiplying by A. Alternatively, the erosion product after dispersion could be used as the *representative PSD*. The erosion product is determined by following the laboratory procedure outlined in Section 4.2.

Table 4.3 – PSD Multiplier, A, based on Sherard and Dunnigan (1985) Filter Design Criteria

Soil Group	Base Soil %<75μm Sieve	Filter Criterion	PSD Multiplier A
1	>85%	$D_{15F}/d_{85B} \leq 9$	$A = 2.25$
2	35% - 85%	$D_{15F} \leq 0.7mm$	$A = \frac{0.7}{4d_{85}}$
3	<15%	$D_{15F}/d_{85B} \leq 4$	$A = 1$
4	15% - 35%	extrapolate between groups 2 and 3 based on %< 75μm.	$A = \frac{0.7}{4d_{85}} + \frac{35-F}{20}\left(1-\frac{0.7}{4d_{85}}\right)$ where F = %Fines Passing 75μm

Vaughan and Soares (1982) showed that the minimum size of particles in filtration is defined by the floc size of clay particles. This size is dependent on the clay material and the eroding fluid chemistry, but is generally within the range of 5-20μm. The base soil PSD should be truncated so that the minimum particle size of the *representative PSD* corresponds to the floc size of particles in a sample of the reservoir water. This does not apply to dispersive clays that may erode as sub-micron sized particles. The representative PSD will be used in Chapter 5 to describe the size of particles reaching the filter and adopting the filter void model developed in Chapter 3.

4.6 Summary of Erosion and NEF Testing

A new laboratory procedure, the modified pinhole test, has been developed to measure the erosion rate and the size of eroded particles due to concentrated flow through a pinhole in a cohesive soil. Erosion rates generally correlated well with the equation: $Erosion\ Rate = \alpha(\tau - \tau_c)$. Many materials exhibited some erosion resistance, as demonstrated by a non-zero critical shear stress, τ_c. If the correlation between this linear equation and the measured results in the modified pinhole test is acceptable, then some erosion resistance can be relied upon in design. The erosion equation will be adopted in the modelling described in Chapter 5.

Particles eroded during the large-scale pinhole test were usually significantly larger than the primary soil particles, indicating that erosion occurred as aggregates of primary particles. This increase in particle size seemed closely related to the fines content of the material. The size of these eroded particles was independent of the flow velocity. Hence, selective erosion of fine particles at relatively low velocity does not occur. These large eroded aggregates were unstable, breaking down quickly to finer particles when ultrasonic dispersion was applied to the particles in suspension in the PSA. This mechanical dispersion was assumed to represent the hydraulic forces present within a granular filter in a dam. The size of particles after dispersion was found to reach a stable minimum distribution, and additional dispersive energy was not able to break down these particles further. For fine materials (d_{85Orig}<75μm), the dispersed eroded particles were generally coarser than the primary particles of the material. The ratio of the size of these eroded particles to the d_{85Orig} size of the primary particles is defined as the *aggregation ratio* (Equation 4.2). The aggregation ratio increased with decreasing d_{85Orig} size. This suggests that clay particles erode as aggregates of many particles that are stable under

hydraulic forces, while coarser materials, eg. sands, erode as individual particles. The PSD of the eroded material after this dispersion was essentially constant for each soil sample and did not vary greatly with moisture content, flow velocity, adsorbed ion content or the eroding fluid ion content.

NEF tests performed on the same materials revealed that there was a relation between these eroded particle sizes and the 'no erosion' filter boundary. The relation D_{15bdy}/d_{85EP}=4-5 was a lower bound for the results in all but three cases. The ratio D_{15bdy}/d_{85EP}=4 was chosen because it represents the controlling constriction size described by Kenney et al. (1985). Hence, it is postulated that it is these stable aggregates of particles (EPdisp) that are captured at the filter interface, rather than the smaller primary particles. Table 4.3 presented a multiplier A, which is multiplied by the original particle sizes to produced a *representative PSD*. This represents the size of aggregates of particles that will remain stable and influence filtration. This multiplier, A, will be used in Chapter 5 to describe the size of particles reaching the filter when modelling the filtration of cohesive soils.

Broadly graded cohesive base soils may be internally unstable, where the coarse fraction of the material is unable to act as a filter for the fine fraction. This means that a filter that can retain the coarse fraction may allow continued erosion of the base soil because self-filtration does not occur. A new procedure has been described to determine this stable fraction, called the *Reduced PSD* method. Re-plotting of the laboratory data based on this *reduced PSD* showed Group 1 materials can be designed using the relation $D_{15bdy}/d_{85reduced}$=12. A design criterion for Group 2 materials was proposed, for clayey materials with PI>10, $D_{15bdy}/d_{85reduced}\leq 9$, and for silty materials with PI<10, use $D_{15bdy}/d_{85reduced}\leq 4$.

5. MODELLING FILTRATION OF COHESIVE SOILS

5.1 Introduction

Chapter 3 saw the development of a theoretical model of transport of non-cohesive base soil particles into a granular filter. Non-cohesive materials were considered first, because it was easier to explain the fundamentals of particle transport using these materials, based on the geometric probabilities of movement. However, in the majority of applications, granular filters are used to protect cohesive materials. As shown in Chapter 4, cohesive materials present further problems to a theoretical description of filtration. Resistance to erosion and the formation of large aggregates of particles rather than individual particles must be considered. In addition, cohesive particles may be subjected to strong inter-particle physico-chemical forces that affect the deposition of particles within the filter. The erosion rate parameters, size of erosion product particles and representative particle sizes determined in Chapter 4, will be used in this chapter to develop a time-dependent model of filtration of cohesive materials.

Recent research has shown that cracks can occur in almost all impervious cores of embankment dams (Sherard, 1986). Cracking can be due to differential settlement, shrinkage, foundation movement, earthquake or hydraulic fracture. These cracks allow water to flow with significantly higher velocity and erosive force than steady state seepage through the intact core. Cohesive core materials can be eroded internally along the walls of these cracks, without collapsing and sealing the crack. This results in an enlargement of the crack, higher flow velocity and greater erosion. Continuation of this process can lead to piping failure.

The aim of this Chapter is to theoretically examine and describe the problem of internal erosion through cracks in cohesive core materials and to produce a time-dependent model of particle erosion, transport and filtration. For the purposes of modelling, the erosion of a dam core due to concentrated flow through a crack can be considered in five stages:

1. The formation of the crack through the core leading to a channel for water flow,
2. The erosion of material from the crack walls due to the shear stress applied by flowing water,
3. The transport of eroded particles to the filter,
4. The retention or transmission of these particles within the filter.
5. Continuation of erosion leading to piping failure, or sealing of the crack as eroded particles form a cake at the filter interface and reduce water flow through the crack.

These processes are shown graphically in Figure 5.1, which is a sketch of the interface between the cracked core and the filter. In order to complete the model, each of these stages will be considered separately in this Chapter.

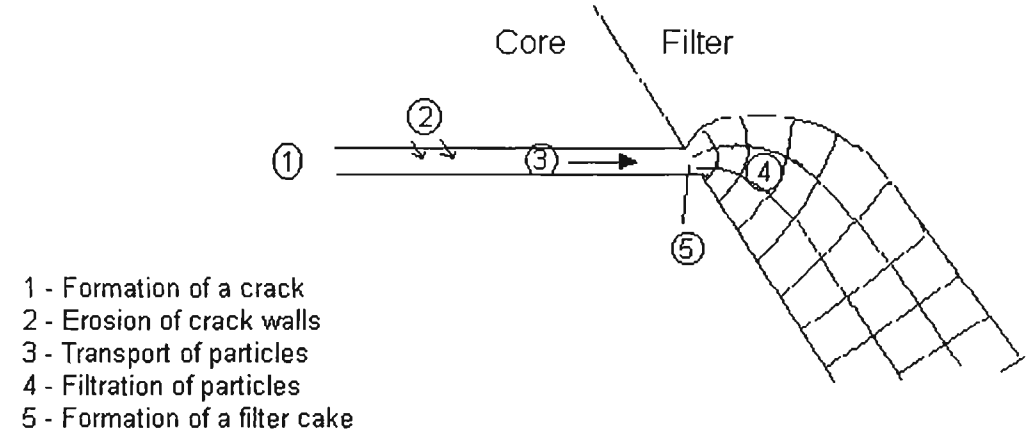

Figure 5.1 Process for modelling cracking, erosion and filtration within an embankment dam

5.2 Formation of the Crack

Many factors may contribute to cracking in embankment dams; some possible causes of cracking include differential settlement of embankment materials, foundation movement, shrinkage, earthquake-induced movement, slope instability and hydraulic fracturing. The hydraulic fracturing process has been described in detail in Chapter 2, it was shown that the minimum pressure required to develop hydraulic fracturing can be estimated based on the minimum principal stress, ie. hydraulic fracture can occur when:

$$\gamma_w h_w \geq T + \sigma'_{min} + p_0 \qquad (5.1)$$

Where, $\gamma_w h_w$ is the hydrostatic water pressure, T is the tensile strength of the core material, σ'_{min} is the minimum effective stress in the core and p_0 is the pore pressure in the core. If the hydrostatic water pressure is sufficiently high then a crack can be opened within the clay core, resulting in water infiltrating the crack and 'jacking' it open. This may result in the crack continuing through the dam core, if the insitu stress conditions allow. However, estimating the re-distribution of internal stresses within a dam is very difficult, and it may be more appropriate to simply consider the likely locations for cracks to occur.

Foster (1999) examined reports of cracking in many embankment dams, and concluded that in most cases the crack occurred at depths from the crest of less than about 30m. The depth of cracking appeared to be related to the source of the low stress condition:

- Cracks associated with small scale irregularities in the foundation profile generally occur close to the foundation surface and usually in the lower half of the dam height.
- Cracks associated with narrow cores and arching of the core between the shell zones are generally located at depths from the crest of 1/3 to 2/3 of the height of the dam.

- Cracks and piping associated with broad changes in the abutment profile are generally located within the upper 1/3 of the height of the dam. This is where tensile stresses might be expected to occur due to large-scale changes in the abutment slope.
- Earthquake induced cracking is usually assumed to induce cracks in the upper 1/3 of the dam, however, foundation movement may lead to cracking in lower sections of the dam.

The most likely location(s) for a crack to develop can be determined based on the observations above and the dam geometry. Modelling the effects of several cracks at likely locations and varying thickness will determine the worst case for each particular dam. Since it is extremely difficult to predict cracking in dams, the modelling developed in this Chapter will assume that a crack has developed and will then consider the effects of flow through this crack.

The width of a crack is very difficult to predict, as a large number of material properties and external stresses control the formation of a crack. Instead, an educated estimate of the crack thickness will be made, depending on the dam geometry. For low dams, the crack thickness is probably only fractions of a millimetre, whereas for high dams, cracks of several centimetres may develop. Sherard (1986) suggests that an excess hydrostatic water pressure of 10-20m of water could result in development of a crack up to 5-10cm thick.

5.3 Erosion Due to Concentrated Flow in a Crack

Following the formation of a continuous crack through the dam core, seepage flow through the crack may cause erosion of the crack walls. To approach the problem of modelling erosion of a crack through a dam core, a number of simplifying assumptions will be made:

1. A single, horizontal crack exists, continuous from upstream to downstream with no adjoining cracks. The theory developed here applies equally well to vertical cracks except that flow rates, and hence, eroding forces at different depths in a vertical crack will vary because of variations in the hydrostatic pressure.
2. The crack can be modelled by an average thickness, w.
3. The crack is effectively infinitely wide along the dam axis, and can be modelled as a 2D problem of erosion due to flow between two parallel plates.

Chapter 4 presented a laboratory study which demonstrated that the erosion rate, E, is dependent on the applied shear stress. For cohesive materials, there is a critical shear stress, τ_c, below which erosion will not occur. At greater flow velocities, the erosion rate increases linearly with shear stress, ie.

$$E = \alpha(\tau_w - \tau_c) \text{ kg/m}^2\text{s} \qquad (5.2)$$

where α=rate of change of erosion rate (g/Ns)

τ_w=wall shear stress per unit width (proportional to flow rate) (N/m)

τ_c=critical shear stress, below which no erosion occurs. (N/m)

Under some flow conditions, re-deposition of particles may occur within the crack. To account for this a deposition coefficient, D, is introduced. This coefficient has the same units as the erosion rate (kg/m^2s). A relation for the deposition coefficient D will be developed in Section 5.5.2.

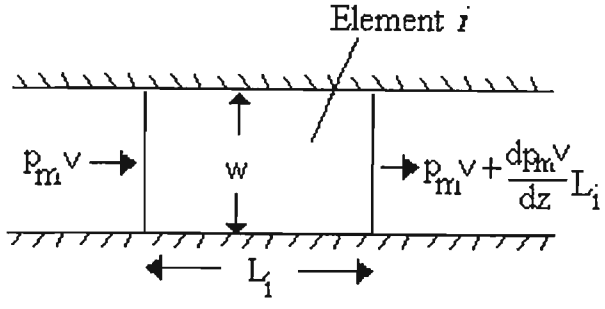

Figure 5.2 Cracked core discretised into elements

The crack can be divided into a number of discrete elements of length L_i, and thickness w, as shown in Figure 5.2. A method to determine the flow rate through the crack elements will be described in Section 5.4.2. Considering the mean slurry density, ρ_m, and the mean flow velocity (determined from the flow rate), v, conservation of mass in the liquid slurry (M_L) can be considered within an element of unit width:

$$\frac{\Delta M_L}{\Delta t} = \frac{M_{in} - M_{out} + \text{erosion} - \text{deposition}}{\text{time}} \tag{5.3}$$

or,

$$\frac{\partial(\rho_m A L_i)}{\partial t} = A(\rho_m v)_i - A\left[(\rho_m v)_i + \frac{\partial \rho_m v}{\partial z} L_i\right] + EL_i - DL_i \tag{5.4}$$

The left-hand side of Equation 5.4 can be expanded:

$$\frac{\partial \rho_m A L_i}{\partial t} = L_i \frac{\partial(\rho_m A)}{\partial t} = \rho_m L_i \frac{\partial A}{\partial t} + A L_i \frac{\partial \rho_m}{\partial t} \tag{5.5}$$

The flow area A, per unit width of crack becomes the crack thickness, w. The rate of change of this thickness is related to the net rate of erosion and deposition:

$$\frac{\partial A}{\partial t} = \frac{\partial w}{\partial t} = \frac{1}{\rho_b}[2\alpha(\tau_w - \tau_c) - D] \tag{5.6}$$

Where, ρ_b is the bulk density of the core material. The erosion rate, E, from Equation 5.2 has been doubled to account for erosion of both walls of the crack. Substituting Equations 5.5 and 5.6 into Equation 5.4 yields:

$$\frac{\partial \rho_m}{\partial t} = -\frac{\partial \rho_m v}{\partial z} + \left(1 - \frac{\rho_m}{\rho_b}\right)\frac{1}{w}[2\alpha(\tau_w - \tau_c) - D] \tag{5.7}$$

Equations 5.6 and 5.7 are the governing differential equations of the erosion process due to confined flow through a crack. Equation 5.6 describes the increase in crack width as erosion occurs, while Equation 5.7 describes the corresponding change in slurry density with time. The equations can be solved by a finite difference procedure with suitable boundary conditions for the slurry velocity and density. Equations to determine the eroding shear stress, τ_w, are developed in Section 5.4.2. The erosion parameters τ_c and α can be determined by following the laboratory procedure described in Chapter 4, or predictive techniques outlined in Chapter 2.

5.4 Transport of Loose Particles

Vaughan and Soares (1982) raised the issue of the transport of eroded particles to the filter, "...The filter must arrest the eroded debris as it is carried through the crack. The extent to which self-filtering occurs will depend on the amount of segregation and deposition of the eroded debris within the crack." The implication here is that at low flow rates, larger particles may not be transported to the filter face, because the flow drag forces are insufficient to move these particles.

Maranha Das Neves (1987) performed a number of "crack erosion tests" which involve a low velocity flow passing over a base soil and then into a filter, to examine the mechanism of crack erosion by concentrated water flows and to investigate the transportation of eroded material. Two important observations were that:

- there was no visible segregation during transportation of the eroded base material,
- even low flow velocities (of about 2cm/s) assure the transportation of sand particles to the filter surface, thus allowing the development of a self-filtering action.

Based on these observations, it is most likely that all particles eroded will be transported through a crack and segregation will not occur. The next section will investigate this further. Both the erosion and transport of cohesive particles are governed by the shear stress, τ_w, applied by the water flowing through the crack. A method to estimate this shear stress will be outlined in Section 5.4.2.

5.4.1 Minimum Shear Stress for Particle Transport

Graf (1971) examined the movement of cohesionless particles in open channel flow. It was shown that there is a minimum shear stress (different to the critical shear stress for

erosion) above which some of the bed load is transported and below which no movement occurs. This minimum shear stress concept is adopted here to estimate the maximum size of particles mobilized by flow through a crack. Graf (1971) suggests that Shields' diagram is suitable for estimating the minimum shear stress to initiate transport of uniform, spherical, non-cohesive particles. Based on the applied shear stress within the crack (determined subsequently in Section 5.4.2), the maximum particle diameter that can move may be estimated from Shields' diagram.

Shields' diagram is based on incipient motion for a bed of uniform size particles, and extrapolating this data to estimate the shear stress at which certain particle diameters in a heterogeneous bed will begin moving is beyond the original experiments. The minimum shear stress predicted by Shields' diagram is expected to increase for non-uniform grain sizes and non-spherical particles. For cohesive particles, forces acting between the particles will have an effect on the critical velocity. However, the larger particles eroded from the core material will be sand or aggregates of clay particles for which the physical forces due to drag and gravity will in most cases be much greater than the physico-chemical attractive forces. It is assumed that, while these effects (heterogeneity, particle shape and cohesion) will increase the minimum shear stress, the concept of a minimum shear stress necessary to move particles still applies. For these reasons, the minimum shear stress, determined from Shields' diagram, has been doubled to produce Figure 5.3, which is a rearrangement of Shields' diagram, assuming a particle density of 2650 kg/m^3. Figure 5.3 demonstrates that at a low shear stress of 0.5N/m^2, transport of particles up to 0.4mm can occur. The flattening of the curve to the left of this point indicates that lower shear stresses will result in little or no movement of particles larger than colloidal size. Higher shear stresses beyond 0.5N/m^2 rapidly increase the size of particles mobilised.

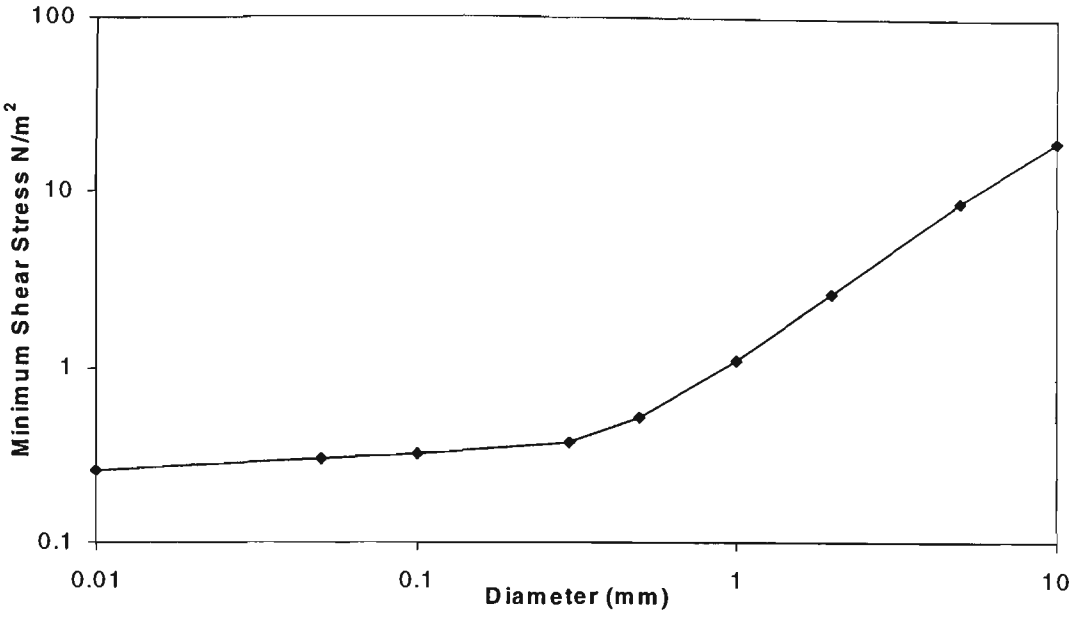

Figure 5.3 Predictions of Shield's diagram for incipient particle movement

Vaughan and Soares (1982) defined a 'perfect' filter as one which will retain the smallest particles that can arise during erosion even if they arrive at the filter interface after complete segregation, unaccompanied by larger particles that would allow self-filtering to occur. Based on Figure 5.3, there is a small range of flow conditions under which segregation could occur because the applied shear stress is sufficient to mobilise fine particles, but not the coarser particles. This suggests that segregation is a risk when the core material is highly erosive, with a critical shear stress to initiate erosion of less than 0.5 N/m^2. In this case, particles can erode but only the fines will be transported and the filter may not be able to retain these mobile fine particles. Arulanandan and Perry (1983) identified highly erodable soils as those with $\tau_c \leq 0.4$ N/m^2, and determined that the risk of failure of these materials was significantly higher than for less erodable materials, if protected by the same filter. Perhaps it is this possibility of segregation that leads to a higher probability of internal erosion. For soils with $\tau_c > 0.5 N/m^2$, it is unlikely that

seepage conditions could exist such that clay and silt sized particles are eroded due to a high eroding shear stress, but coarser particles are not transported because the transporting shear stress is insufficient. Hence, for these more erosion resistant materials, the Vaughan and Soares (1982) perfect filter design criterion is overly conservative.

5.4.2 Flow Rate Through a Cracked Core

Kovacs (1981) examined flow through a single fissure in rock, by assuming the crack could be modelled as flow between two parallel plates. The same model will be adopted here. For laminar flow, the crack is represented by a line element with permeability k_c and width *w*:

$$k_c = \frac{g}{12\eta} w^2 \tag{5.8}$$

where, η is the viscosity of the liquid slurry and *g* represents acceleration due to gravity. Because the slurry contains suspended particles, its viscosity (η) is higher than that of clear water (η_0). A relation developed by Happel and Brenner (1965) is adopted here to determine the increase in viscosity due to interaction effects between the particles and also between the particles and crack walls (Equation 5.9). The diameter, *d*, can be assumed to be the mean diameter of particles in the slurry. The increase in viscosity is based on the slurry volumetric concentration (C_V), as given by:

$$\frac{\eta}{\eta_0} = 1 + 2.5C_V\left(1 + \frac{5dw}{8(2w - d)^2}\right) \tag{5.9}$$

Kovacs (1981) performed a number of experiments to produce a general equation relating the average flow velocity (v) with the hydraulic gradient along the crack (i_{crack}):

$$(i_{crack})^{\frac{3}{4}} = \left(1.25\frac{v}{k_c}\right)^{\frac{3}{4}} + \left(\frac{0.01}{\sqrt{g\eta k_c}}v^2\right)^{\frac{3}{4}} \qquad (5.10)$$

The first term accounts for laminar conditions and the multiplier 1.25 represents the effect of roughness of the crack walls. The second term accounts for turbulent effects and increases with the square of velocity as predicted by conservation of energy from fluid mechanics. The hydraulic gradient, i_{crack}, and flow velocity, v, are still unknown.

The hydraulic gradient acting on the crack is related to the upstream and downstream pressure head. The upstream head can be easily determined from the reservoir head and assumed position of the crack. The upstream fill may reduce the head at the crack inlet, H_{inlet}, depending on the flow rate, dam materials and geometry. The mean hydraulic gradient across the crack can be determined from:

$$i_{crack} = \frac{H_{inlet} - H_{filter}}{CrackLength} \qquad (5.11)$$

The head at the exit of the crack, H_{filter}, is dependent on the filter permeability and flow rate. When the flow reaches the filter, it will spread out from the crack outlet and saturate some portion of the filter. The assumption made here is that the initial spread of water into the filter from the crack outlet will be the same as flow from a point source, with minimal initial effect due to gravity. Further, it is assumed that at some radial distance, R, from the crack, the water pressure is zero, with pressure head H_0. Beyond this initial expansion in flow, the flow will be affected by gravity and tend towards uniform flow draining out of the filter. This saturated flow pattern is sketched in Figure 5.4.

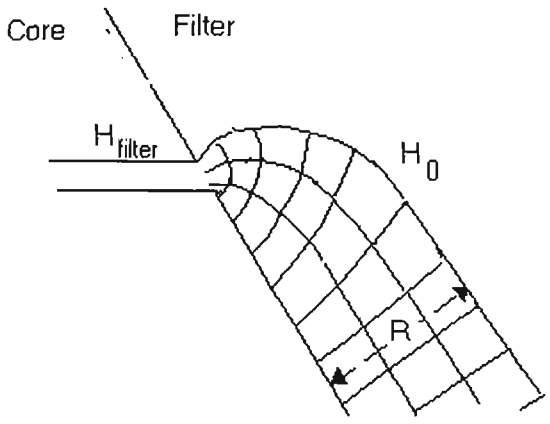

Figure 5.4 Assumed flow paths in filter from exit of cracked core

The radius of the radial seepage from the crack, R, is assumed equal to the width of flow in the filter after uniform flow is established (Figure 5.4). This radius can be estimated using Darcy's law. Assuming the filter to be free draining (ie. the hydraulic gradient in the filter, i_{filter}, is equal to the filter slope), then the drainage capacity of the saturated zone of thickness R per unit width, is given by:

$$Q = k_f i_{filter} R \tag{5.12}$$

In addition, the flow rate from the crack can be determined from the equation for flow from a point source:

$$Q = \frac{\pi k_f \left(H_{filter} - H_0\right)}{\ln\left(\frac{R}{r_{cr}}\right)} \tag{5.13}$$

Where, H_{filter} is the outlet head from the crack, H_0 is the head in the unsaturated filter (pressure=0), and r_{cr} is assumed to be the crack thickness *w*. Substituting R from Equation (5.12) into Equation (5.13) and rearranging gives:

$$H_{filter} = \frac{Q}{\pi k_f} \ln\left(\frac{Q / k_f i_{filter}}{w}\right) + H_0 \tag{5.14}$$

It is possible that a large crack will allow a flow rate greater than the drainage capacity of the filter (the filter capacity is determined by substituting the total filter thickness for R in Equation 5.12). In this case, the downstream embankment will become partially saturated, and the outlet head, H_{filter}, may be greater than that estimated by the method outlined above. In this case a more detailed seepage analysis would be required to estimate the outlet head, however, a simple estimate is to increase the head at radius R, ie. H_0, to represent the head at the filter – fill interface. Depending on the dam materials, geometry and flow rate it may be reasonable to simplify the analysis by assuming the exit pressure, H_{filter}, to be negligible.

An iterative process can be followed to balance equations (5.10), (5.11) and (5.14), in order to calculate i_{crack}. The flow rate, Q, is estimated, and H_{filter} calculated using Equation (5.14). The crack flow velocity, v, is determined from the estimated flow rate and the crack width, *w*. Then Equation (5.10) is used to calculate i_{crack}. This is compared with i_{crack} calculated using Equation (5.11). The flow rate is varied until the correct value of i_{crack} is determined.

Now that the hydraulic gradient across the crack has been defined, the remaining important parameter is the wall shear stress, τ_w, which defines the erosion rate (using Equation 5.2) and the transport of loose particles within the crack (from Figure 5.3). To determine this shear stress, it is necessary to consider the forces acting due to flow through the crack, as shown in Figure 5.5. This diagram can refer to either the entire crack or a single crack element.

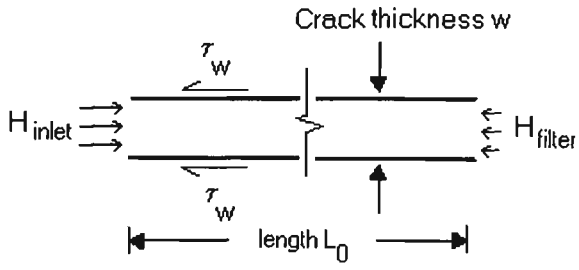

Figure 5.5 Force balance on crack

The forces acting on the flow include the applied pressure head (H_{inlet}-H_{filter}) and the resisting drag caused by shear stress τ_w. In Figure 5.5, a force balance in the direction of flow, per unit width of the crack, gives:

$$\sum F = \rho_m g(H_{inlet} - H_{filter})A - 2\tau_w L_0 = 0 \qquad (5.15)$$

where, ρ_m is the slurry density and A is the cross sectional area of the crack per unit width (equal to the crack thickness, *w*). Rearranging Equation (5.15) gives:

$$\tau_w = \rho_m g \frac{w}{2} \frac{(H_{inlet} - H_{filter})}{L_0} \qquad (5.16)$$

substituting $\frac{H_{inlet} - H_{filter}}{L_0} = i_{crack}$ into Equation (5.16) gives:

$$\tau_w = \rho_m g \frac{w}{2} i_{crack} \qquad (5.17)$$

This wall shear stress can be substituted into Equations (5.6) and (5.7) to calculate the rate of change of the slurry density and crack width. This entire process predicts the changes in flow rate, crack width and density of the slurry in crack elements with time.

5.5 Particle Capture Within the Filter

Retention of cohesive particles within the filter occurs by two mechanisms. The first is physical capture, or particle straining, where base soil particles are larger than the void constrictions they encounter, and are retained by these constrictions. This mechanism is essential for sealing of concentrated leaks, as particles larger than the void constrictions at the filter interface, form a low-permeability cake on the filter face and reduce the flow. The second particle capture mechanism is physico-chemical attraction, where clay particles finer than the void constrictions may adhere to the pore walls due to physico-chemical forces, this process was introduced in Section 2.7.1. This mechanism results in a long-term reduction in the porosity and permeability of the filter, as the void sizes reduce due to the captured particles. A third mechanism due to sedimentation of particles from low velocity flow has been ignored because changes in flow conditions can re-entrain these temporarily stationary particles.

5.5.1 Physical Capture (Straining) of Particles

The physical capture of large particles is a geometric filtration problem, and has been examined in detail in Chapter 3 for non-cohesive base soil particles. The laboratory study of filtration of cohesive materials, described in Chapter 4, determined that the mechanism of physical capture of cohesive particles could be assumed to be similar to the mechanism for non-cohesive particles. The laboratory study also examined the size of particles eroded due to flow through a pinhole, representing a crack, and the effect of these eroded particle sizes on filtration. In order to conservatively estimate the size of eroded particles, Table 5.1 (previously developed in Chapter 4.5), presents a multiplier, A, which is multiplied by the base soil particle diameters to determine the *representative*

PSD for modelling. The representative PSD is considered as defining the size of particles reaching the filter and initiating physical capture. Many cohesive materials appear to have particles significantly larger than the representative PSD, as shown by a large NEF boundary D_{15bdy}/d_{85B} ratio measured in the laboratory. However, the representative PSD (ie. the PSD after multiplying by A) was shown in Chapter 4 to represent a lower bound of the particle sizes measured after erosion tests, and hence, is adopted as a conservative estimate of the particle sizes.

Table 5.1 PSD Multiplier, A, based on Sherard and Dunnigan (1985) Filter Design Criteria

Soil Group	Base Soil %<75μm Sieve	Filter Criterion	PSD Multiplier A
1	>85%	$D_{15F}/d_{85B} \leq 9$	$A = 2.25$
2	35% - 85%	$D_{15F} \leq 0.7mm$	$A = \frac{0.7}{4d_{85}}$
3	<15%	$D_{15F}/d_{85B} \leq 4$	$A = 1$
4	15% - 35%	extrapolate between groups 2 and 3 based on %< 75μm.	$A = \frac{0.7}{4d_{85}} + \frac{35-F}{20}\left(1 - \frac{0.7}{4d_{85}}\right)$ where F = %Fines Passing 75μm

The basic process of the particle capture model is repeated here to explain how the capture of cohesive particles within the filter can be modelled. The development of the model is described in Chapter 3, and equations (5.18) to (5.21) were developed in Chapter 3.

1. The filter void constriction sizes are estimated based on a comparison of the filter particle sizes and relative density, to produce a constriction size distribution (CSD) for each filter element. This procedure is described in Section 3.2.2.
2. The probability, p, that a particle of diameter d can pass any random constriction is the cumulative frequency of constrictions larger than d, found from the CSD. Based on a three dimensional cubic model of the filter pores, the probability that this particle of diameter, d, can move one 'unit step' in the direction of flow, $P(F)$ is given by:

$$P(F) = p + \sum_{i=0}^{\infty} \left[1-(1-p)^4\right](1-p)p\left\{\left[1-(1-p)^3\right](1-p)\right\}^i \qquad (5.18)$$

3. The distance, L, that this particle of diameter d can move into the filter is calculated from:

$$L = \frac{\ln(1-\overline{P})}{\ln P(F)} . D_{f,mean} \qquad (5.19)$$

Where, $D_{f,mean}$ is the 'unit step', estimated as the mean filter particle diameter calculated by number of particles not the mass distribution, and $\overline{P}$ is the probabilistic certainty that the particle will be stopped. A value of $\overline{P}$=95% is usually adopted.

4. The filter is divided into a number of discrete elements. Mobile cohesive particles within each filter element are grouped into three size classes:
   i. Large particles with infiltration distance L<$D_{f,mean}$ cannot move into the next filter element and are retained in their current location. In the case of the first filter element, this means that these large particles collect at the filter face and begin to form a filter cake. The formation of a filter cake is described in Section 5.6. The minimum diameter of particles in this size range, having L=$D_{f,mean}$, is defined as d_r, the retained particle diameter.

ii. Medium size particles with $D_{f,mean} < L <$ *Element Length,* move into the next element and are retained there. These retained particles cannot be later dislodged.

iii. Fine particles with $L >$ *Element Length*, continue to move through the filter.

Note that the *Element Length* is the length from the filter interface to the end of the element being considered.

5. The rate of movement of particles within the filter is determined by the equations of conservation of mass and momentum below (Equations 5.20 and 5.21, from Indraratna and Vafai, 1997). These equations are solved by a finite difference procedure. The boundary conditions for the finite difference analysis are: a) initial density of the flow is equal to ρ_w; b) the density entering the first filter element with time is determined from Equation (5.7), less the fraction of particles retained at the filter face, defined by particles in the size range (i) above.

$$\text{Conservation of Mass: } \frac{d(\rho_m u)}{dz} = \frac{d\rho_m}{dt} \qquad (5.20)$$

$$\text{Conservation of Momentum: } \sum F = \rho_m V_m \left(\frac{du}{dt} + u \frac{du}{dz} \right) \qquad (5.21)$$

6. The particle size distribution, permeability and porosity of each filter element is re-calculated at the end of each time step, based on the mass and size of particles entering and exiting each element.

7. This procedure can be coupled with the crack erosion equations (5.6) and (5.7), and the flow rate equations (5.10), (5.11) and (5.14), and repeated at each time-step, to show the time dependent changes occurring within the crack and filter.

The procedure described above is a summary of the filtration model. The model is described in greater detail in Chapter 3. The important points are that the slurry density

of the first filter element is coupled to the slurry density exiting the last crack element, less the fraction of these transported particles that cannot pass into the filter. In addition, the particle transport equations for the crack, developed in Section 5.4.2, predict the flow rate and flow velocity, u, within the filter. This links the erosion and transport equations developed in this Chapter with the particle capture and transport equations developed in Chapter 3.

5.5.2 Physico-Chemical Capture of Fine Particles

The second particle capture mechanism considered involves physico-chemical attraction, where clay particles finer than the void constrictions may adhere to the pore walls due to these attractive forces. The level of attraction is a complex function of inter-particle forces including gravitational, inertial, hydrodynamic, electric double layer and van der Waals forces. Reddi and Bonala (1997) have examined this physico-chemical capture in granular filters. They define a particle deposition coefficient, λ, which includes all of the forces mentioned above, such that:

$$\frac{d(MassCapture)}{dt} = \lambda C \qquad (5.22)$$

For flow through granular media, the deposition coefficient, λ, is give by:

$$\lambda = \frac{V}{\psi e^{2(b^2+m)}}\left[4(\theta a)^2 - 4(\theta a)^3 e^{(b^2-2m)/2} + (\theta a)^4 e^{2(b^2-m)}\right] \qquad (5.23)$$

Where m and b are, respectively, the mean and standard deviation of the log-distribution of void radii, $ln(D_v/2)$, assuming that the filter void size distribution can be represented as a log-normal distribution. The parameter ψ is the effective length of pore tubes in the direction of flow. Reddi and Bonala (1997) suggest adopting a value of ψ=9.11mm. V is the velocity of flow through the filter pores, 'a' is the radius of the base particles and θ is

a parameter representing the particle attraction forces. These physico-chemical forces essentially apply only to cohesive particles, hence the particle radius, a, should represent the mean radius of clay flocs in the pore water. The meaning of the product θa can be seen conceptually in Figure 5.6. The fraction of flow within the annulus between pore radius r and an inner radius (r-θa) is equivalent to the probability of particle capture.

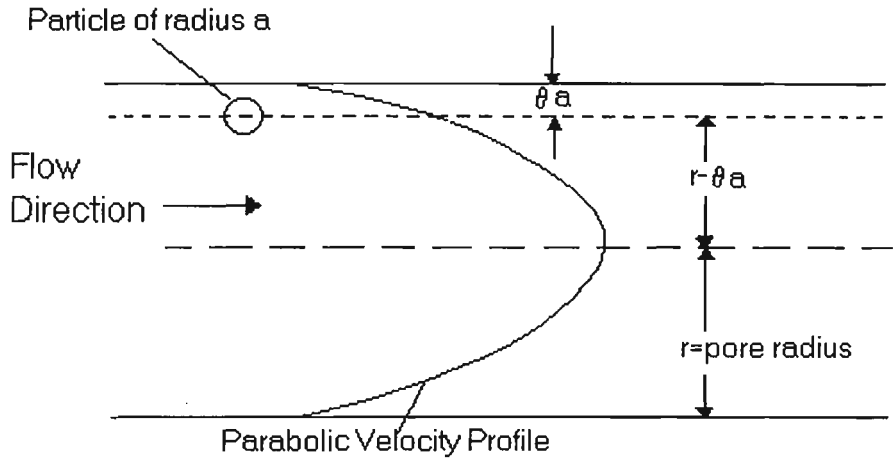

Figure 5.6 Probability of Particle Capture in a Pore Tube (After Rege and Fogler, 1988)

Since the rate of deposition reduces with increasing pore velocity, V, the parameter θ can be estimated by Equation (5.24), developed by Rege and Fogler (1988):

$$\theta = \theta_0 e^{\left(-\frac{V}{V_c}\right)} \qquad (5.24)$$

The particle deposition parameter, θ, is composed of two parameters: θ_0 the particle attraction force constant, and V_c, the critical pore velocity. These constants represent the particle deposition conditions and may vary due to different clay minerals, pore water conditions, temperature, pH etc. While both these constants should be determined by experiment for individual soils and pore fluids, some idea of reasonable values can be obtained from past research. The value of θ_0 is governed by the ionic strength of the pore

fluid and pH, and was found to vary from 1 to 10 in systems with bentonite suspensions with KCl concentrations varying from 0.0 to 0.01M (Rege and Fogler, 1988). For relatively pure dam water and less reactive clay particles a value of θ_0=0.5 to 2 would be expected. Whereas, this value may be more than 10 in situations such as contaminant transport analysis or tailings dams. Rege and Fogler (1988) describe an experimental method to estimate V_c. For bentonite particles filtered in Ottawa sand, they found V_c=0.08cm/s. Reddi and Bonala (1997) have adopted V_c=0.3cm/s in an example using sandy clay base material and a sand filter.

In the current model, the rate of deposition within the filter pores (mass/unit time) is determined from Equation (5.22). This deposition is in addition to the physical capture of large particles. The deposition should occur relatively uniformly over the entire pore surface area. Hence, this process results in an overall reduction in porosity, permeability and void constriction sizes. The porosity reduction can be calculated based on the initial pore volume of the element (n_eV), and the mass of particles retained (from Equation 5.22). The pore void model assumes that the constriction sizes decrease proportionally with a reduction in porosity. Hence, physico-chemical particle deposition will make the constriction size distribution finer. The filter permeability is related to the porosity, so this reduction in porosity will also result in a reduced permeability as expected.

5.5.3 Deposition within the crack

The crack erosion model, developed in Section 5.3, included a rate of deposition, D, to account for re-deposition of some eroded particles as the slurry flows through the crack. The deposition rate, D, is used in Equation (5.6) and (5.7). Many researchers have shown that the rate of erosion decreases as the concentration of particles in the eroding fluid

increases, up to a maximum concentration where no further erosion occurs. This process is often modelled by an erosion rate that decreases proportionally with an increase in the slurry concentration (Govindaraju et al., 1995). In the current model, this reduction in erosion rate is represented by a subsequent re-deposition of particles, increasing proportionally with the slurry concentration. In this way, the processes of erosion and deposition have been de-coupled to allow for changing flow and transport conditions within the crack. A simple model for deposition is to adopt the probability of particle capture model developed by Rege and Fogler (1988), introduced previously in Figure 5.6. Consider now that Figure 5.6 represents a cross section of the crack rather than a pore tube. It is assumed that the slurry concentration is homogeneous across the cross section, while the flow has a parabolic velocity distribution. This can be justified because re-deposition due to particle capture is most likely to affect small cohesive particles that are transported in suspension, rather than the larger silt and sand particles transported as bed load. Sedimentation of large particles in the crack due to low flow drag forces (ie. insufficient shear stress) has been considered in Section 5.4.1.

From Figure 5.6, the probability of particle capture within the crack due to physico-chemical forces, p(r), is the fraction of the total flow within the region between the crack walls and distance (R-θa) from the centreline, where R is half the crack thickness (R=w/2). For a parabolic velocity distribution, the velocity, u, can be defined at any radius, r, based on the velocity at the centre of the crack, u_{max}.

$$u = \left[1 - \left(\frac{r}{R}\right)^2\right] u_{max} \qquad (5.25)$$

The quantity of flow bounded by the crack walls and distance (R-θa) from the centreline and the total flow volume can both be found by integrating Equation (5.25) within the appropriate bounds. In this way, the probability of capture p(r) can be found:

$$p(r) = \frac{2\int_{R-\theta a}^{R}\left[1-\left(\frac{r}{R}\right)^2\right]u_{max}\,dr}{2\int_{0}^{R}\left[1-\left(\frac{r}{R}\right)^2\right]u_{max}\,dr} \tag{5.26}$$

The definite integrals become:

$$p(r) = \frac{\left[r-\frac{r^3}{3R^2}\right]_{R-\theta a}^{R}}{\left[r-\frac{r^3}{3R^2}\right]_{0}^{R}} \tag{5.27}$$

Expanding this, substituting R=w/2 and rearranging gives an equation for the probability of capture of particles:

$$p(r) = \frac{3}{2}\left(\frac{2\theta a}{w}\right)^2 - \frac{1}{2}\left(\frac{2\theta a}{w}\right)^3 \tag{5.28}$$

Where, θ can be estimated using Equation (5.24). The mass of particles captured is dependent on the concentration of particles in the flow, C, as a mass per unit flow volume. This concentration can be related to the slurry density, ρ_m, in each crack element:

$$C = \rho_s\left(\frac{\rho_m - \rho_w}{\rho_s - \rho_w}\right) \tag{5.29}$$

Where ρ_s and ρ_w are the particle and water densities respectively. The deposition rate is then the mass of particles passing a particular point (mean velocity x concentration)

multiplied by the probability of particle capture p(r). Hence, the deposition rate D per unit width of crack is:

$$D = p(r)vC \text{ kg/m}^2\text{s} \tag{5.30}$$

While it appears that the deposition rate increases with the flow velocity, v, the deposition parameter θ decreases exponentially with the flow velocity, leading to a subsequent decrease in p(r). Hence, the overall effect is a decrease in the deposition rate with increased velocity. Equation (5.30) is used in Equations (5.6) and (5.7) to model the effect of particle deposition within the crack elements.

5.6 Formation of a Filter Cake

The preceding sections describe a time dependent model of flow through a crack in a cohesive material leading to particle erosion, transport and capture within a granular filter. This process can lead to either:

- continued erosion and enlargement of the crack until piping occurs or the flow shear stress becomes less than the critical shear stress for erosion, or
- particle capture at the filter interface and formation of a filter cake, producing a reduction in flow rate and subsequent sealing of the crack.

The difference between these two outcomes is dependent on the amount of material retained at the filter interface. Three different particle diameters were defined in Section 5.5.1, corresponding to particles that are too large to move into a filter element, particles that move into the next element and are retained, and finer particles that pass through the filter element. The large particles that cannot pass into the first filter element are retained at the interface, beginning the formation of a filter cake. The finest diameter of these obstructed particles is defined as d_r. Once a sufficient quantity of these coarse particles has been captured, then the filter cake will completely cover the filter face and the voids formed by these retained particles may be sufficiently small to retain progressively finer particles. This time-dependent process leads to the formation of a cake of fine particles and rapidly reduces the flow rate and prevents further erosion due to a significantly reduced shear stress. It is assumed that after the filter interface is sealed, the core material will swell and slake to fill the crack, under a zero stress regime. Hence, if an initial leak will seal with little erosion due to this process of particle capture and formation of a filter cake, then the crack should self-heal.

The filter cake forms a thin layer of low permeability that is sufficient to reduce flow rates to a level where erosion is controlled. The permeability of the filter cake is difficult to determine. The majority of research into the formation of filter cakes is based on surface filtration of bentonite slurries, eg. sealing of surfaces with bentonite. However, it is unlikely that a dam core would be made of a material such as bentonite. More typically, dam cores are constructed of sandy clays with low reactivity and swelling properties. Yuen and Styles (1995) examined the formation of a filter cake by kaolinite slurry, and suggested that the filtration of flocculated slurries (ie. kaolinite) depends primarily on the process of geometric filtration at the slurry/filter interface (ie. capture of particles at voids smaller than the particle diameter as described in Section 5.5.1). Flocculated clay particles are retained and consolidated as water drains into the filter. Nevertheless, very low values of permeability of the cakes were measured, showing that the kaolinite slurry still exhibits reasonably good cake formation ability.

Yuen and Styles (1995) reported that the filter cake generally had a permeability between 10^{-8} and 10^{-9} m/s. Similarly, Sherard and Dunnigan (1989) suggest that in most successful NEF tests, the filter skin is about 1mm thick and has a permeability of $5x10^{-9}$ to $7x10^{-8}$ m/s. In the model developed in Chapter 3, the permeabilities of the non-cohesive materials were estimated based on the fine particle sizes and the porosity of the filter using Equation 5.31 proposed by Koenders and Williams (1992). While this relation was determined for non-cohesive soils, it appears to predict that the permeability of a filter cake consisting of clay flocs will be in the range suggested by Sherard and Dunnigan (1989) and Yuen and Styles (1995). Hence, Equation (5.31) has been adopted for estimating the permeability of the filter cake. This equation predicts a relatively high permeability as sand and silt sized particles are captured at the filter interface, the

permeability then reduces significantly as clay flocs are captured within the voids formed by these sand and silt particles.

$$k = \frac{1}{\eta} D_{f,mean}{}^2 n_e \chi \left(\frac{n_e}{1-n_e} \right)^2 \quad \text{where, } \chi = 0.0035 \pm 0.0005 \qquad (5.31)$$

For modelling purposes, a transition element is required to describe the formation of this filter cake. This element initially has zero length. As eroded particles are captured at the filter face, the transition element length increases. An Equation to calculate the transition element length will be developed in Section 5.8.1, including a change in the transition element width due to erosion around the filter cake. In the filter void model (Section 5.5.1), the distance between each pore constriction is defined as a 'unit step', which is equivalent to the mean filter particle size by number, $D_{f,mean}$. Particles that cannot pass one unit step into the filter are retained in the transition element (ie. particles with a diameter greater than d_r). As the length of the transition element (L_{trans}) increases and becomes close to the unit step length, the transition element becomes a geometric obstruction to movement and is able to retain some finer particles. The function in Equation (5.32) is used to estimate the size of particles retained due to the developing filter cake, d_r:

$$d_r = d_{r,F1} - \left(\frac{L_{trans}}{D_{f,mean}} \right)^2 \left(d_{r,F1} - d_{r,trans} \right), L_{trans} \leq D_{f,mean} \qquad (5.32)$$

Where, d_r is the smallest diameter of particles retained at the filter interface; $d_{r,F1}$ is this diameter calculated based on particles passing the first filter element PSD; and $d_{r,trans}$ is this diameter calculated based on the transition element PSD.

5.7 The Complete Crack Erosion Model

Each of the five parts of the model have now been developed. The following summary highlights the important aspects of the model:

1. The formation of a crack due to hydraulic fracture, embankment movement etc. Rather than attempting to assign a mathematical theory to crack formation, a number of worst case crack locations and sizes are estimated as described in Section 5.2.
2. Erosion of the crack is described by two differential equations predicting the increase in crack width (Equation 5.6) and the changes in slurry density within the crack (Equation 5.7).
3. The transport of eroded particles is predicted using Shield's diagram (Figure 5.3). The shear stress applied by the flow on the crack walls is required to determine both the rate of erosion and the maximum diameter of particles transported. This shear stress, τ_w, is determined by solving Equations (5.10), (5.11) and (5.14).
4. Particle capture within the filter is controlled by two processes. Geometric filtration of coarse particles is considered in Section 5.5.1, two important particle diameters are determined, d_r defines the minimum diameter of particles too coarse to migrate into the next filter element and d_p defines the maximum diameter of fine particles that can move entirely through the filter. Differential equations describing conservation of mass (Equation 5.20) and conservation of momentum (Equation 5.21) determine the rate of movement of the particulate slurry through the filter. The physico-chemical capture of clay flocs is described in Section 5.5.2, based a model proposed by Reddi and Bonala (1997).
5. The formation of a filter cake is described in Section 5.6. Particles that are transported to the filter and are coarser than the diameter d_r, cannot infiltrate the

filter. These particles collect on the face of the filter and begin forming the filter cake. The filter cake is then able to capture progressively finer particles, and produce a low permeability layer that prevents further erosion of the crack.

The differential equations describing crack erosion and particle movement through the filter lend themselves to a finite difference solution. A computer program has been written in Microsoft Excel Visual Basic to implement the model. A likely location and size of crack are estimated based on (1) above, this defines the geometry of the problem. The steps in the computer program are outlined in point form:

- The crack and filter are represented by a number of elements, usually between 2-4 crack and filter elements.
- A time-step small enough to describe the time-dependent changes is adopted. This is often about 0.5s for the initial flow and is increased to about10s as erosion stabilises.
- The initial flow rate and eroding shear stress are determined as outlined in (3) above.
- The erosion equations outlined in (2) are solved using the shear stress τ_w.
- For each filter element, the diameters d_r and d_p are determined.
- The slurry density exiting the last filter element defines both the mass of particles captured in the filter cake (fraction of particles coarser than d_r in the slurry), and the density of particles entering the filter, required for Equations (5.20) and (5.21).
- Changes in the filter element PSD, porosity and permeability are determined.
- The process is repeated for successive time-steps, predicting the time rate of increase in crack width, formation of the filter cake and eventual sealing of the crack.

5.8 Modelling the NEF Test

In order to demonstrate that the model is realistic and to calibrate the model against laboratory data, the equations presented in the previous Sections can be modified to describe the erosion and particle capture occurring during the NEF test, where flow under high pressure erodes material from the walls of a pinhole and formation of a filter cake is essential to prevent further erosion. This Section is included before a discussion of the results of the crack erosion model, in order to show that the model predictions correlate reasonably with the laboratory results. The laboratory work described in Chapter 4 showed the large variation in the ratio of NEF boundary ratio D_{15bdy}/d_{85B} for different materials, and hence, the difficulty of predicting NEF boundaries. Despite these problems, the general process of the NEF test can be modelled. Sherard and Dunnigan (1989) give a detailed description of what occurs during the NEF test. This description is summarised briefly below for fine base soils (d_{85B}<75μm).

Erosion in the NEF test begins with a very high hydraulic gradient acting on the hole, causing erosion and transport of eroded particles to the filter face. Particles that cannot pass through the filter, collect at the filter face and form a cake of low permeability, producing high hydraulic gradients across the cake. This high gradient leads to erosion of the base soil surrounding the filter cake, and erosion of a thin layer of base soil occurs radially outwards from this cake. This material also collects on the filter face so that the filter cake widens with the radial erosion. This action usually continues progressively until, within one to four minutes, a thin water filled slot exists between the base and filter materials. At the end of a successful test, there is a thin zone (cake) over the entire upstream face of the filter. No visible erosion of the original pinhole occurs in a

successful test. The material eroded from the radial slot is sufficient to form a skin of low permeability, reducing the flow velocity and preventing further erosion. In an unsuccessful test, the material eroded from the thin slot and retained on the filter face is not sufficient in volume to prevent further erosion and the preformed hole erodes progressively. The model developed in the following Section will describe this process.

5.8.1 Theoretical Development

The governing erosion equations can be modified to represent a circular pinhole and circular filter. Equation (5.3), considering the balance of mass entering and leaving an element, is repeated to consider the mass entering and leaving element i of a pinhole:

$$\frac{\Delta M_L}{\Delta t} = \frac{M_{in} - M_{out} + \text{erosion} - \text{deposition}}{\text{time}} \tag{5.33}$$

or,

$$\frac{\partial(\rho_m A L_i)}{\partial t} = A(\rho_m v)_i - A\left[(\rho_m v)_i + \frac{\partial \rho_m v}{\partial z} L_i\right] + E - D \tag{5.34}$$

The left hand side of Equation (5.34) can be expanded:

$$\frac{\partial(\rho_m A L_i)}{\partial t} = \rho_m L_i \frac{\partial A}{\partial t} + A L_i \frac{\partial \rho_m}{\partial t} \tag{5.35}$$

The rate of change of the pinhole area is related to the change in solid volume due to erosion, V_s, which in turn is related to the mass eroded per unit time, M_e:

$$\frac{\partial A}{\partial t} = \frac{1}{L_i}\frac{\partial V_s}{\partial t} = \frac{M_e}{L_i \rho_b} \tag{5.36}$$

The erosion rate E is again determined from:

$$E = \alpha(\tau_w - \tau_c) \text{ kg/m}^2\text{s}$$

The mass eroded per unit time, M_e, due to this erosion rate is related to the surface area of the pinhole (S.A.):

$$M_e = S.A.\alpha(\tau_w - \tau_c) = 2\pi r_i L_i \alpha(\tau_w - \tau_c) \text{ kg/s} \qquad (5.37)$$

Because of the high flow velocity through the pinhole, the deposition coefficient, D, is neglected. Substituting (5.35), (5.36), and (5.37) into (5.34) gives:

$$\rho_m L_i \left[\frac{2\pi r_i}{\rho b}\alpha(\tau_w - \tau_c)\right] + \pi r_i^2 L_i \frac{\partial \rho_m}{\partial t} = \pi r_i^2 (\rho_m v)_i - \pi r_i^2 \left[(\rho_m v)_i + L_i \frac{\partial \rho_m v}{\partial z}\right] + 2\pi r_i L_i \alpha(\tau_w - \tau_c) \qquad (5.38)$$

Rearranging this equation gives the modified governing erosion equation for a circular pinhole and circular filter.

$$\frac{\partial \rho_m}{\partial t} = -\frac{\partial \rho_m v}{\partial z} + \left(1 - \frac{\rho_m}{\rho_b}\right)\frac{2}{r_i}[\alpha(\tau_w - \tau_c)] \qquad (5.39)$$

Next consider the rate of increase of the pinhole radius. Since the area $A=\pi r_i^2$, then:

$$\frac{\partial A}{\partial t} = \frac{\partial A}{\partial r_i}\frac{\partial r_i}{\partial t} = 2\pi r_i \frac{\partial r_i}{\partial t} \qquad (5.40)$$

Combining Equations (5.40) and (5.36), and simplifying gives:

$$\frac{\partial r_i}{\partial t} = \frac{1}{\rho_b}\alpha(\tau_w - \tau_r) \qquad (5.41)$$

Equations (5.39) and (5.41) are the governing differential equations describing the pinhole erosion rate. The flow velocity is calculated using the Equation (5.10), as described in Section 5.4.2. To calculate the hydraulic gradient acting on the pinhole, the filter permeability is required. As each filter element (including the filter cake) may have a different permeability, k_i, and length, L_i, the equivalent permeability of the filter with n elements, is given by:

$$k_{e,filter} = \frac{L_{total}}{A}\left[\frac{1}{\sum_{i=1}^{n}\frac{L_i}{k_i A_i}}\right] \qquad (5.42)$$

Using the Darcy flow equation $q=k_e i_{filter} A$ and Equation (5.11) the hydraulic gradient in the filter, i_{filter}, and pinhole, i_h, can be determined. A force balance on the pinhole flow determines that the shear stress in the pinhole, τ_w, is given by:

$$\tau_w = \frac{r_i \rho_s g i_h}{2} \qquad (5.43)$$

Particle capture within the filter is modelled as described in Section 5.5, and the formation of a filter cake is described in Section 5.6. In order to model the radial erosion at the filter face around the filter cake, the transition element representing the filter cake should have a variable radius, r_{trans}, as well as variable thickness, L_{trans} (Figure 5.8). The transition element increases in thickness as more particles are captured, and increases in radius as radial erosion occurs. The volume of particles captured in the transition element depends on the flow rate and density of the slurry exiting the final element of the pinhole and the mass eroded radially from the slot at the filter interface. From this total mass of particles reaching the filter, only the fraction of base particles which are larger than the filter void diameter d_r, are retained in the transition element. The filter cake forms on the filter face by clogging the voids, this means that the length of the transition element will be related to the pore volume (ie porosity) of the filter (n_f):

$$L_{Trans} = \frac{\text{Mass Retained}}{\rho_b \pi \, r_{trans}^2 n_f} \qquad (5.44)$$

As previously described, this filter cake is of low permeability, which will eventuate in high hydraulic gradients across the cake. Sherard and Dunnigan (1989) suggest that because of the low permeability of the filter cake, a high gradient exists across the cake and across the small piece of base soil adjacent to the cake, ie. piece 'A' in Figure 5.7. This small piece is eroded and forms more of the filter cake, thus producing a high gradient on the next piece of base soil. This leads to the progressive process of radial

erosion of the base material surrounding the filter cake. This erosion process can be seen in Figure 5.7.

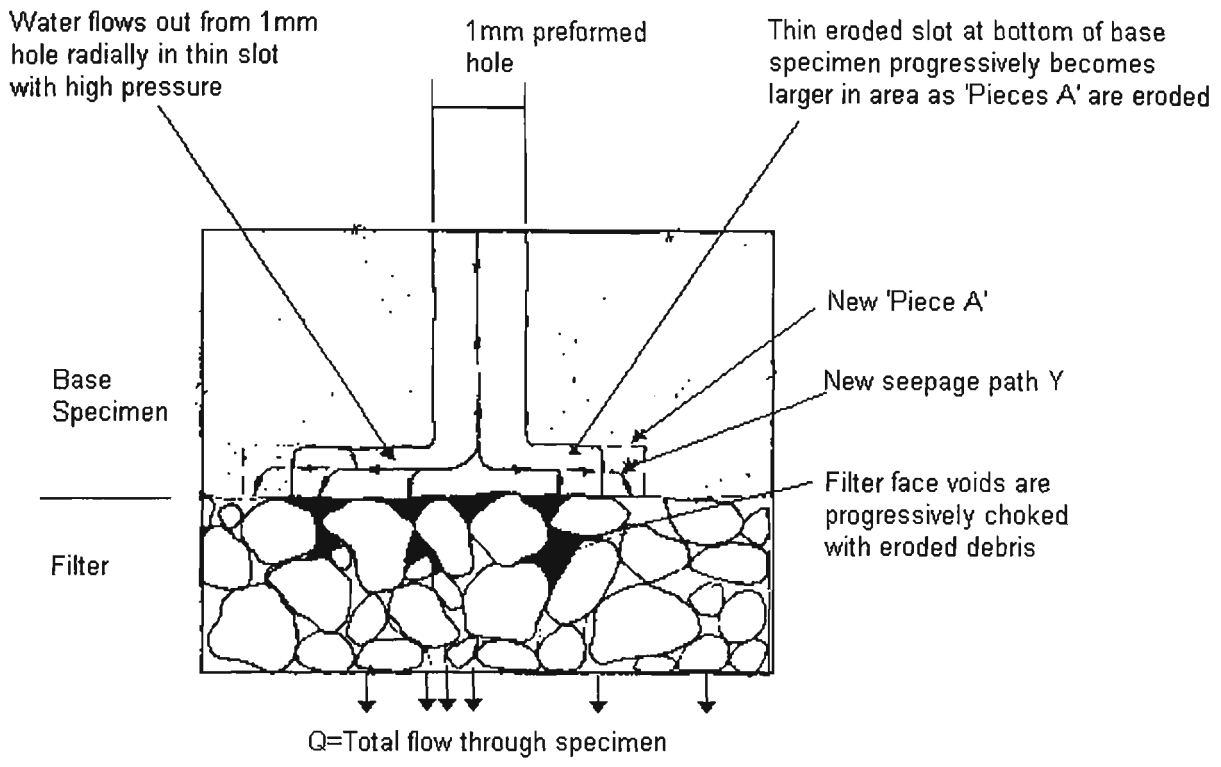

Figure 5.7 Action occurring at bottom of base soil specimen during NEF Test (after Sherard and Dunnigan, 1989)

In order to estimate this radial erosion process, consider the forces acting on the small piece of base soil at the edge of the filter cake ('Piece A' in Figure 5.7). Assuming continuity of flow in the vertical direction, the hydraulic gradient across the filter cake can be found from:

$$Q = k_{trans} i \pi \, r_{trans}^{2} \tag{5.45}$$

Hence, the head difference across the cake, ΔH, is:

$$\Delta H = \frac{Q L_{trans}}{k_{trans} \pi \, r_{trans}^{2}} \tag{5.46}$$

Sherard and Dunningan (1989) suggest that a 1mm gap exists between the base soil and filter cake at the completion of a successful test. Hence, the head, ΔH, acts across a piece of base soil approximately 1mm high. This could be considered as being resisted by a shear stress τ_r as shown in Figure 5.8. Balancing the force due to the applied head and resisting shear force gives:

$$\tau_r = \frac{QL_{trans}}{\sqrt{2}k_{trans}\pi\ r_{trans}^{\ 2}} \qquad (5.47)$$

While not strictly a surface shear stress, this shear τ_r is assumed to produce an erosion mass defined by the erosion equation $E=\alpha(\tau_r - \tau_c)$. The surface area acted on by this shear stress is a 1mm height of the circumference, $2\pi r_{trans}$ (based on Sherard and Dunnigan, 1989). This method of estimating the radial erosion is only approximate, however, the result is an eroding shear stress that is proportional to the length of the filter cake element and inversely proportional to the square of the filter cake radius, which seems likely in practice. Model predictions of the rate of radial erosion, presented subsequently in Section 5.8.2, appear reasonable.

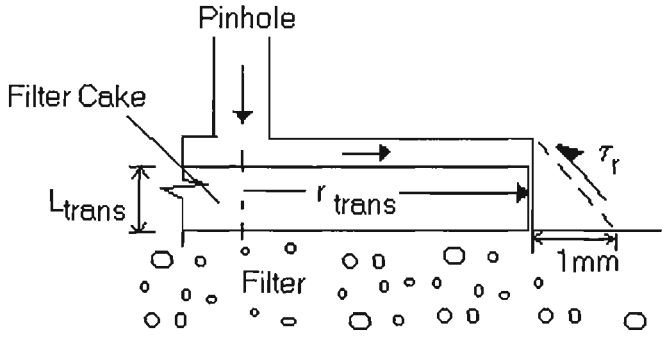

Figure 5.8 Forces on base soil at filter interface causing radial erosion

The rate of radial erosion will control the rate of increase in the radius of the transition (filter cake) element. This increase in radius is calculated using Equation (5.41), replacing r_i with r_{trans}. The capture of particles on the filter face and within the filter is modelled as described in Section5.5. Due to the high velocity flow and short duration of the NEF test, physico-chemical deposition can be ignored. The formation of a filter cake and subsequent reduction in flow rate is the most important aspect in determining the success of a filter in preventing erosion of the base soil.

5.8.2 Application of the NEF model

The application of the NEF model to three materials, representative of different dam core materials, will be described and compared with the results of NEF tests carried out as described in Chapter 4. These materials are:

Kerferd embankment material is a typical group 1 clayey embankment material,

AP1 is a broadly graded sandy clay. The material is gap graded with the coarsest 25-30% unable to influence filtration. This material is considered here to demonstrate that the model can predict the behaviour of internally unstable base soils. By definition, the material is a group 2 soil, but the reduced PSD fits the group 1 grading limits,

The Thomson Dam core material is a sandy clay with a stable coarse fraction. This group 2 material had the coarsest NEF boundary of all the materials tested (D_{15F}=2mm).

Some properties of the materials are listed in Table 5.2. The last column of this table shows the NEF boundary filter D_{15bdy}, determined through laboratory testing. The particle size distributions of the three materials are shown in Figure 5.9, which also shows the particle size distribution of the erosion product, EP. This is the size

distribution of particles collected from the effluent water of erosion tests, as described in Chapter 4. The analytical model will be applied to both the original PSD multiplied by the multiplier 'A' fromTable 5.1, and the erosion product determined from laboratory testing, in order to show the similarity between the predictions.

Table 5.2 Properties of Materials for NEF simulation

Material	d_{85} (μm)	d_{98}/d_{85}	%<75μm	Description	D_{15bdy} (lab)
Kerferd	28	4.3	97	CH	350 μm
AP1	90	7.3	76	CL/SC	190 μm
Thomson	190	2.9	55	SC	2000 μm

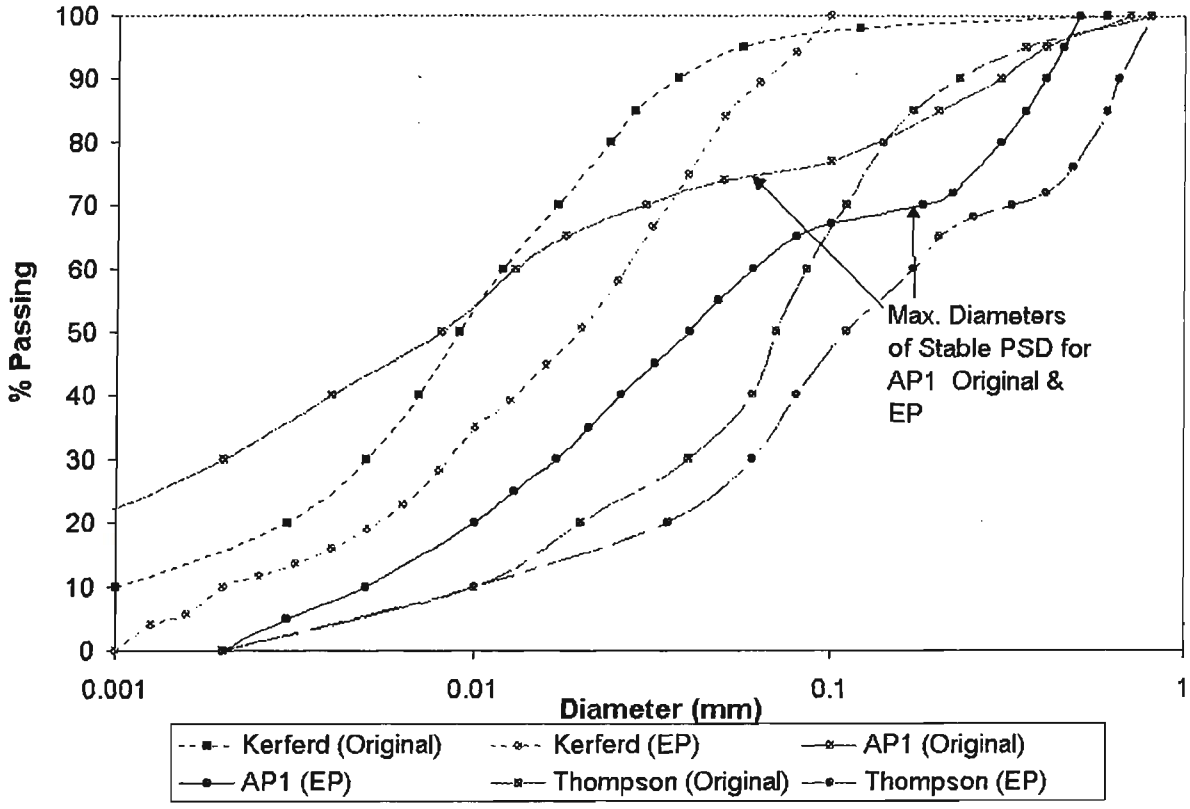

Figure 5.9 Particle Size Distribution of materials for NEF simulation

The NEF test is determined a success or failure based on whether the initial 1mm pinhole shows visible signs of erosion. The measured size of the hole after unsuccessful laboratory tests was subjective, because new holes often developed at the edge of the apparatus, or cracks developed along the base soil and these cracks then eroded. Even in successful tests, some minor erosion is inevitable, since some initial erosion of the pinhole is required to begin forming a filter cake. When considering the model predictions, the NEF boundary is defined as the filter D_{15F} diameter where an increase in filter diameter leads to a rapid increase in the predicted hole diameter. In most simulations, the predicted hole diameter after the test remains at a near constant diameter (usually 1.2-1.3mm) for filters finer than the NEF boundary. The pinhole diameter then increases significantly if the filter diameter is increased above the NEF boundary.

Figure 5.10 shows the measured and predicted pinhole diameter after the NEF test for the two finer materials (Kerferd and AP1). The lines 'Kerferd Model' and 'AP1 Model' refer to the model predictions for the original base soil multiplied by 'A', while the 'EP Model' refers to the model predictions when the base soil is represented by the erosion product determined in the laboratory. The correlation between the model predictions and laboratory measurements is reasonable, considering the difficulty in measuring the hole diameter in the laboratory and the large number of variables required to model the test. The important observations from Figure 5.10 are that, in both the laboratory measurements and the model predictions:

- the pinhole does not erode significantly when $D_{15F} < D_{15bdy}$,
- the amount of pinhole erosion increases rapidly for D_{15F} progressively coarser than D_{15bdy},

- the extent of pinhole erosion is approximately the same for the laboratory measurements and model predictions
- The model predictions, based on the erosion product (EP) and the original PSD multiplied by 'A', are both similar. This suggests that either method is adequate to represent the base soil PSD.

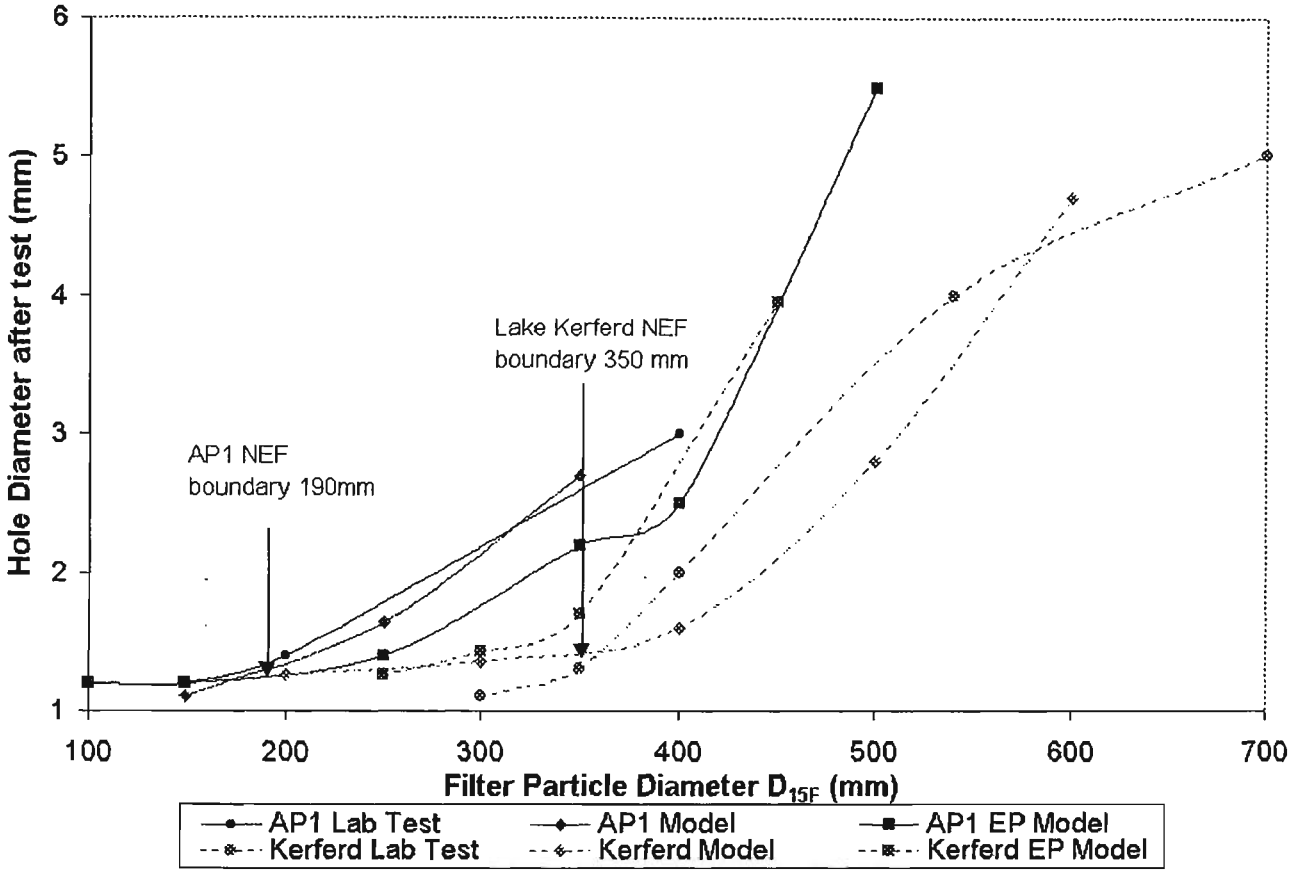

Figure 5.10 Extent of pinhole erosion before steady state for NEF laboratory test and model simulation for fine base soils.

Figure 5.11 presents the laboratory measured pinhole erosion and model simulation results for the Thomson Dam base soil. Because the filter is significantly coarser, and more permeable, than for the finer base soils, the model predicts a greater flow rate through the apparatus. This results in more erosion of the pinhole before the filter cake seals the hole. Hence, the predicted final pinhole diameter for successful tests (about

1.5mm) is greater than the laboratory measured results (approximately 1mm). The predictions are similar to those for fine base soils, ie. the extent of erosion is constant for filters finer than the NEF boundary, while erosion increases rapidly beyond a filter diameter defining the boundary. The correlation with laboratory results is reasonable.

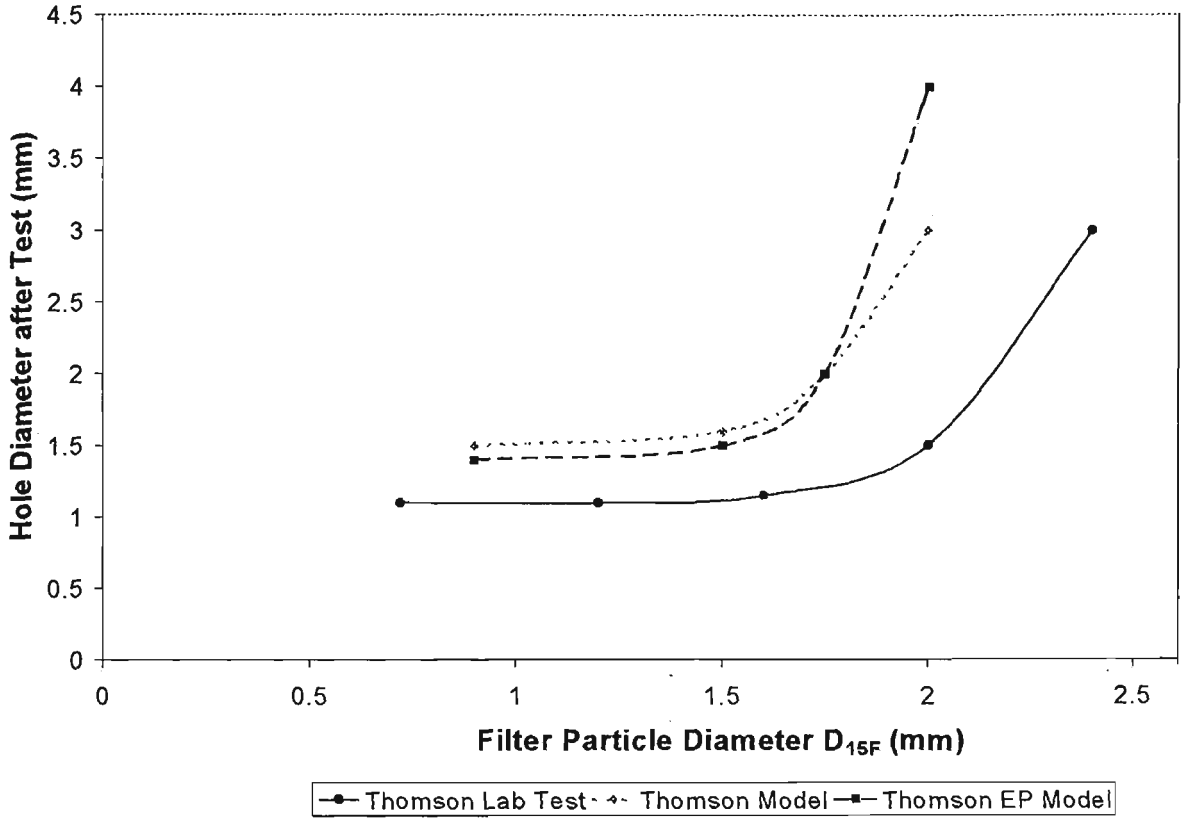

Figure 5.11 Extent of pinhole erosion after test for NEF laboratory test and model simulation for a group 2 base soil

The extent of pinhole erosion, both predicted by the model and measured in the laboratory is normalised against the ratio $D_{15F}/d_{85B(rep)}$ in Figure 5.12. The parameter $d_{85B(rep)}$ is the d_{85} size of the *representative PSD,* after multiplying by the factor 'A', and excluding the coarse fraction of material AP1 that is unable to self-filter the fines. In Figure 5.12, the NEF boundary is assumed to be represented by the point of inflection where the hole diameter increases rapidly. Below the NEF boundary there is very little erosion, while above the NEF boundary, the erosion rate increases rapidly with increased retention ratio. Figure 5.12 demonstrates that the NEF boundary corresponds to

approximately D_{15bdy}=4-5$d_{85(rep)}$ for all three materials. This observation corresponds to the controlling constriction size of Kenney et al. (1985), suggesting that the assumption that cohesive base soils erode as aggregates and flocculated particles, and these larger particles remain stable during filtration, is justified. Both the base soil represented by its erosion product as determined from laboratory tests, and the base soil represented by the original PSD multiplied by the multiplier 'A', produce similar predictions for pinhole erosion, when normalised by the representative base soil particle size, d_{85rep}. The AP1 material has a slightly reduced pinhole erosion for D_{15F}>D_{15bdy} because the large particles that gather at the filter face reduce the flow rate slightly, even though they are unable to retain the fines of the base soil. Above a ratio of D_{15bdy}/d_{85rep}>8 the filter is unable to retain the coarse fraction of the AP1 material and the quantity of erosion increases rapidly.

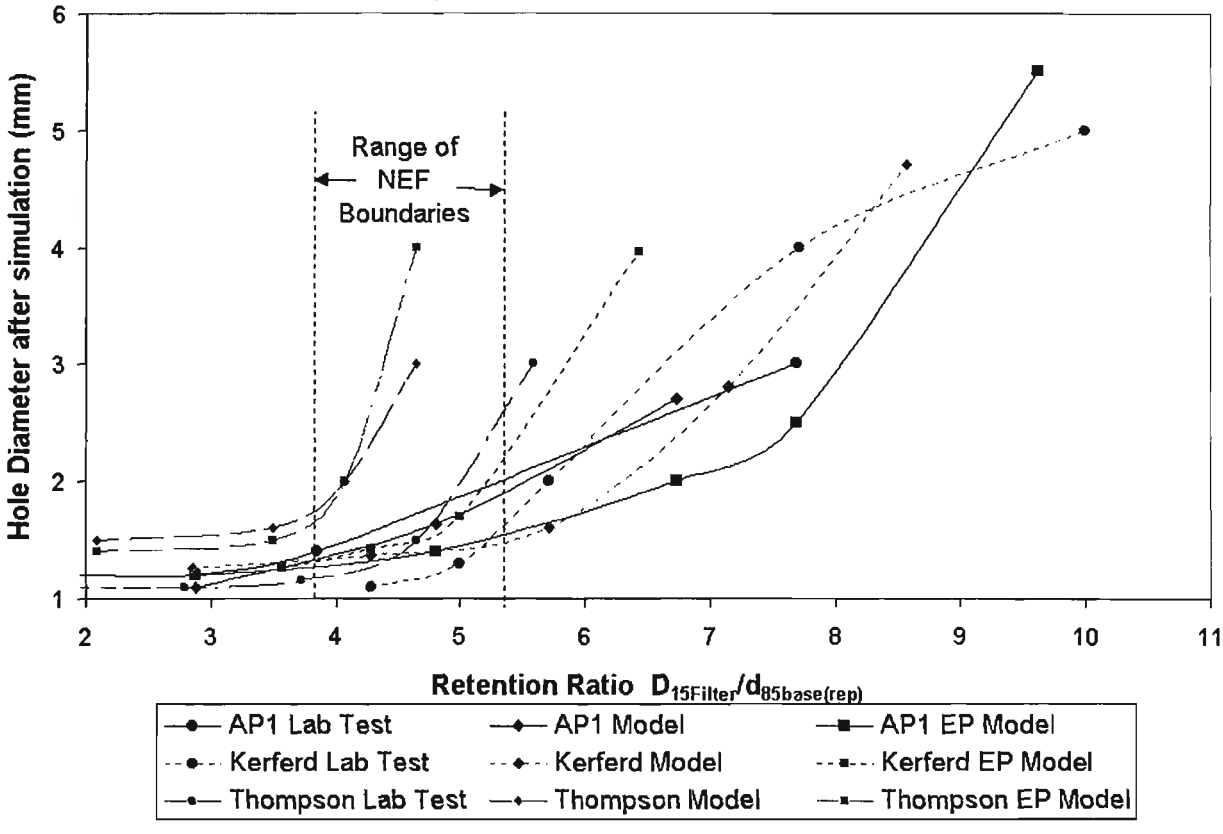

Figure 5.12 Extent of pinhole erosion before steady state related to ratio $D_{15F}/d_{85B(rep)}$ in NEF simulation

The model is able to predict time-dependent changes in particle transport and capture, flow rate, permeability and porosity of the filter during the NEF test. The flow rate through the apparatus is a function of the permeability and porosity of the filter, hole diameter and filter cake formation. Hence, the flow rate combines all the other predictions and is a reasonable indicator of the model performance. The predicted change in flow rate through the apparatus is shown in Figure 5.13 and Figure 5.14 for the AP1 and Lake Kerferd materials respectively. The predictions are shown for several filter diameters, also shown are some laboratory measured flow rates for various filters. The trends for both materials are similar.

For simulations using filters near or below the NEF boundary, the model predicts that the flow rate will reduce rapidly as the filter cake seals the pinhole. Sherard and Dunnigan (1989) determined that at the end of successful NEF tests, the flow rate was in the range 0.02-0.3 ml/s/cm^2. For the 15cm diameter apparatus this corresponds to a flow rate of $3x10^{-6}$ to $5x10^{-5}$ m^3/s. The model predictions for flow rate after a successful test for both materials fall within this range. The flow rate measured in the laboratory test on material AP1 for a filter with D_{15F}=0.15mm is also shown in Figure 5.13. Similarly, the flow rate for a successful test on the Kerferd material with D_{15F}=0.3mm is shown in Figure 5.14. In both cases the predicted and measured flow rates for successful tests do not correlate exactly, but are within one order of magnitude and have a similar trend. Given the potential variations in initial pinhole diameter, applied head from the mains water system, filter particles partially blocking the pinhole, flow restrictions within the apparatus etc, this correlation is good.

In unsuccessful tests, the model predicts that the flow rate will initially increase as the hole erodes. The flow rate later becomes steady and begins to reduce as some retention of particles occurs, and a filter cake begins to form. For filters only slightly coarser than the NEF boundary, the filter cake does form after some erosion, and the flow rate reduces to a level near the flows predicted for successful tests. For filters significantly coarser than the NEF boundary, the flow rate begins to reduce slightly but remains higher than the initial flow rate. Figure 5.13 shows the measured flow rate in a laboratory test on the AP1 material combined with an unsuccessful filter with D_{15F}=0.8mm. Figure 5.14 presents the measured flow rate through the Kerferd base soil, for an unsuccessful filter with D_{15F}=0.6mm. In both cases, the measured flow rate is an order of magnitude lower than the predicted flow for the same filter, but follows a similar trend. This lower measured flow rate is most likely due to flow restrictions in the apparatus such as the inlet and outlet valves, which were not considered in modelling.

The other time-dependent variables, ie. the rate of erosion and transport, permeability and porosity, formation of the filter cake etc. are related to the flow rate, and exhibit similar trends for both successful and unsuccessful NEF tests. Hence, the model is able to predict the extent of pinhole erosion in NEF tests and the time-dependent changes occurring during the test. As demonstrated by the analysis of material AP1, the model can differentiate between internally stable and unstable base soils, allowing continued erosion of the fine fraction of internally unstable soils even though the coarse fraction may be retained.

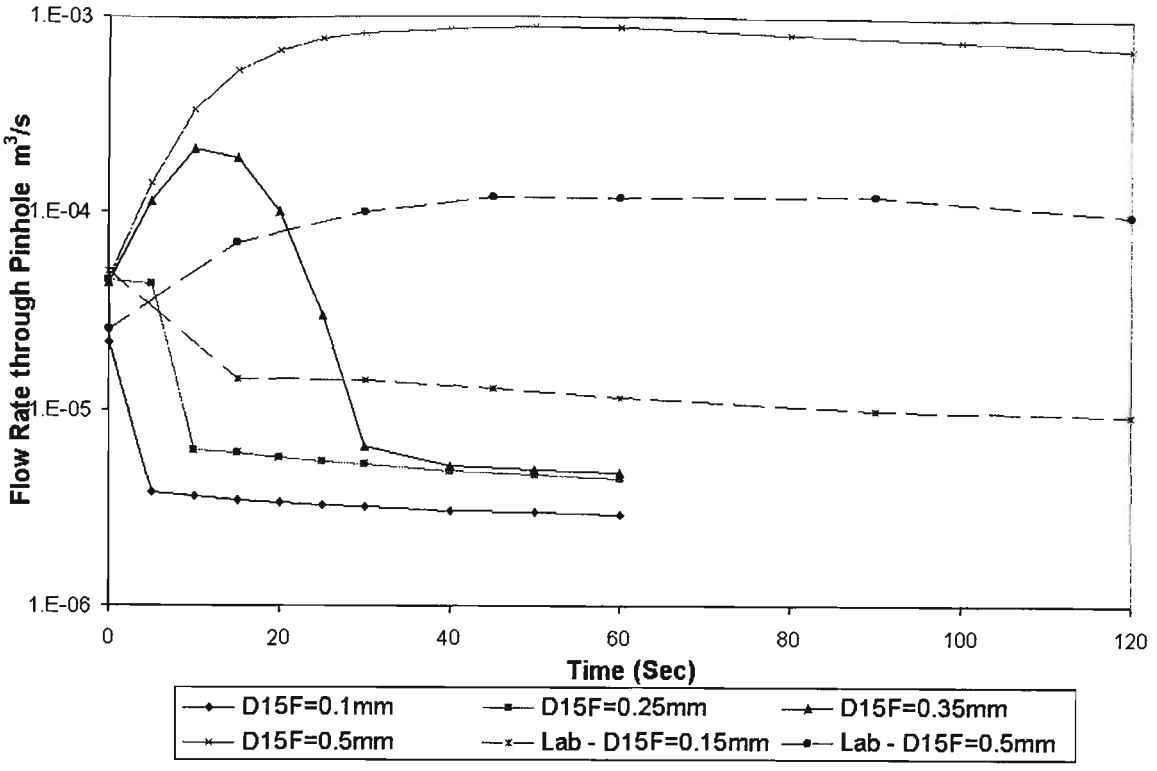

Figure 5.13 Predicted and measured flow rate changes during NEF test for material AP1

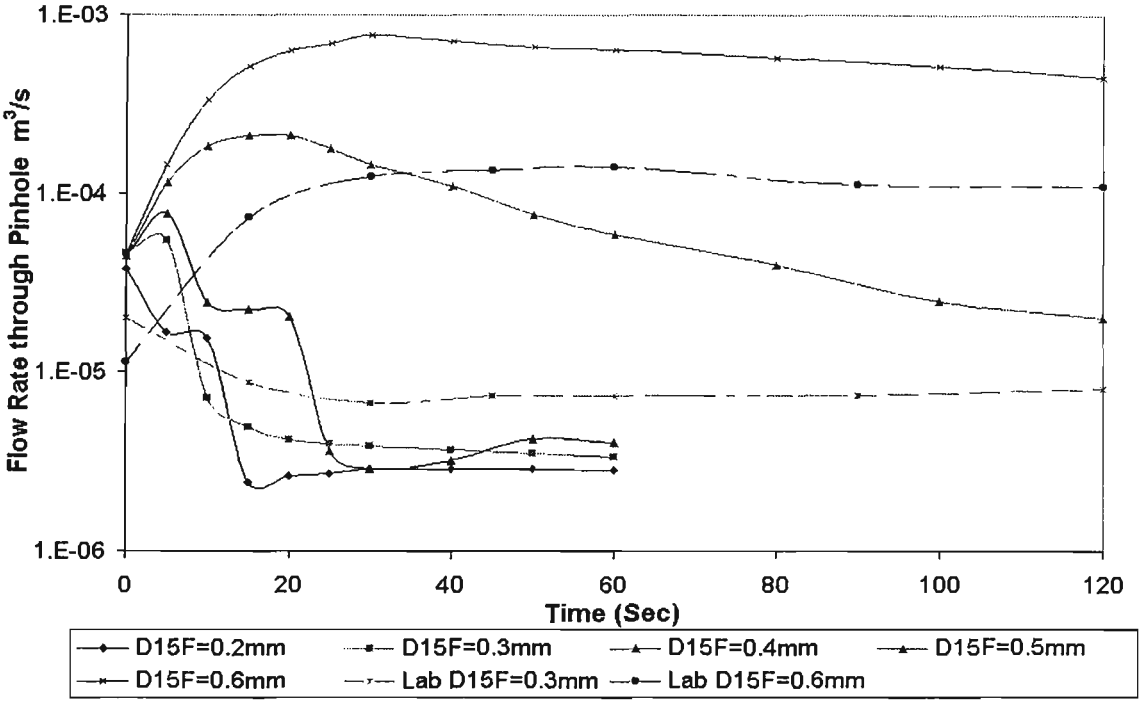

Figure 5.14 Predicted and measured flow rate changes during NEF test for Lake Kerferd embankment material.

5.9 Application of the Cohesive Material Model

The previous section saw the verification of some aspects of the analytical model describing filtration of cracked cohesive material, through a comparison with observations of NEF tests. The comparison was intended demonstrate that the particle size multiplier 'A', and the particle capture models are an adequate description of base soil - filter behaviour. The overall model of filtration of cohesive material has many more aspects that will be considered in this Section. Within a dam, a continuous crack may develop, allowing concentrated flow and erosion of the crack walls. This Section will describe the model predictions for flow rate through a crack, erosion and transport of particles and capture of eroded particles within the filter under changing conditions, and examine the effect of various model parameters. The application of the model is demonstrated by first considering a case study from an Australian dam. Following this, the effects of various model parameters are shown by considering different dam geometry, hydraulic conditions, erodability and physico-chemical characteristics. Chapter 7 will include further case studies showing the application of the model, and further verification against recorded observations.

Figure 5.15 shows a typical dam cross section, identifying dimensions that will be used in modelling. A continuous, horizontal crack of length L and thickness w exists through the dam core. Water flows through the crack under a reservoir head, H. Other important parameters include the critical shear stress, τ_c, and the erosion rate parameter, α, of the core material. The filter PSD is defined by its D_{15F} size. A filter coefficient of uniformity of 3, and an initial density of 40% are adopted for all the analyses in this Chapter.

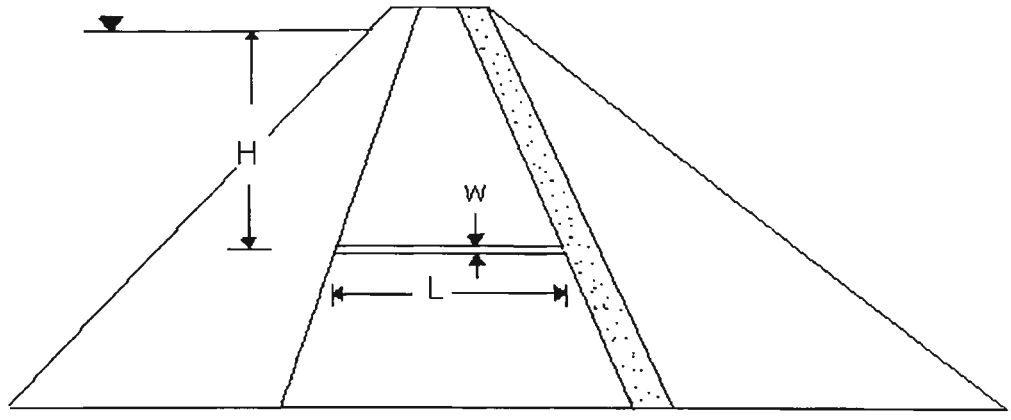

Figure 5.15 Dam cross section defining dimensions for modelling data

5.9.1 Case Study – Kerferd Dam

The application of the analytical model to Kerferd Dam in Victoria, Australia will be described. The dam is a homogeneous earthfill embankment, approximately 20m high at the maximum section, with 17m maximum reservoir height at full supply level, constructed around 1920. Due to concerns about the internal stability as well as slope stability under static and earthquake loading conditions, coupled with observations of high seepage flow rates and previous incidents of piping failure, the dam was rehabilitated recently with a 3-stage granular filter and a stabilising berm, constructed against the downstream embankment and foundation. A typical cross section of this remedial work is shown in Figure 5.16. For modelling purposes, it is assumed that a crack will form at 13m depth (with 10m hydraulic head, H). The crack length, L, at this depth through the entire homogeneous embankment is 65m, the assumed initial average thickness, w, is 1mm. While cracking due to earthquake movement is unlikely at this depth, piping failure would still be possible, as stress re-distribution and strength reduction allowed hydraulic fracture.

The embankment material is a medium plasticity clay. Some properties of this material were previously listed in Table 5.2, and the PSD plotted in Figure 5.9. Erosion tests on this material (described in Chapter 4) determined a critical shear stress of τ_c=0.5 N/m^2 and an erosion rate parameter α=0.04 g/Ns. The clay material seems relatively non-reactive, and the reservoir water has few contaminants. Based on these observations, deposition parameters of θ_0=5 (unit-less) and V_c=0.01m/s were assumed for the modelling. In the laboratory, the NEF boundary filter for this material had D_{15F}=0.35mm.

The model described in this Chapter is used to predict the erosion of a crack through Kerferd dam after construction of a granular filter downstream of the homogeneous embankment. The model was run for four different filters with D_{15F}=0.3mm, 0.4mm, 0.5mm and 0.7mm, using the base soil parameters described above. The model predicts at each time-step the mass entering and leaving each element, the maximum diameter and fraction of eroded particles transported through the crack, the maximum diameter and corresponding fraction of loose particles passing through the filter elements and the permeability and porosity of each filter element. It is not possible to present all of this data here. Table 5.3 presents some of the model predictions for the first 10 minutes of flow after formation of the crack. The model considered 1 second time-steps at this initial stage, but the results are only printed at each 20 second interval. The data clearly shows the reduction in flow rate as the filter cake becomes thicker and the permeability of the filter reduces. The erosion rate and increase in crack thickness can also be seen. The initial drop in flow rate is due to the filter cake sealing the 1mm crack. Subsequent radial erosion enlarges the flow area across the filter cake and the flow rate increases again before steadily decreasing as the crack seals.

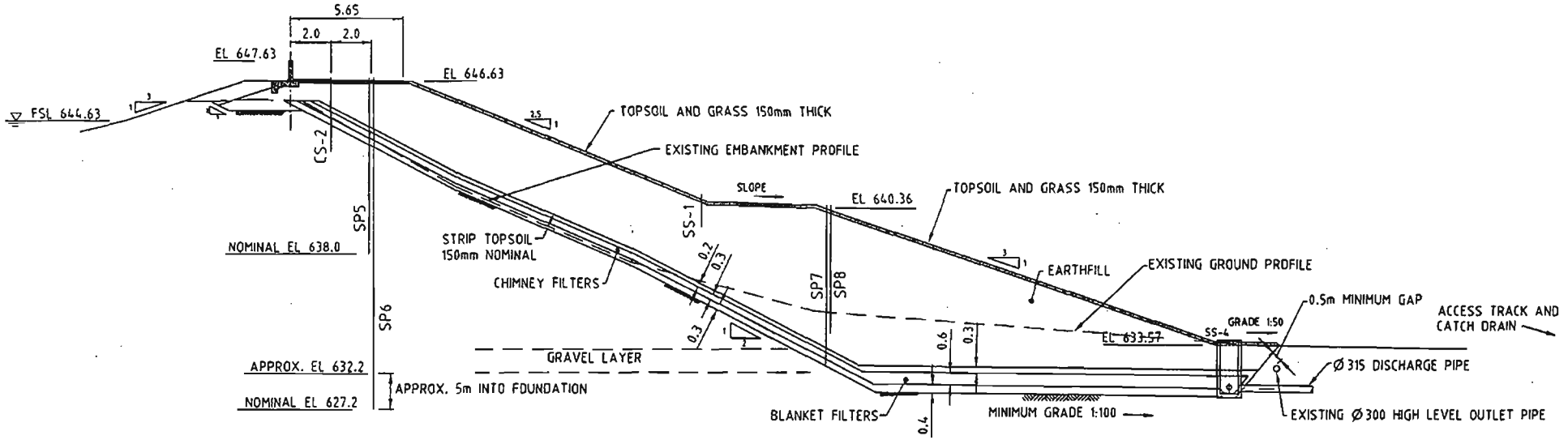

SECTION AT RD 58m

Figure 5.16 Cross Section of remedial works at Kerferd Dam

Table 5.3 Sample of typical data from crack erosion model – Kerferd base soil, D_{15F}=0.5mm

		Base Element 1					Transition Element						Filter Element 1				
Time (Sec)	FlowRate (m3/s)	Percent Mobilised	Crack Width	Diameter Mobilised	Cum. Mass Out (kg)	Conc. (kg/m3)	Percent Passing	Length (mm)	Retained Diameter	kf m/s	Cum. Mass Out (kg)	Conc. (kg/m3)	Percent Passing	Retained Diameter	kf m/s	Cum. Mass Out (kg)	Conc. (kg/m3)
0	4.9E-04	100.00	1.00E-03	4.452	0.00	0.00	94.14	0.00	0.187	4.7E-05	0.00	0.00	0.0	0.187	2.0E-04	0.00	0.00
20	4.8E-05	93.34	1.00E-03	0.175	0.05	9.59	41.55	0.41	0.019	1.4E-08	0.05	9.61	0.1	0.177	1.8E-04	0.03	0.05
40	1.1E-04	100.00	1.00E-03	0.903	0.07	10.88	73.36	0.35	0.048	3.0E-08	0.06	8.30	0.1	0.177	1.6E-04	0.03	0.00
60	1.6E-04	100.00	1.00E-03	1.261	0.10	10.44	71.41	0.41	0.045	5.3E-08	0.08	7.87	0.1	0.177	1.4E-04	0.03	0.00
80	1.5E-04	100.00	1.01E-03	1.201	0.13	10.66	70.42	0.50	0.044	5.9E-08	0.11	7.83	0.7	0.177	1.0E-04	0.04	9.22
100	1.4E-04	100.00	1.01E-03	1.126	0.16	10.75	70.72	0.56	0.044	6.2E-08	0.13	7.60	0.8	0.177	9.6E-05	0.07	11.84
120	1.3E-04	100.00	1.01E-03	1.064	0.19	10.41	69.24	0.62	0.042	6.3E-08	0.15	7.31	0.8	0.177	8.2E-05	0.10	11.72
140	1.2E-04	100.00	1.01E-03	1.017	0.21	10.12	68.76	0.66	0.041	6.4E-08	0.17	7.00	0.8	0.177	9.9E-05	0.13	11.46
160	1.2E-04	100.00	1.01E-03	0.975	0.24	9.94	69.60	0.70	0.042	6.4E-08	0.18	6.68	0.8	0.177	7.7E-05	0.16	11.21
180	1.2E-04	100.00	1.01E-03	0.949	0.26	9.61	69.39	0.73	0.042	6.5E-08	0.20	6.40	0.8	0.177	1.0E-04	0.18	10.91
200	1.1E-04	100.00	1.01E-03	0.923	0.28	9.28	69.25	0.75	0.042	6.5E-08	0.21	6.15	0.7	0.177	9.9E-05	0.21	10.57
220	1.1E-04	100.00	1.01E-03	0.902	0.30	8.99	69.26	0.77	0.042	6.5E-08	0.23	5.92	0.7	0.177	9.1E-05	0.23	10.25
240	1.1E-04	100.00	1.01E-03	0.886	0.32	8.72	69.37	0.79	0.042	6.6E-08	0.24	5.72	0.7	0.177	1.2E-04	0.26	9.95
260	1.1E-04	100.00	1.01E-03	0.872	0.34	8.48	69.53	0.81	0.042	6.6E-08	0.25	5.54	0.7	0.177	9.8E-05	0.28	9.69
280	1.1E-04	100.00	1.01E-03	0.858	0.36	8.04	69.53	0.82	0.042	6.6E-08	0.26	5.38	0.7	0.177	1.0E-04	0.30	9.32
300	1.1E-04	100.00	1.01E-03	0.844	0.38	7.82	67.88	0.83	0.040	6.6E-08	0.28	5.23	0.6	0.177	9.0E-05	0.32	9.03
320	1.1E-04	100.00	1.01E-03	0.831	0.39	7.60	67.89	0.85	0.040	6.6E-08	0.29	5.09	0.6	0.177	1.1E-04	0.34	8.78
340	1.0E-04	100.00	1.01E-03	0.821	0.41	7.41	67.91	0.86	0.040	6.6E-08	0.30	4.96	0.6	0.177	1.3E-04	0.35	8.55
360	1.0E-04	100.00	1.01E-03	0.811	0.42	7.23	67.96	0.87	0.040	6.6E-08	0.31	4.84	0.6	0.177	8.8E-05	0.37	8.35
380	1.0E-04	100.00	1.01E-03	0.804	0.44	7.07	68.11	0.87	0.040	6.6E-08	0.32	4.73	0.6	0.177	8.9E-05	0.39	8.18
400	1.0E-04	100.00	1.01E-03	0.798	0.45	6.93	68.27	0.88	0.041	6.6E-08	0.33	4.64	0.6	0.177	1.3E-04	0.40	8.02
420	1.0E-04	100.00	1.01E-03	0.792	0.47	6.81	68.49	0.89	0.041	6.6E-08	0.34	4.55	0.6	0.177	1.2E-04	0.42	7.88
440	1.0E-04	100.00	1.01E-03	0.788	0.48	6.68	68.54	0.89	0.041	6.6E-08	0.35	4.48	0.6	0.177	1.1E-04	0.44	7.74
460	1.0E-04	100.00	1.01E-03	0.784	0.49	6.58	68.70	0.90	0.041	6.6E-08	0.35	4.41	0.6	0.177	9.2E-05	0.45	7.63
480	1.0E-04	100.00	1.01E-03	0.781	0.51	6.49	68.88	0.90	0.041	6.7E-08	0.36	4.35	0.6	0.177	1.2E-04	0.47	7.52
500	1.0E-04	100.00	1.01E-03	0.778	0.52	6.41	69.12	0.91	0.042	6.7E-08	0.37	4.30	0.6	0.177	9.4E-05	0.48	7.43
600	9.9E-05	100.00	1.01E-03	0.769	0.58	6.12	70.10	0.93	0.043	6.7E-08	0.41	4.11	0.5	0.177	1.6E-04	0.55	7.13

Table 5.3 shows how the computer program executing the mathematical model presents the output data. The PSD of each element is also recorded at various time intervals, hence, the output file for each application of the program is many times larger than shown in Table 5.3. The model predictions will be presented in this Chapter as graphs summarising various aspects of the output data. The model predictions for the mass eroded from the crack during the first day after the formation of a continuous, 1mm thick crack are summarised in Figure 5.17. For the two fine filters below or near the NEF boundary filter size (D_{15F}=0.3mm and 0.4mm), initial erosion occurs, but within the first 20 minutes the filter retains a significant quantity of eroded particles and reduces the flow rate. This reduces the shear stress within the crack to below the critical shear stress, and erosion of the crack walls ceases. Further mass loss after this time is due to the continued flow of slurry in the crack, and radial erosion around the filter cake as the flow finds new paths around the obstruction. After one day, the concentration of the slurry has reduced greatly and the quantity of mass leaving the crack becomes negligible. At this stage it is most likely that slaking and expansion of the clay in the crack walls would seal the crack.

The two coarser filters (D_{15F}=0.5mm and 0.7mm) allow a greater quantity of erosion over the first 200-400 minutes before a sufficient quantity of material is captured at the filter interface to reduce the flow shear stress and prevent erosion. For the coarsest filter (D_{15F}=0.7mm), the sealing is only temporary as increased hydraulic gradients at the filter interface 'blow out' the filter cake and erosion occurs again. This is shown by the increases in erosion rate at 800-1000 minutes and again at 1300-1400 minutes. The total loss of mass, during the first day after formation of the crack, is 2.5kg for the coarsest filter tested. Over a crack length of 65m, this represents only a small increase in the crack

thickness. However, the continuing erosion of the crack protected by a filter with D_{15F}=0.7mm suggests that a piping failure could eventuate in this case.

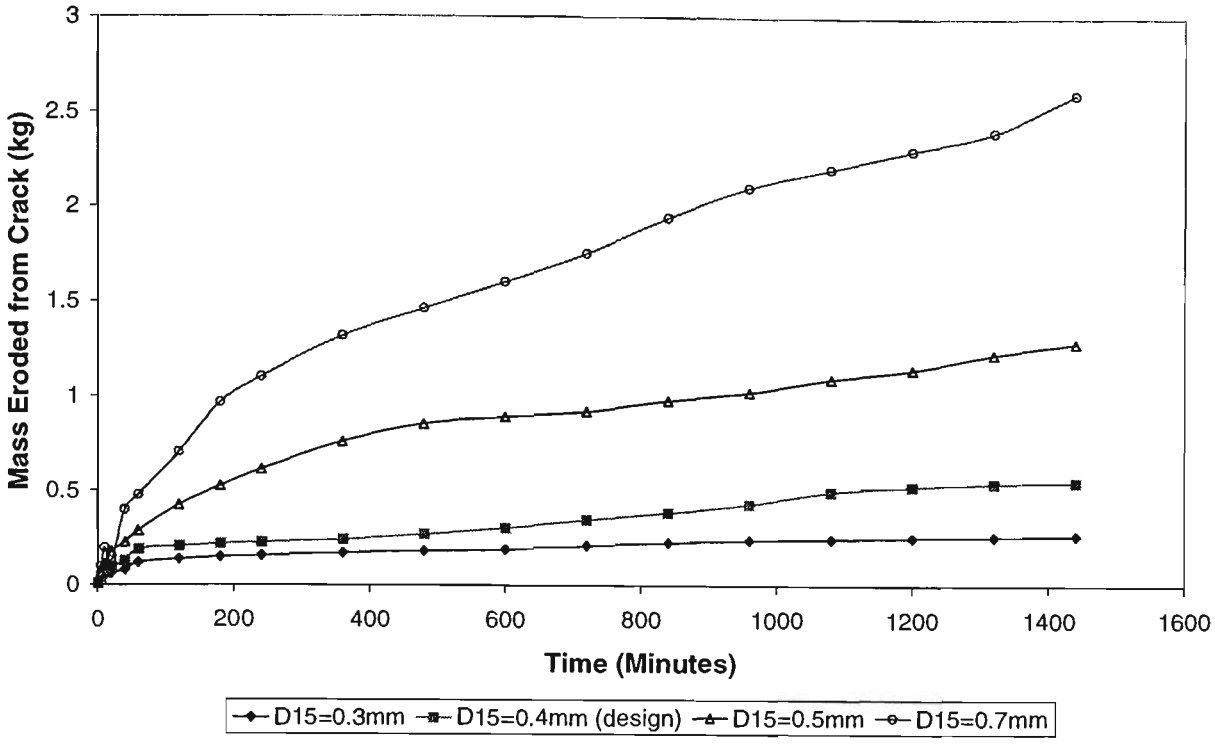

Figure 5.17 Predicted mass of material eroded from a 1mm crack through Kerferd Dam for various filter sizes

5.9.2 Effect of Increased Hydraulic Gradient

In the example above, erosion of the crack ceased because the hydraulic gradient and eroding shear stress were reduced sufficiently to prevent erosion. The filter interface did not seal completely, and an increase in the hydraulic gradient could have continued the erosion process. This demonstrates that the hydraulic conditions within a dam are important to the development of internal erosion and piping failure. In describing the application of the model, it is also important to demonstrate the complete sealing of the filter interface under more severe hydraulic conditions. To simulate these severe hydraulic conditions, consider the case of a central core earth dam constructed using the Kerferd Dam embankment material, with a crack of length L=15m continuous through the core, and reservoir head acting on this crack of H=25m (dimensions are defined in

Figure 5.15). The mass eroded from the 1mm thick crack for various filter diameters is shown in Figure 5.18. The predicted total mass eroded for each simulation is significantly greater than that predicted for the previous example with a lower hydraulic gradient. This is because, under the more severe hydraulic conditions, the erosion process continues until the filter interface seals completely. The general trend for each filter diameter is similar to the previous example, the two finest filters seal the crack with little erosion, while the progressively coarser filters allow significantly more erosion. The D_{15F}=0.5mm filter is able to seal the crack after some erosion, indicating that filters coarser than the NEF boundary are still capable of preventing piping failure. The D_{15F}=0.7mm filter is unable to seal the crack and erosion is still occurring at termination of the model (after 1440 minutes or 24 hours)

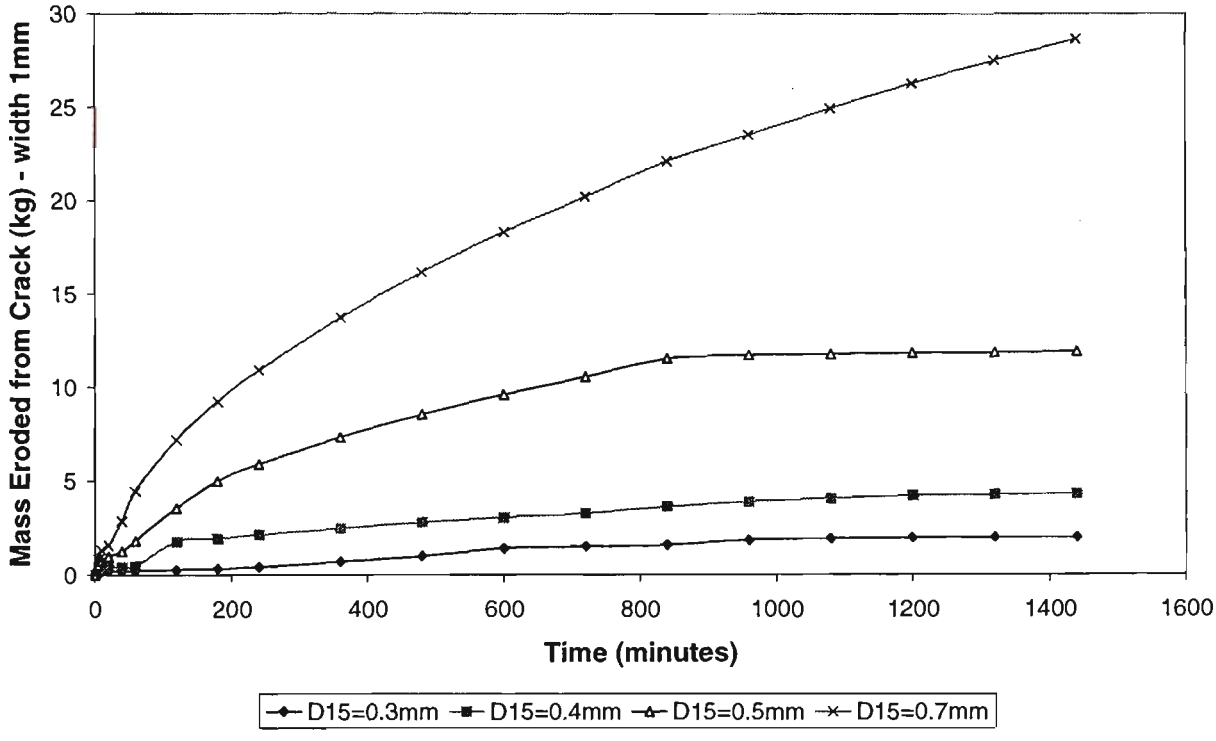

Figure 5.18 Mass eroded from crack with 1mm initial width, under more severe hydraulic conditions

In order to describe the quantities of erosion occurring, the increase in width of the initial 1mm crack is shown in Figure 5.19 for the four different filters under the higher

hydraulic conditions. The two finest filters (D_{15F}=0.3mm and 0.4mm) only allow an increase in crack with of 3-5% before the crack seals. This erosion is insignificant, even under the severe hydraulic conditions. The filter with D_{15F}=0.5mm is coarser than the NEF critical filter boundary (D_{15bdy}=0.35mm). However, it is clearly seen that this filter does seal the crack after a 20% increase in the crack width. This confirms that existing dams with filters coarser than the NEF critical filter may still be safe if a crack through the core does form. The coarsest filter (D_{15F}=0.7mm) does not capture a sufficient quantity of particles to prevent further erosion of the crack within the first day of flow.

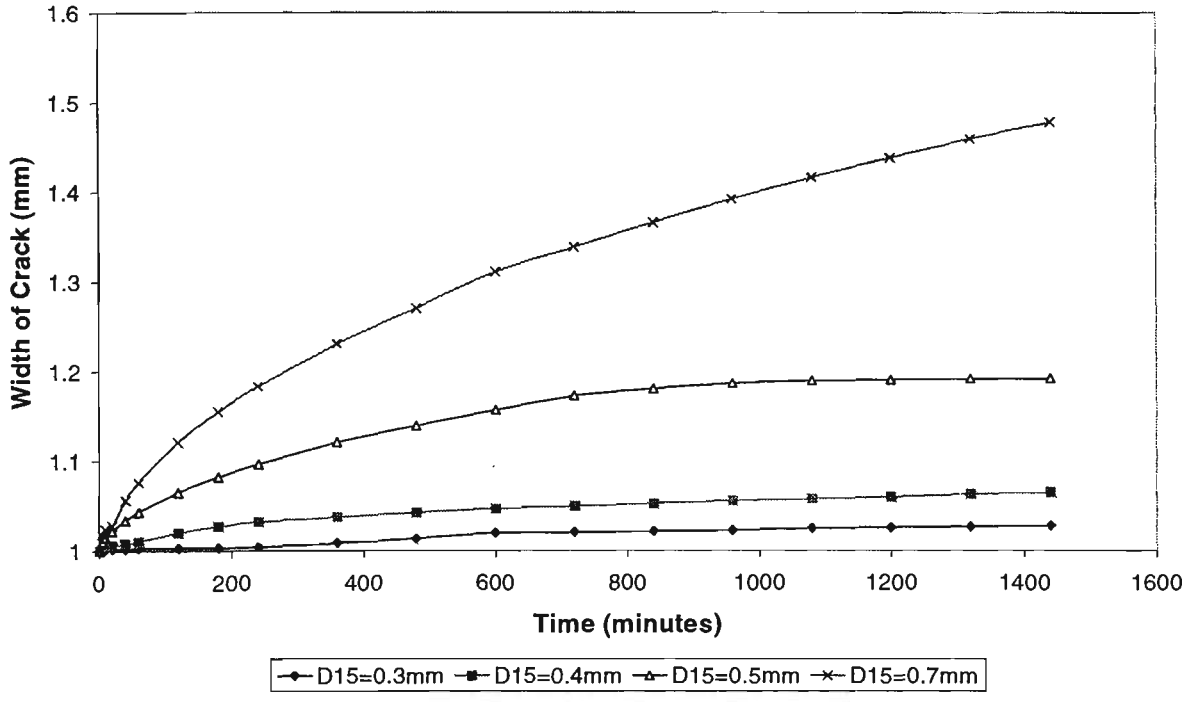

Figure 5.19 Increase in crack width due to erosion of 1mm crack under severe hydraulic conditions

The predicted change in flow rate through the 1mm crack under the severe hydraulic conditions is shown in Figure 5.20. The initial flow rate is controlled primarily by the crack thickness, with a slight variation due to the filter permeability. As mass is eroded and retained at the filter interface, the flow rate reduces rapidly as a filter cake forms. The exposed filter face is only 1mm wide, so the amount of mass required to form a filter cake is small, producing a rapid decrease in flow. This reduction in flow rate is most

pronounced for the two finest filters (D_{15F}=0.3mm and 0.4mm). These filters retain a greater fraction of the base soil, allowing the formation of a thicker filter cake consisting of finer particles. After about 20-40 minutes, the flow rate begins to increase again. This is because the model allows for radial erosion around the filter cake (see Figure 5.7). After the initial formation of the filter cake, this radial erosion occurs at a more rapid rate than erosion of the crack walls, and the filter cake becomes thinner as the radial erosion increases the area covered by the filter cake. This produces the increase in flow rate. The rate of radial erosion decreases and reaches equilibrium with the crack wall erosion after about 200 minutes, and the flow rate stabilises. In all cases, the filter cake becomes the hydraulic control, maintaining constant flow rates through the crack. The thickness and size of particles forming the filter cake determines the final, stable flow rate.

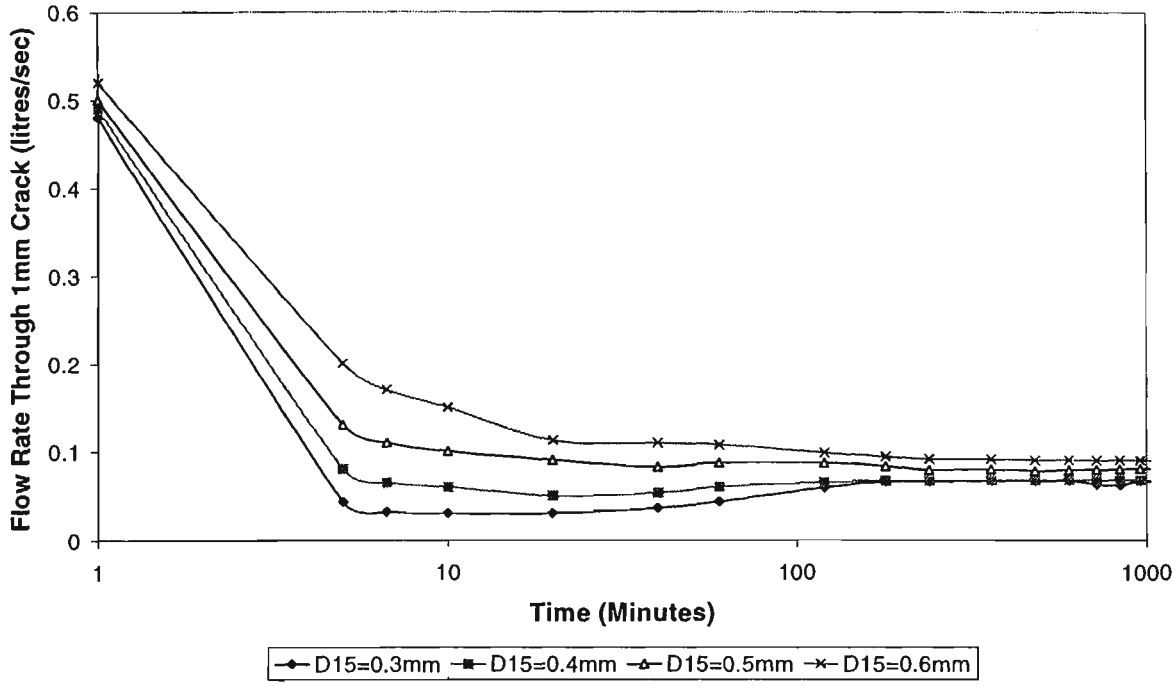

Figure 5.20 Change in flow rate through 1mm crack under severe hydraulic conditions for various filters

5.9.3 *Effect of Crack Width*

For the same dam materials, reservoir head and geometry described in Section 5.8.2, Figure 5.21 shows the mass of material eroded from an initial 10mm crack. The total mass eroded is significantly higher than the 1mm thick crack (Figure 5.18). This is because the larger crack allows greater flow rates and requires a greater mass of material to form a cake over the exposed filter. For the two finest filters (D_{15F}=0.3mm and 0.4mm), the filter retains a sufficient quantity of particles to prevent erosion, after an increase in crack width of about 3-5%. The filter with D_{15F}=0.5mm does reduce the erosion rate and seal the crack after some erosion, while the coarsest filter (D_{15F}=0.7mm) does not adequately seal within the first day. While the mass eroded is significantly higher than the narrower crack, the trends in both cases are similar for each different filter size. Hence, the estimate of initial crack width will affect the total mass eroded, but not the prediction of success or failure of a filter.

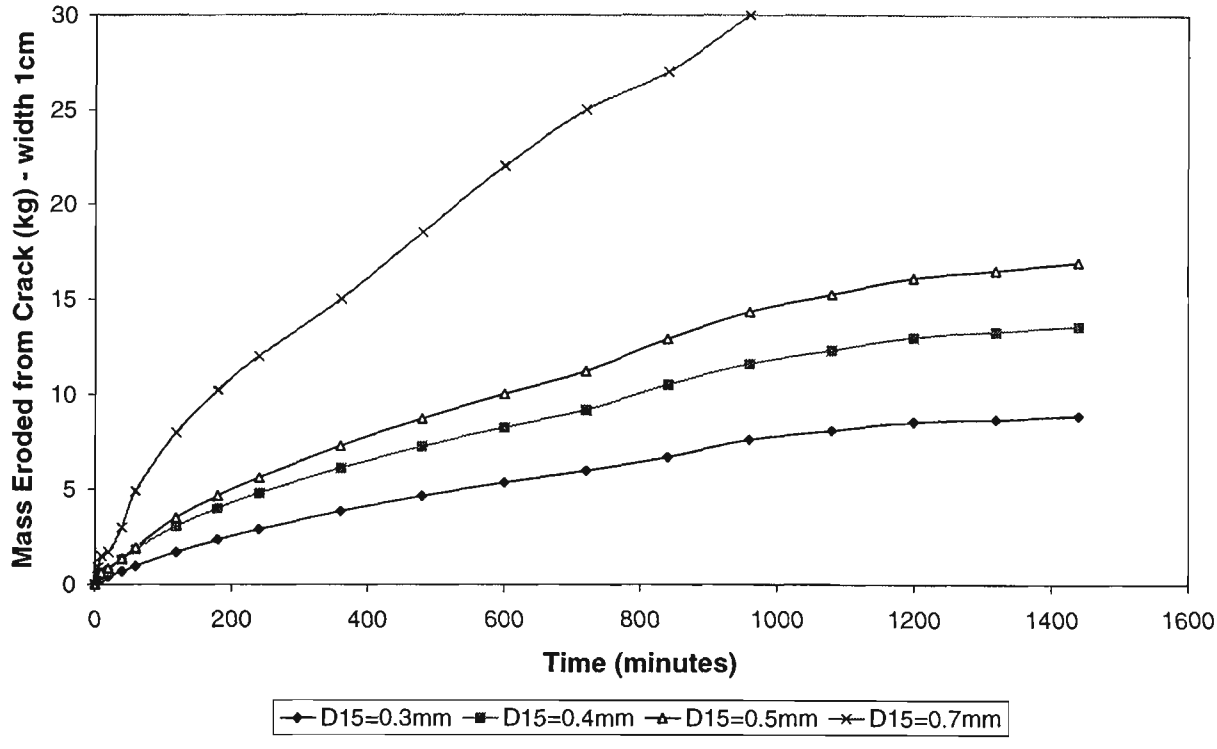

Figure 5.21 Mass eroded from crack with 10mm initial width, under severe hydraulic conditions

5.9.4 *Effect of Erosion Resistance – Critical shear stress* τ_c

The gradation characteristics of the core fines alone (ie. d_{85B}) may not give sufficient information to determine whether or not a certain filter is suitable. Arulanandan and Perry (1983) suggest that consideration of the erodability characteristics of the core material is also necessary in the design of protective filters. The effect of the changing the critical shear stress to initiate erosion is considered in this section. The model has been used to predict the mass eroded from a 1mm crack, with the same geometry and materials as described previously and 25m reservoir head, with varying values of τ_c from 0.05 to 5N/m^2. The simulation is performed for two filters, the first having D_{15F}=0.3mm, and the second having D_{15F}=0.5mm. The results of these simulations are summarised in Figure 5.22, and the effect of changing the critical shear stress by an order of magnitude is clearly demonstrated. An erosion resistant soil with τ_c=5N/m^2 has insignificant erosion through the finer filter before the eroding shear stress is reduced sufficiently to prevent erosion. A coarser filter with D_{15F}=0.5mm also allows minimal erosion, under these hydraulic conditions. This filter is coarser than the NEF boundary. Hence, it may be possible to relax the filter design criteria for erosion resistant materials, depending on the dam geometry and hydraulic conditions.

The moderately erodable material with τ_c=0.5N/m^2, seals quickly when protected by a fine filter with D_{15F}=0.3mm, after minor material loss. The coarser filter, D_{15F}=0.5mm, allows significantly more erosion but does eventually seal the crack. The NEF boundary filter, D_{15F}=0.35mm, would be able to protect this base soil from erosion. This suggests that normal design criteria are adequate to design filters for moderately erodable base soils.

The highly erodable material, with τ_c=0.05N/m^2, when protected by a fine filter (D_{15F}=0.3mm), exhibits an initial decrease in flow rate and consequent erosion rate. After about 600 minutes the erosion rate increases again. This is because the model considers radial erosion around the filter cake. As this radial erosion occurs, the filter cake becomes thinner and the flow rate increases slightly. Due to the very low erosion resistance, a small increase in flow rate can initiate erosion again. The filter finally seals the crack after erosion of 8kg of material. The extent of erosion corresponds to a 15% increase in crack thickness, which is still insignificant. However, continuing radial erosion may result in further erosion and widening of the crack with time. When protected by a coarser filter, D_{15F}=0.5mm, erosion continues at a constant rate over the first 24 hours, and is expected to continue until failure. This demonstrates that a conservative filter is required to protect highly erodable materials. Consideration should be given to providing a filter finer than that predicted by the Sherard and Dunnigan (1985) design criteria.

Critical shear stress is not a normal geotechnical engineering parameter, and is difficult to visualise, or relate to the observed erodability of materials. The standard pinhole test for dispersion is a rough measure of erodability (Sherard et al. 1976). The material classes determined from the pinhole test are listed in Table 5.4. Class D1 erodes rapidly under 50mm head, for the 38mm long sample this corresponds to a hydraulic gradient of 1.3. Using Equation (5.43), this hydraulic gradient produces a shear stress of about 3N/m^2. Arulanandan et al. (1980) showed that the erosion rate increases significantly as τ_c becomes less than 0.5N/m^2. Hence, to produce this rapid erosion, it is most likely that materials in class D1 have a critical shear stress below 0.5N/m^2. Class D2 erodes at a slower rate under the same hydraulic gradient, and erodes to 2mm by the end of a 10 minute test. To produce this amount of erosion, the material probably has a critical shear stress in the range 0.5-1N/m^2. Class ND4 does erode slowly under a 50mm head, and

must have $\tau_c<3N/m^2$. Class ND3 does not erode under 50mm head, but does erode with 180 or 380mm head, corresponding to 10 or 20 N/m^2. Class ND2 is stable under 380mm head but erodes slowly under 1000mm head. Hence, the sample has a critical shear stress in the range 20-50N/m^2. Class ND1 is non-erodable under 1000mm head, and must have $\tau_c>50N/m^2$. These ranges of critical shear stress are shown in Table 5.4. Based on this Table and the predictions of crack erosion related to critical shear stress, it is seen that materials in Class D1 and possibly D2 have a high risk of crack erosion, and may require a filter finer than predicted by design criteria. While materials in classes ND2 and ND1 are erosion resistant and may not require such stringent filter criteria.

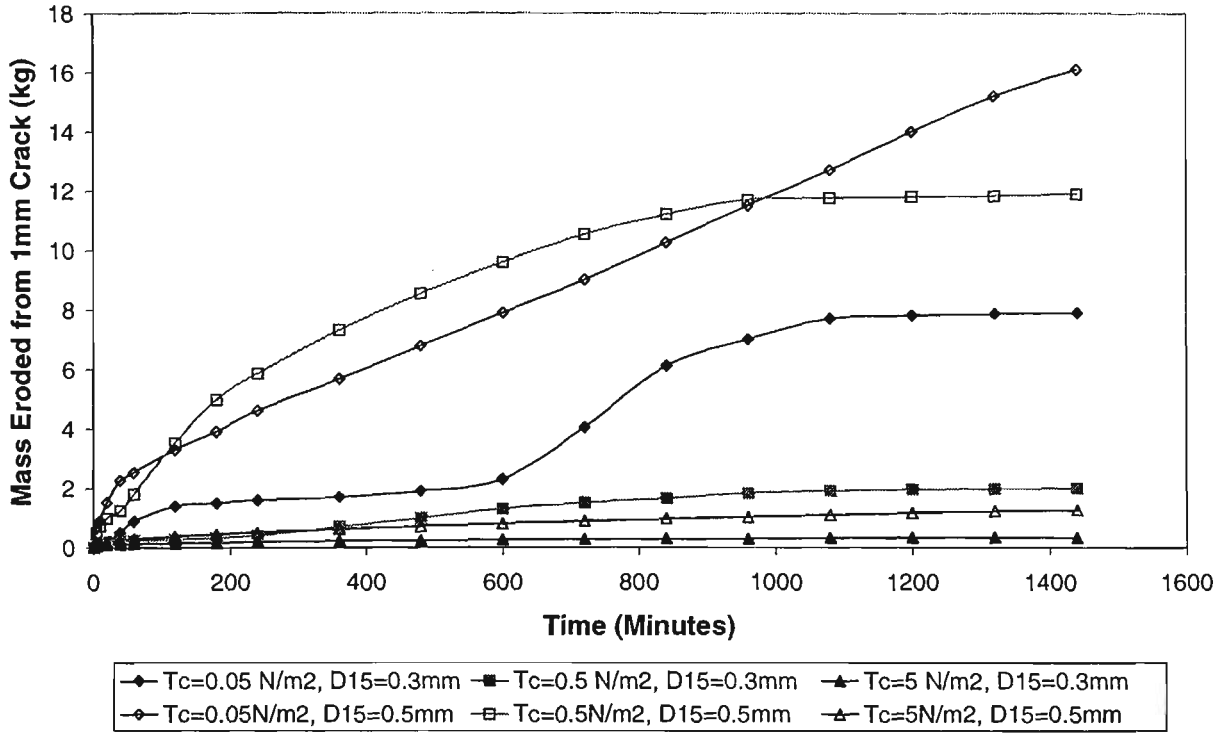

Figure 5.22 Effect of base soil critical shear stress, τ_c, on crack erosion under severe hydraulic conditions (H=25m).

Table 5.4 Pinhole Test Classes and Approximate Critical Shear Stress for Erosion

Classification	Eroding Head	Comments	Crit. Shear Stress
D1 – Highly Dispersive	50mm	Rapidly erodes to >2mm in 2-5 minutes	<0.5 N/m^2
D2 – Dispersive	50mm	Slow erosion to 2mm in 10 minutes	0.5-1N/m^2
ND4	50mm	Erosion under 1.5mm in 10 minutes	1-3N/m^2
ND3	180-380mm	Erodes under higher head	3-20N/m^2
ND2	1000mm	Slow erosion	20-50N/m^2
ND1	1000mm	No erosion	>50N/m^2

5.9.5 Effect of Particle Deposition Conditions

Long-term particle accumulation within filters by physico-chemical attraction can lead to large reductions in the filter permeability and subsequent increases in hydraulic pressures within the dam. This capture of cohesive particles is represented in the model by Equation (5.22), requiring a critical pore velocity, V_c, and a particle deposition parameter, θ_0. Table 5.5 lists the assumed deposition parameters for three different deposition conditions, which may be caused by variations in the reservoir water chemistry or core material. The medium deposition conditions correspond with the case considered in previous examples. The computer model has been run for each of these three cases, using a filter with D_{15F}=0.3mm. Figure 5.23 presents a comparison of the predicted mass loss from a 1mm crack, for the three deposition conditions. The effect of the physico-chemical deposition is clearly shown. An increase in the critical pore velocity, V_c, or the particle deposition parameter, θ_0, results in a decrease in the extent of mass eroded from the crack. This is because more fines are captured and rapidly reduce

the filter porosity and pore constriction sizes. This demonstrates that the physico-chemical particle capture mechanism cannot be ignored in considering the filtration of cohesive materials.

Table 5.5 Parameters for comparison of the effects of deposition conditions on filtration model

Description of conditions	Critical Velocity V_c (m/s)	Deposition Parameter θ_0
Low deposition	0.01	0.5
Medium deposition	0.01	5
High deposition	0.1	10

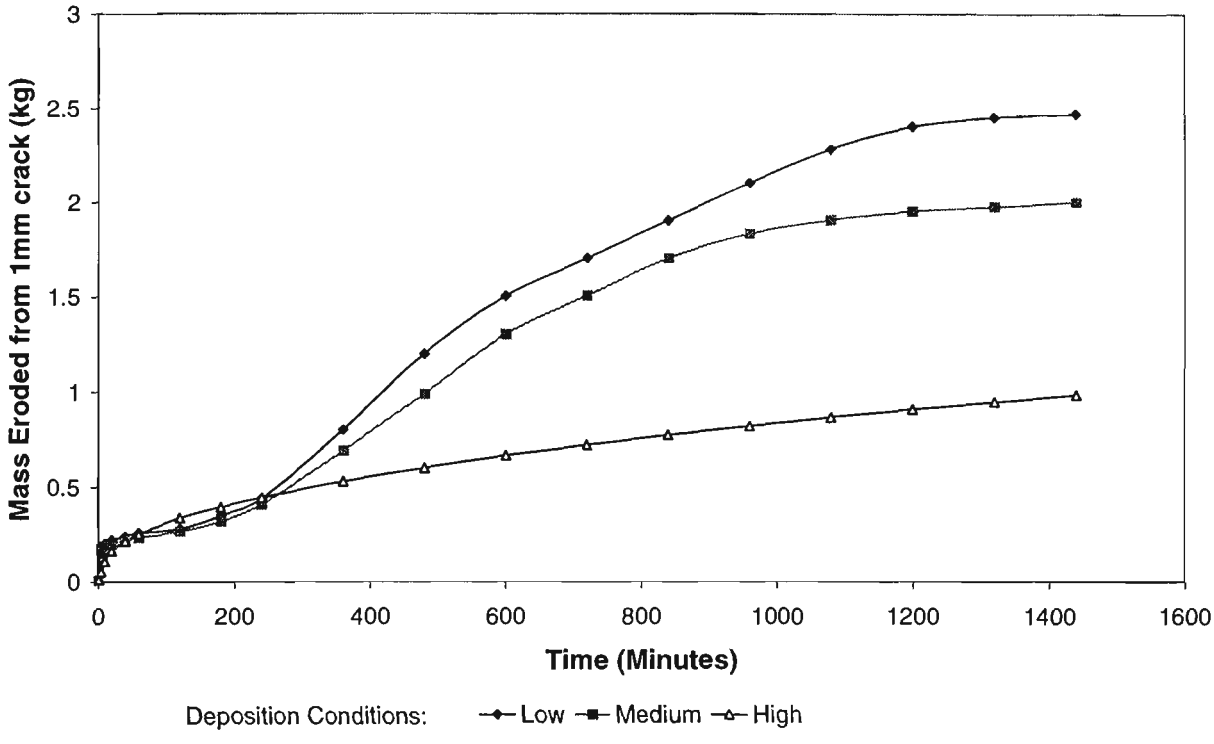

Figure 5.23 Effect of particle deposition conditions on the predicted mass loss from a 1mm crack protected by a filter with D_{15F}=0.3mm

5.9.6 Segregation of Fines

The argument for assuming that segregation of fines may occur, as proposed by Vaughan and Soares (1982), was introduced in Section 5.4. It was shown, in Section 5.4.1, that segregation might be possible when the transporting shear stress is less than $0.5N/m^2$. For this low velocity flow, the applied shear forces are sufficient to mobilize loose clay and silt size particles, but coarser particles will not be transported. To produce conditions such that segregation may occur, consider a highly erodable base soil with $\tau_c=0.05N/m^2$, $\alpha=0.1$ and the same PSD as the previously considered Kerferd material. To produce a low flow rate, a head of 1m is applied to a 15m long crack. This head produces an initial shear stress on the crack walls of about $0.2N/m^2$. A filter with $D_{15F}=0.3mm$ protects the base soil, this filter is finer than the NEF boundary. Figure 5.24 presents the model predictions for erosion of this material. Both the amount of mass eroded from the crack walls and the related change in crack width increase uniformly, as erosion occurs unhindered. The applied shear stress of $0.2N/m^2$ is sufficient to erode the material since the critical shear stress of $0.05N/m^2$ is exceeded, but only particles finer than 20μm are transported. These particles are too fine to be captured by the filter particles, and they move through the filter unhindered. Successful filtration of this base soil would require the coarser silt and fine sand particles to be present at the filter interface to initiate the formation of a filter cake, or a filter capable of retaining the clay flocs.

As shown in Figure 5.24, after 35 hours, the crack width increased from 1mm to 4mm, after loosing 65kg of material per metre width of the 15m long crack. Over this period the shear stress on the crack walls remained reasonably constant at between 0.15-$0.25N/m^2$. This range is insufficient to mobilise coarser particles and the formation of a filter cake cannot be initiated. It is expected that erosion would continue until the crack had widened appreciably (to several centimetres), when transport of coarser particles

may begin as flow rates through the crack increase. The crack may or may not seal at this point, but the risk of failure is high. This analysis shows that the Vaughan and Soares (1982) perfect filter criterion is a sensible design philosophy for highly erodable soils. Materials with a critical shear stress, τ_c<0.5 N/m^2 are at risk of segregation due to erosion at low flow rates, and under certain conditions this may result in extensive erosion before the filter is able to seal the crack. For more erosion resistant materials, the Sherard and Dunnigan (1985) critical filter concept is more appropriate.

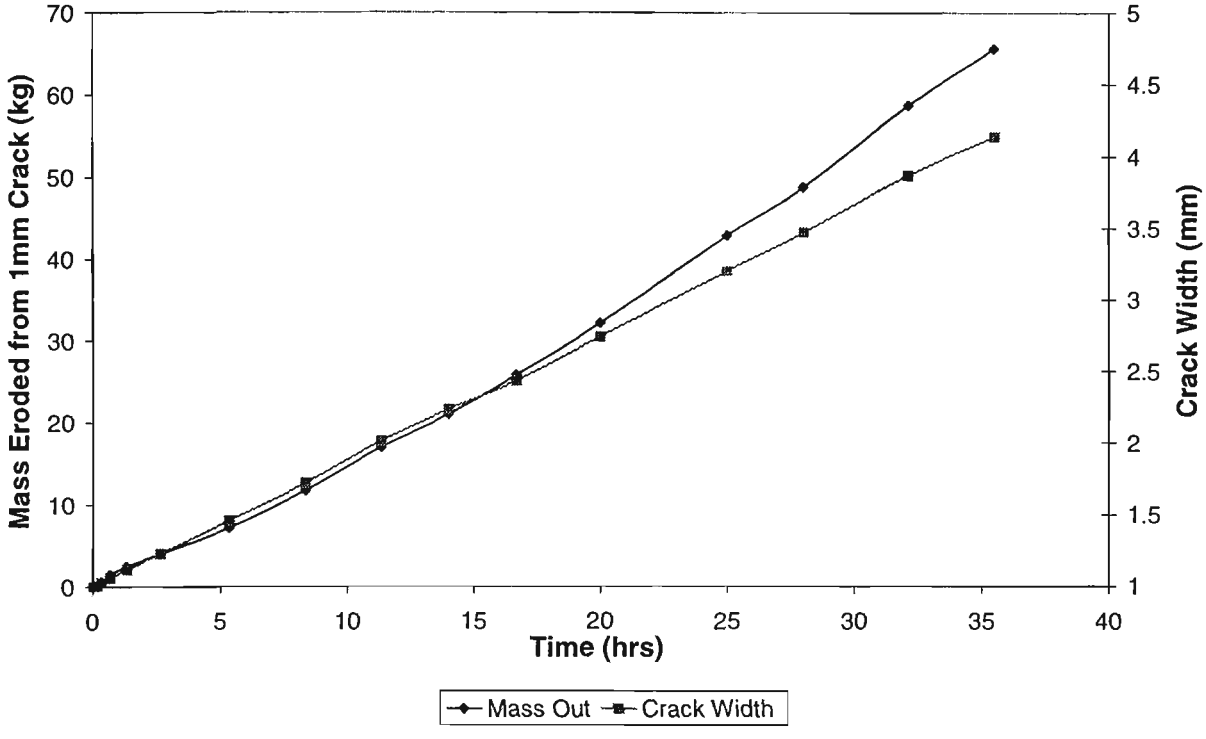

Figure 5.24 Erosion of a 1mm crack through highly erosive material (τ_c=0.05N/m^2) at low flow rate

5.10 Predicting Erosion of Dam Cores

To aid the designer, in this Section some preliminary predictive charts are developed to describe the model predictions of crack erosion under various conditions. The analytical model considers a complex combination of variables that can only be modelled accurately through a time-dependent process, ie. a finite difference solution. To produce simple predictive charts, a number of assumptions and simplifications must be made:

1. The base soil and filter are assumed to be well graded, and are represented by the filter retention ration, D_{15F}/d_{85B}. The base soil is a clay with >85% finer than 75μm. Coarser materials will have an greater increase in crack width for the same retention ratio, as the permeability of the appropriate filter and filter cake formed by these materials is higher, allowing greater flow rates and a higher shear stress for the same filter cake thickness.
2. Arulanandan et al. (1980) presented a correlation to predict the erosion parameter α from τ_c, hence, the erosion properties can be represented by τ_c only.
3. The physico-chemical deposition parameters have been assumed constant with θ_0=5 (dimensionless) and V_c=0.01 (m/s). Actual conditions more prone to particle capture (eg. higher ion content in the eroding fluid) will reduce the extent of crack enlargement, while weak physico-chemical attraction may result in up to 50% more erosion before the crack seals.
4. The dam geometry and reservoir head are represented by the hydraulic gradient along the crack, ignoring the head at the filter interface:

$$i_{crack} \approx \frac{\mathrm{Re}\,servoirHead}{CrackLength} \qquad (5.48)$$

5. The filter will not seal a crack at all, if the coarse base soil particles cannot be captured at the filter interface. This capture of coarse particles can be represented by Equation (5.49), if d_{98B} is large enough to satisfy Equation (5.49), then coarse

particles are captured and will begin forming a filter cake that may be able to capture progressively finer particles. This relation was shown experimentally by Foster (1999).

$$d_{98B} > \frac{D_{15F}}{9} \qquad (5.49)$$

The predictions of the analytical model for well graded clay base soils are summarised in Figure 5.25 for a filter retention ratio $D_{15F}/d_{85B}=10$ and Figure 5.26 for $D_{15F}/d_{85B}=15$. These Figures predict the final crack width based on the initial crack width ($w_{final}/w_{initial}$), for various combinations of critical shear stress τ_c, hydraulic gradient i_{crack}, and filter retention ratio, D_{15F}/d_{85B}. Figure 5.25 shows that at a retention ratio of $D_{15F}/d_{85B}=10$, ie. slightly coarser than allowed by the Sherard and Dunnigan (1985) design criteria, the filter will seal a crack in most base soils with less than 10% increase in crack width. However, at high hydraulic gradients ($i \geq 10$) or for highly erodable materials with $\tau_c < 1N/m^2$, there is a significant increase in the crack width before the filter is able to seal the crack. This suggests that under these conditions of high hydraulic gradient (eg. a narrow core in a high dam) or low erosion resistance (eg. dispersive clays) the filter design criteria should be more conservative than those usually adopted.

Figure 5.26 clearly indicates that at low hydraulic gradients, an erosion resistant dam core will be safe from erosion even when protected by a filter significantly coarser than allowed by the current filter design guidelines, requiring $D_{15F}/d_{85B} \leq 9$. This confirms that coarse filters in existing dams may be adequate provided the expected hydraulic gradients are low and the core material can be shown to have some erosion resistance.

Figures 5.25 and 5.26 can be used as preliminary predictive charts to estimate the extent of erosion through cracks in dam cores, provided the assumptions outlined above are

met, particularly Equation (5.49). The writer does not recommend relaxing the design guidelines for filters in new dams, but these predictive charts may form a useful tool for assessment of filter performance in existing dams.

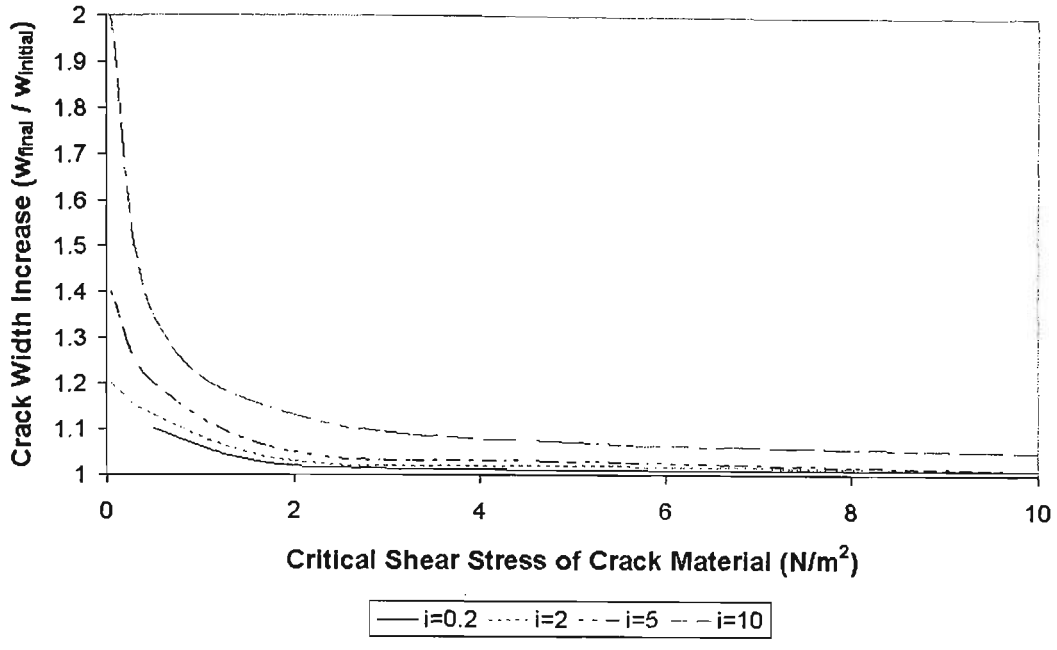

Figure 5.25 Predicted crack erosion for group 1 base soils protected by a filter with $D_{15F}/d_{85B}=10$

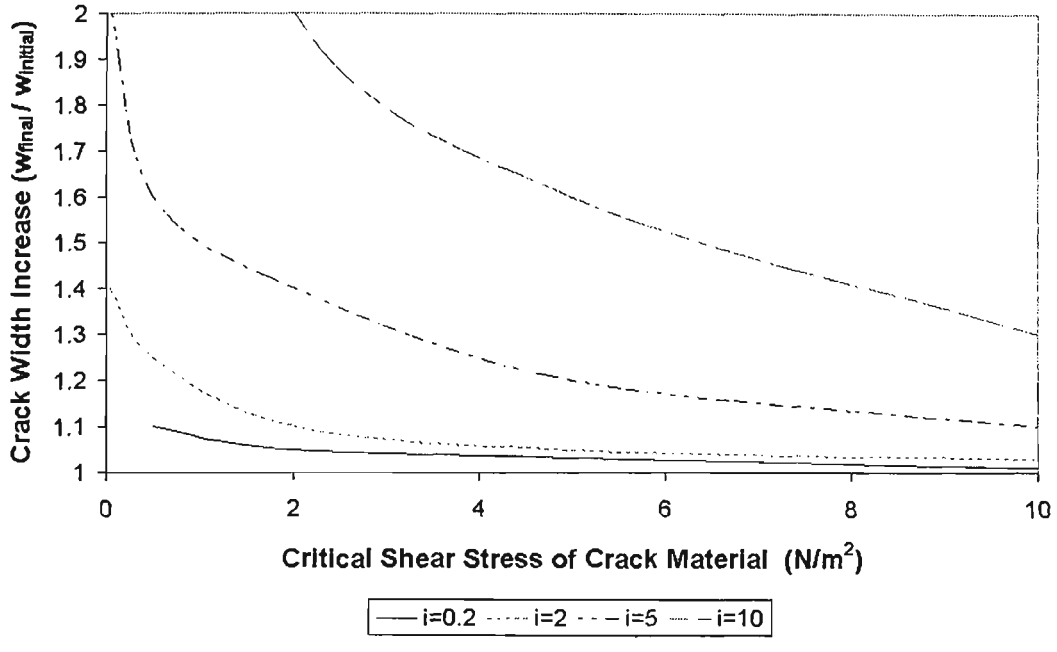

Figure 5.26 Predicted crack erosion for group 1 base soils protected by a filter with $D_{15F}/d_{85B}=15$

5.11 Summary

In this Chapter a mathematical model has been developed to describe the filtration of a concentrated leak through a crack in a cohesive base soil. The model considers five stages of the erosion and filtration processes:

1. Formation of a crack due to hydraulic fracture, differential settlement, earthquake etc. The possible sizes and locations of the crack are estimated based on observations of cracking in other dams and reasonable assumptions.
2. Erosion of the cohesive materials forming the walls of the crack. The erosion rate is related to the shear stress applied by the water flowing through the crack.
3. Transport of particles to the filter face. The maximum size of particles transported is related to the shear stress generated by the flow.
4. Filtration of particles at the filter interface. This is based on the theory developed in Chapter 3 for modelling non-cohesive base soils, and observations of eroded particle sizes in laboratory experiments described in Chapter 4.
5. The formation of a filter cake at the filter interface. If particles are retained, they form a low permeability cake, which reduces the flow rate through the crack and allows it to seal.

Some aspects of the model have been verified through comparison with the results of NEF tests. Simulations for three NEF tests were shown. The first material was a medium plasticity clay, typical of dam core materials. The second material was a very broadly graded sandy clay which has been shown to be unable to self-filter. The third material was a coarse group 2 clayey sand. The NEF model predicted pinhole enlargement and NEF boundaries similar to those measured in the laboratory, for all three materials. Flow rates predicted for NEF tests on two of the materials were similar to those measured in

the laboratory. These comparisons verified the use of a PSD multiplier, A, as defined in Chapter 4 to produce a *representative PSD* for modelling, or the use of the laboratory determined erosion product PSD. The model will be used in Chapter 6 to predict the NEF boundary for the 12 other base soils tested in the laboratory.

The application of the crack erosion model to a real design problem was demonstrated, even though field verifications were not possible. The model predicted that filters finer than the NEF boundary would seal a crack rapidly with little erosion, while increasingly coarse filters allow some erosion before sealing. Larger hydraulic gradients resulted in more erosion before the filter sealed, because the filter cake had to be thicker to reduce the flow rate to a level below the erosion threshold. The critical shear stress to initiate erosion is an important parameter in determining the extent of crack erosion, a high critical shear stress resulted in very little erosion, and a filter coarser than the NEF boundary was adequate. However, a material with a low critical shear stress eroded significantly and a conservative filter was required, approaching the Vaughan and Soares (1982) perfect filter criterion. The deposition conditions, which are a result of the pore water and core material chemistry, had a marked effect on the filtration efficiency. Conditions more conducive to physico-chemical capture of fine particles resulted in more rapid sealing of the filter and a significant reduction in the amount of erosion from the crack.

Highly erodable materials were shown to be prone to segregation during erosion. Flows producing shear stresses smaller than $0.5N/m^2$ were unable to transport sand sized particles within a crack. If the cracked material had a critical shear stress for erosion of less than 0.5 N/m^2, then erosion occurred, but coarse (sand size) particles were not transported and could not influence filtration. The analytical model was shown to

produce conditions such that very low flow rates occurred through a crack or high permeability zone in a dam core, and erosion and segregation of fines occurred. Based on this observation, the Vaughan and Soares (1982) perfect filter design concept should be adopted for highly erodable materials, with τ_c<0.5N/m^2. Erosion resistant materials, eg. plastic non-dispersive clays, may be protected by filters designed using the less stringent Sherard and Dunnigan (1985) design criteria.

The modelling described in this chapter, and in Chapter 3, describes in detail the formation of a stable self-filtering interface for filters protecting either cohesive or cohesionless base soils. Chapter 6 will describe a comparison of both of these models with empirical filter criteria in an attempt to define which criteria are appropriate for different materials and design situations. Some practical applications of the models to dam design and review are presented with the use of case studies in Chapter 7

6. COMPARISON OF MODELLING AND EMPIRICAL CRITERIA

6.1 Introduction

Novel analytical models describing filtration of non-cohesive and cohesive base soils were developed in Chapters 3 and 5, respectively. These models are able to predict the time-dependent changes in flow rate, base soil mass loss, permeability and porosity, the movement and capture of particles within the filter, and changes in the filter permeability and porosity. The predictions of the models have been verified in Chapters 3 and 5, through laboratory testing and comparison with published data. This Chapter compares the model predictions with some of the many empirical design criteria that are more commonly used in filter design, the aim of this comparison is to examine which empirical criteria are suitable for different materials and applications.

Several empirical design criteria were introduced in the literature review of Chapter 2, and are listed again in Table 6.1. These criteria can be divided into two categories; the first category includes those relating to non-cohesive base soils:

- Sherard and Dunnigan (1985) group 3 soils,
- Karpoff (1955),
- US Army Corps of Engineers (1971),
- Honjo and Veneziano (1989).

The second category includes empirical criteria relating to cohesive base soils:

- Sherard and Dunnigan (1985) group 1 and 2 soils,
- Vaughan and Soares (1982),
- Khor and Woo (1989),
- Indraratna et al. (1996).

Table 6.1 Empirical design criteria for granular filters

Author	Base Material	Filter Criteria	Comments
Karpoff (1955)	C_u=3-4	$5 < D_{50F}/d_{50B} < 10$	Also required: 100% passing 75mm sieve, <5% passing 75μm sieve, finer section of base and filter should have parallel grading.
	C_u>4	$9 < D_{50F}/d_{50B} < 30$ and $6 < D_{15F}/d_{15B} < 18$ for crushed rock filters	
		$12 < D_{50F}/d_{50B} < 58$ and $12 < D_{15F}/d_{15B} < 40$ for natural graded filters	
U.S. Army Corps of Engineers (1971)	uniform base Cu<6	$D_{15F}/d_{85B} \leq 5$ and $5 < D_{15F}/d_{15B} < 20$ and $D_{50F}/d_{50B} \leq 25$	For medium to high plastic clays use D_{15F}=0.4mm also require $C_{uF} \leq 20$
Vaughan and Soares (1982)		$k_{filter} < 6.7 \times 10^{-6} \times \delta^{1.52}$ where δ is a representative base particle size (usually d_{85B})	δ in μm, k in m/s
Sherard and Dunnigan (1985)	1) Fine Silts/Clays (>85% <75μm)	$D_{15F}/d_{85B} \leq 9$	% Passing 75μm is based on the base soil fraction finer than 4.76mm. Filters for group 1 and 2 also should have <60% coarser than 4.76mm and maximum particle size 50mm
	2)Silty/Clayey Sand (40-85%<75μm)	$D_{15F} \leq 0.7$mm	
	3) Coarse impervious material (<15% < 75μm)	$D_{15F}/d_{85B} \leq 4$	
	4) Intermediate (15-40% passing 75μm)	interpolate based on % passing 75μm	
Honjo and Veneziano (1989)	Broad grading up to $d_{95B}/d_{75B} \leq 7$	$D_{15F}/d_{85B} \leq 5.5\text{-}0.5\ d_{95B}/d_{75B}$	Based on statistical analysis of compiled previous research.
Khor and Woo (1989)	Cohesive materials	$D_{15F}/d_{85}^* \leq 12$ where d_{85}^* is the 85% largest particle of the fraction passing 75μm	Developed for broadly graded cohesive materials
Indraratna et al. (1996)	Lateritic soils	For d_{85} 50 to 60 μm: D_{15F}/d_{85B} <5 to 5.5 for d_{85} 60 to 80 μm: D_{15F}/d_{85B} <4 to 5	Based on slurry tests

6.2 Predictions and Design Criteria for Non-Cohesive Base Soils

The majority of empirical design criteria have been developed through laboratory tests on non-cohesive soils. These tests are significantly easier to interpret than tests on cohesive materials. In vertical tests, erosion of the base soil occurs at relatively low hydraulic gradients, and the movement of particles can be easily seen. The most commonly adopted design criterion is based on the observations of NEF tests by Sherard and Dunnigan (1985) for coarse, group 3 soils, ie. $D_{15F}/d_{85B}<4$.

The various empirical criteria from Table 6.1 and the predictions of the analytical model are compared for two non-cohesive base soils. The first is a well-graded sand with d_{85B}=1mm and C_u=6. The second sample is a broadly graded silty-sand with d_{85B}=1mm and C_u=20. The PSDs of the two materials are shown in Figure 6.1. Some properties of the two base soils are described in Table 6.2, along with the filter particle sizes required by the various design criteria from Table 6.1. The USACE (1971) design criteria only apply for base soils with $C_u \leq 6$, and for this reason, no design criteria are predicted for the broadly graded material with C_u=20.

Table 6.2 Properties of base soils and corresponding filter design criteria.

Base Soil				Filter Design Criteria			
Sample No.	d_{85} mm	C_u	d_{50} mm	Sherard & Dunnigan (1985)	Karpoff (1955)	USACE (1971)	Honjo & Veneziano (1989)
1	1mm	6	0.29	$D_{15}<4$mm	$0.97<D_{15}<3.2$ $3.4<D_{50}<16.5$	$0.4<D_{15}<1.6$ $D_{50}<7.1$mm	$D_{15}<4.5$mm
2	1mm	20	0.12	$D_{15}<4$mm	$0.18<D_{15}<0.6$ $1.46<D_{50}<7.1$		$D_{15}<3.9$mm

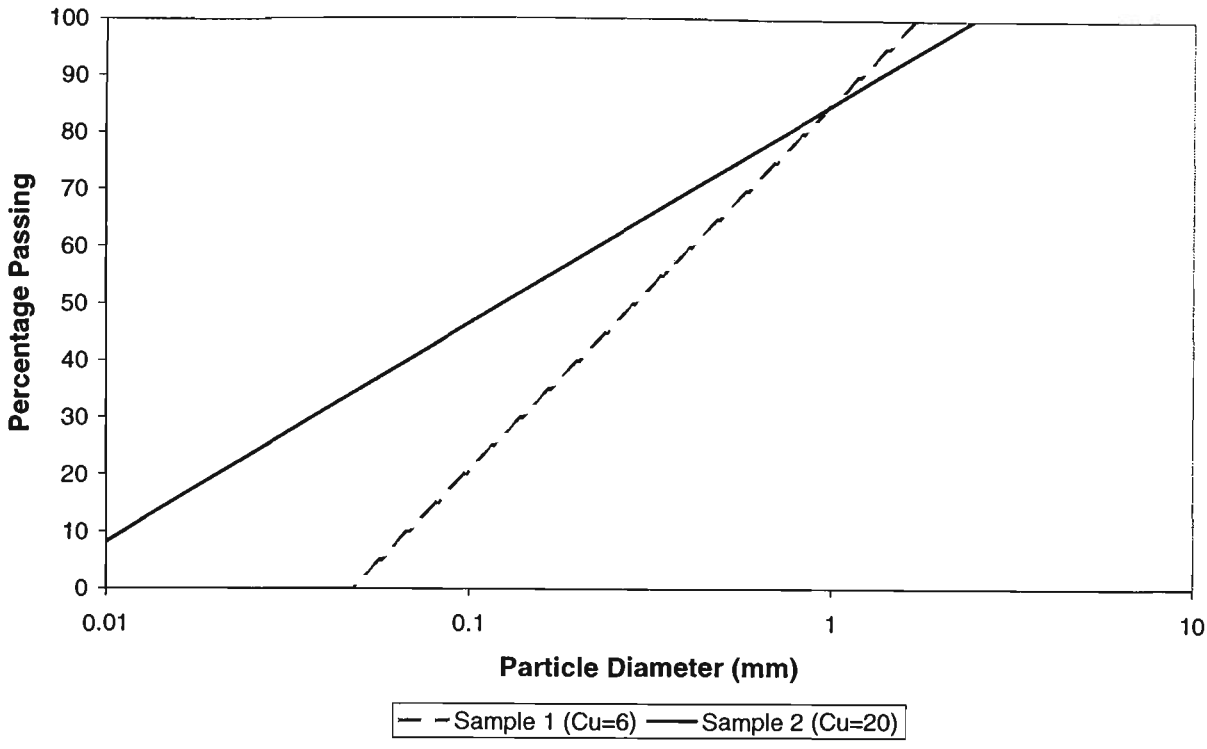

Figure 6.1 Particle size distribution of base soil samples

6.2.1 Well Graded, Non-cohesive Base Soils

Considering first the well graded base soil (Sample 1, C_u=6), the design criteria all require similar filter sizes within the range D_{15F} < 3.2 to 4.5mm. The exception is the USACE (1971) guidelines, which require a significantly finer filter particle size (D_{15F}<1.6mm). The USACE (1971) fine size requirement, D_{15F}/d_{15B}<20, produces this low D_{15F} diameter. The various base/filter ratios (eg. D_{15F}/d_{85B}, D_{15F}/d_{15B} etc.) were discussed in Section 2.4.4. It was shown that the d_{15B} size of the base soil has little effect on filtration, and hence, the ratio D_{15F}/d_{15B} does not relate to filtration and this design requirement should be ignored.

The model predictions of base soil erosion and retention for Sample 1, are summarised in Figure 6.2. This figure shows the mass of base soil passing into the filter for various retention ratios, D_{15F}/d_{85B}. In Figure 6.2, a steep upward slope identifies an area of high base soil erosion, a steep downward slope shows high particle retention within the filter,

and a near flat slope suggests that particles continue to move through this region with little net erosion or retention. The self-filtering zone within the filter can be clearly seen within the first 50-100mm of the filter. The majority of particles passing beyond this self-filtering zone migrate through the filter without being captured. Figure 6.2 clearly demonstrates the effect of increasing the retention ratio, ie. increasing the filter D_{15F} size. Below a retention ratio of 3, the mass loss increases slowly with retention ratio. Above a retention ratio of 3, the mass loss increases more rapidly with further increases in retention ratio. Beyond a ratio of 10, the model predicted failure of the base soil since the filter is no longer able to retain any base soil particles. These predictions suggest that a retention ratio of about 4-5 allows an acceptable amount of particle movement, necessary to form a self-filtering layer, without significant risk of extensive erosion and failure.

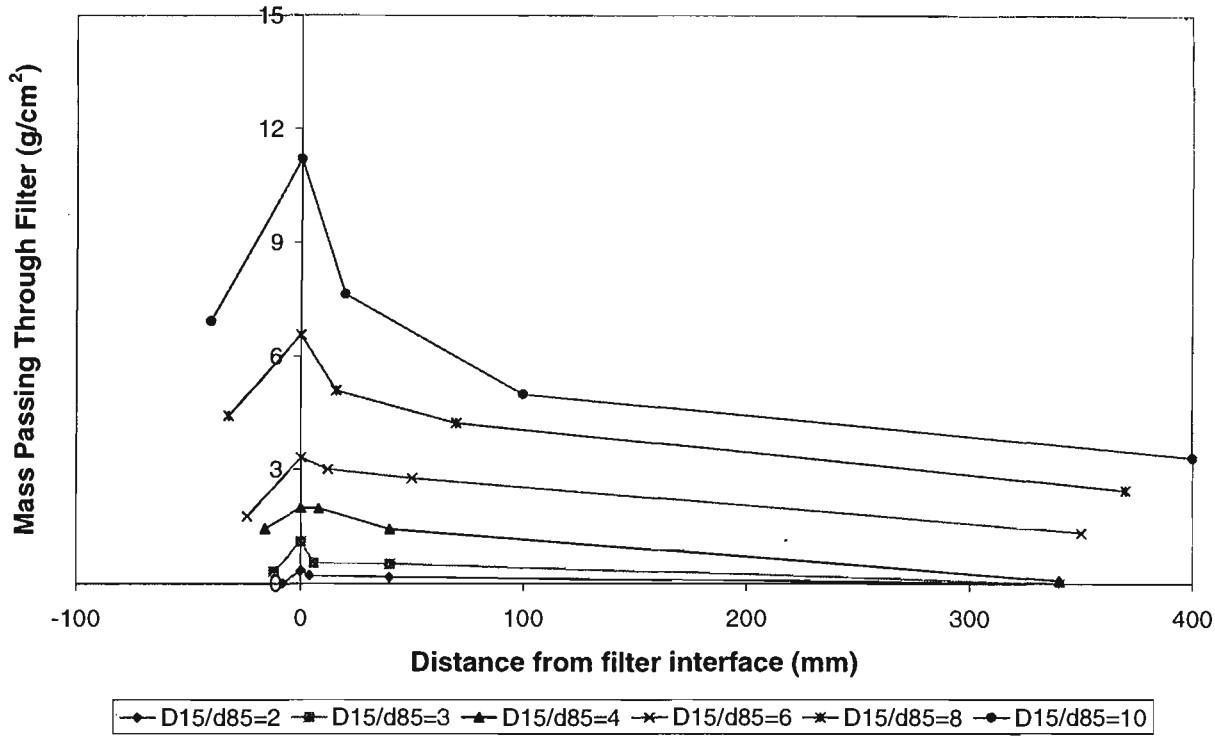

Figure 6.2 Predicted mass of base soil passing into the filter – Sample 1: d_{85B}=1mm, C_u=6.

The model predictions for Sample 1 are compared with the design criteria (from Table 6.2) in Figure 6.3. The figure shows the model prediction of the mass of base soil passing

a depth of at least 100mm into the filter, against the retention ratio. This depth represents the maximum extent of the self-filtration layer within the filter, and it is assumed particles migrating this distance will pass entirely through the filter. The filter design criteria are represented by a vertical line defining the maximum allowable values of D_{15F} from each design method (from Table 6.2). The maximum values for D_{50F} are not shown. The design criteria of Sherard and Dunnigan (1985) and Honjo and Veneziano (1989) are shown to allow a similar quantity of erosion (about 1.3-1.8 g/cm^2) before steady state conditions occur. The Karpoff (1955) criterion requires a slightly finer filter that allows less erosion (0.7g/cm^2). The USACE (1971) criteria require a significantly finer filter allowing almost no erosion. This fine filter seems unduly conservative. Based on these observations, the Karpoff (1955), Sherard and Dunnnigan (1985) and Honjo and Venziano (1989) design criteria all require similar filters for a well graded base soil (C_u=6) and any of these criteria could be adopted for filter design.

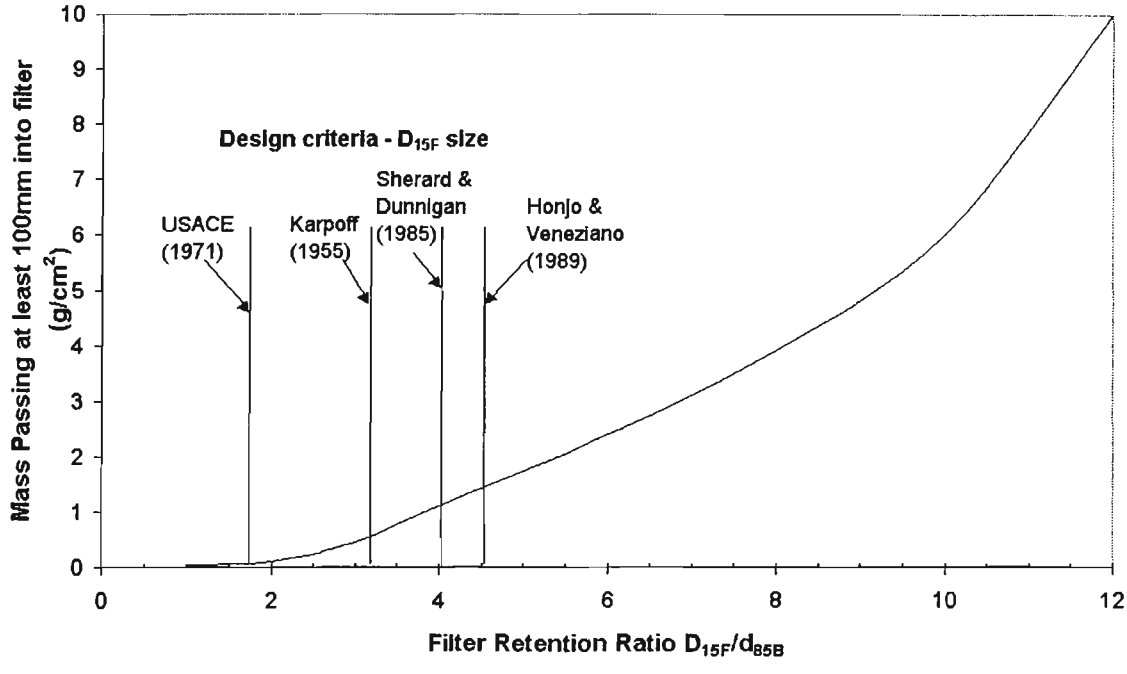

Figure 6.3 Comparison of predicted mass loss and empirical design criteria – Sample 1: d_{85B}=1mm, C_u=6.

6.2.2 *Broadly Graded, Non-cohesive Base Soils*

Now consider the broadly graded base soil (Sample 2) with C_u=20 and PSD shown in Figure 6.1. The model predictions for extent of mass lost before formation of a stable filter interface for this base soil in combination with various filters are shown in Figure 6.4. The model predicts that the amount of mass lost into the filter will be low for filter retention ratios less than 3 to 4, although the quantity of base soil mass lost is greater than that predicted for Sample 1. This greater mass loss is as expected, since a large quantity of very fine particles from the broadly graded base soil will be lost before a sufficient number of coarser base soil particles are captured and are able to self-filter these finer particles. Above a retention ratio of 6, the mass loss increases rapidly with increasing retention ratio. Complete erosion of the base soil is predicted for a retention ratio exceeding 10, and hence, model predictions of mass loss cannot be plotted since the filter does not stabilise.

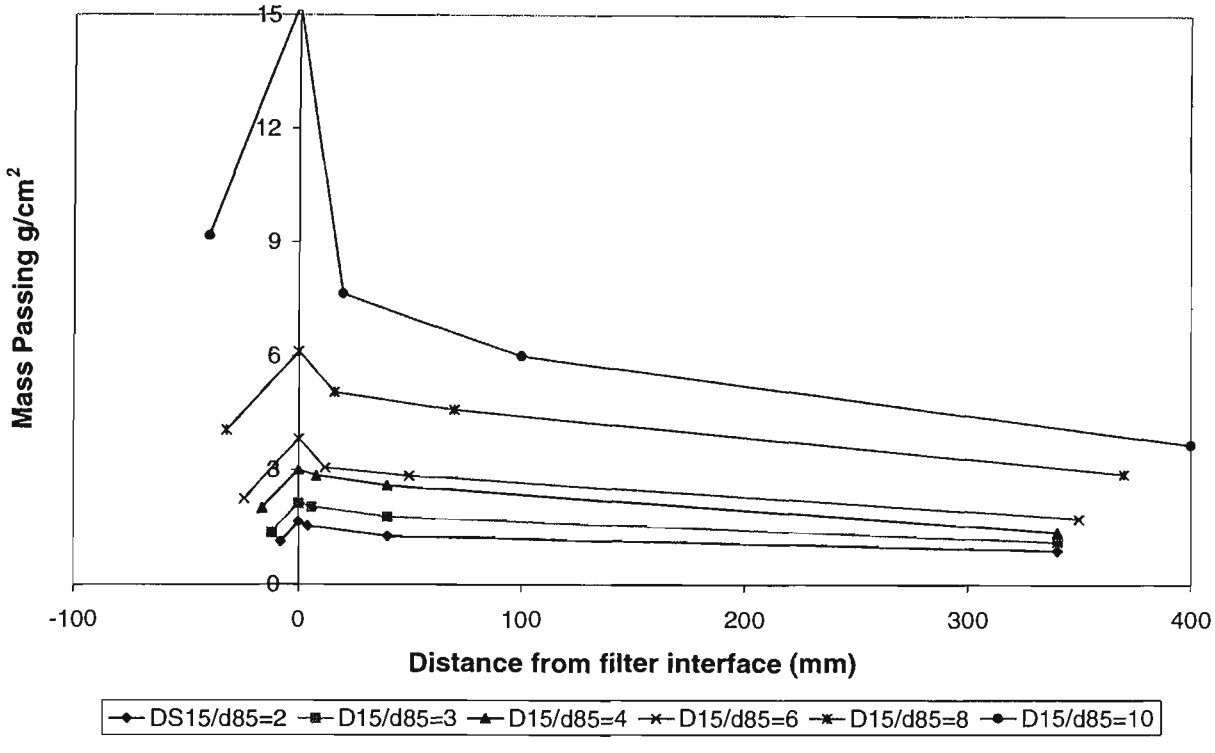

Figure 6.4 Predicted mass of base soil passing into the filter – Sample 2: d_{85B}=1mm, C_u=20.

These model predictions are summarised in Figure 6.5, which again shows the mass of base soil passing at least 100mm into the filter against the retention ratio, for Sample 2. The criteria of Sherard and Dunnigan (1985) and Honjo and Veneziano (1989) again permit a similar maximum D_{15F} size; both methods are shown to allow approximately 1.8 g/cm^2 of erosion. The Karpoff (1955) criteria require $D_{15F}/d_{15B}<40$, which results in a very fine filter for the broadly graded base soil. This filter will still allow about 0.9g/cm^2 of erosion before the filter seals. There seems little justification in requiring such a fine filter for a low reduction in erosion, and hence, the Karpoff (1955) design criterion is overly conservative for broadly graded materials.

Based on these observations, the design criteria of Sherard and Dunnigan (1985) and Honjo and Venziano (1989) predict similar filter D_{15F} sizes for both the well graded and broadly graded base soils examined. The extent of base soil erosion, through the coarsest allowable filter permitted by these two design criteria, is similar for both base soils. This suggests that the criteria are consistent for various values of C_u. In contrast, the criterion of Karpoff (1955) requires a significantly finer filter for the broadly graded base soil, with only a small reduction in the predicted base soil erosion. Hence, the Karpoff (1955) criterion, $12<D_{15F}/d_{15B}<40$, is not justified by the model predictions. The USACE (1971) criterion, $5<D_{15F}/d_{15B}<20$, similarly requires excessively fine filters for well graded base soils.

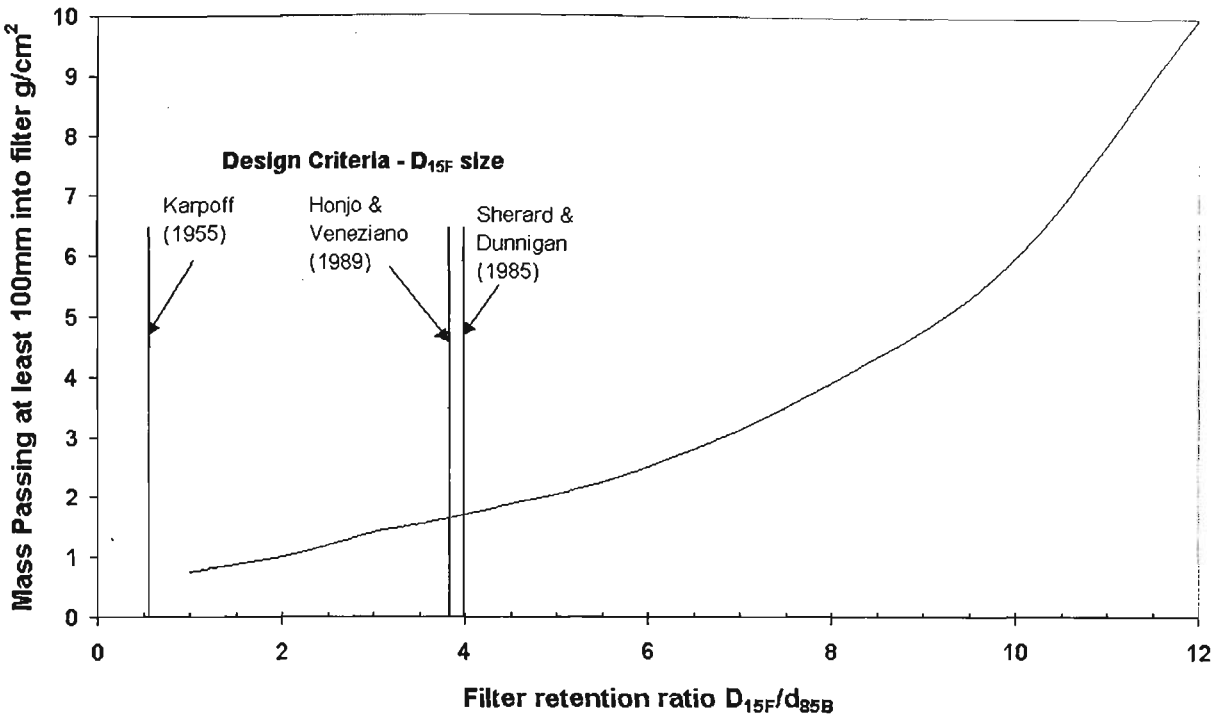

Figure 6.5 Comparison of predicted mass loss and empirical design criteria – Sample 2: d_{85B}=1mm, C_u=20.

6.2.3 Design Criterion for Non-Cohesive Soils

The previous analysis has shown that the design criteria of Sherard and Dunnigan (1985) and Honjo and Veneziano (1989) are suitable for the design of filters for non-cohesive base soils. These two criteria require slightly different filters for various base soil gradings and should be investigated further. The Sherard and Dunnigan (1985) criterion requires $D_{15F}/d_{85B} \leq 4$ for any base soil with <15% finer than 75μm. In contrast, the Honjo and Venziano (1989) criterion requires a reduction in the retention ratio with increasing base soil broadness coefficient, ie.

$$D_{15F}/d_{85B} \leq 5.5 - 0.5*d_{95B}/d_{75B} \qquad (6.1)$$

To compare these two criteria, the analytical model is used to predict the extent of base soil erosion before steady filtration occurs, for a range of sandy base soils coupled with the coarsest allowable filter from these two design criteria. The base soils have d_{85B}=1mm, a linear grading (on log scale) and C_u varying from 2 to 40, in increments of

2. The model was used to predict the extent of base soil erosion for each base soil protected by the coarsest allowable filter determined from both design criteria. The predicted mass of base soil passing through the self-filtration zone (ie. infiltrating more than 100mm), is plotted against C_u in Figure 6.6.

The Sherard and Dunnigan (1985) criterion allows very little mass loss (about 0.2 g/cm^2) for uniform base soils. As the base soil coefficient of uniformity increases, the mass of base soil passing through the filter also increases rapidly up to 1.6 g/cm^2 for a base soil with C_u=12. As increasingly broadly graded base soils are considered, the amount of base soil erosion continues to increase up to about 2.0g/cm^2 for a base soil with C_u=40. These model predictions are consistent with the observations of Lafleur et al. (1989), who suggested that the extent of base soil loss before self-filtration can occur, increases with more broadly graded materials. Hence, adopting a constant retention ratio for any non-cohesive base soil, regardless of the broadness of grading, seems unsatisfactory.

The Honjo and Venziano (1989) design criterion allows coarser filters for uniform materials (D_{15F}=5.3mm). Consequently, the predicted mass loss for a uniform base soil (C_u=2), protected by a filter designed by this criterion, is about 1.0 g/cm^2. This is five times that predicted for the Sherard and Dunnigan (1985) filter, having D_{15F}=4mm. The mass of base soil lost rapidly increases to 1.8g/cm^2 as the coefficient of uniformity is increased to 6. For the well graded and broadly graded base soils (with C_u from 6 to 40) the predicted quantity of erosion of the base soil is nearly constant. This is because the allowable filter diameter D_{15F} becomes finer with increasing broadness of the base soil, as represented here by C_u. Hence, the Honjo and Venziano (1989) design criterion is more consistent than the Sherard and Dunnigan (1985) criterion for a wide range of base soils. The difference between the two methods is maximum at low values of C_u (less than

10). Based on this analysis, the writer recommends using the Honjo and Venziano (1989) criterion for the design of filters for non-cohesive, internally stable base soils. Internal stability can be determined by the *Reduced PSD* method (Chapter 4).

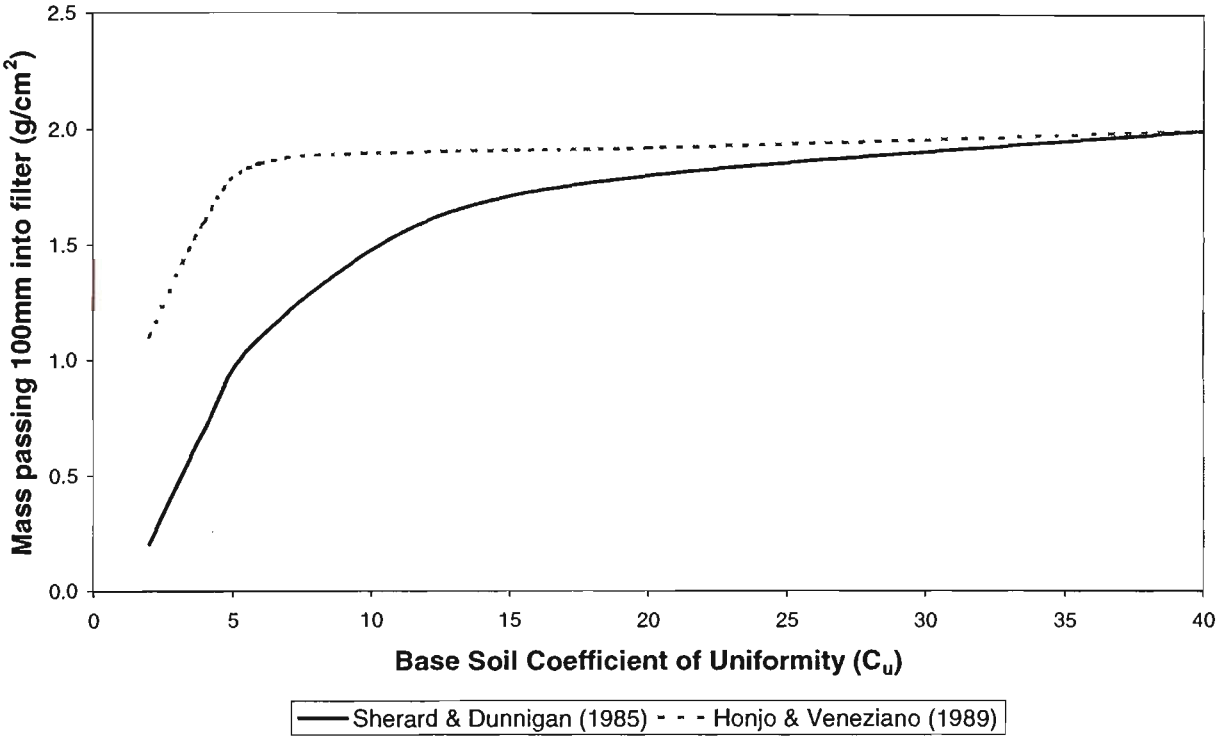

Figure 6.6 Mass of erosion before steady state conditions for various base soils

6.3 Predictions and Design Criteria for Cohesive Base Soils

The methods of designing filters for cohesive base soils can be sub-divided into two design concepts: the critical filter concept developed by Sherard and Dunnigan (1985), and the perfect filter concept proposed by Vaughan and Soares (1982). These were both discussed in detail in Chapter 2. Because the design concepts are so different, it is difficult to compare the predictions directly. Instead, this Section will compare the model predictions with each design concept separately.

6.3.1 Comparison with Critical Filters and NEF Test Results

The No Erosion Filter (NEF) test is used to determine the critical filter for a base soil. Sherard & Dunnigan (1985) and Khor & Woo (1989) have used this test in developing their filter design criteria. During the current research project, NEF tests were performed on 15 different base soils from dams and other sources throughout Australia. The results of these tests were presented in Chapter 4. In Chapter 5 an analytical model of the NEF test was developed, describing the time-dependent changes occurring during the test. In this Section, the laboratory results from Chapter 4 will be compared with the model predictions, and with the design criteria of Sherard & Dunnigan (1985) and Khor & Woo (1989). Delgado (2000) performed NEF tests on 6 group 2 materials, the results of these tests are also considered here for comparison.

In Chapter 4, a new method to determine the critical filter size for cohesive base soils was described, called the *Reduced PSD* method. This method required analysis of the base soil PSD, to examine the self-filtration properties of the material. If the coarse particles are unable to self-filter the fines within the soil, then the PSD is truncated to produce a *Reduced PSD*. This Reduced PSD represents the self-filtering fine fraction of

the base soil. The critical filter size D_{15F} could be found from the Reduced PSD. For group 1 soils with >85% finer than 75μm, use $D_{15F} \leq 12d_{85Reduced}$, and for group 2 soils (with 40-85% finer than 75μm):

- If PI>10 then $D_{15F} \leq 9d_{85Reduced}$
- If PI<10 then $D_{15F} \leq 4d_{85Reduced}$

Where $d_{85Reduced}$ is the 85% largest particle from the Reduced PSD. The critical filter determined from the Reduced PSD method will also be considered.

Table 6.3 presents some properties of the base soils tested, and the measured and predicted critical filter D_{15F} diameter, determined by the various methods. This data is summarised in Figure 6.7 for group 1 base soils (with >85% finer than 75μm), and Figure 6.8 for group 2 base soils (with 40-85% finer than 75μm). Consider first the group 1 base soils (Figure 6.7). Each material is labelled above the laboratory results, the critical filters determined by the design criteria and model predictions are not labelled, but can be located since they have the same D_{15F} size. It is evident that there is a large scatter in the predicted and measured critical filter sizes. This illustrates the complex combination of factors that influence filtration of fine cohesive materials. A design criterion based solely on particle size ratios cannot describe the effect of hydraulic gradient, erosion resistance, inter-particle forces etc. Despite this, the design criteria and modelling predictions cluster around the Sherard and Dunnigan (1985) design criterion of $D_{15F}/d_{85B}=9$, suggesting that this criterion is adequate for design. The Khor and Woo (1989) design criterion has the widest scatter from the $D_{15F}/d_{85B}=9$ line, and from the measured laboratory results. This criterion usually requires a more conservative filter diameter.

Of the group 1 base soils, only samples BB4 and BB3 have a laboratory measured critical filter diameter, D_{15bdy}, finer than the diameter predicted by the design criteria and model. These materials have a very uniform coarse fraction ($d_{98}/d_{85}<3$), and are expected to have an NEF boundary filter slightly finer than predicted (as described in Chapter 4). NEF tests performed on all the group 1 base soils, using filters meeting the design criteria, allowed no erosion or a small amount of erosion before stabilising. This suggests that all of the design methods are adequate for predicting safe filters for these eleven group 1 base soils. In most cases, the filters required by the design criteria will be significantly finer than the actual NEF boundary filter. The modelling results and Reduced PSD method predict a critical filter diameter similar to the other design criteria, with no apparent advantage or disadvantage in adopting these methods for the group 1 soils.

Table 6.3 NEF Test results compared with model and design criteria

Base Soil	%<75μm	Base Soil Properties d_{85Orig} (μm)	d_{85}* (μm)	$d_{85Reduced}$ (μm)	Laboratory NEF Bdy D_{15F} (mm)	Sherard & Dunnigan D_{15F} (mm)	Khor & Woo (1989) D_{15F} (mm)	Reduced PSD D_{15F} (mm)	New Model NEF Bdy D_{15F} (mm)
BB3	95	16	15	16	0.13	0.14	0.18	0.19	0.21
BB4	100	11	11	9	0.10	0.10	0.13	0.11	0.15
CA1	95	36	22	24	0.33	0.32	0.26	0.29	0.3
CO1	90	45	28	37	0.80	0.41	0.34	0.44	0.4
RO1	92	35	20	27	0.75	0.32	0.24	0.32	0.35
SF1	98	23	23	23	0.54	0.21	0.28	0.28	0.24
AS1	98	38	38	38	0.27	0.34	0.46	0.46	0.32
YanYean	98	34.5	33	35	0.63	0.31	0.40	0.42	0.32
Cowarra	96	25	18	19	0.53	0.23	0.22	0.23	0.25
Kerferd	95	28	26	28	0.35	0.25	0.31	0.34	0.37
Hume	98	33	22	26	0.37	0.30	0.26	0.31	0.3
AP1	76	190	18	17	0.19	0.70	0.22	0.15	0.23
AS2	82	90	27	85	1.10	0.70	0.32	0.77	0.75
BB1	82	120	35	48	0.78	0.70	0.42	0.43	0.37
Thompson	55	180	60	160	2.00	0.70	0.72	1.44	1.7
BFA-C1	65	776	30	109	1.40	0.70	0.36	0.98	-
BFA-C2	66	630	22	104	1.20	0.70	0.26	0.94	-
BJV-C1	65	300	51	183	1.30	0.70	0.61	0.73	-
BJV-C3	68	270	50	177	1.10	0.70	0.60	0.71	-
BJV-C7	62	1250	45	68	1.40	0.70	0.54	0.61	-
BP-C2-0.32	80	100	30	43	0.95	0.70	0.36	0.39	-
BSC-C4	81	93	25	42	0.60	0.70	0.30	0.38	-

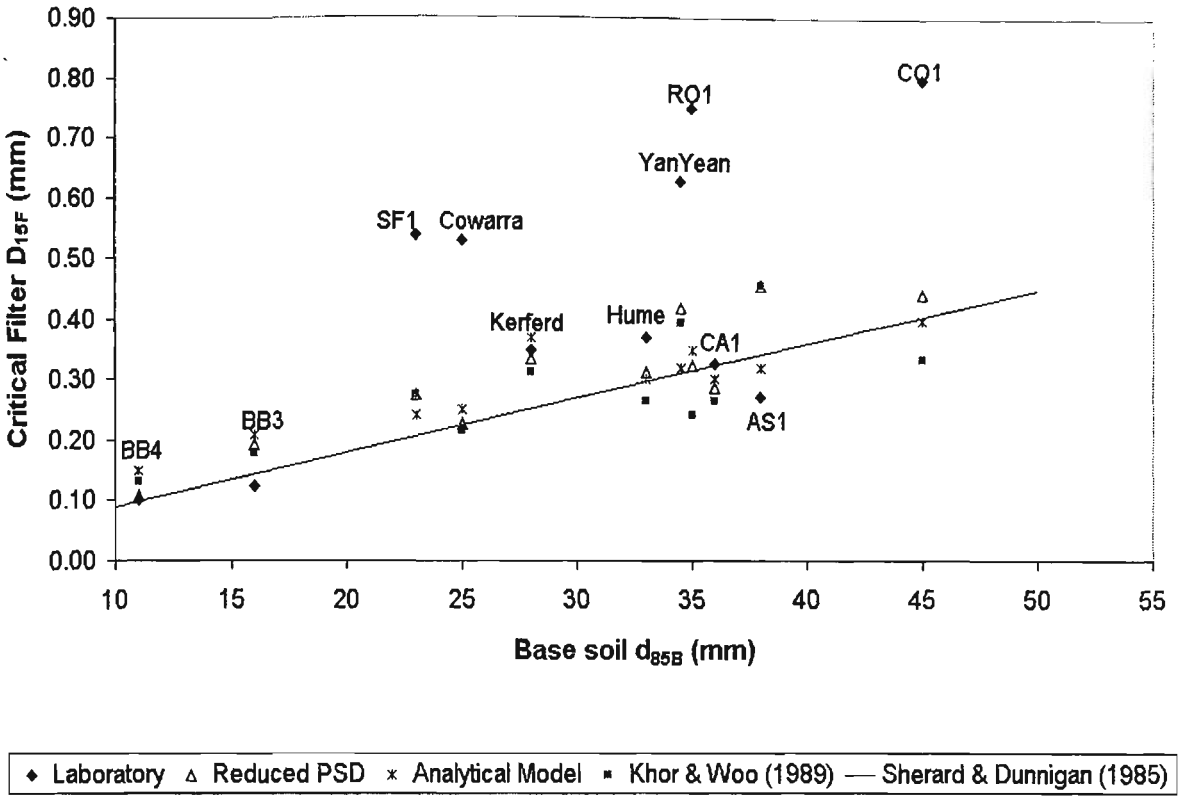

Figure 6.7 Critical filter diameter determined through laboratory testing, design criteria, new Reduced PSD method and modelling for group 1 base soils with d_{85B}<75μm.

The comparison of the design criteria, model predictions and laboratory results for group 2 base soils is shown in Figure 6.8. There were four materials tested in the current laboratory investigation from group 2, also the results of NEF tests on 6 materials from Delgado (2000) have been included in the analysis. The analytical model could not be applied to the Delgado (2000) data because the erosion parameters were not determined, and hence, model predictions are only shown for the four materials tested in the laboratory. The Sherard and Dunnigan (1985) design criterion is represented by the straight line, D_{15F}=0.7mm. The scatter of results and predictions from this design criterion is very wide. For the majority of samples, the various design criteria predict filters finer than the laboratory NEF boundary. The Reduced PSD method appears to yield filters closest to the laboratory results, while still requiring a filter finer than the NEF boundary. The Thompson Dam core material has a very high laboratory D_{15bdy},

because this coarse material is internally stable. The Sherard & Dunnigan (1985) and Khor & Woo (1989) design criteria ignore the coarse fraction of group 2 soils, and require a filter significantly finer than that determined in the laboratory. The Reduced PSD method and the analytical model were able to recognise that the coarse fraction of this material is able to self-filter the fine fraction, and predicted a filter diameter close to the laboratory results. The AP1 material is gap graded, containing both coarse sand and fine silt/clay fractions. This material was described in detail in Chapter 4. Only the soil fraction finer than about 50μm is able to self-filter. Because the Sherard and Dunnigan (1985) method ignores the self-filtering requirement of the base soil, it allows a filter significantly coarser than the safe filter in the NEF test. All other design methods were able to predict the finer critical filter diameter.

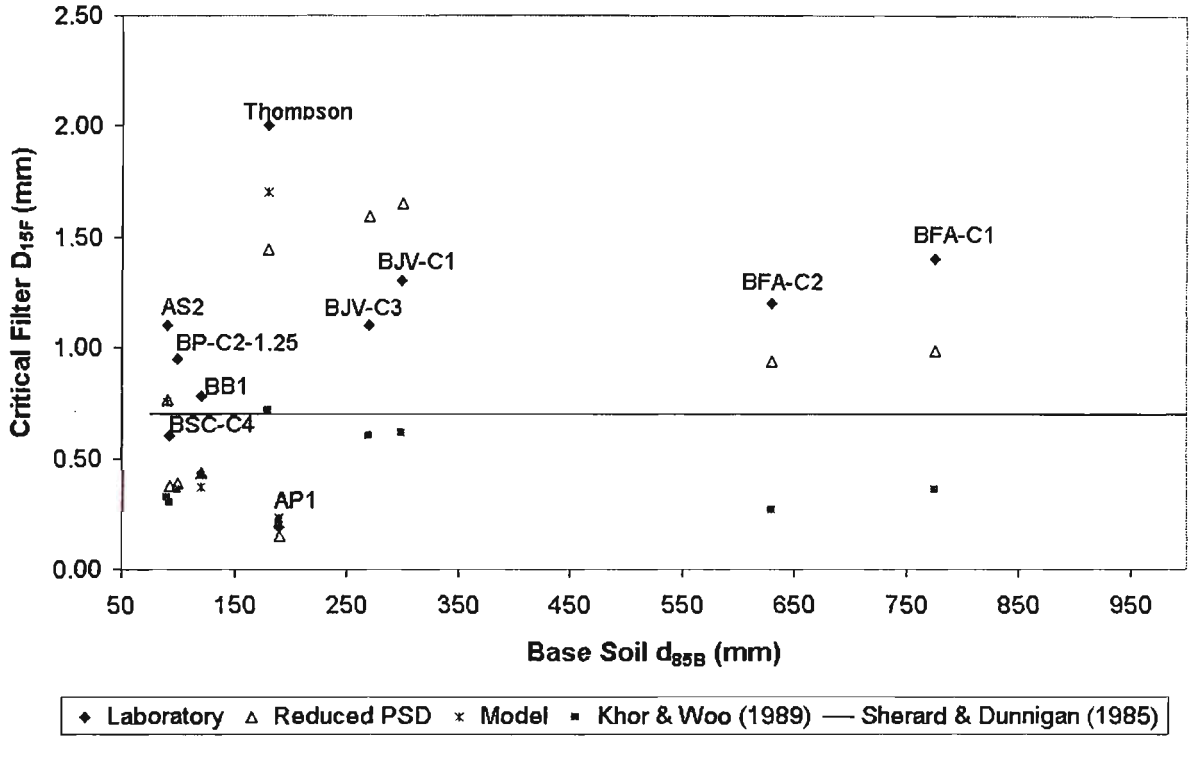

Figure 6.8 Critical filter diameter determined through laboratory testing, design criteria, new Reduced PSD method and modelling for group 2 base soils, d_{85B} >75μm.

This analysis of 25 group 1 and 2 base soils suggests the following conclusions:

- While the Sherard and Dunnigan (1985) design criteria were developed from an extensive laboratory testing program, the criteria do not predict a conservative filter diameter in all cases. Notable exceptions include fine base soils with a uniform coarse fraction and broadly graded base soils that are unable to self-filter.
- The Khor and Woo (1989) design criterion is conservative in most cases. The criterion is often unduly conservative, as it does not consider the coarse fraction of internally stable materials even when these materials can self-filter.
- The analytical model predicts a critical filter in close agreement with the empirical design criteria. The model is able to recognise broadly graded base soils that are unable to self-filter. In addition, the advantages of the model are the full description of the NEF test including changes in flow rate, time taken until steady state conditions and the extent of infiltration of particles into the filter.
- The *Reduced PSD* method of filter design, described in Chapter 4, has been shown to predict a critical filter diameter close to the NEF filter diameter measured in the laboratory. The method is particularly effective for group 2 base soils, which are often broadly graded and the coarse fraction may be unable to self-filter the fine fraction.

This analysis suggests that currently adopted design criteria may not be adequate for all cohesive materials. Laboratory testing is the best approach to determine a critical filter for individual cohesive base soils. If this is not possible, the writer recommends that both the Sherard and Dunnigan (1985) criteria and the Reduced PSD method be used to determine a critical filter diameter, and the finer of these diameters be used to determine a safe filter. The use of analytical models such as that developed in Chapter 5, can improve designer confidence in the expected behaviour of filters.

6.3.2 *Comparison with the 'Perfect Filter' Concept*

The 'perfect filter' was defined by Vaughan and Soares (1982) as a filter that is able to retain the finest base soil particles, even if they arrive at the filter interface alone, after complete segregation of the base soil. In other words, no self-filtration occurs and the filter must be able to retain the mean clay floc size of the cohesive soil. Vaughan and Soares (1982) also define a design criterion for retention of the base soil, based on the filter permeability:

$$k_f = 6.7 \times 10^{-6} \times \delta^{1.52} \quad \text{m/s} \qquad (6.2)$$

Where δ is the particle diameter to be retained (in μm). For the perfect filter concept, δ is the mean floc size of the base material. The 15 base soils used in NEF tests, described previously, were examined using the laser particle size analyser (PSA). The mean floc size for clayey materials was determined from the PSA results. The mean floc size generally corresponded to a pronounced peak in the frequency distribution graph. It was not possible to define a mean floc size for samples RO1 and AP1, because these materials had fine particles spread over a range from 0.3-40μm with no discernible peak.

An alternative base soil particle size – filter permeability relationship for safe filters was determined by Indraratna et al. (1996) for tropical, lateritic clays. This relationship is based on the d_{85B} size of the base soil:

$$k_f = 6.3 \times 10^{-4} (d_{85B})^{1.25}, \; d_{85} \text{ in mm}, \; k_f \text{ in cm/s} \qquad (6.3)$$

In addition, Indraratna et al. (1996) determined the equivalent particle size ratios for protection of lateritic soils:

For d_{85B}=50-60μm: D_{15F}/d_{85B}=5 - 5.5

For d_{85B}=60-80μm: D_{15F}/d_{85B}=4 - 5 (6.4)

Table 6.4 lists the mean floc size for the base soils tested. The maximum filter permeability calculated using the perfect filter concept (Equation 6.3), and the Indraratna et al. (1996) relation (Equation 6.4), are also listed. The analytical model is able to predict the filter permeability based on the fine particle sizes and porosity. This predicted permeability for the critical filter allowing no erosion is also listed in Table 6.4 for comparison. The data is presented graphically in Figure 6.9, where the allowable filter permeability is plotted against the mean floc size. The Vaughan and Soares (1982) perfect filter concept generally requires a less permeable (ie. finer) filter to protect the base soil than the Indraratna et al. (1996) method and the model predictions. As the mean floc size increases, this perfect filter permeability becomes similar to the other predictions. The Indraratna et al. (1996) permeability relation (Equation 6.3) defines a filter permeability close to that predicted by the model for most cases.

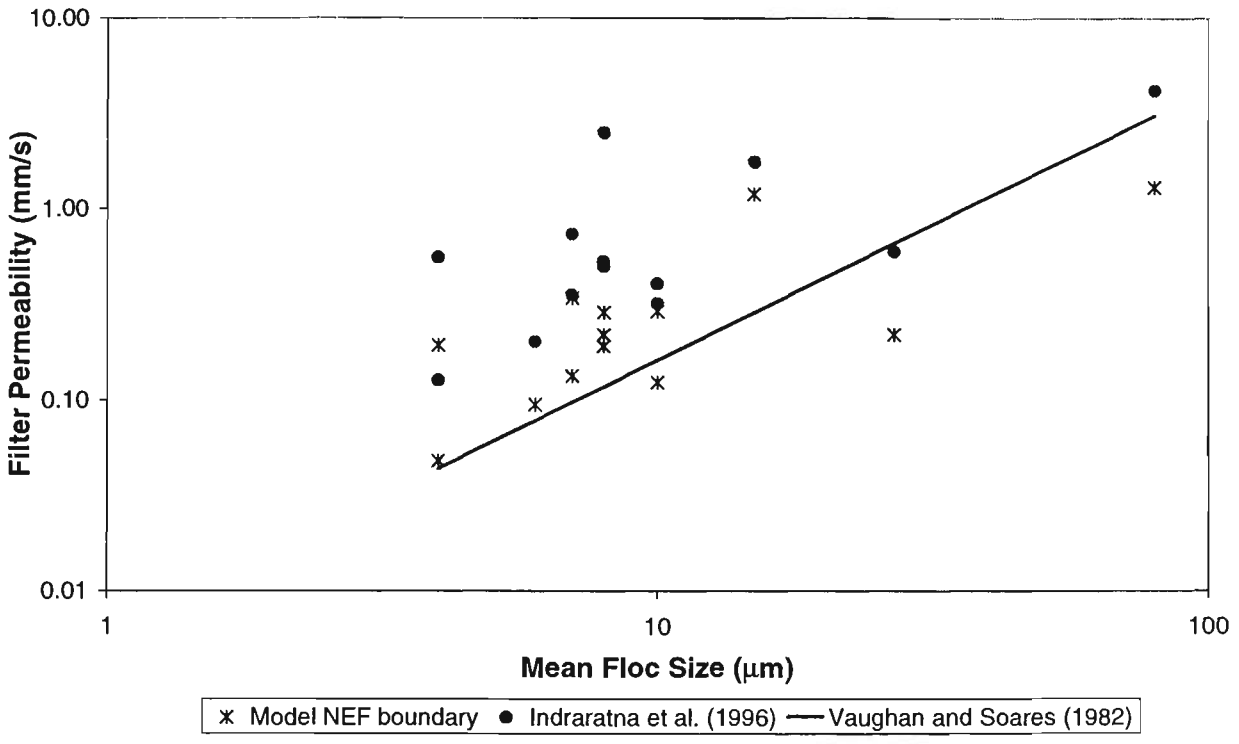

Figure 6.9 Maximum Permeability of Safe Filters against Mean Floc Size of the Base Soils Tested

Indraratna et al. (1996) present a number of simple equations to estimate the permeability of a granular material, based on various particle sizes in the fine fraction. While an equation developed using D_{5F} and D_{10F} gave the best correlation with laboratory results, it is not possible to directly compare these fine particle sizes with the filter design criteria adopting D_{15F}. The relation in Equation (6.5) was also found to be satisfactory, and relates the filter permeability k_f with the filtration parameter D_{15F}:

$$k_f\,(cm/s) = 0.7(D_{15F})^{1.8}\,(mm) \qquad (6.5)$$

For comparison with the other filter criteria, Equation (6.5) is used to convert the Vaughan and Soares (1982) allowable filter permeability predictions to an equivalent D_{15F} size. This data is listed in Table 6.4. Also shown in Table 6.4 are the maximum filter diameters defined by the Indraratna et al. (1996) particle size relations (Equations 6.4), the critical D_{15F} filter size determined in the laboratory, and the allowable D_{15F} from the design criteria of Sherard and Dunnigan (1985). Note that the Indraratna et al. (1996) filter criteria were developed for soils with particle sizes in the range d_{85B}=50-80μm, but have been extended well beyond this range for comparison with other criteria. The data in Table 6.4 suggests that, in general, the perfect filter permeability is smaller than the critical filter permeability determined by the analytical model. This is to be expected since the perfect filter concept usually requires a filter capable of retaining finer materials.

Table 6.4 Comparison of model predictions and perfect filter permeability and particle size from various design criteria.

Base Soil	Mean Floc Size (microns)	Vaughan & Soares K_f (mm/s)	Indraratna et al. (1996) K_f (mm/s)	Model Permeability K_f (mm/s)	Vaughan & Soares D_{15F} (mm)	Indraratna et al. (1996) D_{15F} (mm)	Laboratory NEF Bdy D_{15F} (mm)	Sherard & Dunnigan D_{15F} (mm)
BB3	6	0.08	0.20	0.09	0.08	0.08	0.13	0.14
BB4	4	0.04	0.13	0.05	0.06	0.06	0.10	0.10
CA1	4	0.04	0.56	0.19	0.06	0.19	0.33	0.32
CO1	7	0.10	0.73	0.34	0.09	0.24	0.80	0.41
RO1		0.00	0.54	0.26	0.00	0.18	0.75	0.32
SF1	10	0.16	0.32	0.12	0.12	0.12	0.54	0.21
AS1	27	0.66	0.59	0.22	0.27	0.20	0.27	0.34
YanYean	8	0.12	0.53	0.22	0.10	0.18	0.63	0.31
Cowarra	7	0.10	0.35	0.13	0.09	0.13	0.53	0.23
Kerferd	10	0.16	0.41	0.29	0.12	0.15	0.35	0.25
Hume	8	0.12	0.50	0.19	0.10	0.17	0.37	0.30
AP1		0.00	4.44	0.11	0.00	0.86	0.19	0.70
AS2	15	0.29	1.75	1.18	0.17	0.41	1.10	0.70
BB1	8	0.12	2.50	0.29	0.10	0.54	0.78	0.70
Thompson	80	3.07	4.15	1.29	0.63	0.81	2.00	0.70

The predicted D_{15F} particle sizes from the Vaughan and Soares (1982), Sherard and Dunnigan (1985) and Indraratna et al. (1996) design criteria, and the laboratory measured critical filter size, are plotted against the base soil d_{85B} size in Figure 6.10. In almost all cases, the perfect filter is finer than the Sherard and Dunnigan (1985) critical filter and the laboratory NEF boundary. The Indraratna et al. (1996) design criterion predicts a filter boundary only slightly coarser than the perfect filter particle size. This criterion could be used to estimate the perfect filter boundary with reasonable accuracy if the mean floc size is not known.

This analysis has shown that the critical filter diameter is consistently coarser than the perfect filter diameter, as expected. In order to adopt a filter designed by the critical filter concept, it is necessary to discount the design philosophy of the perfect filter concept, ie. considering segregation of the base soil and designing a filter to retain only the finest particles. This issue was considered in Chapter 5, where it was shown that erosion resistant materials with a critical shear stress of $\tau_c > 0.5$ N/m^2 are not likely to be prone to

segregation since an eroding shear stress exceeding this critical shear stress is able to transport particles of up to 75μm diameter, which is significantly more than the mean floc size. Materials with a critical shear stress below 0.5N/m^2 were shown to be prone to segregation. Hence, the perfect filter concept should be adopted for erodable materials with τ_c<0.5 N/m^2, while the critical filter concept may be adopted for more erosion resistant materials.

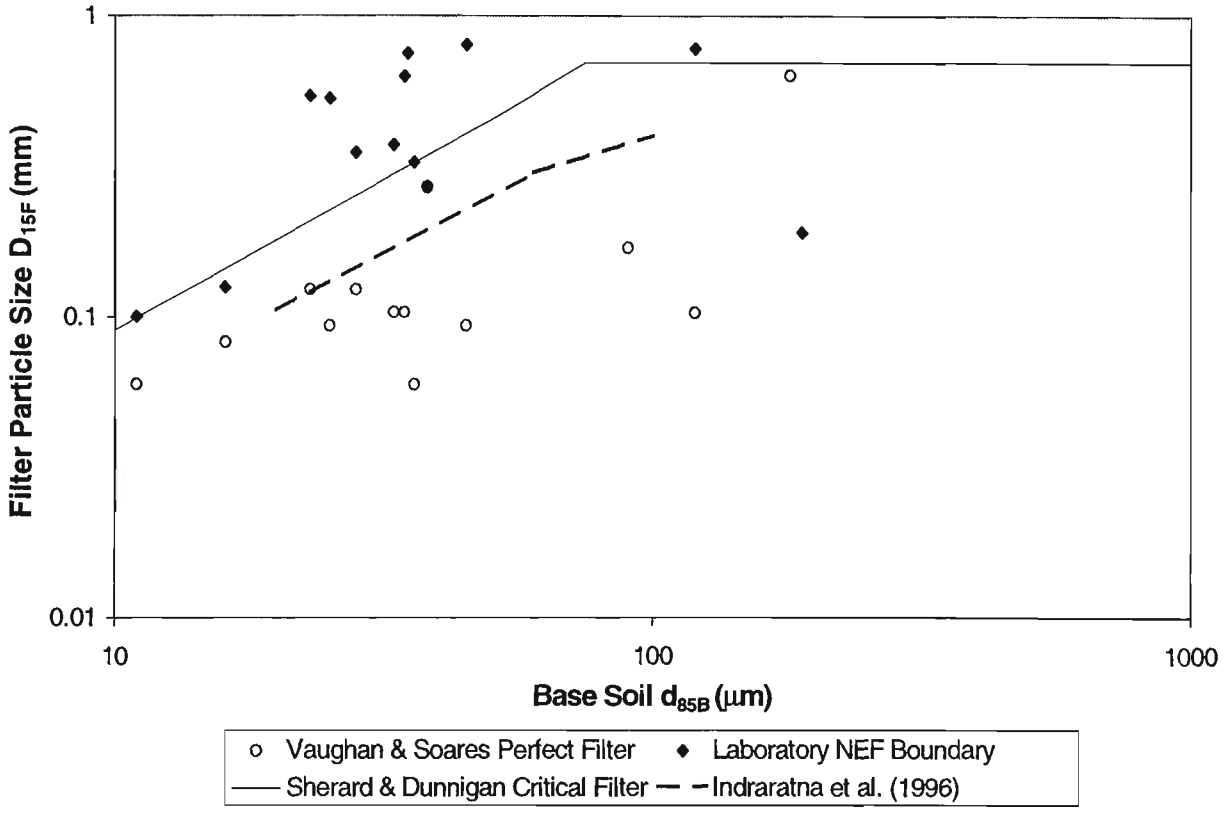

Figure 6.10 Comparison of Vaughan and Soares (1982) perfect filter with Sherard and Dunnigan (1985) critical filter

6.4 Recommended Empirical Design Criteria for Granular Filters

Various filter design guidelines have been used in the past to design filters for embankment dams, and few failures have been recorded. However, it is now recognised that many of these criteria have limited application in general practice. The design criteria recommended here are appropriate for most design situations. These criteria are based on a critical review of previous literature (Chapter 2), new laboratory data (Chapter 4) and the comparison of newly developed model predictions with the design criteria requirements (this Chapter). While these criteria are appropriate in most situations, it is still recommended to perform laboratory tests on core and filter samples proposed for dam construction. The No Erosion Filter (NEF) test (Sherard and Dunnigan, 1985) is the most suitable test available for determining suitable filters for embankment dams. The writer also recommends the use of analytical modelling, such as that outlined in Chapters 3 and 5, to better describe the expected behaviour of particular base soil - filter combinations.

For all materials excluding group 1 and 2 materials with an erosion resistance τ_c<0.5 N/m^2, the recommended retention criteria are set out in Table 6.5. These design criteria are based on the recommendations of Sherard and Dunnigan (1985). The criteria are modified for coarse soils (with less than 15% by mass passing the 75μm sieve), to the criterion proposed by Honjo and Veneziano (1989). Group 1 and 2 soils are modified to consider the self-filtering requirement, defined by the *Reduced PSD*. The boundary between soil groups 2 and 4 has been changed to 35%, as proposed by Foster and Fell (1999). Filters for soil groups 1 and 2 (>35% passing 75 μm), should have no more than 60% coarser than 4.76mm and a maximum particle size 50mm. The filter coefficient of uniformity, C_u, should not exceed 20. The requirements for filter permeability and no

cohesion are not addressed here. Locke et al. (2000) have addressed these design requirements in detail. For group 1 and 2 materials with an erosion resistance τ_c<0.5 N/m^2, the Vaughan and Soares (1982) perfect filter design concept should be adopted, ie. the filter must be able to retain the mean floc size rather than the d_{85B} size.

Table 6.5 Recommended Filter Design Criteria for base soils with τ_c>0.5N/m^2.

Soil Group	Base Soil Type	Base Soil % Passing 75μm Sieve (of portion <4.75mm for groups 1-3)	Filter Criterion
1	Fine Silt or Clay	>85%	$D_{15F}/d_{85B} \leq 9$ and If PI>10 $D_{15F}/d_{85Reduced} \leq 12$ [(a)] If PI<10 $D_{15F}/d_{85Reduced} \leq 4$ [(a)]
2	Sandy Silts / Clays & Silty / Clayey Sands	35% - 85%	$D_{15F} \leq 0.7$mm and If PI>10 $D_{15F}/d_{85Reduced} \leq 9$ [(a)] If PI<10 $D_{15F}/d_{85Reduced} \leq 4$ [(a)]
3	Soils intermediate between groups 2 and 4	15% - 35%	interpolate between groups 2 and 4 based on %passing 75μm sieve.
4	Sands, Sandy Gravels with few fines	<15% and $d_{95B}/d_{75B} \leq 7$ [(b)]	$D_{15F}/d_{85B} \leq$ 5.5 - 0.5 d_{95B}/d_{75B}

[(a)] $d_{85Reduced}$ is the d_{85} size of the base soil reduced PSD, determined as outlined in Chapter 4.4.

[(b)] When $d_{95B}/d_{75B} > 7$, recalculate the grading by truncating the coarse fraction at the most coarse particle such that, in the new grading, $d_{95B}/d_{75B} = 7$.

7. APPLICATIONS IN PRACTICE

7.1 Introduction

The preceding chapters have demonstrated the development and verification of new analytical models, designed to predict the time-dependent changes occurring during the filtration process. Laboratory procedures have also been developed to describe aspects of filtration. This chapter will show some potential applications of these models and laboratory procedures, through selected case studies from Australia and the UK. Some modelling predictions are described although the details of the computer simulation are not reproduced.

The first case study will examine Cowarra Dam, currently under construction in New South Wales, Australia. The filter and blanket drain materials are assessed using the non-cohesive model, NEF tests and large scale laboratory tests. The modified erosion test and the crack erosion model are used to assess the potential damage due to a crack through the narrow dam core. The second case study considers Wartook Dam, 110 year old, homogeneous embankment in Victoria, Australia, constructed of silty fine sand. The efficiency of a new granular filter and stabilising berm to retain this material is assessed, using the non-cohesive model. The third case study uses the non-cohesive model to assess the internal stability of an existing broadly graded filter from a dam in Victoria. The final case study is Balderhead Dam in England, which failed 14 months after first filling. The failure has been described in detail by Vaughan and Soares (1982). The crack erosion model and Reduced PSD method are used to predict why the dam failed.

7.2 Case Study 1 – Cowarra Dam

Cowarra Dam is an off-river water supply dam, near Port Macquarie in New South Wales, which is expected to be completed by October 2001. It is an earthfill dam, with a narrow, central clay core and sand/gravel filters, and has a maximum height of 43m and crest length of 545m. A typical cross section of the dam is shown in Figure 7.1. The dam is protected by granular filters which consist of a single sand zone, F2A(1), against the clay core, and a 3-layer filter and drainage blanket above the downstream foundation. The 3-layer filter consists of a coarse F2B zone, sandwiched between two F2A sand zones (Figure 7.1b). Further details about the dam can be found in Thompson and Chenhall (2000). The dam owners, Hastings Council, were concerned about the filter 2A material supplied to site and wanted to confirm that this material was adequate to protect the core material. This Section will describe the laboratory experiments and analytical modelling carried out to examine many aspects of the expected behaviour of Cowarra Dam.

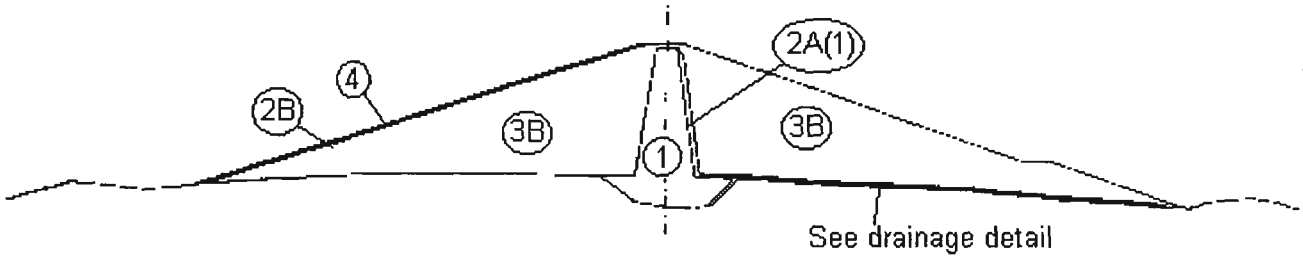

a) Typical Cross Section

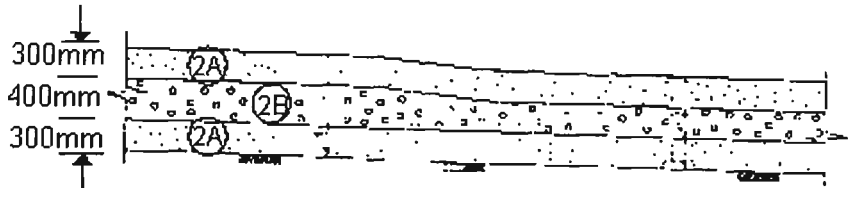

b) Drainage Blanket Detail

Figure 7.1 Typical Cross Section of Cowarra Dam

7.2.1 Assessment of Filter 2A and 2A(1) Suitability

A fine sand filter is placed against both the core and the downstream foundation, to protect the dam. The clay core material has a slightly finer particle size distribution than the weathered rock foundation. Hence, a slightly finer filter, called F2A(1), was required to protect the core, while the coarser filter for the foundation was called F2A (Figure 7.1). The design gradings of these two filter materials are shown in Figure 7.2. After commencement of the dam construction, the river sand that was originally proposed as filter material became unavailable. Local quarries could not provide filter materials to accurately match the design gradings. Consequently, three materials were provided as possible filter 2A and 2A(1) materials. The particle size distributions of the three samples are shown in Figure 7.2

- Sample 1 is a crushed rock; this material fits the design grading for material 2A, but not 2A(1),
- Sample 2 is a crushed material from another quarry; this material is too coarse in the fine-mid size range (10-60% passing) for both the 2A and 2A(1) envelopes,
- Sample 3 is a 50:50 blend of sample 1 and river sand. This material is linearly graded and fits the 2A(1) envelope, but is more expensive to manufacture.

The filter materials were first tested in the laboratory to determine their suitability. The NEF test was used to examine the filtration of samples from the dam core using the three filter materials, the results are presented in Table 7.1. All the proposed filter materials were coarser than the Sherard and Dunnigan (1985) design guidelines ($D_{15F}/d_{85B}<9$), based on the finest core particle size distribution measured ($d_{85B}=30\mu m$). Despite this, the three filter materials were able to protect the clay core successfully in the NEF test. Further testing, with progressively coarser filters, revealed that the boundary between a

successful and unsuccessful filter could be represented by D_{15bdy}≈0.56mm. Sample 2 had a D_{15F} size of 0.53mm, indicating that it was close to this boundary. While these materials are coarser than permitted by design guidelines, they are suitable as filters for the clay sample obtained from the dam core, based on the NEF test results.

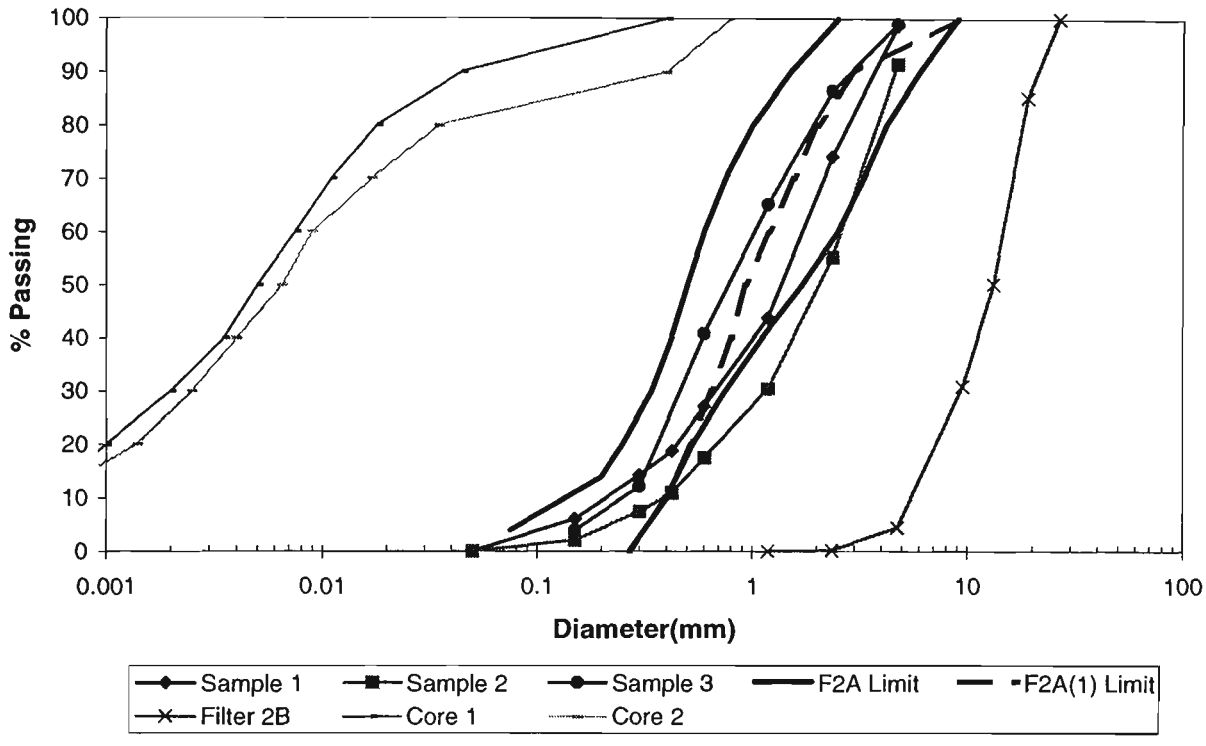

Figure 7.2 Particle Size Distributions of core and proposed F2A and F2B filter zone materials for Cowarra dam

Table 7.1 NEF Test Results – Cowarra Dam (See Appendix 1 for NEF test procedure)

Material	D_{15F}	D_{15F}/d_{85B}	Max Flow Rate	Final Hole Diam.	Outcome
Sample 1	0.3mm	10	0.2 l/min	1.0mm	Success
Sample 3	0.33mm	11	0.4 l/min	1.0mm	Success
Sample 2	0.53mm	17	0.9 l/min	1.0mm	Success
Blended sand	0.6mm	20	1.9 l/min	1.5mm	Failure
Blended sand	0.7mm	23	1.9 l/min	2.0mm	Failure

Internal stability of the two crushed filter materials (Samples 1 and 2) was considered a risk since both samples had a concave upward PSD. If the materials were to lose fines due to internal instability, they may become too coarse to retain the core material. The non-cohesive analytical model was used to simulate the effect of water flowing through each of the three samples, to predict the possible loss of fines from the filter. The model used five cylindrical elements, 100mm long and 500mm diameter, each with the same initial PSD. Vertical flow of water was simulated at 30s time steps until no further migration of particles occurred, requiring approximately 10 hours of water flow under the assumed hydraulic gradient of 2. The simulations predicted that all three F2A materials were internally stable, with only minor wash out of the fines (<75μm), while the larger particles did not move. The model predictions for the internal stability of Sample 2 are presented in Figure 7.3, and will be discussed shortly. Sample 2 is the most broadly graded of the materials, and it is considered to be the worst case.

To verify this modelling, the internal stability of Sample 2 was examined in the laboratory. The material was compacted into the small permeameter (150mm diameter, 200mm high sample), and vertical flow applied with a hydraulic gradient of 10. The hydraulic gradient in the laboratory was greater than in the simulation to allow a shorter test duration. During the test, the apparatus was regularly tapped with a rubber mallet to avoid particle bridging over pores. After 30 minutes of vertical (downwards) flow, the material was removed in five layers of 40mm thickness, and the PSD of each layer was examined. Figure 7.3 shows the changes in grading of Sample 2 after this experiment. In both the analytical model and laboratory test, a small amount of fines washed out of the top layer of the material (Element 1), but there was no noticeable change measured or predicted in the lower layers, which is why elements 3 to 5 are shown as the same line.

Hence, the material is internally stable. The model predictions and laboratory observations are very similar. All three materials were confirmed as adequate for preventing erosion of the core and foundation. The dam owner chose to adopt the blended Sample 3 material for the chimney filter (Filter 2A(1)), and the sample 2 material for the foundation blanket filter (F2A).

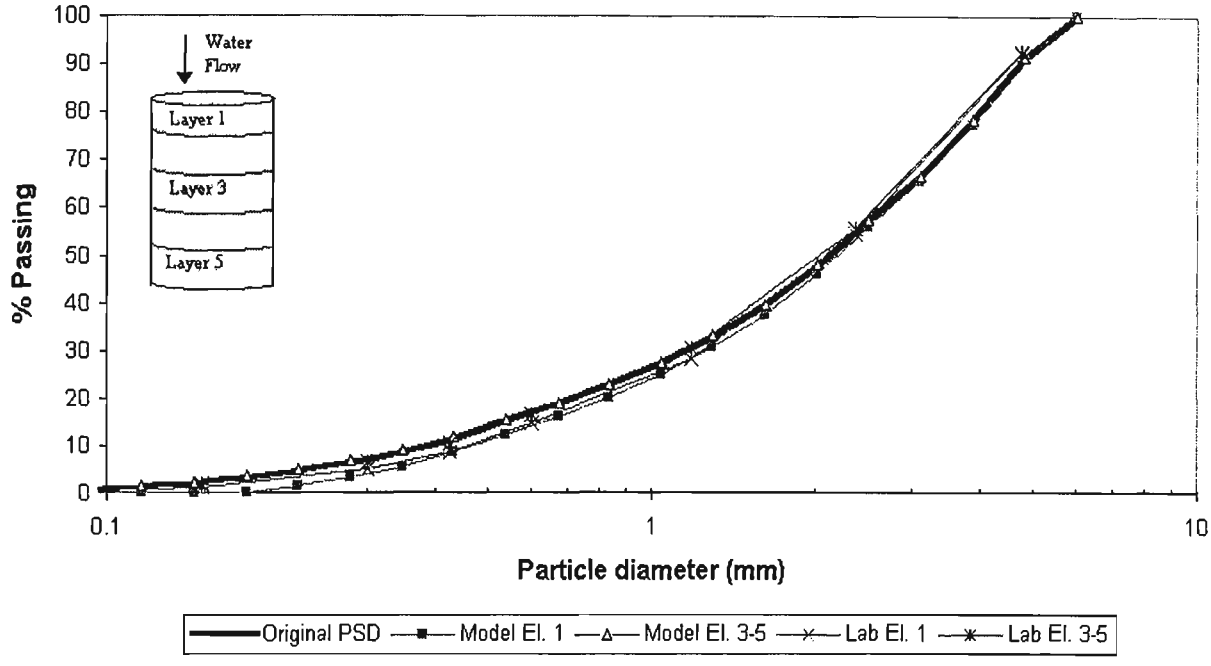

Figure 7.3 Predicted change in PSD of sample 2 after prolonged flow

7.2.2 Filter 2B Material

A uniform crushed gravel was supplied as the F2B material used in the foundation drainage blanket (Figure 7.1b). The PSD of the F2B material is shown in Figure 7.2. The analytical model was used to examine the potential infiltration of the three F2A samples into the F2B drainage material, in order to determine the suitability of the F2B material as a filter for the F2A material. In Chapter 3 it was shown that important changes during filtration occur initially near the base soil – filter interface. This interface was represented in the model by 100mm of base soil (F2A) divided into three elements, and a 200mm depth of filter (F2B) divided into three elements. A hydraulic gradient of unity across this

interface was adopted as a worst case for design. The model was run for 6 hours, with a time step of 30 seconds. The model was applied to each of the 3 different F2A materials, but only the simulation adopting Sample 1 is shown here. The time-dependent changes in flow rate and mass passing through Sample 1 base soil protected by the F2B filter are shown in Figure 7.4. Particles finer than about 1.4mm were initially able to migrate into the filter. These base soil fines eroded steadily within the first few hours, some coarser particles (1.2-1.4mm) were retained within the filter, while the fines passed through the filter unhindered. The retained particles eventually reduced the diameter of particles able to migrate through the filter and beyond the third hour, no particles passed a distance greater than 100mm into the filter, because the filter interface had stabilised and any eroded material was captured within this interface. The flow rate increased steadily for the first four hours, as the base soil continually eroded into the self-filtration zone, resulting in a subsequent increase in the base soil permeability. After four hours no further erosion occurred and the flow rate stabilised. The best summary of the final, stable interface is the plot of mass lost from the base soil and retained at increasing depth in the filter material (Figure 7.5). The base soil erosion near the filter interface, and capture of particles within a short distance in the self-filtration zone are clearly demonstrated. The extent of base soil erosion is only small, 0.9g/cm^2 of base soil was mobilised and only 0.3g/cm^2 passed through the self-filtration zone. For comparison, in Chapter 3.3.4 filtration of broadly graded materials was considered successful if the mass passing through the self-filtration zone was <1g/cm^2.

A large-scale laboratory test was carried out to examine the potential erosion of Sample 1 into the F2B filter, to confirm the model predictions. The large scale test procedure was outlined in Chapter 3. Visual observation during the experiment revealed that after an

initial outflow of dirty water, the effluent quickly cleared and no particles eroded entirely through the filter. After the experiment, the filter was carefully removed in layers and the change in PSD of each layer measured. The extent of base soil movement was estimated based on the change in PSD, and this is shown in Figure 7.5. Comparing the model predictions and laboratory results, the analytical model predicts a greater mass movement than measured in the laboratory, which is due to the assumption that all particles finer than the filter constriction sizes will move. In addition, the short test duration (1 hour) may have resulted in incomplete particle migration. The predicted trends are similar for both the laboratory test and the analytical model predictions. Based on the modelling and laboratory results, the F2B material is considered a successful filter for the three F2A materials, hence, little erosion is expected to occur during extended seepage. This is explained by the low filter retention ratios of: D_{15F}/d_{85B}=1.9 (Sample 1), 1.6 (Sample 2), and 2.9 (Sample 3). Normal design guidelines for filtration of coarse particles would suggest a maximum retention ratio of D_{15F}/d_{85B}=4.

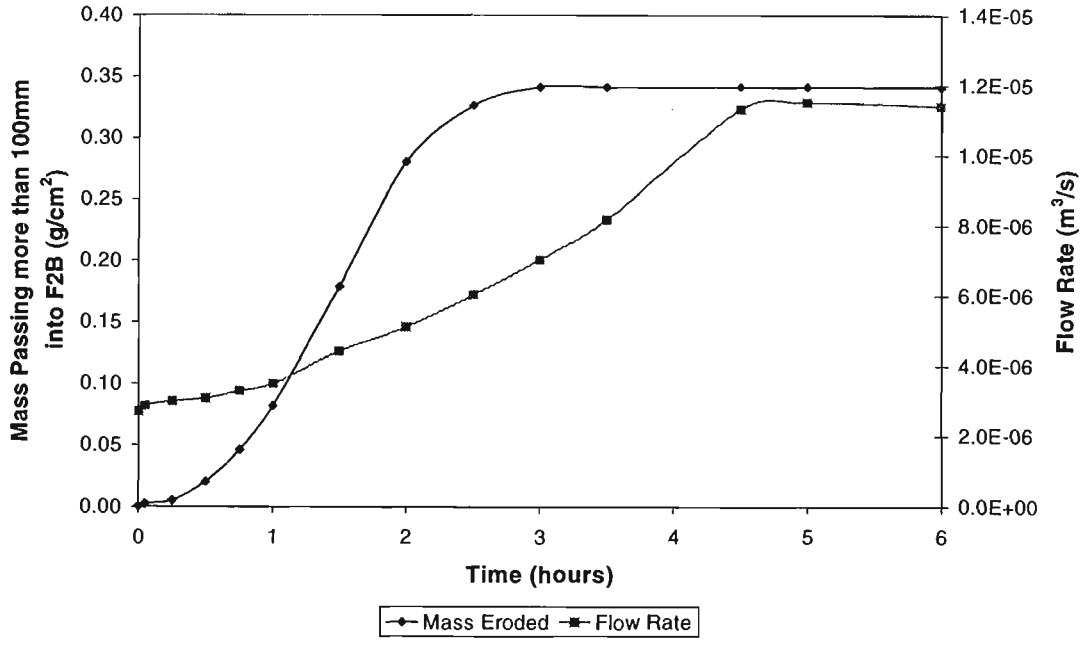

Figure 7.4 Time-dependent changes in mass transport and flow rate through F2A – F2B combination.

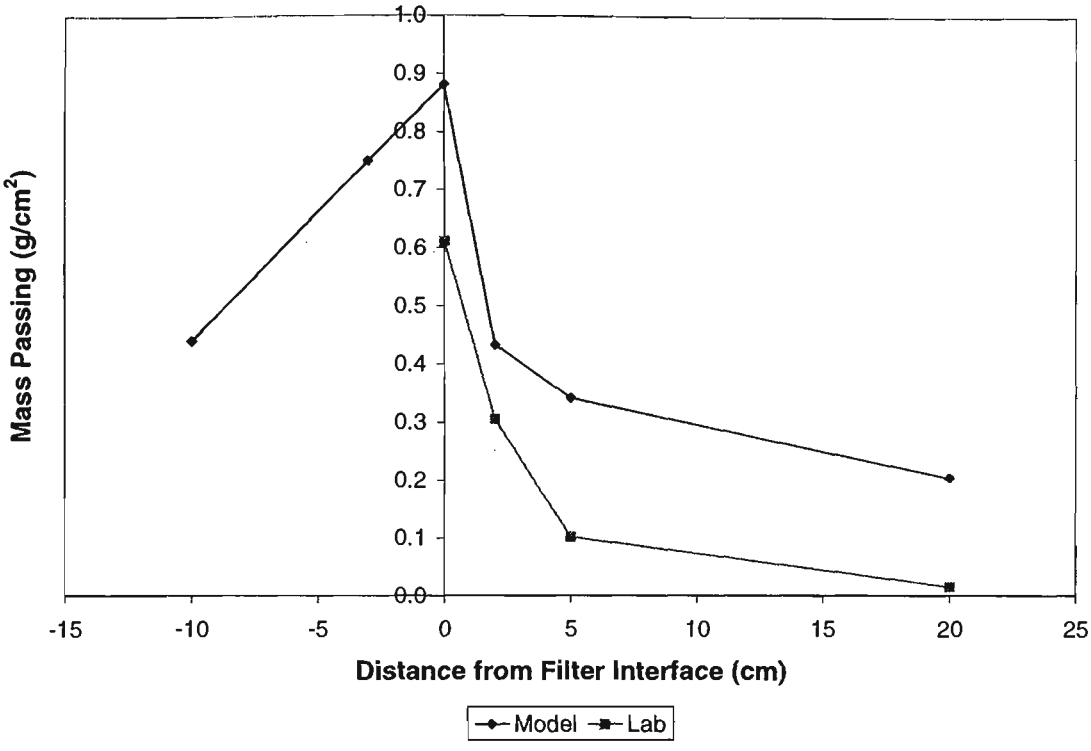

Figure 7.5 Predicted Infiltration of Sample 2 fine filter material into supplied F2B material

7.2.3 Cracking of the Core Material

The dam core material is a low plasticity clay containing some sand and gravel sized particles. Because the core is relatively narrow, hydraulic fracture and the formation of a continuous crack through the core material is a real risk. The analytical model describing cracking in cohesive cores, developed in Chapter 5, was used to assess the potential damage due to a 1mm wide crack through the core at one third of the dam height, protected by the filter 2A(1) material (Sample 3). The measured particle size distribution of two samples from the core, and the boundary grading limits from previous investigations are shown in Figure 7.6. Modified pinhole erosion tests on the material, following the procedure described in Chapter 4, revealed that the clay has a low erosion resistance, with a critical shear stress of τ_c=0.5N/m^2, and an erosion rate parameter of

α=0.09. The maximum reservoir head acting on the 10m long crack at the highest cross section was 28m.

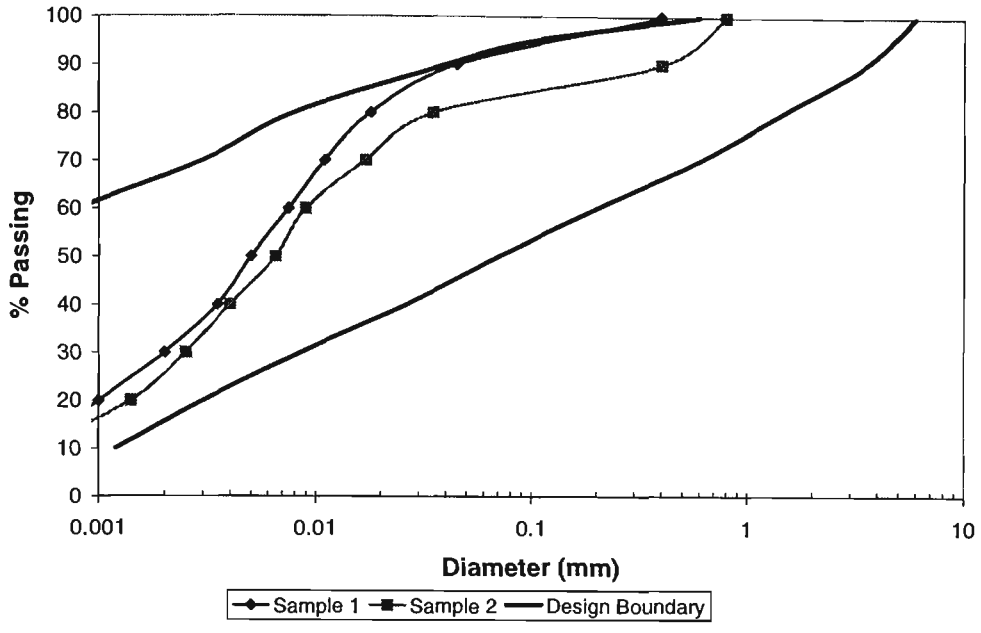

Figure 7.6 PSD of Cowarra dam core material

The analytical model was used to describe the erosion of a 1mm wide crack protected by the Sample 3 filter material, having D_{15F}=0.3mm, for the first 24 hours after the crack formed (Figure 7.7). The model predicted a very small amount of erosion of the crack (0.1-0.2g) before sealing after about 1 hour. After this first hour, erosion perpendicular to the crack, as the flow found new paths around the filter cake, continued to occur slowly. After one day, the predicted mass eroded from the crack walls was negligible (0.4g). For comparison, the model was used to analyse the effectiveness of a coarser filter, with D_{15F}=0.7mm (Figure 7.7). The extent of erosion was significantly greater than for the finer filter (note the log scale on the y-axis). During the first hour, the 1mm wide crack lost about 5kg of material, corresponding to a crack enlargement of 50%. After this first hour, the crack partially sealed, and the erosion rate reduced. A near constant erosion rate over the next 23 hours led to a total mass loss of about 10kg after 24 hours. This coarser

filter was not effective in completely sealing a crack, and slow erosion and enlargement of the crack was predicted. The 'as constructed' filter was shown to be effective in quickly sealing a continuous crack through the dam core, with minimal erosion.

The analytical modelling and laboratory experiments outlined in this Section, confirm that the dam filter materials are suitable to protect the dam core and foundation from erosion. The F2A material is finer than the experimentally determined NEF filter boundary, and modelling predicts that the filter will rapidly seal a crack through the core with minimal erosion. The F2B material has been shown through experiment and modelling to be a suitable filter for the F2A material, and hence, the drainage blanket is expected to function correctly without clogging.

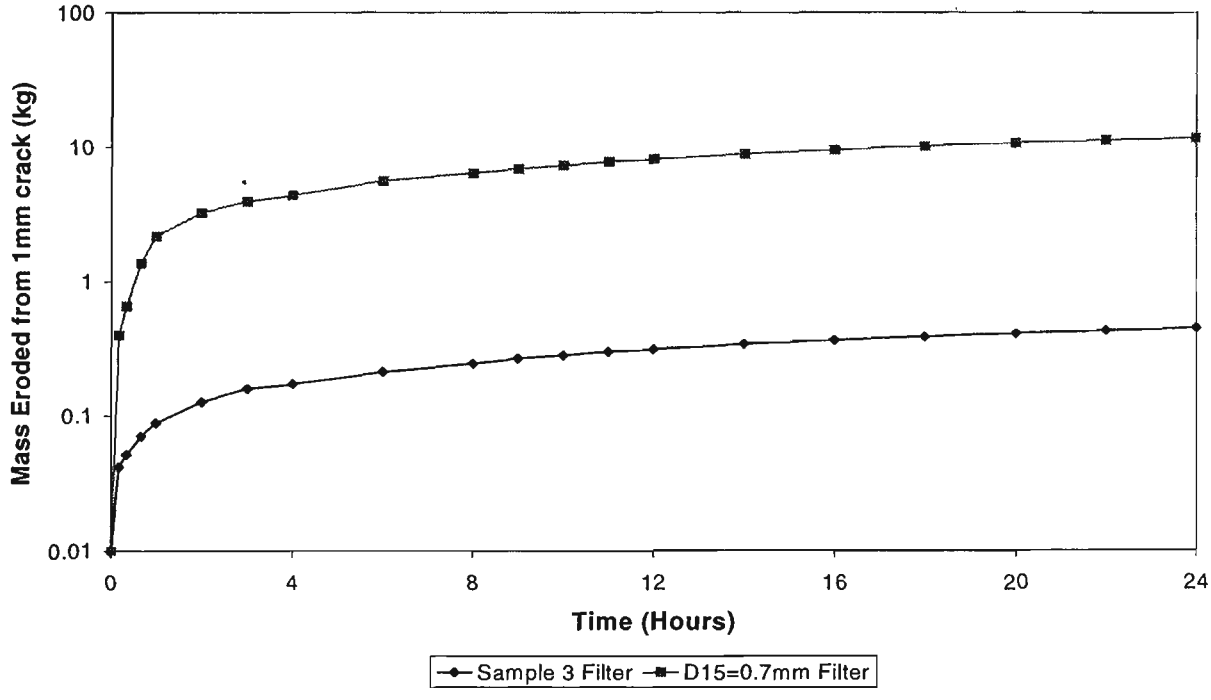

Figure 7.7 Predicted mass eroded from a 1mm crack through Cowarra Dam core - filter as constructed and coarser filter (D_{15F}=0.7mm)

7.3 Case Study 2 – Wartook Reservoir Embankment

Wartook Dam, constructed in the late 1880's, is 11m high at the maximum section and 1100m long. The embankment is homogeneous, being constructed of a silty fine sand. The materials and construction techniques used resulted in the establishment of a high phreatic surface through the dam, with high seepage flows and susceptibility to liquefaction under moderate seismic loading. Visual inspection records noted that seepage from the downstream embankment had been evident, possibly as high as one-third of the height above the toe, for almost the entire length of the bank. Geotechnical investigations of the embankment materials revealed loose to medium density, silty fine sands with little cohesion. The material is characterised by d_{85B}=0.27mm, PI<5 and C_u=8-10, the PSD of this material is shown in Figure 7.9.

In order to ensure the internal and static stability of the dam, a two-stage protective filter and stabilising rockfill berm were recently constructed against the downstream face of the homogeneous embankment. The risk based approach adopted for rehabilitation of this dam is such that the embankment will fail due to liquefaction under the maximum design earthquake but there will be no overtopping of the dam, hence, preventing uncontrolled release of stored water from the reservoir. The typical cross section of the dam after these remedial works is shown in Figure 7.8. The gradings of the fine and coarse filters are shown in Figure 7.9. The core material is a silty sand with little cohesion. Piping failure through this material could occur as progressive erosion from the downstream interface, as modelled by the non-cohesive model, developed in Chapter 3. This model is used here to determine the rate of erosion of the embankment material into the filter after liquefaction of the embankment, and examine whether the filters will act to successfully retain the mobilised particles.

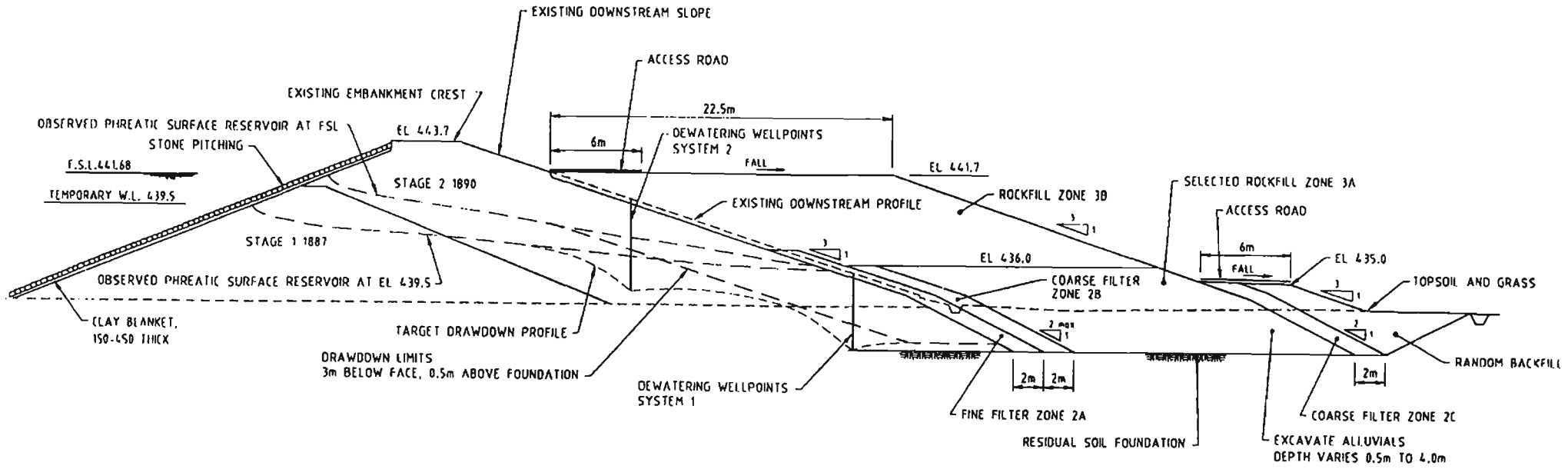

Figure 7.8 Wartook Embankment - typical cross section after remedial works

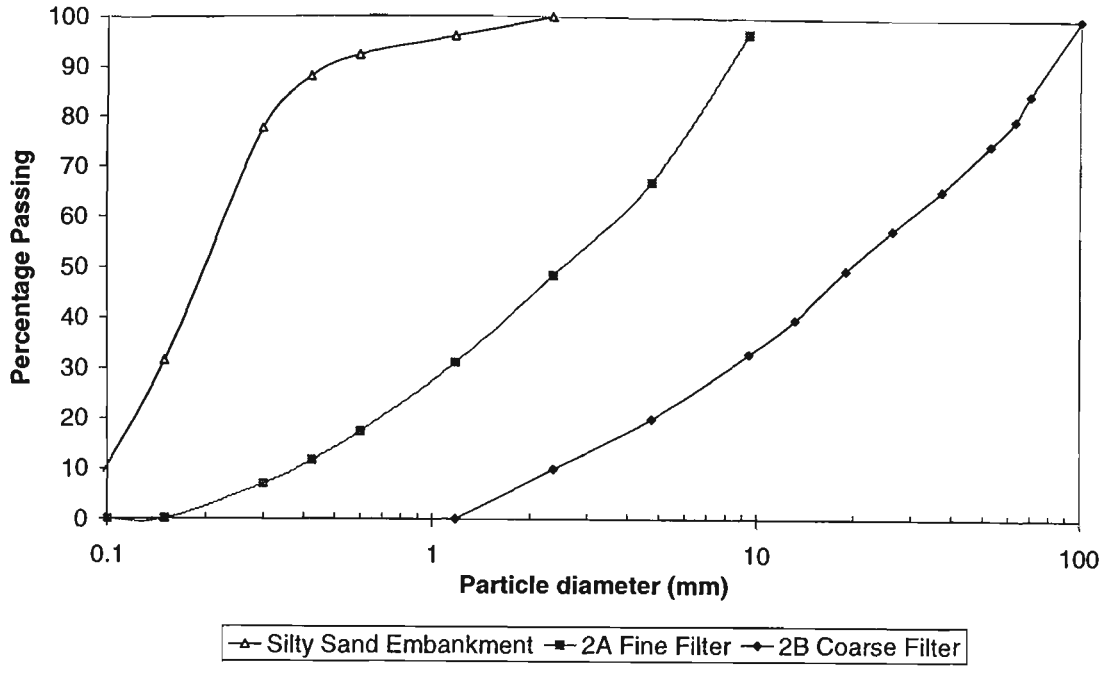

Figure 7.9 PSD of Wartook Embankment materials.

It is assumed that, if earthquake induced liquefaction were to occur, the steady-state seepage forces driving particle movement would be the same as those existing in the dam previously, and the short term increases in pore pressures are ignored. Flow through the embankment was estimated based on the observed flow exiting the downstream face of the dam, and the embankment permeability was estimated from the fine particle sizes of the silty-sand. The computer program Seep/W was used to determine the steady state flow regime through the embankment, this seepage analysis is shown in Figure 7.10a. In modelling the flow, it was assumed that the embankment was 10 times more permeable in the horizontal than the vertical direction due to horizontal layering during construction. This produced a flow rate of 0.02 litres/s per metre width out of the downstream face of the embankment, or a mean flow exit velocity of 1.2×10^{-5} m/s. Flow paths across the filter interface were divided into a number of elements, as shown in Figure 7.10b. The particle movement and filtration can then be simulated as a pseudo one-dimensional problem in the non-cohesive model, to predict particle movement along the flow path.

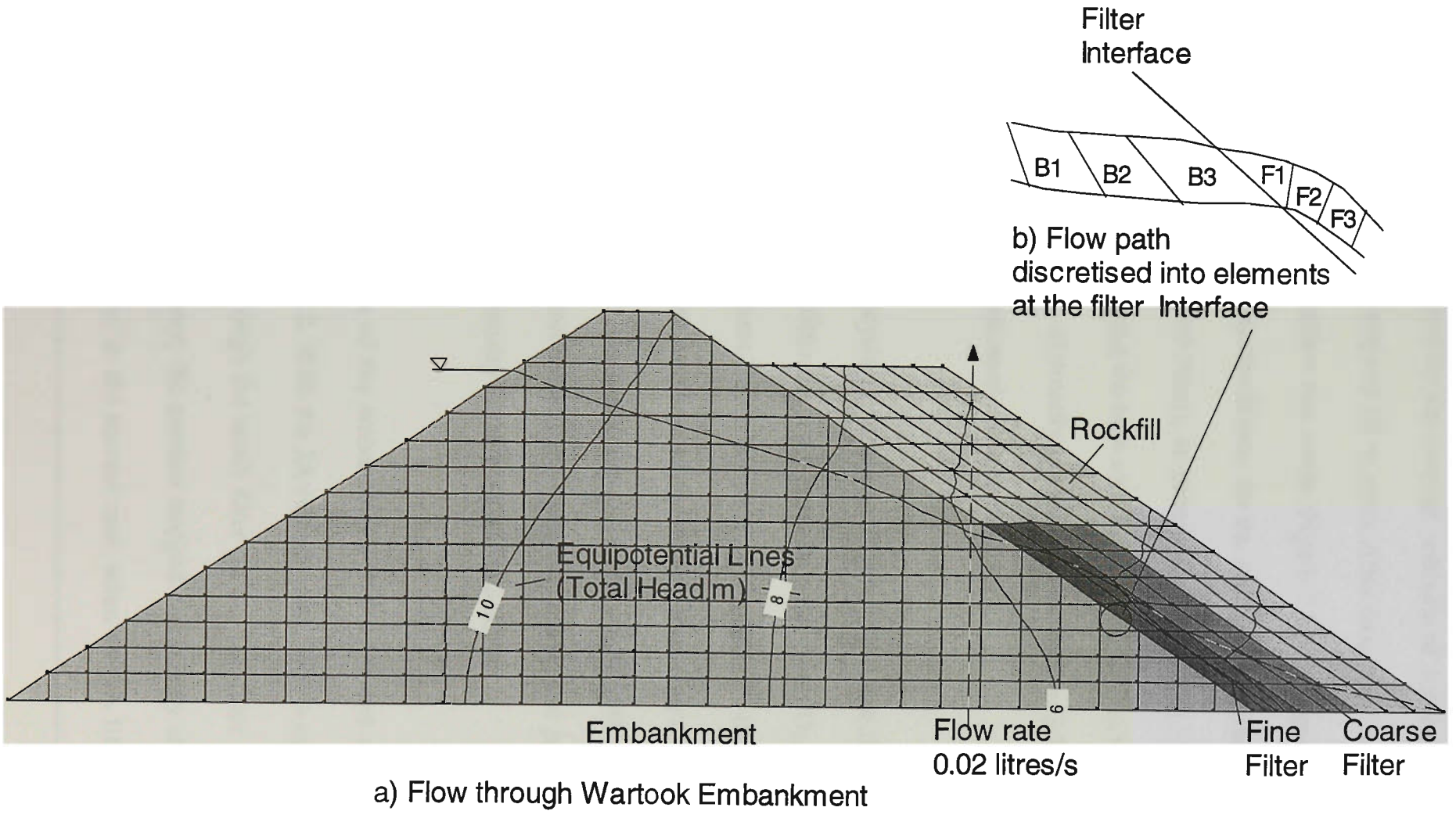

Figure 7.10 a) Steady state seepage flow through Wartook Embankment

b) Flow path discretised into elements

The model considered a 100mm thickness of embankment material divided into three elements, protected by a 200mm length of fine 2A filter, also divided into three elements. The hydraulic gradient across this interface was varied to produce a flow rate corresponding to that estimated by the seepage analysis of 1.2×10^{-5} m/s. Five hours of flow were modelled, in time-steps of 10 seconds. After five hours the erosion of material had ceased and the filter interface was stable (Figure 7.12). The predicted movement of mass after attaining steady state conditions, for the case of the embankment protected by the fine 2A filter (with D_{15F}=0.7mm), is plotted in Figure 7.11. This sand filter was shown to be effective in retaining the base soil, limiting the erosion to less than 0.1g/cm^2. Based on modelling filtration of broadly graded soils in Section 3.3.3, a predicted mass loss of less than 1g/cm^2 is considered a successful filter.

For comparison, another analysis is shown in Figure 7.11, considering the extent of erosion without the fine 2A filter, ie. the coarse 2B filter (with D_{15F}=3.5mm) is placed directly against the embankment. In the absence of the fine 2A filter, the mass eroded after 5 hours was predicted to be close to 6g/cm^2. At this stage, the model predicted failure of the base soil due to excessive mass loss and consequent increase in porosity. Figure 7.11 shows the predicted erosion and transport of base soil just before the model terminates due to excessive porosity of the base soil (n_e>60%).

The predicted rate of erosion of the embankment, both with and without the fine 2A filter, are shown in Figure 7.12. With the 2A filter present, only a small amount of fines was able to initially wash through the small filter pores. The filter rapidly retained the eroding embankment, and hence, the erosion stopped completely after about 1.5 hours due to successful self-filtration. In the second case, when the 2A filter was not present,

erosion continued to occur rapidly through the coarse filter and the rockfill. After about three hours, the rate of erosion began to drop, as some fines were retained in the 2B filter. Note that the log scale exaggerates this drop in the erosion rate, and erosion still occurred at a rate of 0.75kg/hr. After 5 hours the model execution terminates as the base soil reached a porosity of 60% at the filter interface.

Based on these model predictions, the protective 2A filter will be successful, and is an essential part of the upgrade works to prevent excessive erosion and potential piping of the embankment after liquefaction. The coarse 2B filter was shown to be unsuccessful in retaining the silty-sand embankment material. Hence, the two-layer filter is essential to protect the embankment from potential piping erosion.

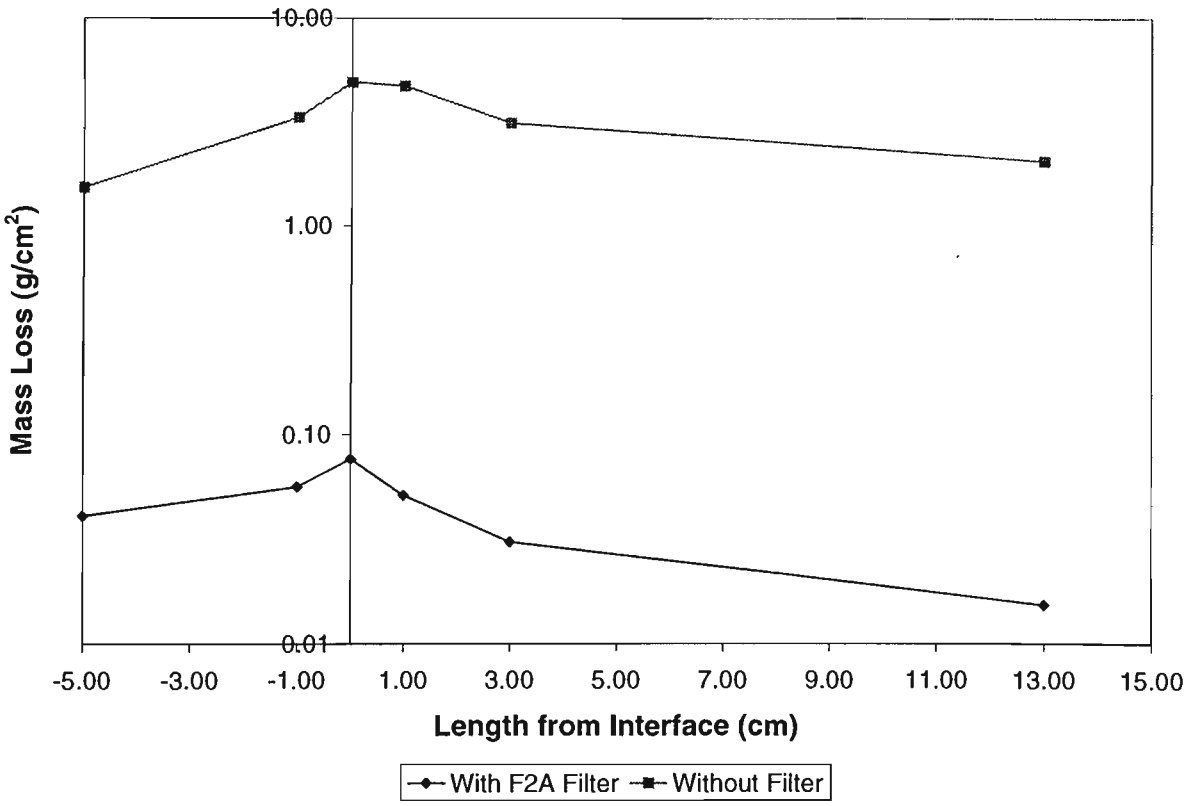

Figure 7.11 Predicted mass loss from Wartook Embankment with and without the F2A fine filter

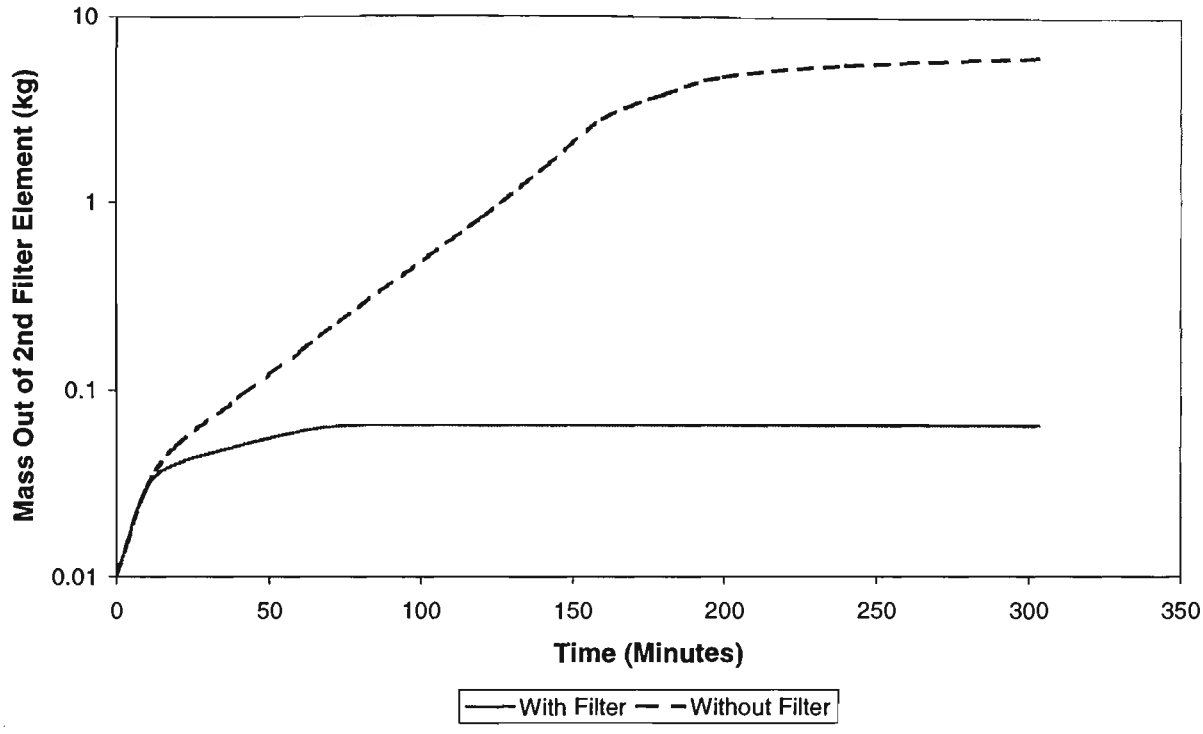

Figure 7.12 Time Rate of Erosion of Wartook Embankment into Rockfill Berm, With and Without the F2A Fine Filter

7.4 Case Study 3 – Transition Zones in Existing Dams

Australia has a large number of older embankment dams some of which comprise a central earthfill core surrounded by a transition zone and outer rockfill shell. Although not intended, the transition zone in some cases acts as a filter for the clay core. Often these transition zones do not meet current filter design criteria, for instance, being too broadly graded or containing too large a quantity of fines. Dam engineers assess these transition zones to determine their suitability to act as a filter in a design review process. The analytical modelling has been used to assist in this filter assessment. Broadly graded transition zones are at risk of internal erosion, ie. loss of the fine fraction through the internally unstable soil matrix. The non-cohesive model is able to assess the internal stability of these transition zones, and its application to assess the internal stability of a transition zone material from an Australian embankment dam, is described here.

The example considered is an 80m high earth and rockfill dam with a broadly graded, sandy clay core, having about 10% sand and gravel, and the remainder of particles finer than 0.3mm. This material would classify as a group 2 soil based on Sherard and Dunnigan (1985), having 80% finer than the 75μm sieve. For such a core material, the design criteria would suggest a suitable filter should have D_{15F}=0.7mm. The *Reduced PSD* method suggested that the coarsest particle in the stable PSD is about 0.5mm, and the reduced d_{85B} size is 0.07mm. The safe filter boundary predicted by the Reduced PSD method is D_{15F}=0.84mm, similar to the Sherard and Dunnigan (1985) requirement.

Figure 7.13 Sandy gravel 'transition zone' material from an embankment dam

A photograph of the transition zone material sampled from a test pit is shown in Figure 7.13. The PSD of the transition (filter) material is plotted in Figure 7.14 as the 'before test' data. This material has a D_{15F} size of about 0.1mm, significantly finer than the required D_{15F} size predicted by either the Reduced PSD method or the Sherard and Dunnigan (1985) criterion. As can be clearly seen, the transition material is broadly graded, with a significant fraction of fine particles that may be internally unstable, as well as having a significant fraction of gravel and cobbles. The non-cohesive model was used to assess the internal stability of this material. The simulation considered five elements of 100mm thickness and 250mm diameter, subjected to vertical flow with a hydraulic gradient of 2. The analysis was performed for 6 hours, after which time no further particle movement occurred. Figure 7.14 plots the initial PSD of the transition

zone and the predicted final PSD of three elements of the material after 6 hours of seepage. The figure clearly predicts that the transition material is internally unstable, since the finest 15-20% of the material was washed out of each element. Layer 1 became significantly coarser than the other layers because all the fine particles eroded and were not replaced, whereas in layers 3 and 5, some fine particles from previous elements were retained. The model predicted that the permeability of this transition material increased by 2-3 orders of magnitude as the fines were washed out. These model predictions suggest that after extensive initial wash-out, the transition material became stable, with a PSD close to that shown for layers 3 and 5. No further erosion of this material was predicted. This stable PSD has a D_{15F} size of about 1.3mm, coarser than that required by both the Sherard and Dunnigan (1985) design guidelines, and the Reduced PSD method.

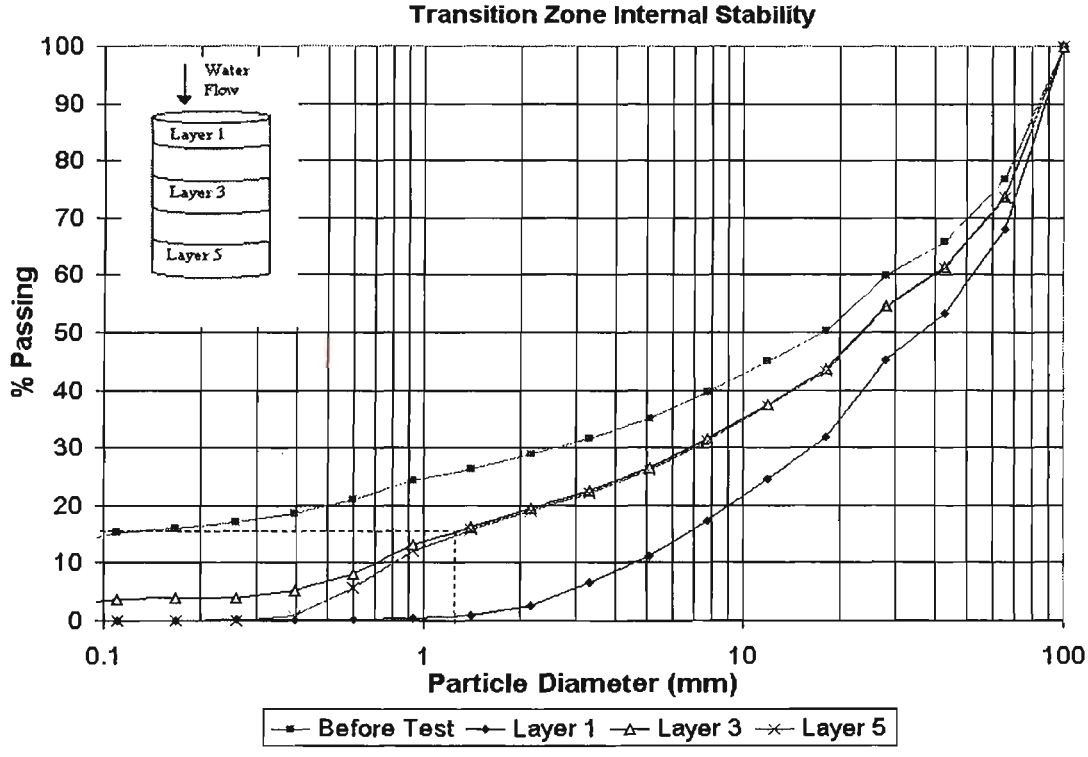

Figure 7.14 Change in PSD of transition zone after extended seepage

The previous analysis using the non-cohesive model suggests that all particles finer than 1mm are potentially unstable. However, it requires a significant flow velocity to mobilise

these sand-sized particles. For an assumed permeability of the core material of 10^{-8} m/s, the expected flow rate through the intact embankment is approximately $q=4x10^{-7}$ m^3/s per unit width of core. This steady state flow through the embankment is unlikely to erode any of the transition zone material. However, higher velocity flows may occur if a crack were to appear in the core.

The crack erosion model was used to estimate the flow rate through a crack in the core material. It was assumed that a continuous single crack developed through the core at two thirds of the total dam height (26m from the crest), where the width of the core is 50m, the likelihood of this crack is considered very small, however it is considered to show the potential application of the model. The crack erosion model was used to predict the initial flow rate through several cracks of various widths, with a maximum reservoir head of 23m. The filter permeability was estimated as somewhere between 10^{-5} to 10^{-4} m/s. Predicted flow rates were determined for both extremes of the predicted filter permeability. The results of the simulations are summarised in Table 7.2. The flow rate through the cracked core produced significant flows of 3-4 orders of magnitude higher than the flow rate through the intact core. It is very unlikely that a continuous crack of 50mm thickness and a high filter permeability could occur concurrently. For this model, a design flow of $1x10^{-3}$ m^3/s (or 1.0 litre/sec) was adopted. This flow would saturate the transition zone at the crack outlet. It is very difficult to estimate the hydraulic gradients required to cause internal erosion in the slightly cohesive transition zone. As a conservative estimate it was assumed that this flow would result in hydraulic gradients sufficient to mobilise the fine particles of the transition material, and potentially lead to the loss of fines described in Figure 7.14. The erosion resistance of the core material was not determined in the laboratory. Due to this lack of information, it was assumed that the

flow of 1 litre/sec would be sufficient to erode the walls of a crack through the core. The crack erosion model predicted that the three cracks (1mm, 10mm and 50mm) would seal after some erosion, since initially 10% of the coarser particles of core material would be retained by the transition zone and initiate self-filtration, even after wash-out of the transition fines. Based on this prediction, complete piping failure would be very unlikely. Hence, a hypothetical case of a wide, continuous crack through the entire core was predicted to seal after some erosion and the transition zone was judged an effective filter. The propagation of a crack through the transition zone material, which contains 15-20% fines, was not considered in this theoretical study. It is believed likely that the gravels and cobbles present would rapidly collapse on a crack through the transition zone and rapidly seal any cracks. The details of the crack erosion model are not shown here, because the erosion parameters were not determined in the laboratory.

Table 7.2 Flow Rate through cracked core

Crack Thickness	Q ($k_f=10^{-5}$) m^3/s	Q ($k_f=10^{-4}$) m^3/s
1mm	$4.5x10^{-6}$	$4.6x10^{-6}$
10mm	$2.2x10^{-4}$	$1.6x10^{-3}$
50mm	$3.2x10^{-4}$	$3.1x10^{-3}$

7.5 Case Study 4 – Balderhead Dam

The failure and subsequent investigation of Balderhead Dam were described in detail by Vaughan and Soares (1982). Balderhead Dam is located in Northern England, designed in 1959 and completed in 1965. The reservoir was impounded between October 1964 and February 1966, and it remained full until April 1967, when a large sinkhole appeared in its crest. A further sinkhole developed later, while the reservoir was being drawn down. It was determined that the core had suffered cracking by hydraulic fracture shortly before impounding was complete. The loss of core material by internal erosion occurred over a period of 14 months. The filter provided downstream of the core had not prevented this loss of material. A cross section of the dam core and the erosion damage is shown in Figure 7.15. A number of researchers have postulated the reason for failure of Balderhead Dam. Vaughan and Soares (1982) suggested that the core cracked and subsequent low velocity flow through the crack initiated gradual erosion of the core. Segregation of the eroded core material occurred, and only the eroded fines were transported into the filter, while the coarse material remained in place. The filter could not retain particles finer than about a medium sand, hence the filter was unable to retain the fines that were transported. This lead to continued erosion at low flow rates, without initiating self-filtration. Arulanandan and Perry (1983) suggested that the core material had a low erosion resistance (τ_c=0.4N/m^2), which increased the risk of failure by piping rather than by segregation. This section will show the application of the crack erosion model and Reduced PSD method to describe the consequences of a crack through the Balderhead dam core , in order to produce an alternative explanation for the failure of the dam.

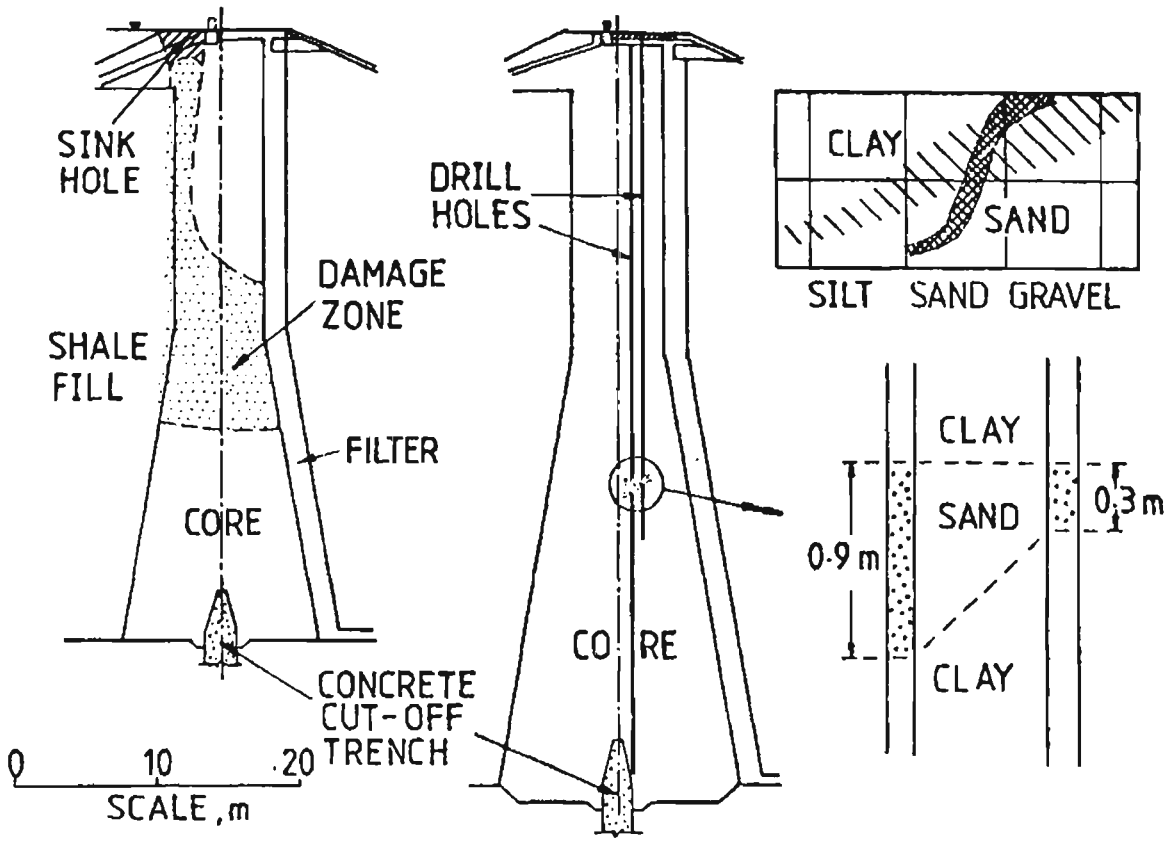

Figure 7.15 Cross Section of the Balderhead Core showing Erosion Damage (Vaughan and Soares, 1982)

Balderhead dam is an earthfill embankment with a narrow central core of broadly graded boulder clay with 20% of particles finer than 2μm, and cobbles up to 0.15m and larger. The core is protected by a sandy gravel filter (Figure 7.15). The gradings of the core and filter materials are shown in Figure 7.16 (after Vaughan and Soares, 1982). The *Reduced PSD* method was used to determine the stable PSD of the core material, this is also shown in Figure 7.16. The reduced PSD was determined from the mean grading of the core material, the coarsest particle of this stable PSD had a diameter of about 1.2mm, and $d_{85reduced}$=0.3mm. Adopting the Reduced PSD design rule for retention of materials with PI<10, ie. $D_{15F}/d_{85B}<4$, a maximum safe filter diameter of 1.2mm was obtained. In comparison, the Sherard and Dunnigan (1985) design criteria suggest that this material may be protected by a filter with $D_{15F}\leq 0.7$mm. The average filter grading in Balderhead

Dam had D_{15F}=1.4mm, while the coarsest measured grading had D_{15F}=10mm. Hence, the filter in many locations was likely to be too coarse to retain the stable fine fraction of the core material. While the coarse fraction may have been mobilised and captured at the filter interface, the Reduced PSD method suggests that erosion could occur regardless, since this internally unstable material was unable to self-filter, and the coarse fraction did not influence filtration. Hence, segregation of the fines is not the only possible explanation for the failure of Balderhead Dam. In the following, the analytical model for crack erosion will be used to investigate whether segregation is the likely cause of the failure.

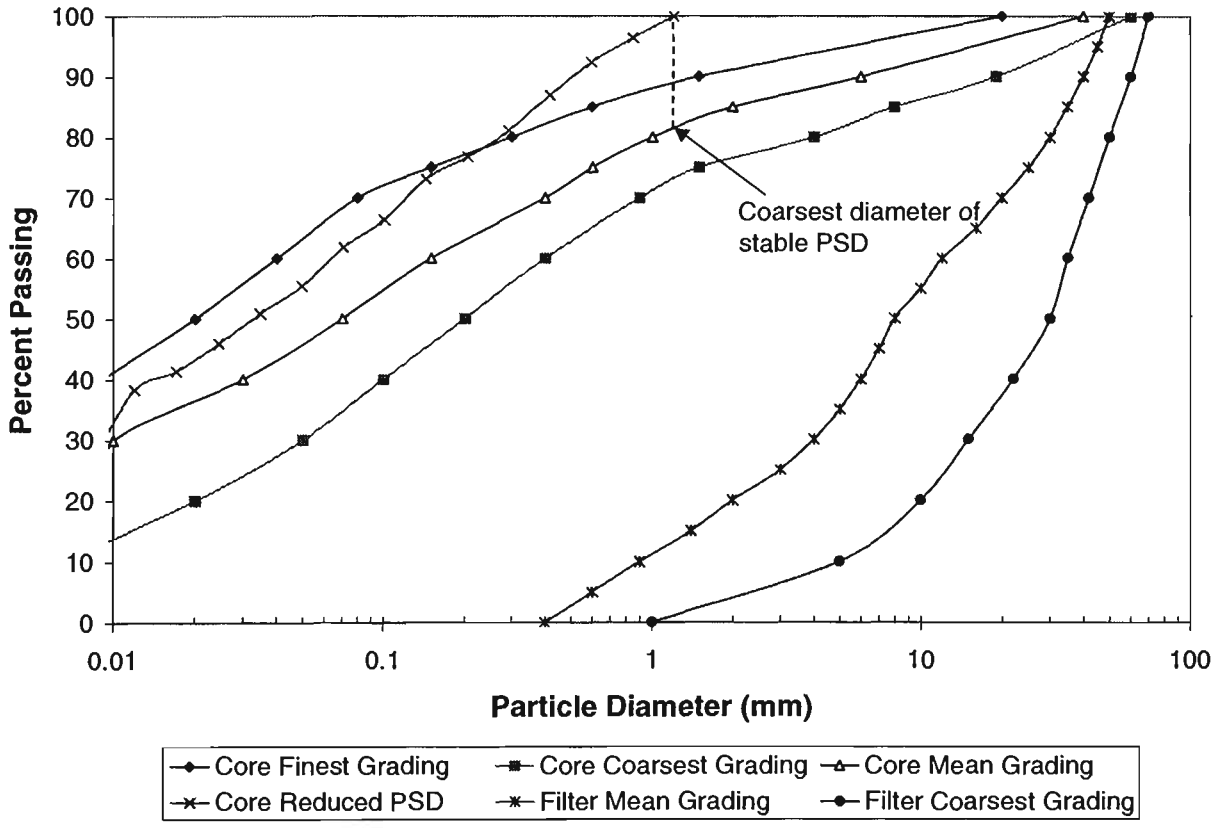

Figure 7.16 Particle size distribution of Balderhead Dam core and filter materials and Reduced PSD of the core material.

Investigations into the cause of the piping failure revealed a large damage zone in the core, beginning at a depth of about 30m and migrating upwards to the dam crest (Figure

7.15). It was determined that a crack had most likely developed near the base of the damage zone (at 30m depth). This crack enlarged slowly by erosion until it reached a size where the cohesive strength of the clay was no longer sufficient to prevent collapse. After collapse, damage migrated upwards as further erosion and collapse occurred. When excavated, the damage zone was filled with very soft clay, lumps of unsoftened clay and lenses of water-washed sands and gravels, indicating obvious segregation.

The erosion most likely began through a narrow crack of about 1-10mm, continuous across the 9m wide core at 30m depth (the base of the damage area). Vaughan and Soares (1982) performed an erosion test on the core material, to show that a 6mm hole through a sample eroded to 12mm diameter after 5 weeks of water flow through the hole at a hydraulic gradient of 10. This slow erosion rate identified that the material was moderately resistant to erosion, although it was not possible to assign erosion parameters based on the reported experiment. For modelling purposes, it was assumed that the compacted core material is characterised by a critical shear stress of τ_c=3N/m^2, and an erosion parameter, α=0.01. The upstream fill was significantly more permeable than the core material, and the full reservoir pressure, ie. 30m reservoir head, was assumed to act on a 9m long, 10mm wide crack. Based on these modelling parameters, the crack erosion model was used to examine the potential erosion of the Balderhead Dam core. The crack was represented by 2 elements, both 4.5m long. And the first 300mm of the filter was represented by 3 elements. A transition element of variable length (initially zero) and width was used to describe the formation of a filter cake.

The predicted mass of core material eroded during the first 20 days after a 10mm crack appeared in the core is shown in Figure 7.17. In the initial period, erosion occurred

rapidly, but reduced to a relatively gradual erosion rate as sand and gravel sized particles were captured at the filter interface. These particles formed the beginnings of a filter cake element, which reached a length of about 2mm after the first 3 hours of the simulation. The filter cake had a slightly lower permeability than the filter material, and hence, the flow rate and erosion rate reduced. Despite this reduction in flow rate, the sand sized particles in the filter cake were unable to self-filter the finer particles. A sufficient flow rate and shear stress passed through the crack to enable continued erosion of the crack walls, while the eroded fines continued to pass through the sand filter cake. Thereby continual erosion of the fine particles occurred over the next 20 days. This is consistent with the predictions of the Reduced PSD method which suggested that particles coarser than 1mm did not influence filtration of the fine fraction. While the total eroded mass was low (only 14kg after 20 days), the erosion rate was near constant, suggesting that the erosion would continue unhindered. The increase in crack width is also shown in Figure 7.17. The crack width increased gradually to 18mm after 20 days. This demonstrates that very slow erosion of the core was possible, without the crack sealing effectively. Vaughan and Soares (1982) determined that erosion of the core took 14 months to cause a visible sinkhole in the dam crest. This is consistent with the predicted slow, but constant, erosion rate.

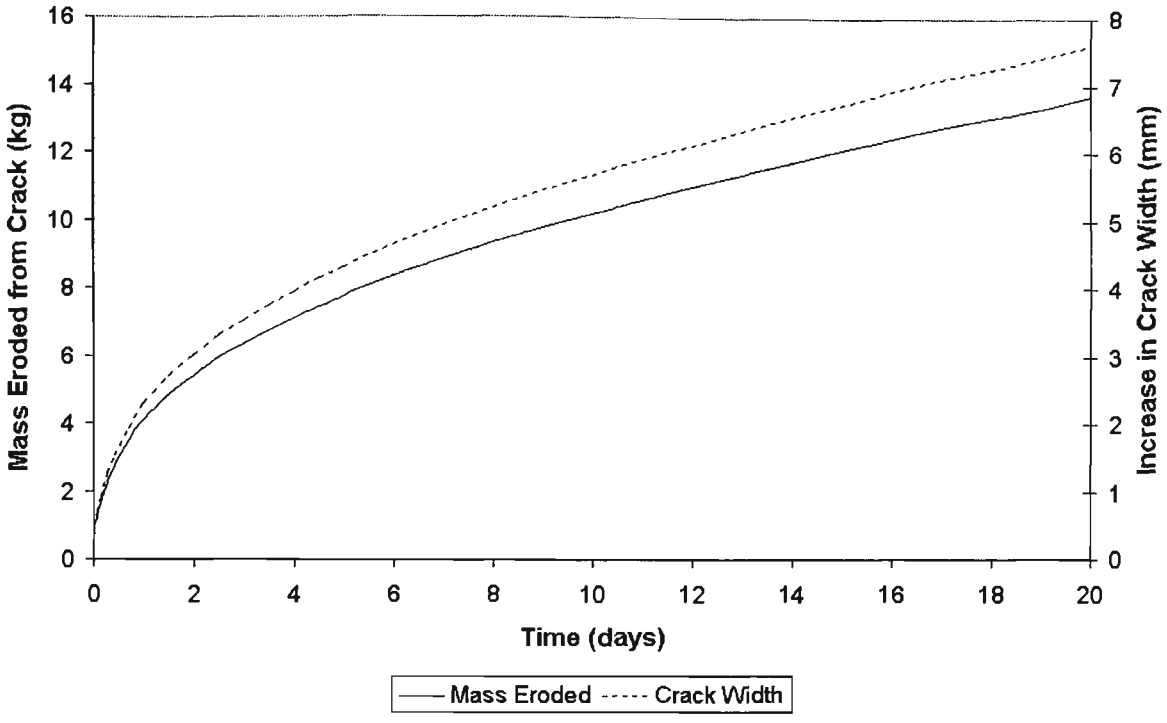

Figure 7.17 Mass Eroded from 10mm crack through Balderhead Dam Core

Figure 7.18 shows the predicted minimum particle diameter that was retained in the filter cake, this is described in the figure as "Min. Diam. Retained". Also shown in Figure 7.18, the "Max Diam Transported" line represents the maximum diameter of particles that can be mobilised within the crack by the flow shear forces. Particles coarser than the maximum transported diameter remained stationary in the crack. Particles finer than the maximum transported diameter but coarser than the minimum retained diameter, were transported to the filter interface and began to form a filter cake, because they could not infiltrate the filter. This means that initially particles in the size range 0.6-8mm were captured at the filter interface (Figure 7.18). Over the first 3 hours, these sand and gravel sized core material particles were captured at the filter face, and began a self filtering layer of voids smaller than the filter voids. These smaller voids resulted in a rapid reduction of the maximum diameter able to pass through to the filter from 0.6mm to 0.08mm within 3 hours, as progressively finer particles were captured in the filter cake.

This retained diameter tended to a constant value of 0.08mm over the next 20 hours. The self-filtration process failed because the coarse fraction of the core material was too coarse to retain any particles finer than 0.08mm. While only the first day of modelling is shown in Figure 7.18, there was no change in the particle diameter retained by the filter cake over the next 19 days of the simulation. Particles finer than 0.08mm continued to pass through the filter unhindered. The filter cake, consisting of particles from 0.08mm to 8mm was too permeable to completely prevent further erosion and the erosion would continue at a very slow rate. The filter cake became slightly thicker, reaching 4mm after 20 days as more sand particles were retained, but was still unable to retain finer particles. The increase in crack width to 17mm after 20 days offset the increase in filter cake thickness, and the flow rate remained near constant. Constant erosion then occurred and the fines continued to erode through the filter without sealing the crack.

The "Max. Diam. Transported" in Figure 7.18 is the predicted maximum diameter that can be mobilised due to the hydraulic forces, and hence, can be used to examine potential segregation. The initial burst of flow through the crack was able to transport large particles up to 8mm diameter. As the filter cake formed, the flow rate reduced, and the model predicted that the flow rate reduced to 0.3 litres/sec per metre width of crack, which was still able to transport particles up to 2.2mm in diameter. Because the flow rate remained nearly constant after this initial drop, this maximum diameter of transported particles did not change appreciably during the 20 day simulation. While particles coarser than 2.2mm were not transported, the important silt and sand sized particles that may influence filtration were mobilised, and particles between 0.08mm to 2.2mm continued to be captured in the filter cake. Hence, the model predicted that segregation is

not the only possible cause of failure of Balderhead Dam, but the continuous erosion of the finer fraction through the coarser fraction is a definite contributor.

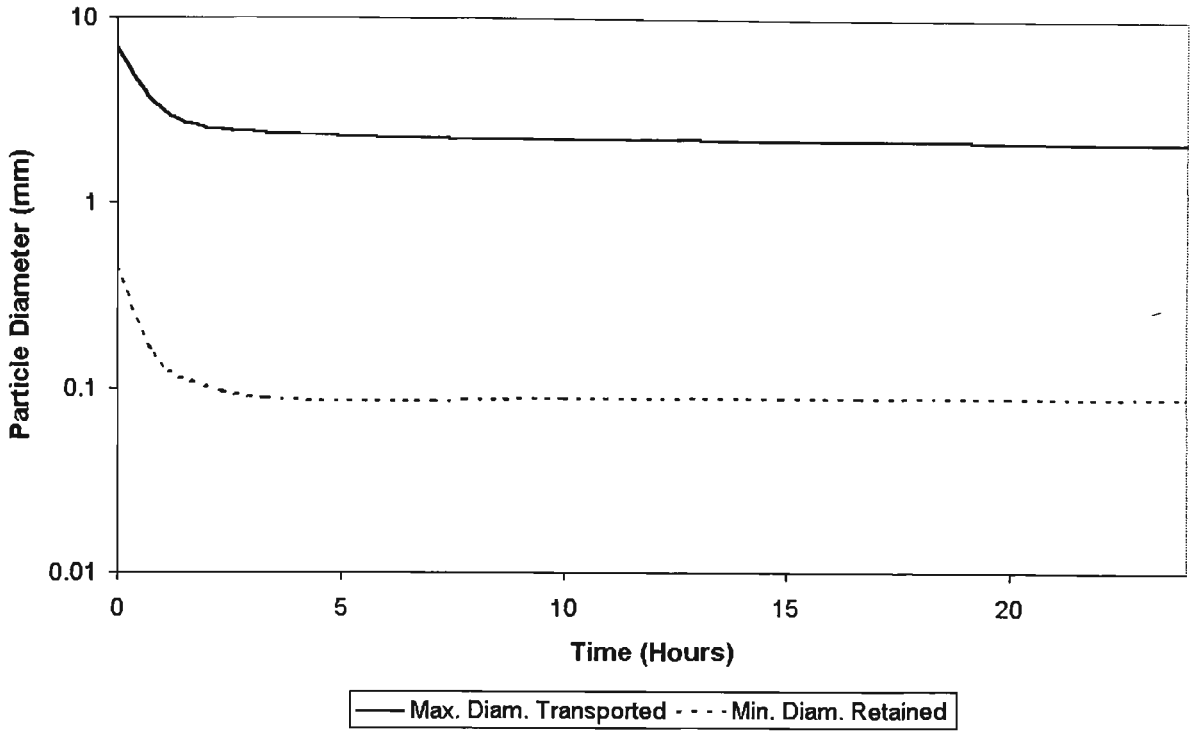

Figure 7.18 Balderhead Dam - Maximum diameter of particles transported through the crack and minimum diameter of particles retained in the filter cake.

To summarise, the sand size fraction of the Balderhead Dam core material was unable to self-filter particles finer than 80μm, even when the coarser fraction of the material was retained at the filter interface. This may have resulted in continued, slow erosion of the clay matrix through the coarser material by both crack erosion and suffusion processes. These fines made up 40% by mass of the material, and loss of these fines would result in a significant reduction in volume, until collapse of the wet crack occurred and the piping failure progressed vertically through the core. The presence of large stones over 0.15m diameter in the core material would increase the potential for crack collapse in the core and vertical migration. Some coarse particles would migrate to the filter interface, while others would simply fall to the bottom of the 'pipe' and resemble washed sand sitting in

the damage zone. These predictions match the observations of Vaughan and Soares (1982). A filter designed by the Sherard and Dunnigan (1985) design criteria would have D_{15F}=0.7mm, significantly finer than the as constructed filter with an average D_{15F}=1.4mm. This design filter should be able to retain this core material with no erosion.

8. CONCLUSIONS AND RECOMMENDATIONS

8.1 Role of Dam Filters

Granular filters are used in earth structures such as embankment dams where erosion of base material may occur due to piping or incidents of high seepage. This study was focussed on the role of filters in embankment dams, placed downstream of the dam core. It is essential that these filters be coarse enough to allow seepage flow and preventing saturation of the downstream embankment, while being fine enough to protect (retain) any eroding core material. Granular filters must also be non-cohesive so that a crack developed within the core is not propagated into the filter, as well as not sustaining a crack itself, due to deformation or elevated hydraulic gradients. Methods of filter design based on these three essential criteria have been reviewed in detail in this thesis.

The largest particle that can pass through a filter is determined by the size of the constrictions between pores of the filter. Constrictions are the smallest two-dimensional openings formed between two pores in a granular material. If the larger particles of the base material can be retained by these constrictions, then smaller constrictions will be formed, which progressively retain smaller base particles and produce a stable base soil - filter interface. This process is called self-filtration, and it is essential for the filtration of internally stable soils. Hence, the retention requirement of a filter is dependent on some of the coarse base soil particles being retained by the pore constrictions. Failure or success of the filter should be judged by the amount of base soil particles lost before self-filtration halts erosion.

8.2 Analytical Modelling of Non-Cohesive Materials

An analytical model for the time-dependent movement of non-cohesive base soil particles through granular filters has been described in Chapter 3. This model significantly extends the particle transport concept of Indraratna and Vafai (1997), describing the time-dependent processes occurring during self-filtration in detail. The model consists of three important sections:

4. A filter pore model based on a three dimensional cubic network proposed by Schuler (1996), where pores are interconnected by constrictions in a regular cubic network. The size of the pore constrictions is determined from a new relationship considering both the filter particle size distribution and relative density.
5. A new equation for the infiltration of particles into the filter model, based on the probability of movement of particles of varying diameter through the filter pore constrictions. This equation governs the retention of particles within the filter.
6. Particle transport equations of conservation of mass and momentum, proposed earlier by Indraratna and Vafai (1997), have been modified to consider the increased viscosity of the flow due to suspended particles in the pore water. This particle transport model determines the rate of erosion and transport of base soil particles.

Within broadly graded filters, some fine particles may not be part of the skeleton of fixed particles that form the structure of the soil. These particles are loose within the pores of the soil skeleton and do not contribute to particle capture during filtration. Hence, these particles should not be considered when determining the size of constrictions between the filter voids. At the other extreme, some coarse particles may be 'floating' in a matrix of fines. In this case, the coarser particles do not contact each other to form large constrictions, although they still contribute to the formation of constrictions along with

the smaller particles. Within the analytical model, a method has been described to determine which particle sizes should be excluded from the particle size distribution (PSD), when determining the constriction size distribution of a broadly graded material.

The analytical model considers the transport and capture of non-cohesive base soil particles and predicts, for a suitable base soil - filter combination, the time-dependent formation of a stable filter interface. In a typical analysis, fine particles are initially able to infiltrate the filter, but as some coarse base soil particles are captured within the filter, the model predicts that void constriction sizes will decrease and finer base soil particles will be retained. By modelling these time-dependent changes within a suitable filter, the model predicts the formation of a stable self-filtering layer, where a sufficient quantity of base soil particles have been captured and are able to prevent further erosion of the base soil. This self-filtration layer thickness is usually between 10-30cm thick, which corresponds to 5-10 times the mean filter particle diameter by number (usually in the range D_5-D_{10}). Beyond this self-filtering layer, there is little retention of particles, suggesting that increasing the filter thickness does not greatly affect the capture of particles.

The model was shown to predict particle movement and time-dependent changes in flow-rate, permeability and porosity for non-cohesive, uniform and broadly graded base and filter materials, and is a significant extension of the original analysis of Indraratna and Vafai (1997). In addition, this revised model has been shown to predict internal stability to some extent, based on fine filter particle washout. Comparison with published results of internal stability tests showed a good correlation, the model predicted very similar quantities of material wash out for an internally unstable material, while no movement was predicted for an internally stable material.

A novel large-scale laboratory equipment was constructed as part of the project, to examine the filtration of coarse, non-cohesive materials. The new apparatus was better suited to examining in detail the behaviour of coarse materials, and reduce the potential errors due to edge effects in a smaller cell. The filtration chamber is a 500mm diameter and 1m high acrylic cylinder, sealed with circular steel endplates. Flow rates up to 2.5 litres/s were applied to a wide range of base soil and filter combinations, providing visual verification of the model predictions and accurate laboratory data describing particle infiltration lengths and the depth of self-filtration zones. These laboratory results and some previously published experimental findings were compared with the model predictions. The analytical model predicted particle movement and capture similar to the measured data for non-cohesive, uniform and well graded base and filter materials. Predicted changes in particle size distribution at increasing depths within the filter were similar to the measured data.

The analytical model was used to compare the various design criteria for filters to protect non-cohesive base soils. It was determined that the criteria of Karpoff (1955) and the USACE (1971) are not suitable design criteria for broadly graded base soils. The Honjo and Venziano (1989) design criterion was found to be the most consistent for design of filters for a broad range of base soils with C_u varying from 2-40. Some practical applications of the non-cohesive model were demonstrated in Chapter 7. Common applications include predicting the success of fine filters next to coarse drainage blanket zones, and the assessment of internal stability and wash out of fines from broadly graded filter materials.

8.3 Effect of Cohesive Core Materials

The majority of dam core materials are cohesive. Most modern design criteria recognise that cracking of cohesive materials, and the erosion of the crack walls often represents a worst case scenario in design. Empirical filter design criteria and models developed to describe filtration of intact, non-cohesive base soils cannot adequately describe the erosion and filtration of cohesive materials, where an arch may be sustained over the crack due to the material cohesion, allowing continued erosion of the crack. The analytical model was extended in Chapter 5 to describe the erosion and filtration of a cracked cohesive material. This new 'crack erosion model' considered five steps in the filtration process for a cohesive base soil:

1. Formation of a crack by hydraulic fracture or differential settlement: the model adopted the assumption that a crack had occurred, and the location and size of the crack was estimated based on published observations of cracked cores in dams.
2. Erosion of the crack walls due to the flow: the large scale pinhole test was developed to measure the erosion rate and the size of eroded particles due to concentrated flow through a pinhole in a cohesive soil. Erosion rates generally correlated well with the equation, $Erosion\ Rate = \alpha(\tau - \tau_c)$, and many materials exhibited some erosion resistance, as demonstrated by a non-zero critical shear stress, τ_c. Conservation of mass of the solid fraction and the eroding fluid were considered in the model, to develop equations predicting the time-dependent erosion of the crack walls based on the erosion equation.
3. Transport of the eroded particles to the filter interface was based on the flow velocity, and corresponding shear stress. Shield's diagram was used to determine the maximum size of particles mobilised, which is dependent on the shear stress generated by the flow.

4. Filtration or transmission of the particles through the filter was considered to be similar to the non-cohesive model, ie. the particles finer than the pore constrictions can pass through the filter, while coarser particles are retained. Physico-chemical retention of clay flocs was also considered.
5. The essential part of successful filtration of flow through a crack is the formation of a low permeability filter cake, leading to lower flow rates and sealing of the crack. The model assumed that particles that are too coarse to pass into the filter were retained at the filter face, initiating the formation of a filter cake. As the thickness of this cake increased, it was able to retain finer base soil particles and form a skin over the filter face, thus sealing the crack and preventing further erosion.

Some aspects of this crack erosion model were verified through comparison with the results of No Erosion Filter (NEF) tests performed in the laboratory. Three materials were considered, representing a group 1 clay (with >85% finer than 75μm), an internally unstable group 2 sandy clay (with 40-85% finer than 75μm), and a coarse group 2 sandy clay. The predicted quantity of erosion and enlargement of the pinhole before the filter sealed the pinhole and prevented further erosion, was very close to the erosion measured in the laboratory for the three materials. Predicted flow rates through the NEF apparatus were similar to those measured in the laboratory. This verified the use of a PSD multiplier, A, as defined in Chapter 4.5, to produce a *representative PSD* to describe the size of particles reaching the filter interface in the model. Alternatively, the size of particles eroded through a pinhole, as measured in the laboratory, was used successfully in the model to describe the size of particles reaching the filter. This was called the laboratory determined *erosion product* PSD.

The crack erosion model was shown to predict that filters finer than the NEF boundary filter would seal a crack rapidly with little erosion, while increasingly coarse filters allowed increasing amounts of erosion before sealing. Larger hydraulic gradients resulted in more erosion before the filter sealed. This suggests that an embankment dam with a broad core, and hence, low hydraulic gradients at the filter interface may be adequately protected by a filter significantly coarser than the NEF boundary filter.

Through new experimental data and study of previous literature, it was shown that the erodability of cohesive materials could be represented by two erosion parameters, the critical shear stress to initiate erosion, τ_c, and the erosion rate parameter α. The critical shear stress was shown to be an important parameter in determining the extent of crack erosion. A high critical shear stress (τ_c=5N/m^2) resulted in very little erosion, and a filter coarser than the NEF boundary may have been adequate to protect the base soil. However, a base soil with a very low critical shear stress (τ_c=0.05N/m^2) eroded significantly, and a conservative filter was required to protect the base soil, approaching the Vaughan and Soares (1982) perfect filter criterion.

The physico-chemical conditions leading to the deposition of clay particles on the pore walls (related to the pore water and core material chemistry) had a marked effect on the filtration efficiency. Conditions more conducive to physico-chemical capture of fine particles resulted in more rapid sealing of the filter and a significant reduction in the amount of erosion from the crack. The model has demonstrated the significant effect of erosion rate parameters, size of particles eroded and the physico-chemical deposition of particles. Hence, existing models of filtration are unable to describe the behaviour of cohesive base soils and a more rigorous analysis such as that proposed in this thesis is necessary.

Highly erodable materials were shown to be prone to segregation during erosion. Flows producing shear stresses smaller than $0.5N/m^2$ were unable to transport sand sized particles within a crack. If the cracked material had a critical shear stress of less than 0.5 N/m^2, then erosion was possible due to these creeping flows, but coarse (sand size) particles were not transported and could not influence filtration. Using the analytical model, it was possible to produce conditions such that very low flow rates could occur through a crack or high permeability zone in a dam core, and erosion and segregation of the fines would occur. Based on this observation, the Vaughan and Soares (1982) perfect filter design concept should be adopted for highly erodable materials, with $\tau_c<0.5N/m^2$. This shear stress was shown to correspond approximately with the highly dispersive category D1 of the standard pinhole test (Sherard et al. 1976a), and would include dispersive clays and non-cohesive silts and fine sands. More erosion resistant materials may be protected by filters designed using the less stringent Sherard and Dunnigan (1985) design criteria.

The modelling described in this thesis is a major advancement on the Indraratna and Vafai (1997) analytical model for non-cohesive base soils. The combination of a 3D filter pore model, consideration of broadly graded materials and time-dependent modelling provides a significantly more accurate description of filtration than previous published models. To the writers knowledge, the complete model of filtration of cohesive soils is the first to consider the combination of the processes of cracking, erosion, transport, filtration and formation of a filter cake, thereby providing a comprehensive description of filtration from the inception of a crack through a dam core.

8.4 Broadly Graded Materials – The Reduced PSD Method

Broadly graded cohesive base soils may be internally unstable, where the coarse fraction of the material is unable to act as a filter for the fine fraction. This means that a filter that can retain the coarse fraction may still allow continued erosion of the base soil as self-filtration may not occur. Laboratory tests and modelling predictions verified this observation. A suitable filter must be designed to retain the stable fine fraction of the base soil. This problem has been noted in filtration of non-cohesive base soils (Sherard, 1979), but has not been previously described in cohesive soils. The results of 47 NEF tests were compared, including 15 tests performed during this study, 17 test results published by Delgado (2000), 8 from Khor and Woo (1989) and 7 from Sherard (1984). Based on these test results and predictions from the analytical model, a new procedure was described to determine a safe filter for fine base soils, called the *Reduced PSD* method.

The *reduced PSD* is produced by determining the stable, self-filtering fine fraction of the base soil. The method is described in detail in Section 4.4. Re-examination of the laboratory determined NEF critical filter diameter and the 85% coarsest particle of this reduced PSD, $d_{85reduced}$, showed that Group 1 materials, having >85% finer than 75μm, can be designed using the relation $D_{15bdy}/d_{85reduced}=12$. It was shown that the uncertainty in designing filters for Group 2 materials (ie. using $D_{15F}=0.7$mm for a wide range of materials), is due to the inability of many broadly graded cohesive materials to self-filter. In the laboratory, several materials that were able to self-filter had NEF boundaries significantly coarser than 0.7mm, and this coarser boundary was predicted by the *Reduced PSD* method.

A new design criterion for Group 2 materials, based on the *Reduced PSD*, was proposed:

- for clayey materials with PI>10, adopt $D_{15bdy}/d_{85reduced} \leq 9$,
- for silty materials with PI<10, adopt $D_{15bdy}/d_{85reduced} \leq 4$.

The model for erosion through a crack in cohesive materials was compared with the design criteria of Sherard and Dunnigan (1985), Khor and Woo (1989), the *reduced PSD* method and 21 laboratory NEF results. This comparison demonstrated that the commonly adopted Sherard and Dunnigan (1985) criteria are adequate for design of filters in most cases. However, some exceptions were found, including fine clays with uniform coarse fractions and broadly graded materials that are unable to self filter. For these broadly graded materials, the *reduced PSD* method provided a good estimate of the NEF boundary. Hence, it is recommended that the *reduced PSD* method be combined with the Sherard and Dunnigan (1985) criteria, to design a safe filter.

8.5 Recommendations for Improved Filter Design

Based on the extensive analytical modelling, laboratory experiments and the critical review of previous literature presented in this thesis, the following guidelines are proposed for the design of granular filters for embankment dams. These guidelines are appropriate for most design situations, however, it is still recommended to perform laboratory tests on core and filter samples proposed for dam construction. The No Erosion Filter (NEF) test (Sherard and Dunnigan, 1985) is the most suitable test available for determining suitable filters for embankment dams. A detailed procedure for the NEF test, developed during this study, is presented in Appendix 1.

The filter design guidelines are presented as three *flow charts*. The first *flow chart* (Figure 8.1) describes the application of simple empirical criteria. These criteria are based on the recommendations of Chapter 6, reproduced in Table 8.1, and consist primarily of the recommendations of Sherard and Dunnigan (1985), and the criterion proposed by Honjo and Veneziano (1989) for coarse soils (with less than 15% by mass passing the 75μm sieve). Group 1 and 2 soils are modified to consider the self-filtering requirement, defined by the *Reduced PSD*. Highly erodable materials, having τ_c<0.5N/m^2, have been shown to be at risk of segregation at low flow rates, and should be protected by filters designed following the Vaughan and Soares (1982) 'perfect filter' design concept.

Once a base soil and filter material are chosen based on the empirical design flow chart, they can be examined in more detail using the simplified analytical approach shown in Figure 8.2. This procedure adopts design charts and equations developed throughout this thesis to quickly estimate the extent of erosion of the base soil. This simplified procedure provides an overview of the behaviour of the base soil – filter combination, but cannot describe the full range of time-dependent changes and will not be valid for unusual materials such as uniform or very broadly graded soils or cohesive materials with a low erosion resistance.

For comprehensive design of granular filters, the writer recommends following the detailed analytical procedures outlined in Figure 8.3. This flow chart is a summary of the modelling described in Chapters 3 and 5 of this thesis. Computer programs have been written to implement these models, and by following the Users Manual written for these programs, it is now convenient to determine the predicted, time-dependent behaviour of the proposed base soil – filter combinations.

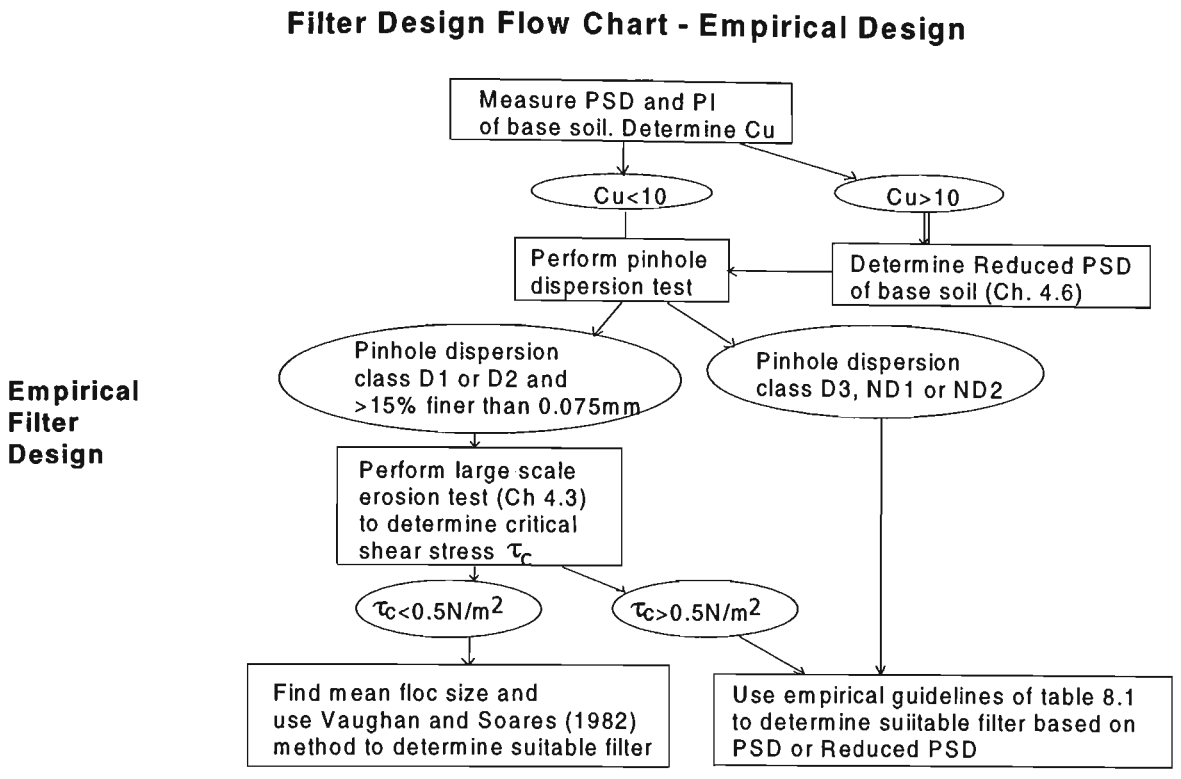

Figure 8.1 Flow chart for empirical filter design procedure

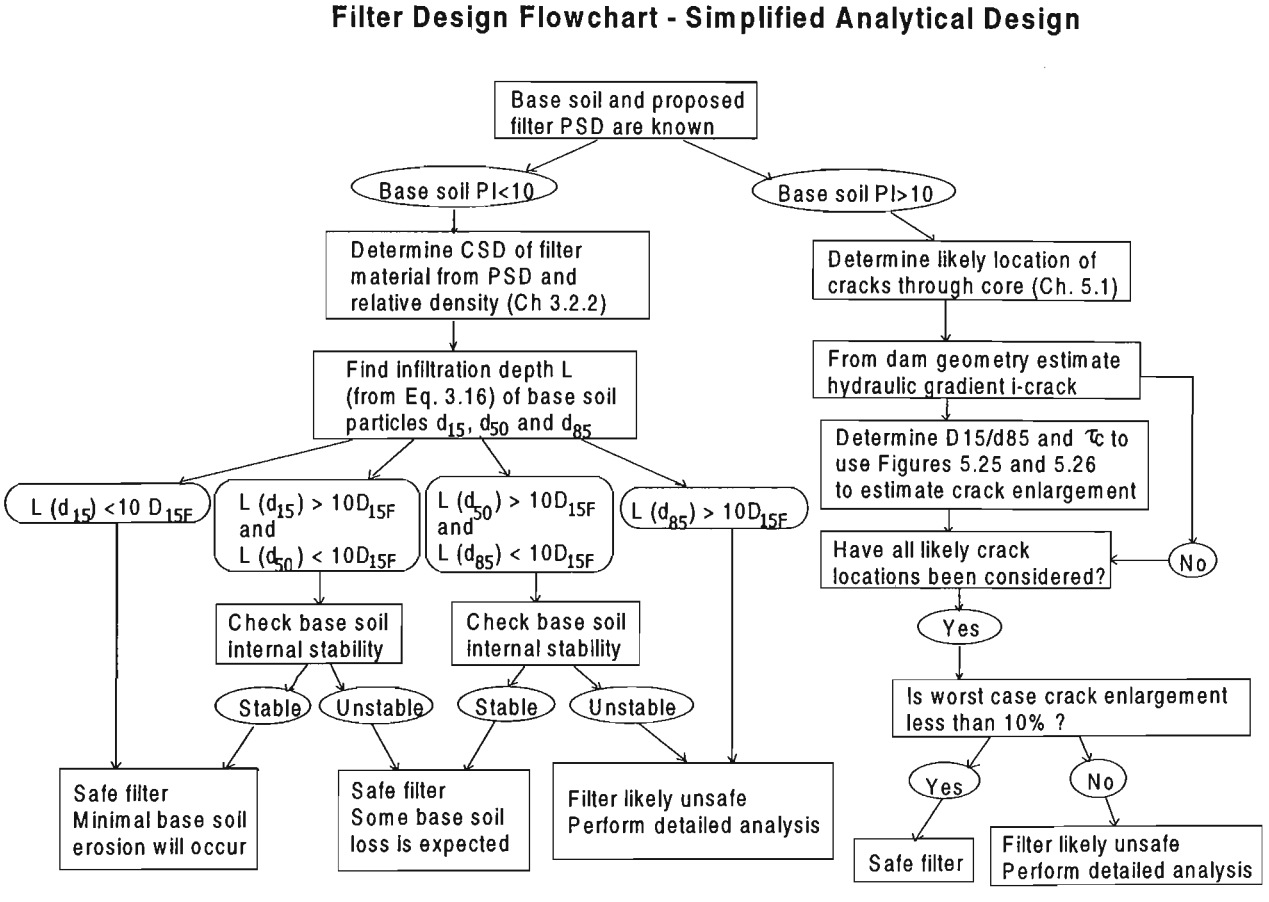

Figure 8.2 Flow chart for simplified analytical filter design procedure

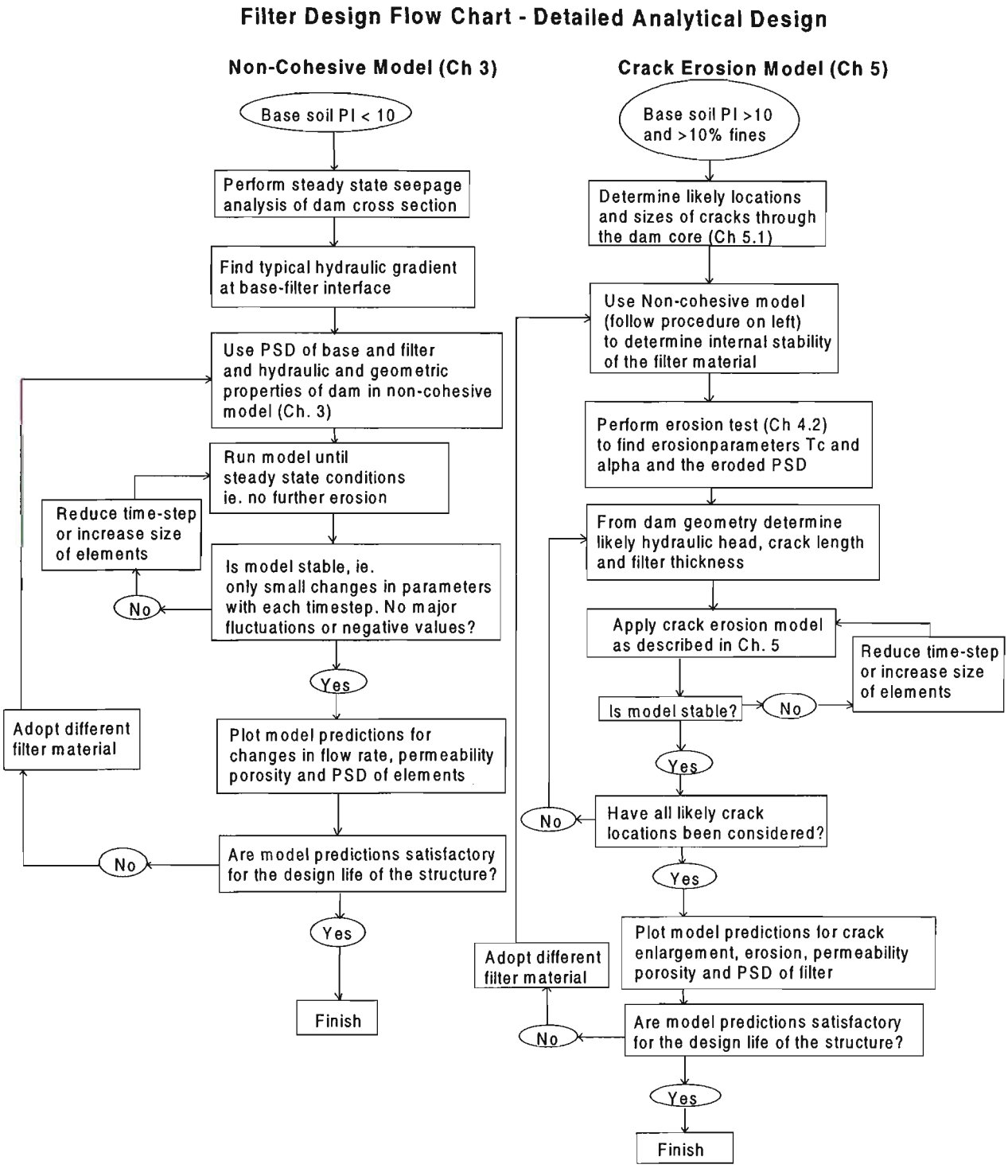

Figure 8.3 Flow chart for detailed analytical filter design procedure

Table 8.1 Revised Filter Design Criteria.

Soil Group	Base Soil Type	Base Soil % Passing 75μm Sieve (of portion <4.75mm for groups 1-3)	Filter Criterion
1	Fine Silt or Clay	>85%	$D_{15F}/d_{85B} \leq 9$ and If PI>10 $D_{15F}/d_{85Reduced} \leq 12$ [(a)] If PI<10 $D_{15F}/d_{85Reduced} \leq 4$ [(a)]
2	Sandy Silts / Clays & Silty / Clayey Sands	35% - 85%	$D_{15F} \leq 0.7$mm and If PI>10 $D_{15F}/d_{85Reduced} \leq 9$ [(a)] If PI<10 $D_{15F}/d_{85Reduced} \leq 4$ [(a)]
3	Soils intermediate between groups 2 and 4	15% - 35%	interpolate between groups 2 and 4 based on %passing 75μm sieve.
4	Sands, Sandy Gravels with few fines	<15% and $d_{95B}/d_{75B} \leq 7$ [(b)]	$D_{15F}/d_{85B} \leq$ 5.5 - 0.5 d_{95B}/d_{75B}

[(a)] $d_{85Reduced}$ is the d_{85} size of the base soil reduced PSD, determined as outlined in Chapter 4.4.

[(b)] When $d_{95B}/d_{75B} > 7$, recalculate the grading by truncating the coarse fraction at the most coarse particle such that, in the new grading, $d_{95B}/d_{75B} = 7$.

8.6 Future Studies

There is still scope for further advancement of the modelling details. Some potential future improvements to the analytical procedures and to our overall understanding of filter behaviour are presented below.

- Effect of hydraulic gradient - the non-cohesive model adopted the assumption that any particle finer than the pore constrictions will move through the filter until it is retained. In reality, hydraulic conditions will have a major influence on the movement of particles. Low flow rates may not be sufficient to erode the base soil. Within the filter, low flow rates may result in sedimentation of particles in the filter voids. Very high flow rates or hydraulic gradients may result in dilation of the filter voids and allow coarser particles to move through the filter. These hydraulic conditions should be investigated in detail.
- Effect of particle shape - Spackman (2000) showed that filters with rounded particles allow decreased loss of base soil compared with filters of crushed material with angular particles, when compacted under the same conditions. Karpoff (1955) also provided different filter design criteria for rounded or angular filters. Indraratna and Vafai (1997) adopted a particle shape factor to allow for different particle shapes. This shape factor could be adopted in the current model and correlated with laboratory data to reflect more accurately, the effect of particle shape.
- Flocculation and aggregation in cohesive materials – in NEF tests on cohesive base soils, both in the current laboratory program and in previous published studies, the ratio D_{15bdy}/d_{85B} has varied between 6 and 40. In this study, it was suggested that strong bonds between particles in cohesive materials produce aggregates and flocs of larger particles, which are stable at the filter interface and are unable to move through the filter voids. The size of these aggregates was shown to vary considerably between

materials and was proposed as the reason for the large variation in filter retention ratio. This aspect of filtration should be investigated further.

- Prediction of cracking in dam cores - little is known of the initial orientation and size of cracks and the processes of erosion of cracks through dam cores. As more knowledge becomes available, the erosion model can be improved to better describe what has been observed in the laboratory and in engineering practice.
- Transition zones in existing dams - investigation of older Australian dams often reveals that the core is protected by a 'transition zone', intended to act as a filter. This material is typically a broadly graded sandy gravel, which often contains a substantial proportion of fines. The issue of internal stability and wash-out of fines within these materials has been considered in this thesis. The high fines content also raises concerns about the ability of the filter to self-heal over a crack. Further research is required to examine the effect of these fines on the crack filling ability of a filter. The amount and type of fines, particle size distribution, capture of fines from the core and long term changes may all have a significant effect on the filter function.

8.7 Summary

This thesis has presented a major extension to existing analytical models of the behaviour of granular filters. Complete models have been presented which are able to predict time-dependent changes occurring during the filtration process, including changes in particle size distribution, permeability and porosity of the base and filter materials and the changes in flow rate and mass transfer within the system. This description of the time-dependent changes greatly improves our understanding of how the filtration process transpires and more accurately predicts the extent of mass movement and time required to form a stable filter interface. The two models presented are able to describe the mechanisms of piping failure, which can occur either by backwards erosion of non-cohesive materials due to mobilisation of particles due to seepage forces, or through erosion of the walls of a pre-formed crack in cohesive materials.

The laboratory program described in this thesis has examined various aspects of filter behaviour. The correlation between erosion tests and NEF tests has improved the description of fundamentals behind filtration of cohesive materials. The *Reduced PSD* method, developed after a series of NEF tests on various base soils, is an important advance in predicting safe filters for broadly graded base soils. Large scale laboratory tests were used to verify the model predictions, examine the filtration of coarse base soils, investigate the infiltration of particles into a long filter, and study the effect of filter length. New filter design procedures have been proposed, incorporating existing empirical design criteria, the Reduced PSD method, and the application of analytical models to describe the behaviour of the base soil and filter.

REFERENCES

Aberg (1993) "Washout of Grains from Filtered Sand and Gravel Materials", Jour. Geotechnical Engineering, ASCE, Vol. 119(1), pp. 36-53.

Arulanandan K., Loganathan P., Krone R. (1975) "Pore and Eroding Fluid Influences on Surface Erosion of Soil", Jour. Geotechnical Engineering Div., ASCE, Vol. 101, No. GT1, pp 51-66.

Arulanandan K., Gillogley E., Tulley R. (1980) "Development of a Quantitative Method to Predict Critical Shear Stress and Rate of Erosion of Natural Undisturbed Cohesive Soils", Tech Rep. GL-80-5, U.S. Army Engrs, Waterways Experiment Station, Vicksburg, Miss.

Arulanandan K. and Perry B. (1983) "Erosion in Relation to Filter Design Criteria in Earth Dams", Jour. Geotechnical Engineering Div., ASCE, Vol. 109, No. 5, pp 682-697.

Carter J., Booker J., and Yeung S. (1986) "Cavity Expansion in Cohesive Frictional Soils" Geotechnique, Vol. 36(3), pp. 349-358.

Delgado Ramos F. (2000) *Laboratory Simulation of the Internal Erosion Phenomenon to determine the Variables that Influence the Efficiency of Filters for Cohesive Soils.* PhD Thesis, University of Granada, Spain (in Spanish).

Delgado Ramos F. and Locke M. (2000) "Design of Granular Filters: Guidelines and Recommendations for Laboratory Testing", *Filters and Drainage in Geotechnical and Environmental Engineering,* Wolski & Mlynarek Eds., Balkema, Rotterdam, pp. 115-122.

DeMello V. (1977) "Reflections on Design Decisions of Practical Significance to Embankment Dams", Geotechnique Vol. 27(3), pp. 279-355.

Faure Y. and Gendrin P. (1989) "Filtration of a Granular Medium by Textiles" *Powders and Grains*, Biarez & Gourves (Eds.) Balkema, Rotterdam, pp. 425-432.

Faure Y., Farkouh B., Delmas Ph., Nancey A. (1996) "Valcros Dam: Summary of Tests and Analysis of Filter Criteria", *Geofilters '96, Comptes Rendus Proceedings*, Lafleur & Rollin (Eds.), Bitech Publictions, Canada.

Federico F. and Musso A. (1993) "Some Advances in the Geometric-probabilistic Method for Filter Design", in *Filters in Geotechnical and Hydraulic Engineering*, Brauns, Heibaum & Schuler (eds.), 1993 Balkema, Rotterdam

Fischer G. and Holtz R. (1996) "A Critical Review of Granular Soil Filter Retention Criteria", *Geofilters '96, Comptes Rendus Proceedings*, Lafleur & Rollin (Eds.), Bitech Publictions, Canada. pp. 409-418.

FosterM., Fell R., and Spannagle M. (1998) *Analysis of Embankment Dam Incidents*, UniCiv Report No. R-374, University of New South Wales, Australia.

Foster M. (1999) *The Probability of Failure of Embankment Dams by Internal Erosion and Piping,* PhD Thesis, University of New South Wales, Australia, 482p.

Foster M. and Fell R. (1999) "Filter Testing for Dams - No Erosion and Continuing Erosion Boundaries", Proc. 8th Aust/NZ Conf. on Geomechanics, Hobart, Australia. Vol.2 pp. 503-511

Giroud J. "Granular Filters and Geotextile Filters", *Geofilters '96, Comptes Rendus Proceedings*, Lafleur & Rollin (Eds.), Bitech Publictions, Canada, pp. 565-680.

Govindaraju R., Reddi L., Kasavaraju S. (1995) "A Physically Based Model for Mobilization of Kaolinite Particles under Hydraulic Gradients" Journal of Hydrology, Vol 172, pp. 331-350.

Graf W. (1971) *Sediment Transport*, McGraw-Hill, 513p.

de Groot M., Bakker K., Verheij H. (1993) "Design of Geometrically Open Filters in Hydraulic Structures", in *Filters in Geotechnical and Hydraulic Engineering*, Brauns, Heibaum & Schuler (eds.), 1993 Balkema, Rotterdam

Happel J. and Brenner H. (1965) *Low Reynolds Number Hydrodynamics*, Noordhoff, Leyden, The Netherlands.

Heinzen R. and Arulanandan K. (1977) "Factors Influencing Dispersive Clays and Methods of Identification" *Dispersive Clays, Related Piping, and Erosion in Geotechnical Projects,* ASTM STP 623, J.L. Sherard and R.S. Decker, Eds., ASTM 1977, pp. 202-217.

Hjeldnes E. and Lavania B. (1980) "Cracking, Leakage and Erosion of Earth Dam Materials" Jour. Geotechnical Engineering Div., ASCE, Vol. 106, No. GT2, pp. 117-135.

Honjo Y. and Veneziano D. (1989) "Improved Filter Criterion for Cohesionless Soils", Jour. Geotechnical Engineering Div., ASCE, Vol. 115, No. 1, pp 75-94.

Humes C. (1996) "A New Approach to Compute the Void-Size Distribution Curves of Protective Filters" *GeoFilters '96*, Lafleur & Mlynarek (Eds.), Bitech Publishing, Canada, pp. 57-66.

ICOLD (1994) "Embankment Dams – Filters and Drains" Bulletin No. 95, ICOLD, France.

Imdakm A. and Sahimi M. (1987) "Transport of Large Particles in Flow Through Porous Media", Physical Review A, Vol. 36 No. 11, pp. 5304-5309.

Indraratna B. Dilema E., Nutalaya P. (1990) "Design of Granular Filters for a Lateritic Residual Soil", Dam Engineering Vol. 1(3), AIT Bangkok, Thailand, pp. 201-220.

Indraratna B., Vafai F., Dilema E. (1996) "An Experimental Study of the Filtration of a Lateritic Clay Slurry by Sand Filters", Proc. Instn Civ. Engrs. Geotechnical Engineering, Vol 119, pp. 75-83.

Indraratna B. and Vafai F. (1997) "Analytical Model for Particle Migration Within Base Soil - Filter System", Jour. Geotechnical and Geoenvironmental Engineering, ASCE, Vol 123, No. 2, pp. 100-109.

John N. and Watson P. (1996) "Soil Particle Bridge Development at the Soil – Geotextile Interface", *Geofilters '96, Comptes Rendus Proceedings*, Lafleur & Rollin (Eds.), Bitech Publictions, Canada, pp. 57-66.

Joy D., Lennox W., Kouwen N. (1993) "Stochastic Model of Particulate Transport in Porous Medium" ASCE Jour. Hydraulic Engineering, Vol. 119, pp. 846-861.

Karpoff K. (1955) "The Use of Laboratory Tests to Develop Design Criteria for Protective Filter", Proc. 58th Annual Meeting ASTM, pp. 1183-1198.

Kenney T., Chahal R., Chiu E., Ofoegbu G., Omange G., Ume C. (1985) "Controlling Constriction Sizes of Granular Filters", Canadian Geotechnical Journal, Vol. 22, pp. 32-43

Kenney T. and Lau D. (1985) "Internal Stability of Granular Filters", Canadian Geotechnical Journal, Vol. 22, pp. 215-225.

Khilar K., Fogler H., Gray D. (1985) "Model for Piping-Plugging in Earthen Structures", Jour Geotechnical Engineering, ASCE, Vol. 111(7), pp. 833-846.

Khor C. and Woo H. (1989) "Investigation of Crushed Rock Filters for Dam Embankment", Jour of Geotechnical Engineering, ASCE, Vol. 115(3), pp. 399-412.

Koenders M. and Williams A. (1992) "Flow Equations for Particle Fluid Mixtures" *Acta Mechanica*, Vol. 92, No. 1, pp. 91-116.

Kovacs G. (1981) *Seepage Hydraulics,* Elsevier Publishing, Amsterdam, 570p.

Kulhawy F. and Gurtowski T. (1976) "Load Transfer and Hydraulic Fracturing in Zoned Dams" Jour. Geotechnical Div. ASCE, Vol 102(GT9), pp. 963-974.

Kwang T. (1990) " Improvement of Dam Filter Criterion for Cohesionless Base Soil" M. Eng. Thesis, Asian Institute of Technology, Bangkok, Thailand.

Lafleur J. (1984) "Filter Testing of Broadly Graded Cohesionless Tills" Canadian Geotechnical Journal, Vol. 21, pp. 634-643.

Lafleur J., Mlynarek J., Rollin A. (1989) "Filtration of Broadly Graded Cohesionless Soils", Jour. Geotechnical Engineering, ASCE, Vol 115, No. 12, pp. 1747-1768.

Lo K. and Kaniaru K. (1990) "Hydraulic Fracture in Earth and Rockfill Dams" Canadian Geotechnical Jour.,Vol. 27, pp. 496-506.

Maranha das Neves E. (1989) "Analysis of Crack Erosion in Dam Cores. The Crack Erosion Test" *De Mello Volume*, pp. 284-298

Penman A. and Charles J. (1981) "Assessing the Risk of Hydraulic Fracture in Dam Cores" 10th ICSMFE, Stockholm, Vol. 3, pp. 457-461.

Rallings R. (1966) "An Investigation into the Causes of Failure of farm Dams in the Brigalow Belt of Central Queensland" Water Research Foundation Aust. Bull. No. 10.

Reddi L. and Bonala M. (1997) "Analytical Solution for Fine Particle Accumulation in Soil Filters", Jour. Geotechnical Engng Div. ASCE, Vol. 123, No. 12, pp. 1143-1152.

Reddi L. Ming X., Hajra M., Lee I. (2000) "Permeability Reduction of Soil Filters due to Physical Clogging" Jour. Geotechnical and Geoenvironmental Engineering, ASCE, Vol. 126(3), pp. 236-246.

Rege S. and Fogler H. (1988) "A Network Model for Deep Bed Filtration of Solid Particles and Emulsion Drops" Jour. AIChE, Vol. 34, No. 11, pp. 1761-1772.

Ripley C. (1982) Discussion of "Design of Filters For Clay Cores for Dams" by Vaughan and Soares (1982), Jour. Geotechnical Engng Div. ASCE, pp 1193-1195.

Schuler U. (1996) "Scattering of the Composition of Soils. An Aspect for the Stability of Granular Filters", *Geofilters '96, Comptes Rendus Proceedings*, Lafleur & Rollin (Eds.), Bitech Publictions, Canada. pp. 21-34

Sherard J., Dunnigan L., Decker R., Steel E. (1976a) "Pinhole Test for Identifying Dispersive Soils" Jour. Geotech. Engineering Div. ASCE, Vol 102, No. GT1, January 1976, pp 69-85.

Sherard J., Dunnigan L. and Decker R. (1976b) "Identification and Nature of Dispersive Soils", Jour. Geotechnical Engng Div. ASCE, Vol. 102, No. GT4, pp 287-301.

Sherard J. and Decker R. (1977) "Some Engineering Problems With Dispersive Clays" *Proceedings, Symposium on Dispersive Clays, Related Piping, and Erosion in Geotechnical Projects,* ASTM, Special Technical Publication 623, 1977, ASTM, Philadelphia, Pennsylvania, pp 3-12.

Sherard J. (1979) "Sinkholes in Dams of Coarse, Broadly Graded Soils" Trans. 13th International Congress on Large Dams Vol 2, p. 25.34.

Sherard J. (1982) Discussion of "Design of Filters For Clay Cores for Dams" by Vaughan and Soares (1982), Jour. Geotechnical Engng Div. ASCE, pp 1195-1197.

Sherard J. (1984) Data from NEF laboratory tests, presented in Foster M. (2000).

Sherard J., Dunnigan L., Talbot J. (1984a) "Basic Properties of Sand and Gravel Filters" Jour. Geotech. Engineering Div. ASCE, Vol 110, No. GT6, June 1984, pp 684-700.

Sherard J., Dunnigan L., Talbot J. (1984b) "Filters for Silts and Clays" Jour. Geotechnical Engineering, ASCE, Vol. 110(6), pp. 701-718.

Sherard J. and Dunnigan L. (1985) "Filters and Leakage Control in Embankment Dams" *Proceedings, Symposium on Seepage and Leakage from Dams and Impoundments,* R.L. Volpe and W.E. Kelly eds., ASCE 1985, pp 1-30.

Sherard J. (1986) "Hydraulic Fracturing in Embankment Dams" Journal Geotech. Engineering, ASCE, Vol. 112, GT10, pp. 905-927.

Sherard J. and Dunnigan L. (1989) "Critical Filters for Impervious Soils" Jour. Geotech. Engineering Div. ASCE, Vol 115, No. GT7, July1989, pp 927-947.

Silveira A. (1965) "An Analysis of the Problem of Washing through in Protective Filters", Proc. 6th Int. Conf. Soil Mechanics and Foundation Engineering, Canada, Vol. 2, pp. 551-555.

Silveira A., de Lorena Peixoto T., Nogueira J. (1975) "On Void Size Distribution of Granular Materials", Proc. 5th Pan-Am Conf. Soil Mech and Fnd. Engng, pp. 161-176.

Silveira A. (1993) "A Method for Determining the Void Size Distribution Curve for Filter Materials" *Filters in Geotechnical and Hydraulic Engineering*, Brauns, Heibaum & Schuler (eds.), 1993 Balkema, Rotterdam, pp. 71-74.

Skempton A. and Brogan J. (1994) "Experiments on Piping in Sandy Gravels", Geotechnique, Vol. 44, No. 3, pp. 449-460.

Soria M., Aramaki R., Viviani E. (1993) "Experimental Determination of Void Size Curves" *Filters in Geotechnical and Hydraulic Engineering*, Brauns, Heibaum & Schuler (eds.), 1993 Balkema, Rotterdam, pp. 43-48.

Spackman D. (2000) "An Investigation into the Effects of Particle Shape in Granular Filter Design" Engineering Honours Thesis, University of Wollongong, NSW, Aust.

Terzaghi K. (1922) "Der Grundbruch an Stauwerken und Seine Verhuntung Forcheimer-Nummer Wasserkr, 17, pp. 445-449, quoted by Vafai (1996).

Thompson M. and Chenhall G. (2000) "Protecting Environmental Flows While Catering for Urban Water Supply Demand, The Cowarra Off-creek Storage Dam Experience" Aust. National Committee on Large Dams, 2000 Conference on Dams.

U.S. Bureau of Reclamation, USBR, (1963) *Earth Manual, First Edition (revised)*, US Govt. Printing Office, Washington D.C., 751p.

U.S. Army Corps of Engineers, USACE, (1971) "Dewatering and Groundwater Control for Deep Excavations", Technical Memorandum No. 5-818-5 (April), Office of Chief of Engineers, US Army, Washington D.C.

Vaughan P. and Soares H. (1982) "Design of Filters for Clay Cores of Dams", Jour. Geotech. Engineering Div., ASCE, Vol. 108, pp. 17-31.

Vaughan P. (2000) "Filter Design for dam cores of clay, a retrospect" *Filters and Drainage in Geotechnical and Environmental Engineering,* Wolski & Mlynarek Eds., Balkema, Rotterdam, pp. 189-196.

Vafai F. (1996) "Analytical Modelling and Laboratory Studies of Particle Transport in Filter Media", PhD Thesis, University of Wollongong, NSW, Australia.

Witt K. (1993) "Reliability Study of Granular Filters", in *Filters in Geotechnical and Hydraulic Engineering*, Brauns, Heibaum & Schuler (eds.), 1993 Balkema, Rotterdam

Wittmann L. (1979) "The Process of Soil Filtration – its Physics and the Approach in Engineering Practice" Proc. 7th EuroConf. Soil Mech. and Fnd. Engng, pp. 303-310.

Wolski (1970) "Model Tests on the Seepage Erosion in the Silty Clay Core of an Earth Dam", 6th Int. Conf. On Soil Mech and Foundation Eng., Canada, Vol II, pp 583-587

Yuen S. and Styles J. (1995) "Use of Sand Washing Slimes as a Landfill Liner Material", Australian Civil Engineering Transactions, Australia, Vol. CE37 No. 3, pp. 201-209.

Appendix 1 – Procedure for No Erosion Filter (NEF) Test

Introduction

The No Erosion Filter (NEF) test was proposed by Sherard and Dunnigan (1985), to simulate filtration of cohesive base soils after the formation of a crack. The typical apparatus is shown in Figure A1.1. In the test, a sample of base soil is compacted on top of the filter. A pinhole is pushed through the base soil to simulate a concentrated leak through a crack. Water is forced through the pinhole under a high pressure, which is sufficient to erode the base soil. The test is considered successful if no visible erosion occurs before the filter interface seals, and unsuccessful if some erosion is necessary to reach steady filtration. This Section outlines a detailed procedure for the NEF test developed by Delgado and Locke (2000), based on the recommendations of Sherard and Dunnigan (1985). This Appendix outlines some recommendations regarding the apparatus, and preparation and interpretation of the NEF test.

NEF Apparatus

The apparatus is typically a cylinder of 100-200mm diameter and 200-300mm high, capable of handling pressures up to 600kPa or more. Top and bottom plates are connected to the cylinder, possibly with continuous rods running between both plates external to the cylinder. The plates should be machined to provide a locating lip and a recess for an o-ring, which provides a water tight seal. As well as a water inlet valve, it is recommended to install a second valve in the top plate to allow air out of the top of the cylinder as it is filled with water. The details of the apparatus are shown in Figure A1.2.

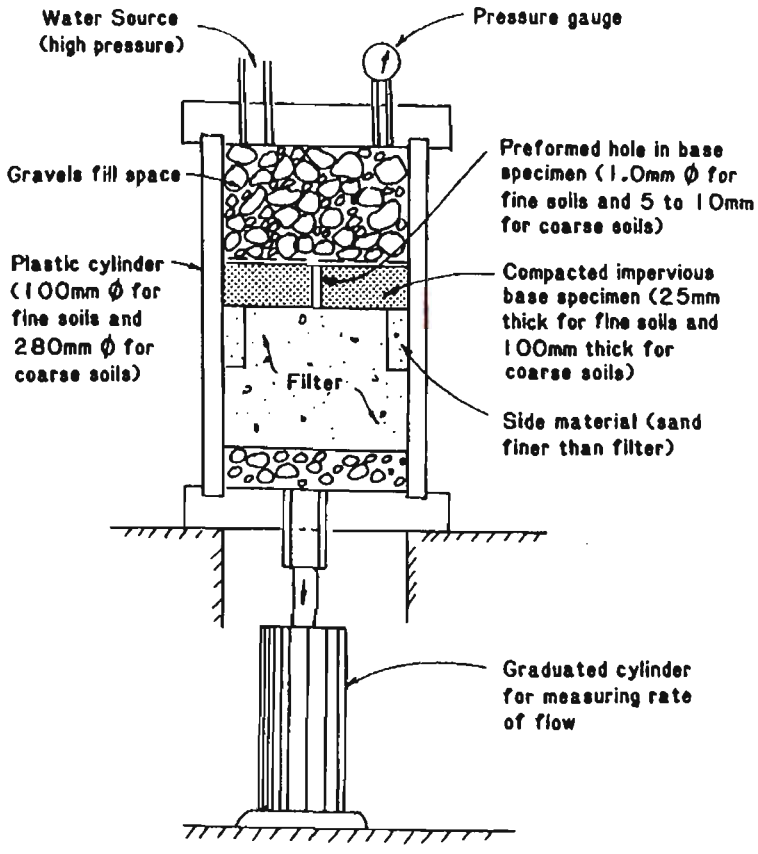

Figure A1.1 Typical NEF Apparatus (Sherard and Dunnigan (1985)

If there is a concern with the quality of water supply it is recommended that some form of water filter be used to ensure no particles enter the test cylinder. A geotextile could be used for this purpose. If the water supply pressure is either insufficient (<200kPa) or highly variable then it may be necessary to use a large capacity holding tank. Water drawn from this tank is pumped at the desired pressure into the apparatus. It may be convenient to use the NEF apparatus for measuring the permeability of the filter material.

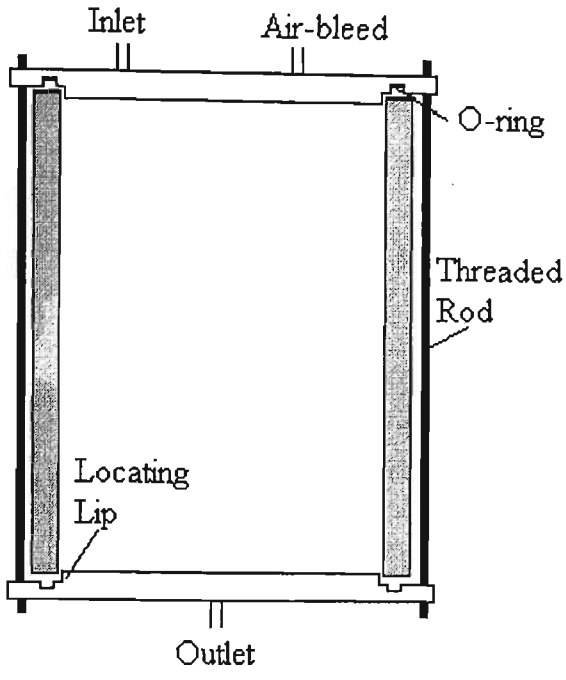

Figure A1.2 Schematic diagram of NEF apparatus

Filter Preparation

Except in the case where real filter materials are sourced from the proposed stockpile or natural deposit, it is necessary to produce a filter material to a particular grading. The required grading is usually determined from the D_{15} size and the coefficient of uniformity, although other factors such as maximum and minimum particle size may also control the grading. In order to prepare such a sample, the material should be split into distinct fractions, by sieving and washed on a 75μm sieve to remove any cohesive fines. Fujisawa et al. (1997) have shown that increased fines content greatly improves the filter effectiveness, and to remove these fines produces a more conservative test. If the required filter gradation requires some fines content, this fraction can be re-blended, ensuring the fines are non-cohesive. Sufficient material for only one test should be produced in each batch. In this way, problems of segregation due to excessive splitting of samples are avoided.

Compaction of the filter material can lead to breakdown of particles, which produces finer particles than the original grading. This is very dangerous as it produces false results, predicting success whereas the real filter will fail. To control this the particle size distribution (PSD) of a filter sample after compaction should be measured and compared with the original sample.

After completion of a test, the filter material can be recovered, washed and separated into size fractions again, to provide material for another filter test. The filter particles should be examined to ensure they have not broken down during this process to different sizes and shapes, as particle shape has been shown to effect filtration efficiency.

Many authors employ a "side material" of sand finer than the filter to avoid the formation of preferential flow paths down the side of the material (Sherard et al. 1984, Khor and Woo 1989). The writer has found that compaction of the filter by vibration can lead to migration of the side material into the filter, with a subsequent improvement in the filtration efficiency. It is recommended instead that a strip of modelling clay (air drying clay has been found to work well) be placed around the edge of the apparatus, approximately 15mm high, such that it is centred over the base - filter interface. This material will prevent erosion down the side of the apparatus.

Preparation of the Base Soil

The base soil should only contain the fraction passing the 4.75mm sieve, as the coarser fraction has no influence on filtration. It is important to determine the complete PSD of the base soil with and without a chemical dispersant. This demonstrates the tendency of the base soil to form flocs or aggregates of many cohesive particles. If the soil is found to be dispersive, distilled water is often used in the NEF test to ensure conservative testing

conditions. Distilled water is not necessary for non-dispersive materials. Although no published research has yet related the influence of clay mineralogy to filtration efficiency, the mineralogy could be determined as this information provides some insight into the expected behaviour of the material.

In order to obtain the desired moisture content in a cohesive base soil, it is important to leave the sample in a moist environment (such as a sealed plastic bag or a humidifier), after mixing, for at least 24 hours to ensure the moisture is distributed homogeneously throughout the sample. It is often easier to prepare many samples at the one time to ensure homogeneity and because the process is time consuming.

Preparation and Execution of the NEF Test

Details of the proposed NEF test method follow this section, a few recommendations are given here. It is important that coarse particles are not present on the filter surface after compaction, as these particles may block the pinhole through the base soil. Some authors suggest the pinhole should be formed by compacting the base soil around a needle, however the sample is more homogeneous, and it is certainly easier, if the pinhole is formed after compaction by pushing a needle or fine wire through the base soil. The needle should penetrate about 5mm into the filter material to avoid obstructing the exit. The upper surface of the base soil should be protected with a solid disc to prevent the gravel, which is placed on top, penetrating into the sample.

Erosion of the base soil occurs during the first moments of flow. In a successful test the filter usually seals and clear water flows within the first few minutes. Hence, a duration of 20 minutes is sufficient for the test. Several tests of longer duration have been performed with no change in results. Because successful filtration occurs rapidly, it is

recommended to take measurements of flow rate and turbidity every 30 seconds during the first five minutes, this can be relaxed to once per minute for the following five minutes and at two-minute intervals during the final 10 minutes. Turbidity can be measured using a turbidimeter. This must be calibrated to the particular base soil and can then give good estimates of turbidity at each time interval. It is very interesting to analyse the particle size distribution of the particles in the effluent water, a laser particle size analyser can do this quickly and accurately. To save time the effluent water could be analysed only for the two samples on the borderline between success and failure.

Interpretation of Results

On completion of the test, the apparatus should be dismantled and the filter material recovered carefully with a spatula, so as not to disturb the base soil. The final part of filter material can be washed away from the base soil with a gentle stream of water. The base soil should then be gently removed so that the pinhole remains intact. A disc which closely fits the inside diameter of the apparatus (the surcharge weight is ideal) can be used to press the block of base soil out.

The NEF test is considered a success when there is no visible erosion of the 1mm pinhole, and failure if the pinhole erodes to more than 2mm diameter. The hole can be examined with a magnifying glass to confirm these measurements. In intermediate cases, with a final diameter between 1mm and 2mm it is recommended to consider the effluent water flow rate and turbidity and perhaps the mass of eroded material, to judge the test. In these cases the result is "intermediate", and the NEF boundary is determined based on the results of other tests using slightly coarser and finer filters.

The NEF test is very sensitive, the border between success and failure often being detected over a variation of 0.1mm in the D_{15} size of the filter. Erratic results are sometimes encountered, this may be because there is a large filter particle blocking the pinhole, or large eroded aggregates or surface slaking of base soil block the pinhole before significant erosion can occur. These erratic results can generally be noticed because they do not comply with the results of the next coarser or finer filter test. If this is the case the erratic result should be discarded and the test repeated.

Laboratory Method for NEF test

Sherard and Dunnigan (1985, 1989) briefly describe the NEF test procedure used to determine their design criteria. However, these papers do not describe in detail the preparation of materials and problems encountered with testing. This section outlines a detailed procedure, which was followed for the NEF tests described in the thesis.

Compaction of the Filter

1. Divide the filter into fractions by sieving. Wash and remix to produce 1.5kg of material. The mass of each size fraction to include is determined from the required PSD.
2. Add 3% water by weight, mix so that the material is homogeneous.
3. Divide into 4 parts of equal weight, taking care to remove all the material which may have adhered to the apparatus or containers.
4. Place a disc of wire mesh, approximately 1-2mm opening size over the base plate of the apparatus. Weigh the apparatus and record the height above the wire mesh.
5. For fine filter materials, it may be necessary to place a thin layer of coarser material to avoid the filter washing out through the wire mesh.

6. Place the apparatus on a vibrating table and attach it firmly. Place filter material in the cylinder to approximately 2.5cm height (approximately 260g). Apply a 9kg surcharge to the filter material and vibrate for 1 minute.
7. Remove the surcharge carefully so that no material adheres to it. Repeat the process for the next two layers of filter material.
8. Mould and attach a strip of modelling clay or plastacine to the sides of the cylinder. This should be approximately 15mm deep and located so that the compacted final layer of filter material will reach approximately the middle of the strip.
9. Place the 4^{th} fraction of filter material and compact by vibration again.
10. Use the remaining filter material from the 4 fractions to determine the moisture content of the material.
11. Remove the apparatus from the vibrating table and weigh.
12. Measure the height of the filter material, using a minimum of 4 readings over the surface.

Compaction of the Base Soil

1. Take a representative sample of the base material to determine the moisture content.
2. Place approximately 140g of base material on top of the filter and smooth the surface with a spatula. Put the surcharge weight on top without pressing on it.
3. Compact the base soil with 25 blows of a standard compaction hammer on top of the surcharge. Remove the surcharge and scarify the surface.
4. Place another layer of base soil so that the base soil sample is approximately 2.5cm deep in total. Compact again with 25 blows, without scarifying the final surface.
5. Lift off the surcharge and remove any material adhering to the walls of the cylinder.
6. Perforate the base soil with a 1mm diameter needle or wire, until it reaches 5mm into the filter material. Remove the needle, taking care not to deform the hole.

7. Weigh the entire apparatus again and measure the height of the base soil with a minimum of four readings. Determine the density and moisture content of the base soil.
8. Put a disc or mesh on top of the base soil and place gravel, of 2-5mm diameter that has been washed and sieved, inside the cylinder without affecting the base soil. Place another disc on top of the gravel and place the top plate on the test cell.

Execution of the Test

1. Fill the cylinder with water, without pressure, until the apparatus is completely full, ensuring all the air has been removed from the cylinder.
2. Apply the required pressure, as rapidly as possible, controlling it with the valve at the inlet to the apparatus.
3. For the 20 minute test, record the time interval, turbidity of water, entrance pressure, and flow rate or volume. Take measurements every 30 seconds in the first 5 minutes, then every minute for the next 5 minutes and every 2 minutes for the final 10 minutes. This describes the behavior of the base-filter interface.
4. Finish the test, open the apparatus without disturbing the base soil and observe the pinhole entrance and exit. Record the diameter of the pinhole and any other items of interest.

APPENDIX 2 - NOTATION

a - particle radius

A - multiplied to determine representative PSD of base soils

b - standard deviation

C - volume concentration of slurry flow

C_u - coefficient of uniformity (D_{60}/D_{10})

d_{iB} - diameter of *i%* coarsest base soil particle, eg. d_{85B}

d_p - maximum particle diameter passing through element

d_r - maximum particle diameter entering an element and then retained

d_{85EP} - 85% largest particle of erosion product after dispersion

d_{85red} - 85% largest particle of *reduced PSD*

d_{85Rep} - 85% largest particle of representative PSD for modelling cohesive soils

D - deposition rate

D_c* - controlling constriction size

D_{iF} - diameter of *i%* coarsest filter particle, eg. D_{15F}

$D_{f,mean}$ - mean filter particle diameter (calculated from PSD by number rather than mass)

D_{max} - largest particle diameter

D_v - void constriction diameter

D_{VLD} - constriction diameter from least dense packing model of four particles

D_{VMD} - constriction diameter from most dense packing model of three particles

D_{15bdy} - D_{15} of the coarsest filter able to retain a base soil with no erosion in the NEF test

E - erosion rate

F - mass fraction passing diameter D

ΣF - sum of forces on the seepage flow within an element

g - acceleration due to gravity

H - mass fraction between diameters D and 4D

H_{inlet} - head at inlet to crack

H_{filter} - head at filter interface

H_0 - head at free surface of flow (pressure=0)

i_{crack} - hydraulic gradient in crack

i_{filter} - hydraulic gradient in filter

i_h - hydraulic gradient in pinhole

k - permeability

K_1 - representative permeability of crack element

l_e - depth of penetration into filter

L - length a particle can infiltrate the 3D pore model

L_I - length of element I

L_{trans} - length of transition element

m - mean

n - number of layers (or forward steps) a particle will infiltrate the 3D pore model

n_e - porosity

O_f - allowable filter opening size

p - probability that a particle of diameter d can pass through a random pore constriction

p(r) - probability of capture of particles of diameter r

p_0 - pore pressure

$\overline{P}$ - certainty in probabilistic infiltration depth model

P_i - probability of occurrence (frequency) of particles of diameter *i* (from PSD)

P_v - probability of occurrence (frequency) of void constrictions of diameter D_v

P(F) - probability of a forward step (movement of a particle from one void to another in the direction of flow) in the 3D pore model.

P(F|1S) - probability of a forward step from either the initial void or after one perpendicular (sideways) step, in the 3D pore model

q - flow flux (flow rate/unit area)

Q - flow rate

r_i - radius of pinhole element i

r_j - number of times particles of diameter D_j appear in the combination of particles forming a constriction

r_{trans} - radius of transition element

R - radius of saturated zone in filter

R' - hydrodynamic number

R_D - relative density

s - unit step or distance between confrontations in filter model

S_n - mass fraction passing diameter D_n from PSD

T - tensile strength of cohesive material

u - slurry velocity

V_c - critical pore velocity

V_m - volume of slurry within an element

$(V_s)_j$ - volume of solid particles in slurry in element j

$(V_{s\text{-}out})_j$ - volume of solid particles in slurry leaving element j

w - crack thickness

α - erosion rate parameter (also shape factor in Chapter 2 only)

χ - non-dimensional permeability coefficient

δ - Representative particle size

ϕ' - effective friction angle

λ - deposition coefficient

η - viscosity

θ - parameter representing particle attraction forces

ρ_b - bulk density of material

ρ_m - slurry density

ρ_s - particle density

τ_w - shear stress on wall of crack

τ_c - critical shear stress to initiate erosion

ψ - effective pore length